Western Graduate&PostdoctoralStudies

Western University
Scholarship@Western

Electronic Thesis and Dissertation Repository

4-20-2012 12:00 AM

Gasification of Bio-oils to Syngas in Fluidized Bed Reactors

Mohammad Latifi, *The University of Western Ontario*

Supervisor: Dr. Franco Berruti, *The University of Western Ontario*
Joint Supervisor: Dr. Cedric Briens, *The University of Western Ontario*
A thesis submitted in partial fulfillment of the requirements for the Doctor of Philosophy degree in Chemical and Biochemical Engineering
© Mohammad Latifi 2012

Follow this and additional works at: https://ir.lib.uwo.ca/etd

Part of the Catalysis and Reaction Engineering Commons

Recommended Citation

Latifi, Mohammad, "Gasification of Bio-oils to Syngas in Fluidized Bed Reactors" (2012). *Electronic Thesis and Dissertation Repository*. 490.
https://ir.lib.uwo.ca/etd/490

This Dissertation/Thesis is brought to you for free and open access by Scholarship@Western. It has been accepted for inclusion in Electronic Thesis and Dissertation Repository by an authorized administrator of Scholarship@Western. For more information, please contact wlswadmin@uwo.ca.

Gasification of Bio-oils to Syngas in Fluidized Bed Reactors

(Spine Title: Gasification of Pyrolytic Bio-oils to Syngas)

(Thesis format: Integrated-Article)
by
Mohammad Latifi

Graduate Program in Engineering Science
Department of Chemical and Biochemical Engineering

Submitted in partial fulfillment
of the requirements for the degree of
Doctor of Philosophy

School of Graduate and Postdoctoral Studies
Western University
London, Ontario

April 2012

© Mohammad Latifi 2012

WESTERN UNIVERSITY
SCHOOL OF GRADUATE AND POSTDOCTORAL STUDIES

CERTIFICATE OF EXAMINATION

Joint-Supervisor

____
Dr. Franco Berruti

Joint-Supervisor

____
Dr. Cedric Briens

Examiners

____
Dr. Argyrios Margaritis

____
Dr. Dimitre Karamanev

____
Dr. Ken Yeung

____
Dr. Guus van Rossum

The thesis by

Mohammad Latifi

entitled:

Gasification of Bio-oils to Syngas in Fluidized Bed Reactors

is accepted in partial fulfillment of the

requirements for the degree of

Doctor of Philosophy

Date__________________________

____
Chair of the Thesis Examination Board

ABSTRACT

Bio-fuels are renewable and clean which can be used as alternatives to fossil fuels or can be used in combination with them. Biomass is a main source of bio-fuels production: it is a renewable resource and its conversion to energy releases no net CO_2 to the environment.

Bio-oil, the valuable liquid product obtained from biomass through pyrolysis, may be either combusted to generate carbon-neutral electricity or converted to a synthesis gas from which chemicals or clean fuels can be produced. Producing bio-oil from biomass and then converting the bio-oil to syngas has several advantages: The bio-oil may be generated in distributed or mobile plants and then shipped to a central facility for conversion to syngas, thus avoiding the expensive transportation of bulky and perishable biomass. The syngas produced from bio-oil is cleaner than syngas produced directly through biomass gasification. Finally, valuable green chemicals may be extracted from the bio-oil before it is converted to syngas.

This thesis focuses on investigation of syngas production from bio-oil through thermal and catalytic reactions. Low bio-oil conversion and syngas yield were achieved from thermal cracking experiments in a pilot plant bubbling fluidized bed at moderate temperatures. A novel induction heated batch-wise micro reactor was designed and developed to test catalysts for bio-oil gasification. Catalytic gasification of bio-oils in this micro reactor revealed that a syngas with desired yield can be produced from bio-oil with maximum conversion provided there is a suitable catalyst and sufficient operating conditions such as temperature, residence time and steam in the reactor.

KEYWORDS: Biomass, Bio-oil, Gasification, Syngas, Hydrogen, Fluidized bed, Thermal cracking, Catalytic cracking, Catalyst, Jiggle Bed Reactor, JBR, Vibration, Pneumatic actuator, Induction heating, Amplitude and Frequency, Image processing, Signal processing, Acetic acid, Thermodynamic, Equilibrium, Olivine, Calcination.

STATEMENT OF CO-AUTHORSHIP

Chapters 1 through 6 encompass research studies which are going to be published in the peer-refereed journals. Individual contributions of all authors for each journal article are briefly stated below.

CHAPTER 1

Article Title	**Production of Syngas from Bio-oil and its Model Compounds- A Literature Review**
Authors	M. Latifi, C. Briens, F. Berruti
Current Status	To be submitted to the *International Journal of Chemical Reactor Engineering*
M. Latifi reviewed the literature and wrote the manuscript. C. Briens and F. Berruti jointly supervised, reviewed and revised several drafts of the work.	

CHAPTER 2

Article Title	**Effects of Residence Time and Temperature on the Thermal Cracking of Bio-oil for Syngas Production**
Authors	M. Latifi, L. Ferrante, C. Briens, F. Berruti
Current Status	Presentation and Poster in *ECI Conference, Bioenergy II*, Rio de Janeiro, Brazil, March 2009 Presentation and Poster in *ABIN Conference* 2010 To be submitted to the *Canadian Journal of Chemical Engineering*
M. Latifi designed and developed the gas-atomized bio-oil injector, the cyclonic condenser and two gas analysis systems which were used by other students in the lab. M. Latifi conducted the experimental work, performed the data analysis and wrote the manuscript. L. Ferrante had a significant contribution in preliminary steps of running the bubbling bed, design of the cyclonic condenser and development of the first gas analysis system. Various drafts of the manuscript were reviewed and revised by C. Briens and F. Berruti. The work was jointly supervised by C. Briens and F. Berruti.	

CHAPTER 3

<table>
<tr><th>Article Title</th><th>A Novel Fluidized and Induction Heated Micro Reactor for Catalyst Testing</th></tr>
<tr><td>Authors</td><td>M. Latifi, L. Ferrante, C. Briens, F. Berruti</td></tr>
<tr><td>Current Status</td><td>Presentation and poster in ECI conference, Bioenergy III, Lanzarote, Spain, May 2011
To be submitted to the <i>AICHE Journal</i></td></tr>
<tr><td colspan="2">M. Latifi designed and developed the Jiggle Bed Reactor setup and operation procedure and conducted the experimental and theoretical work including the induction heating method and the image analysis technique. M. Latifi performed the data analysis and wrote the manuscript. L. Ferrante introduced the idea of image analysis and provided his comments during the experimental work. C. Briens and F. Berruti introduced the idea of the jiggle bed reactor. C. Briens provided the signal processing program and assisted in the development of the heat transfer modeling. Various drafts of the manuscript were reviewed by C. Briens and F. Berruti. The work was jointly supervised by C. Briens and F. Berruti.</td></tr>
</table>

CHAPTER 4

<table>
<tr><th>Article Title</th><th>Non-catalytic and Catalytic Steam Reforming of Acetic Acid in the Jiggle Bed Reactor</th></tr>
<tr><td>Authors</td><td>M. Latifi, C. Briens, F. Berruti</td></tr>
<tr><td>Current Status</td><td>To be submitted to the <i>Journal of Fuel Processing Technology</i></td></tr>
<tr><td colspan="2">M. Latifi conducted all the design modifications and the experimental work. M. Latifi developed the gas analysis technique with a micro GC which was used by several students and post docs in the lab. M. Latifi performed the data analysis and wrote the manuscript. Various drafts of the manuscript were reviewed by C. Briens and F. Berruti. The work was jointly supervised by C. Briens and F. Berruti.</td></tr>
</table>

CHAPTER 5

<table>
<tr><th>Article Title</th><th>Thermal and Catalytic Gasification of Bio-oils in the Jiggle Bed Reactor for Syngas Production</th></tr>
<tr><td>Authors</td><td>M. Latifi, C. Briens, F. Berruti</td></tr>
<tr><td>Current Status</td><td>To be submitted to the <i>International Journal of Hydrogen Energy</i></td></tr>
<tr><td colspan="2">M. Latifi conducted the experimental work and wrote the manuscript. Various drafts of the manuscript were reviewed by C. Briens and F. Berruti. The work was jointly supervised by C. Briens and F. Berruti.</td></tr>
</table>

CHAPTER 6

Article Title	Development of a Thermodynamic Model to Predict the Equilibrium Concentration of Gases from Bio-oil Gasification with Sand or Olivine Catalyst
Authors	M. Latifi, F. Berruti, C. Briens
Current Status	To be submitted to the *International Journal of Hydrogen Energy*
M. Latifi developed the thermodynamic model, conducted all the experimental work and wrote the manuscript. Various drafts of the manuscript were reviewed by C. Briens and F. Berruti. The work was jointly supervised by F. Berruti and C. Briens	

APPENDIX I

Article Title	A Novel Induction Heated Microreactor for Gasification Catalyst Testing
Authors	S. Rohani, M. Latifi, L. Ferrante, C. Briens, F. Berruti
Current Status	Presentation and conference in *GPE-EPIC; 2nd International Congress on Green Process Engineering; 2nd European Process Intensification Conference; 14-17 june 2009 - Venice (Italy)* Presentation in *8th World Congress of Chemical Engineering*, Montreal, Canada, August 2009
M. Latifi assisted S. Rohani in the experimental work. S. Rohani conducted the experimental work wrote the manuscript. L. Ferrante set up the experimental plant and assisted in the experiments and technology development. Various drafts of the manuscript were reviewed by C. Briens and F. Berruti. The work was jointly supervised by C. Briens and F. Berruti.	

APPENDIX II

Article Title	Characterization of Moisture Distribution in a Fluidized bed
Authors	M. Farkhondeh, M. Soleimani, M. Latifi, C. Briens, F. Berruti
Current Status	To be submitted to Journal of Powder Technology
M. Latifi assisted M. Farkhondeh to develop a new image analysis technique to analyze her experimental recordings to observe moisture distribution in her fluized bed setup. M. Farkhondeh conducted all experimental work and wrote the manuscript. M. Soleimani assisted M. Farkhondeh in her experimental work. Various drafts of the manuscript were reviewed by C. Briens and F. Berruti. The work was jointly supervised by C. Briens and F. Berruti.	

ACKNOWLEDGEMENTS

This research project would not have been possible without the support of many people. I would like to extend my deepest appreciation and gratitude to my supervisors, Professor Franco Berruti and Professor Cedric Briens, for being truly my teachers and for their continuous encouragement, constructive criticism, enthusiastic guidance, support, trust and understanding throughout my doctoral program. Besides, I have been extremely fortunate to work with them during this important period of my life and have them as one of the best examples of good researchers and great academic supervisors. I will never forget the practical lesson I learned from them: As an engineer, we are supposed to learn how to find the solution for the problems in life because there is always a solution for any problem.

Especially, I wish to express my sincere gratitude to my fellow graduate student, post doctoral fellow and summer student collegues at the former WFG and currently the Institute for Chemicals and Fuels from Alternative Resources (ICAFR); I am so proud of working with such amazing people who made this challenging period of my life an enjoyable and a memorable experience. I wish all the best for them in their life being full of prosperity, health and wealth.

My special gratitudes and appreciation go to Robert Taylor who patiently dedicated his valuable time to my project to design and develop the micro reactors.

In particular, I would like to express my gratitude to Chantal Gloor, Pina Sorbana and Christine Ramsden for their invaluable and excellence administration and financial service at ICFAR.

I am also thankfully acknowledging University Machine Services (UMS), Information Technology Service (ITS) and Engineering Financial Store (EFS). Moreover, the any-time advice and assistance from Mr. Brian Dennis, Mr. Souheil Afara and Mr. Joel Eckert are greatly appreciated.

I would like to sincerely express my appreciations to David Lunn from the department of Mechanical and Material Engineering, Norbet Ban from COWPER, David Magellan from AMERITHERM, Elyse Barone from KYOCERA, Annabel from CERAMTEC and Joy Jennison from AGILENT for their continuous, great and invaluable technical advice at different levels of design and development of the jiggle bed reactor.

My gratitude is also extended to the Ontario Centres of Excellence (OCE), the Natural Sciences and Engineering Research Council of Canada (NSERC), and Western University for the financial support of the research program. I gratefully acknowledge the Faculty of Engineering Science in the Western University for the financial support in the forms of Western Engineering Scholarships (WES) and Graduate Thesis Research Awards (GTRA).

Last, but not the least, I would like to thank, from the bottom of my heart, my family for being my best people in the world: my late, but always in my heart, father, my amazing and extraordinary kind mother, my great and priceless brother and systers, my nieces and my in-laws and, in particular, my lovely fincee. All my honors are for my family. I am especially grateful to them who have been continuously supporting me and giving me the best education throughout my entire life. Without their optimism, trust, love, motivation, inspiration, sympathy and support, any accomplishment would not have been possible. I owe everything that I am and I have to the greatest teachers in my life: my father and mother.

DEDICATIONS

I would like to dedicate this achievement to my best people in the world:

My amazing late father who is always in my heart and I feel so proud of being his son

My kindest mother who did everything she could do for me to reach this moment and step of my life, an amazing mother who never forgot to call me a single day and supported me with her advice, pure love and sympathy

My siblings, in-laws and nieces for their love, encouragements, supports and inspirations

My fiancée who gave me her true love and made my life deeply meaningful, beautiful and and delightful

TABLE OF CONTENTS

CERTIFICATE OF EXAMINATION ii

STATEMENT OF CO-AUTHORSHIP iv

ACKNOWLEDGEMENTS vii

DEDICATIONS ix

TABLE OF CONTENTS x

LIST OF TABLES xvii

LIST OF FIGURES xxi

LIST OF ABBREVIATIONS xxix

OVERVIEW 1

CHAPTER 1: Production of Syngas from Bio-oil and its Model Compounds - A Literature Review 6

1.1. Introduction 7

1.2. Bio-oil gasification reaction and kinetics 12

1.2.1. Biomass 12

1.2.2. Bio-oil 12

1.2.3. Steam reforming reactions of bio-oil and its model compounds: 15

1.2.4. Thermodynamics of gasification 19

1.2.5. Gasification kinetics 21

1.3. Review of experimental results from gasification of bio-oil and its model compounds 26

1.3.1. Experimental objectives and setups 26

  1.3.1.1. Bio-oil model compounds 26

1.3.1.2. Bio-oil 29

1.3.1.3. Summary 36

1.3.2. Composition and effect of the catalysts 36

1.3.2.1. Bio-oil model compounds 36

1.3.2.2. Bio-oil 51

1.3.2.3. Summary 65

1.3.3. Effect of temperature 66

1.3.3.1. Bio-oil model compounds 66

1.3.3.2. Bio-oil 67

1.3.3.3. Summary 69

1.3.4. Effect of residence time and GHSV 70

1.3.4.1. Bio-oil model compounds 70

1.3.4.2. Bio-oil 71

1.3.4.3. Summary 74

1.3.5. Effect of excess steam, hydrogen and CO_2 74

1.3.5.1. Bio-oil model compounds 74

1.3.5.2. Bio-oil 79

1.3.5.3. Summary 83

1.3.6. Effect of oxygen 83

1.3.6.1. Bio-oil model compounds 83

1.3.6.2. Bio-oil 84

1.3.6.3. Summary 86

1.5. Thesis objectives 92

References 93

CHAPTER 2: Effects of Residence Time and Temperature on the Thermal Cracking of Bio-oil for Syngas Production 99

2.1. Introduction 100

2.2. Pilot plant set-up 101

2.3. Experimental procedure 105

2.4. Gasification reactions..106

2.5. Results and discussion 108

2.5.1. Effect of residence time 109

2.5.2. Effect of temperature 111

2.5.3. Effect of bed mass.. 116

2.5.4. Effect of particle size 119

2.5.5. Syngas (H_2+CO) production 120

2.6. Conclusions 122

References 123

CHAPTER 3: A Novel Fluidized and Induction Heated Micro Reactor for Catalyst Testing 127

3.1. Introduction 128

3.2. Equipment 132

3.2.1. The Jiggle Bed Reactor.. 132

3.2.2. The Motion system 135

3.2.3. The induction heating system 136

3.3. Optimization of fluidization dynamics - Cold study..137

3.3.1. Particle mixing in the jiggle bed reactor 137

3.3.2. Experimental set-up 138

3.3.3. Image processing methodology 140

3.3.4. Results and discussion 144

    3.3.4.1. Relation between the air pressure and the frequency of the actuator 144

    3.3.4.2. Frequency of the actuator versus frequency of the bed 145

    3.3.4.3. Effect of amplitude of the pneumatic actuator motion on fluidization........ 145

    3.3.4.4. Effect of mass and size distribution of the catalyst particles 147

3.4. Optimization of fluidization dynamics- Heat transfer study..................................149

3.4.1. Heat transfer modeling.. 150

3.4.2. Results and discussion 152

    3.4.2.1. Effect of the delivered power... 152

    3.4.2.2. Effect of frequency of the pneumatic actuator... 156

3.5. Conclusions 159

Acknowledgments...160

Nomenclature 160

References 161

Appendix A. Sizing the air cylinder 163

CHAPTER 4: Non-catalytic and Catalytic Steam Reforming of Acetic Acid in the Jiggle Bed Reactor 166

4.1. Introduction 167

4.2. Experimental setup and procedure 170

4.3. Catalyst preparation 175

4.4. Catalyst characterization...176

4.5. Experimental results and discussion 179

4.5.1. Non-catalytic results of the acetic acid steam reforming 182
    4.5.1.1. Effect of molar S/C ratio and residence time 182
    4.5.1.2. Effect of temperature 185
4.5.2. Catalytic results of the acetic acid steam reforming 186
    4.5.2.1. Effect of molar S/C ratio and residence time 186
    4.5.2.2. Effect of catalyst mass 189
4.5.3. Comparison with literature data 192
4.6. Conclusions 193
References 194
CHAPTER 5: Thermal and Catalytic Gasification of Bio-oils in the Jiggle Bed Reactor for Syngas Production 197
5.1. Introduction 198
5.2. Experimental setup and procedure 203
5.3. Bio-oils 205
5.4. Preparation of the bed material 206
5.5. Catalyst characterization 207
5.6. Experimental results and discussion 211
5.6.1. Thermal cracking of the bio-oils 214
5.6.2. Catalytic cracking of the bio-oils 217
    5.6.2.1. Effect of catalyst type and mass 217
    5.6.2.2. Effect of residence time 219
    5.6.2.3. Effect of temperature 220
5.7. Conclusions 224
References 225

CHAPTER 6: Development of a Thermodynamic Model to Predict the Equilibrium Concentration of Gases from Bio-oil Gasification with Sand or Olivine Catalyst 229
6.1. Introduction 230
6.2. Equilibrium model for bio-oil gasification 231
6.2.1. Development of equations 232
6.2.2. Development of the solving program 238
6.2.3. Validation of the equilibrium model 238
6.3. Experimental setup and procedures 239
6.4. Experimental materials 241
6.4.1. Bio-oil characteristics 241
6.4.2. Preparation of the bed material 242
6.4.3. Catalyst characterization 242
6.5. Experimental results and discussion 245
6.5.1. Equilibrium composition of the product gases versus experimental data.... 248
6.5.2. Effect of the bed material on hydrogen yield and bio-oil carbon conversion.... 255
6.6. Conclusions 258
Nomenclatures 258
References 260
CHAPTER 7: Conclusions and Recommendations 266
7.1. Conclusions 267
7.2. Recommendations 271
APPENDIX I: A Novel Induction Heating Micro Reactor for Gasification Catalyst Testing 275

APPENDIX II: Characterization of Moisture Distribution in a Fluidized bed................283

CURRICULUM VITAE 317

LIST OF TABLES

Table 1.1. Composition of different bio-oils (Yields in wt % of dry biomass). Adapted from [20] 13

Table 1.2. Stoichiometric yield of H_2 at equilibrium from steam reforming of a water free poplar bio-oil with formula of $CH_{1.33}O_{0.53}$. Adapted from [20] 19

Table 1.3. Estimated optimum conditions for steam reforming of model compounds. Adapted from [28] 21

Table 1.5. Kinetic data for thermal decomposition of biomass and tar 24

Table 1.6. Properties of Dynamotive's bio-oil. Adapted from [63] 30

Table 1.7. Elemental analysis and water content of BTG bio-oils. Adapted from [67] ... 32

Table 1.8. Elemental analysis of Dynamotive's bio-oil and bio-char. Adapted from [71]34

Table 1.9. Elemental composition of rice husk bio-oil. Adapted from [73] 34

Table 1.10. Elemental composition of pine wood bio-oil. Adapted from [74] 35

Table 1.11. Bio-oil characteristics supplied by the BTG. Adapted from [75] 36

Table 1.12. Catalysts used in screening tests. Adapted from [20] 37

Table 1.13. Conversion (%) of model compounds by catalytic steam reforming. Adapted from [20]. Experimental conditions: 700°C, S/C= 5, GHSV= 6725 h^{-1} and t= 0.01s 38

Table 1.14. Activity of various catalysts for steam reforming of model compounds in term of CO_x yield; adapted from [54]: (-) 20-40%; (0) 40-60%; (+) 60-80%; (++) >80% 39

Table 1.15. Activity of various catalysts for steam reforming of model compounds in term of hydrogen yield; adapted from [54]: (--) <20%; (-) 20-40%; (0) 40-60%; (+) 60-80%; (++) >80% 39

Table 1.16. Results of Catalytic Steam Reforming: Influence of Catalyst Composition and W/m_a Ratio. Adapted from [55] 42

Table 1.17. Carbon deposition with respect to the catalyst composition and temperature. Adapted from [21]; Ratio of H_2O/AA= 3 43

Table 1.18. Results of Acetol Catalytic Steam Reforming: Influence of Catalyst Composition at 650°C. Adapted from [57] 46

Table 1.19. Commercial and laboratory catalysts and surface areas. Adapted from [62] 52

Table 1.20. Effect of catalytic activity on the concentration of product gases. Adapted from [67] 60

Table 1.21. Metal Analysis of the Catalyst (RK-212) and the Sand. Adapted from [71]. 61

Table 1.22. Gasification results done at different temperatures of the staged system. Adapted from [68]........ 69

Table 1.23. Experimental results of acetol steam reforming at 650 °C with Ni/Al catalyst, S/C=5.58, 2 h reaction time. Adapted [77] 70

Table 1.24. Conversion of bio-oil and Volume of Product Gas Formed over a Period of 30 min at different Temperatures and Nitrogen Flow Rates at bio-oil Flow Rate of 4.5 g/h. Adapted from [63] 71

Table 1.25. Steam Reforming of Mono- and Disaccharides Using the ICI 46/1 Catalyst; Experimental Conditions, Carbon Balance, and Hydrogen Yields. Adapted from [53]... 76

Table 1.26. Results of Acetol Catalytic Steam Reforming: Influence of S/C Ratio at 650°C Using Ni-Al Catalyst. Adapted from [57] 78

Table 1.27. Product Gas Composition as a Function of CO_2 Concentration in a Feed Gas Mixture of N_2 and CO_2 at a bio-oil Flow Rate of 5.0 g/h at 800 °C. Adapted from Panigrahi et al. [64]........ 79

Table 1.28. Product Gas Composition as a Function of H_2 Concentration in a Feed Gas Mixture of N_2 and H_2 at a bio-oil Flow Rate of 5.0 g/h and at 800 °C. Adapted from [64] 80

Table 1.29. Product Gas Composition as a Function of Steam Flow Rate at a Nitrogen Flow Rate of 30 mL/min and BDO Flow Rate of 5.0 g/h at 800 °C. Adapted from [64] 80

Table 1.30. Experimental results at 650°C, with a catalyst weight of 1.1 g of Ni/Al catalyst calcined at 750°C with oxygen addition. Adapted from [58] 84

Table 1.31. Experimental results of pyrolysis liquid aqueous phase steam reforming at 650 °C, u/u_{mf} =10, 2 h reaction time, catalyst MgAl 0.26. Adapted from Medrano et al. [74] 85

Table 2.1. Elemental analysis and HHV of bio-oil 108

Table 3.1. Required data for heat transfer calculations 153

Table 3.2. Measured temperatures on the surface of wires and inside the reactor 154

Table 3.3. Consumed power, heat loss heat transfer coefficient and heat transfer coefficient between wires and bed; air pressure 207 kPa, sand particles 10 g 155

Table 3.4. Consumed power, heat loss heat transfer coefficient and heat transfer coefficient between wires and sand particles; power outlet 20%, sand particles 10 g, amplitude 6.4 cm 158

Table 4.1. Surface and pore analysis of the catalyst X 176

Table 4.2. XRF analysis data of the steam reforming catalyst X 178

Table 4.3. TPR-TPO analysis results on the fresh and reduced catalyst X 178

Table 4.4. Carbon conversion, molar H_2/CO and CO/CO_2 ratios as a function of catalyst mass and S/C ratio 191

Table 4.5. Comparison between catalytic experimental data from this study and literature data 193

Table 5.1. Elemental analysis of Dynamotive (DMB) and ICFAR (BWB) bio-oils 206

Table 5.2. Surface and pore analysis of the steam reforming catalysts 207

Table 5.3. XRF analysis data of the steam reforming catalysts X and Y 209

Table 5.4. Estimated Ni^0 on the catalyst surface by TPR-TPO analysis (wt%)............. 209

Table 6.1. Gibbs energy and enthalpy of formation of products at equilibrium [67]..... 236

Table 6.2. Coefficients for the special heat capacity of gasification products 237

Table 6.3. Comparison of results between equilibrium model and references data 239

Table 6.4. Elemental analysis of the Dynamotive bio-oils 242

Table 6.5. Surface and pore analysis of olivine 243

Table 6.6. XRF analysis data of fresh olivine 243

Table 6.7. Comparison between estimated equilibrium and experimental mole fractions (dry basis) from olivine calcined at 1000°C. Temperature: 800°C, Residence time: 240s 250

LIST OF FIGURES

Figure 1.1. Diagram of syngas conversion processes taken from [7] 9

Figure 1.2. Block flow diagram of Hydrogen via Steam Methane Reforming taken from [6] 9

Figure 1.3. Shares of alternative fuels in total fuel consumption in the world taken from [8] 10

Figure 1.4. Syngas production from an aqueous fraction of bio-oil taken from [26] 15

Figure 1.5. Sketch of the two parallel reactors performing acetic acid cracking/regeneration sequences in opposition for continuous hydrogen production taken from [60] 28

Figure 1.6. Schematic overview of the staged setup; taken from [68] 33

Figure 1.7. H_2 and total gas yields obtained with and without previous reduction of the catalyst. Bold symbols correspond to yields with reduction and open symbols correspond to yields without reduction taken from [55] 40

Figure 1.8. CO and CO_2 yields obtained with and without previous reduction of the catalyst. Bold symbols correspond to yields with reduction and open symbols correspond to yields without reduction taken from [55] 41

Figure 1.9. Comparison of conversion and H_2 yields between steam reforming of AcOH and acetone over Pt/ZrO_2 catalyst (875K, S/C=5, GHSV=40000h^{-1}; diamond: coversion; circle: yield; taken from [56] 44

Figure 1.10. Diagram for the possible reactions of acetic acid (and acetone) over ZrO_2 catalyst taken from [56] 44

Figure 1.11. Schematic structural evolution of Ni/Al_2O_3 catalyst during repeated cracking/regeneration sequences taken from [60] 51

Figure 1.12. Hydrogen yield obtained by catalytic steam reforming of bio-oil aqueous fraction. Reference catalyst: ×; (a) commercial catalysts; (b) research catalysts; T=825°C, S/C= 4.92, $G_{C1}HSV$= 126000 h^{-1}. Taken from [62] 53

Figure 1.13. Yield of hydrogen from co-reforming of bio-oil fraction with natural gas at 850°C, S/C=4.6 and $G_{C1}HSV$=1000 h^{-1}. Taken from [26] 54

Figure 1.14. Time-dependent concentration profiles (% mole fraction) and H_2 yield (% stoichiometric) during reforming of the three component mixture at 750°C and H_2O/C=6. Taken from [65] 55

Figure 1.15. Effect of reaction temperature on H_2 yield and gas proct compositions. Black symbols for GHSV=300 h^{-1} and White symbols for GHSV=600 h^{-1} .Taken from [65]... 56

Figure 1.16. Gaseous product formation during a single cracking/regeneration sequence on Ni-K/La_2-O_3-Al_2O_3 (600 mg catalyst, T= 700°C). Taken from [23].......................... 57

Figure 1.17. Proposed reaction network during the bio-oil cracking . Taken from [23] .. 59

Figure 1.18. Effect of catalysis on (a) carbon yield (mol %, atomic) as CO, CO_2, CH_4, and hydrocarbons (C_2-C_4) and (b) hydrogen yield (mol %, atomic) as H_2, CH_4, and hydrocarbons (C_2-C_4) on the dry feed stock basis; under steam gasification, $H_2O/C \approx 5.5$, and GC1HSV ≈ 340 h^{-1}. Taken from [71] 62

Figure 1.19. Comparison of feedstock under catalytic and noncatalytic steam gasification on (a) carbon yield (mol %, atomic) as CO, CO_2, CH_4, and hydrocarbons (C_2-C_4) and (b) hydrogen yield (mol %, atomic) as H_2, CH_4, and hydrocarbons (C_2-C_4) at $H_2O/C \approx 5.6$ and GC1HSV ≈ 320 h^{-1}. Taken from [71] 63

Figure 1.20. Effect of space velocity on (a) carbon yield (mol %, atomic) as CO, CO_2, CH_4, and hydrocarbons (C_2-C_4) and (b) hydrogen yield (mol %, atomic) asH_2, CH_4, and hydrocarbons (C_2-C_4) on the dry feed stock basis at T ≈ 800°C and GHSV ≈ 320 h^{-1} under noncatalytic steam gasification. Taken from [71] 72

Figure 1.21. Steam reforming of bio-oil at different LHSV. (a) Fixed bed, experimental conditions: 1 g catalyst, T = 800 °C, S/C = 9.8, reaction time = 60 min. (b) Fluidized bed, experimental conditions: 100 g catalyst, T = 750 °C, S/C = 18, reaction time = 60 min. Taken from [73] 73

Figure 1.22. Pathway for the steam reforming of AcOH involving bi-functional catalysts of Pt/ZrO_2 . Taken from [22] 77

Figure 1.23. Steam reforming of bio-oil at different rates of steam to carbon. (a) Fixed bed, experimental conditions: 1 g catalyst, T = 800 °C, LHSV = 1.8 h^{-1}, reaction time = 60 min. (b) Fluidized bed, experimental conditions: 100 g catalyst, T = 750 °C, LHSV = 0.8 h^{-1}, reaction time = 60 min. Taken from [73] 82

Figure 2.1. Schematic diagram of the bubbling fluidized bed set-up 104

Figure 2.2. Hydraulic pumping system and nozzle to feed bio-oil into reactor........ 105

Figure 2.3. Yield of total gas production versus versus residence time as moles produced per injected grams of bio-oil; Mass of the sand bed: 1.5kg, sauter mean diameter of the sand: 200μm........ 110

Figure2.4. Yield of syngas production versus residence time as moles produced per injected grams of bio-oil; Mass of the sand bed: 1.5kg, sauter mean diameter of the sand: 200μm 110

Figure 2.5. Yield of molar H_2/CO versus residence time; Mass of the sand bed: 1.5kg, sauter mean diameter of the sand: 200μm 111

Figure 2.6. Yield of hydrogen as moles produced per injected grams of bio-oil; Mass of the sand bed 1.5kg, sauter mean diameter of the sand: (a) 200μm, (b) 80μm........ 112

Figure 2.7. Yield of CO as moles produced per injected grams of bio-oil; Mass of the sand bed 1.5kg, sauter mean diameter of the sand: (a) 200μm, (b) 80μm........ 113

Figure 2.8. Yield of CO2 as moles produced per injected grams of bio-oil; Mass of the sand bed 1.5kg, sauter mean diameter of the sand: (a) 200μm, (b) 80μm........ 113

Figure 2.9. Yield of CH_4 as moles produced per injected grams of bio-oil; Mass of the sand bed 1.5kg, sauter mean diameter of the sand: (a) 200μm, (b) 80μm........ 114

Figure 2.10. Yield of total gas production as grams produced per injected grams of bio-oil; Mass of the sand bed 1.5kg, sauter mean diameter of the sand: (a) 200µm, (b) 80µm 115

Figure 2.11. Yield of liquid production as grams produced per injected grams of bio-oil; Mass of the sand bed 1.5kg, sauter mean diameter of the sand: (a) 200µm, (b) 80µm .. 115

Figure 2.12. Yield of hydrogen as moles produced per injected grams of bio-oil; Mass of the sand bed 3.0kg, sauter mean diameter of the sand: (a) 200µm, (b) 80µm 117

Figure 2.13. Yield of CO as moles produced per injected grams of bio-oil; Mass of the sand bed 3.0kg, sauter mean diameter of the sand: (a) 200µm, (b) 80µm 117

Figure 2.14. Yield of CO_2 as moles produced per injected grams of bio-oil; Mass of the sand bed 3.0kg, sauter mean diameter of the sand: (a) 200µm, (b) 80µm 118

Figure 2.15. Yield of CH_4 as moles produced per injected grams of bio-oil; Mass of the sand bed 3.0kg, sauter mean diameter of the sand: (a) 200µm, (b) 80µm 118

Figure 2.16. Yield of total gas production as grams produced per injected grams of bio-oil; Mass of the sand bed 3.0kg, sauter mean diameter of the sand: (a) 200µm, (b) 80µm 119

Figure 2.17. Effect of sauter mean diameter of the sand on total yield of gasification. Empty symbols: mass of bed 1.5kg, bold symbols: mass of bed 3.0kg.......................... 120

Figure 2.18. Yield of syngas production as moles produced per injected grams of bio-oil; solid lines: mass of bed 1.5kg, dashed lines: mass of bed 3.0kg; sauter mean diameter of the sand: 200µm 121

Figure 2.19. Yield of molar H2/CO ratio; solid lines mass of bed: 1.5kg, dashed lines mass of bed: 3.0kg; sauter mean diameter of the sand: 200µm 122

Figure 3.1. Diagram of the jiggle reactor: 1. on/off feed valves 2. Inlet of carrier gas 3. Thermocouple 4. Inlet of feed and carrier gas 5. Ceramic crucible with insulation 6. Insulation disk 7. Insulation disk 8. Linear pneumatic actuator 9. Outlet gas valve 10.

Stainless steel support rods 11. Copper coil 12. Copper disk 13. Aluminum disk mounted on the actuator 14. Stainless steel scalloped disk 134

Figure 3.2. Reaction chamber of the jiggle bed reactor: a) ceramic crucible b) heating element assembly (dimensions are in mm) 135

Figure 3.3. Schematic of the linear pneumatic actuator... 136

Figure 3.4. Sequences of mixing of catalyst particles in the jiggle bed reactor: (a) bed expansion during downward actuator retraction (b) bed contraction during upward actuator extension 138

Figure 3.5. Visual set-up to investigate mixing of sand particles in a transparent crucible 139

Figure 3.6. Digitized gray pictures for a bed of the sand particles with 10 g mass and size distribution of 149-212 µm. Actuator frequency 4Hz: a) Retracted bed b) Expanded bed c) Variation of the horizontally averaged gray value along the crucible length............ 142

Figure 3.7. Variation of $\mathbf{CVspace}$ versus time; sand particles 10 g, size distribution of 149-212 µm, air pressure of 345 kPa 143

Figure 3.8. Power spectrum of the bed motion; sand particles 10 g, size distribution of 149-212 µm; amplitude 6.4 cm 143

Figure 3.9. Variation of frequency of the pneumatic actuator versus air pressure. 144

Figure 3.10. Frequency of bed of the sand particles versus frequency of the actuator; (a) effect of mass; size 149-212 µm (b) effect of size distribution; mass 10g 145

Figure 3.11. Effect of amplitude on variation of $\mathbf{CVspace, min}$ versus air pressure; sand particles: mass 10 g and size 149-212 µm 146

Figure 3.12. Comparison of power of dominant frequencies versus air pressure and amplitude; sand particles: mass 10 g and size 149-212 µm... 147

Figure 3.13. Effect of mass of the particles on dominant frequency power of the particle mixing; sand particles with size of (a) 212-355 µm, (b) 149-212 µm and (c) 75-149 µm 148

Figure 3.14. Effect of size distribution of the sand particles on dominant frequency power of the particle mixing; mass of sand particles: (a) 5 g, (b) 10 g and (c) 20 g 149

Figure 3.15. Effect of power outlet of the power supply on rate of heating of the sand particles; mass 10 g, size 149-212 µm, air pressure 207kPa, amplitude 6.4cm 153

Figure 3.16. Consumed power inside the reactor versus partial power outlet of the power supply 156

Figure 3.17. Effect of the actuator air pressure on the rate of temperature rise inside the reactor during the heating step; power outlet 20%, mass of sand particles 10 g, amplitude 6.4 cm 157

Figure 3.18. Effect of air pressure of the actuator on rate of temperature drop inside the reactor during the cooling step; power outlet 20%, mass of sand particles 10 g, amplitude 6.4 cm 158

Figure 3.19. Temperature recovery for endothermic reactions taking place in the JBR 159

Figure 3.A1. Schematic of the flat air cylinder with the dual rods presenting position of the reed switches (RS) and the brake length (Δx) at the end of extension (left) and retraction (right) modes 165

Figure 4.1. Design and dimensions of the ceramic crucible 171

Figure 4.2. Configuration of the ceramic crucible and clamp on the jiggle bed reactor 172

Figure 4.3. Position of the in-situ tube and internal heating wires in the jiggle bed reactor 173

Figure 4.4. Schematic of the JBR experimental setup for the catalytic gasification tests 175

Figure 4.5. XRD graphs of the fresh (a) and reduced (b) catalyst. Square symbols (■) present phases of NiO and diamond symbols (♦)present phases of Ni^0 179

Figure 4.6. Non-catalytic steam reforming of acetic acid. Effect of S/C ratio versus residence time; T= 700 °C 184

Figure 4.7. Non-catalytic steam reforming of acetic acid. Effect of temperature. Residence time= 30s. Left, middle and right hand side bars present data of S/C ratios of 0, 3 and 6, respectively 186

Figure 4.8. Catalytic steam reforming of acetic acid. Effect of S/C ratio versus residence time; T= 700 °C, catalyst mass= 0.5 g. In case of hydrogen yield: empty symbols present catalytic yields and bold symbols present the non catalytic yields................................ 188

Figure 4.9. Catalytic steam reforming of acetic acid. Effect of catalyst mass on gas yields. Residence time= 10s, Temperature= 700°C 191

Figure 5.1. Schematic of the JBR experimental setup for the catalytic gasification tests 205

Figure 5.2. XRD patterns of the catalysts X and Y: (a) fresh catalyst (b) reduced catalyst; square symbols (■) presents phases of NiO and diamond symbols (♦) presents phases of Ni^0 211

Figure 5.3. Yield of product gases from thermal cracking of the DMB and the BWB versus temperature. Residence time= 30 s.. 216

Figure 5.4. Yield of molar H_2/CO and CO/CO_2 ratios from thermal cracking of the DMB and the BWB; Residence time= 30 s 216

Figure 5.5. Effect of the catalyst type and mass on yield of product gases from catalytic gasification of the DMB and the BWB, temperature= 800°C, residence time= 30 s. Full and dashed lines represent trend of yields with the catalysts X and Y, respectively...... 219

Figure 5.6. Effect of the catalyst type and mass on carbon conversion from catalytic gasification of the DMB and the BWB, temperature= 800°C, residence time= 30 s. Full and dashed lines represent trend of yields with the catalysts X and Y, respectively...... 219

Figure 5.7. Effect of residence time on yield of product gases from catalytic gasification of the DMB and the BWB, temperature= 800°C, mass of the catalyst X= 1 g 220

Figure 5.8. Yield of product gases from catalytic cracking of the DMB and the BWB versus temperature. Residence time= 30s; left hand side bars: mass of the catalyst X= 0.5 g; right hand side bars: mass of the catalyst X= 1 g. Yield of hydrogen is shown with continuous and dashed lines for 0.5 g and 1 g catalyst masses, respectively 223

Figure 5.9. Yield of molar H_2/CO and CO/CO_2 ratios from catalytic cracking of the DMB and the BWB; residence time= 30 s. Mass of the catalyst X= 0.5g (continuous lines) and 1g (dashed lines) 223

Figure 6.1. Schematic of the JBR experimental setup for the catalytic gasification tests 241

Figure 6.2. XRD patterns of the (a) original Olivine (b) Olivine calcined at 850°C (c) Olivine calcined at 1000°C and (d) Olivine reduced with hydrogen. • presents phases of $(Mg,Fe)_2SiO_4$, + presents phase of $MgSiO_3$, Δ presents phase of Mg,Si_2O_5, ♦presents phase of α-Fe_2O_3 and ■ presents phases of metallic iron (Fe^0)..................................... 245

Figure 6.3. Measured mole fraction of hydrogen compared to its predicted equilibrium mole fraction, on a dry basis. Bed materials: olivine and sand. Temperature: 800°C.... 250

Figure 6.4. Measured mole fraction of CO compared to its predicted equilibrium mole fraction, on a dry basis.. Bed materials: olivine and sand. Temperature: 800°C............ 251

Figure 6.5. Measured mole fraction of CO_2 compared to its predicted equilibrium mole fraction, on a dry basis. Bed materials: olivine and sand. Temperature: 800°C............ 252

Figure 6.6. Measured mole fraction of CH_4 compared to its predicted equilibrium mole fraction, on a dry basis. Bed materials: olivine and sand. Temperature: 800°C............ 253

Figure 6.7. Measured mole fraction of (C_2H_6+C_2H_4) compared to its predicted equilibrium mole fraction, on a dry basis. Bed materials: olivine and sand. Temperature: 800°C 254

Figure 6.8. Experimental molar H_2/CO ratio versus predicted molar H_2/CO ratio at equilibrium. Bed materials: olivine and sand. Temperature: 800 °C............................ 255

Figure 6.9. Yield of hydrogen versus residence time. Bed materials: olivine and sand, Temperature 800°C... 257

Figure 6.10. Bio-oil carbon conversion versus residence time. Bed materials: olivine and sand. Temperature 800°C 257

LIST OF ABBREVIATIONS

AA	Acetic Acid
ADP	Adenosine dephosphate
BDO	Biomass Drived Oil
BWB	Birchwood Bio-oil
CH_mO_n	General formula of bio-oil with 1 atom C, m atom H and n atom O
CV	Coefficient of Variation
DMB	Dynamotive Bio-oil
ESP	Electrostatic Precipitator
FB	Fluidized Bed
GC	Gas Chromatography
GHSV	Gas Hourly Space Velocity
HHV	High Heat Value
ICFAR	Institute for Chemical and Fuels for Alternative Resources
I.D.	Internal Diameter
JBR	Jiggle Bed Reactor
LHSV	Liquid Hourly Space Velocity
NPOX	Non-catalytic Partial Oxidation
O/C	Molar Oxygen to Carbon Ratio
O.D.	External Diameter
PLC	Programmed Logic Controller
RS	Reed Switch
RSD	Reed Switch Distance
S/C	Molar Steam to Carbon Ratio
SCT-RT	Short Contact Time Riser Test
TCD	Thermal Conductivity Detector
TPR	Temperature Programmed Reduction
TPO	Temperature Programmed Oxidation
u	Superficial Gas Velocity in the Gas /Solid Fluidized Reactors
u_{mf}	Minimum Fluidization Velocity
XRD	X-ray Diffraction
XRF	X-ray Fluorescence

OVERVIEW

Fossil fuels including petroleum oil, natural gas and coal are the most common fuels. However, such fuels are not renewable and many countries have to resort to imports to meet their energy needs. Another challenge with these fuels is that they are sources of large amount of pollutants such as nitrogen oxides, sulfur dioxide, volatile organic compounds and etc that create human health problems and CO_2 which caused global warming. Many governments have chosen to promote new technologies to substitute renewable fuels for fossil fuels to reduce greenhouse gas emissions, adhere to environmental regulations, provide some security of supply, and reduce imports.

Bio-fuels are renewable and clean and can be used as alternatives to fossil fuels or can be used in combination with them. Another advantage of using bio-fuels would be in regards to economical interests in the agricultural sector. In addition, bio-fuels can be upgraded to value added chemicals for a variety of applications. Biomass, agricultural and forestry residue, is a main source of bio-fuels production: it is a renewable resource and its conversion to energy releases no net CO_2 to the environment. In fact, it can be carbon negative: Biomass converted to bio-oils produces carbon-rich bio-char as a co-product; if bio-char was dispersed into the ground, it would represent a stable form of carbon sequestration. In the case of an increase in the price of fossil fuels or depletion of their resources, biomass can be counted as a safe and reliable resource of energy.

Bio-oil is the liquid product of the fast pyrolysis of biomass, which is a renewable source of energy and fuels. Bio-oil can be either used directly as a fuel or it can be upgraded to some chemicals for different applications. Since the late 1990s, this liquid has been considered as a source of syngas (H_2+CO) and, in particular, for hydrogen production. Syngas can be produced also through direct gasification of biomass. However, biomass is produced over wide areas; it is seasonal and not available at a constant rate, and its transportation is expensive because it has a low density, it is bulky and polluting. Conversion of biomass to syngas is, therefore, problematic and impractical as both biomass and syngas are not easily transportable. On the other hand, conversion into a high density easily transportable material (bio-oil) at the site of production of the biomass and at the time of its availability would make more sense. The bio-oil would then be gasified at a centralized processing plant where it will be utilized as a building block for production of high value chemicals.

To expand the knowledge and commercial opportunities in this field, this thesis focuses on investigation of syngas production from bio-oil through thermal and catalytic reactions in the novel fluidized bed reactors.

This thesis is divided into seven chapters describing the research as follows:

Chapter 1: *Production of Syngas from Bio-oil and its Model Compounds- A Literature Review. D*ue to the special chemical and physical properties of bio-oil and the dependence of its composition on the original biomass, gasification results would be different from a bio-oil to another under similar operating conditions, so it is important to critically analyze and integrate findings in literature to obtain a comprehensive understanding of the recent developments in this field. Chapter 1 is a literature review about the importance of bio-oil for syngas production, illustrating the chemical and physical properties of bio-oils, the kinetics of chemical gasification reactions of bio-oil and its model compounds, and finally the effect of reactor design, operating conditions and catalyst composition on the syngas yield.

Chapter 2: *Effects of Residence Time and Temperature on the Thermal Cracking of Bio-oil for Syngas Production*. A fluidized bed reactor operating in the bubbling regime has been used for the conversion of bio-oil to syngas. The reactor consists of a 3 inch I.D. bed, with an expanded freeboard, whose volume can be adjusted to vary the gas residence time. This reactor has been used to carry out either thermal or catalytic cracking/reforming of bio-oil. A gas-atomized injector has been especially developed to feed bio-oil, which may be viscous and contaminated with small ash and char particles, allowing it to remain cool until coming in contact with the fluidized particles inside the bed. This chapter presents the product yields and compositions obtained by thermally cracking the bio-oil at various temperatures and gas residence times. The bed temperature was varied from 500 ºC to 700 ºC and the vapor residence time ranged from 7.8 to 27.6 seconds. Effect of particle size and mass of bed was also investigated. The conversion of bio-oil to gas increased with increasing temperature and residence time.

Chapter 3: *A Novel Fluidized and Induction Heated Micro Reactor for Catalyst Testing.* The jiggle bed reactor is a state-of-the-art batch fluidized micro reactor designed and developed to test catalysts for endothermic reactions. The solid particles in the micro reactor are mechanically fluidized by agitating the reactor using a linear pneumatic actuator. An external induction field heats up vertical metal wires installed inside the reactor bed to generate heat rapidly and uniformly within the bed of solid particles, while eliminating hot spots and large temperature gradients. Image and signal processing techniques were utilized to investigate how the fluidization dynamics of the solid particles are affected by the amplitude and frequency of the vibrations, the size distribution and the mass of the particles. The results show that the micro reactor is very flexible: operating conditions can be optimized to successfully fluidize any type of catalyst.

The preliminary results of the heat transfer studies indicate that induction heating allows for responsive and accurate temperature control of the catalyst bed while eliminating hot spots and greatly reducing temperature gradients.

Chapter 4: *Non-catalytic and Catalytic Steam Reforming of Acetic Acid in the Jiggle Bed Reactor.* In order to evaluate the performance of the jiggle bed reactor in producing reliable and reproducible data and its functionality in relation to changes in operating parameters, non-catalytic and catalytic steam reforming of acetic acid (model compound) was investigated. Silica sand was used as the bed material for non-catalytic tests and a commercial steam reforming catalyst was used for the catalytic tests. Testin parameters included temperatures between 650°C and 750°C, residence times between 10s and 90s and molar steam to carbon ratio (S/C) equal to 0, 3 and 6. Atmospheric pressure was used in all experiments.

Analysis of the product gas yield shows that the jiggle bed reactor allows for a series of precise experiments over a short period of time in a small scale setup. In addition, the effects of operating parameters, such as temperature, residence time, S/C ratio as well as type and mass of the bed particles on product gas yields, were clearly observed and reliable consistency between trends from the JBR data and the literature was confirmed.

Non-catalytic experiments achieved a high carbon conversion of acetic acid, but the hydrogen yield was very low. Complete carbon conversion and high hydrogen yield were achieved in the catalytic experiments. Catalytic steam reforming data reveal that maximizing the hydrogen yield and the H_2/CO ratio requires the appropriate molar S/C ratio and catalyst mass.

Chapter 5: *Thermal and Catalytic Gasification of Bio-oils in the Jiggle Bed Reactor for Syngas Production.* Thermal and catalytic gasification of two bio-oils were then carried out in the jiggle bed reactor to investigate carbon conversion of the bio-oils and the syngas yield as functions of catalyst type and mass, residence time and temperature. Two commercial nickel based steam reforming catalysts were used. Temperature ranged from 700 °C to 800 °C and residence times varied between 10 and 30s.

In thermal gasification, both carbon conversion and hydrogen yield increase with increasing temperature, but both remained relatively low. Production of CO was relatively quite high, so that the molar H_2/CO ratios were below 2.

The catalyst X gave better results in terms of carbon conversion of bio-oils and hydrogen yield at 800°C. Catalytic experiments showed that increasing the temperature decreases the molar H_2/CO ratio because of a lack of steam, while it increases the carbon conversion. Therefore, either steam should be added to the gasification reactor or a secondary water gas shift reactor should be used downstream of the gasification reactor to maximize the H_2/CO ratio.

Chapter 6: *Development of a Thermodynamic Model to Predict the Equilibrium Concentration of Gases from Bio-oil Gasification with Sand or Olivine Catalyst.* In order to investigate the catalytic activity for bio-oil gasification to syngas, pretreated olivine (calcined with air at 850°C and 1000°C and reduced with hydrogen at 800°C) as well as silica sand were tested in the jiggle bed reactor. Temperature was 800°C and residence time ranged from 10 to 240s. A thermodynamic model was developed based on the equilibrium constants of the independent reactions between the final gasification products to predict the product mole fraction at various operating conditions. This model can be applied for any feedstock that contains carbon, hydrogen and oxygen, regardless of its molecular composition.

Results show that olivine is an active catalyst for bio-oil gasification when it is reduced with hydrogen, providing complete bio-oil conversion as well as maximum syngas yield. However, calcined olivine is inappropriate, as it releases oxygen that reacts with the combustible products. Thermodynamic analysis showed that mole fractions of the product gases would reach predicted equilibrium values when the reduced olivine was the material of the catalytic bed; on the other hand, when calcined olivines were the catalytic bed materials, product gas would tend to reach a new equilibrium state.

Chapter 7: *Conclusions and Recommendations.* Main conclusions from the experimental and theoretical work of the thesis are listed in this chapter. In addition, there are some recommendations in this chapter as guidelines for the future work in related and similar projects.

CHAPTER 1:

Production of Syngas from Bio-oil and its Model Compounds - A Literature Review

1.1. Introduction

An increase in energy demand is seen in the recent decades in different sectors of society. Between 1990 and 2008, total energy consumption in the transportation sector increased from 10,051 to 12,510 peta joules in Canada and from 89,312 to 104,875 peta joules in the United States [1]. Fossil fuels have been the main source of energy supply. For example, fossil fuel consumption in Canada and the United States were respectively 75.1% and 84.4% of the total fuel used in 2010 [2]. There is also a big dependence on this energy source. For example, Consumption of petroleum was about 19 million barrel per day in 2010 in the United States while 49% of this consumption was supplied from imports [3]. Another challenge with these fuels is that they are sources of large amount of pollutants that create human health problems and global warming. Similar patterns of fossil fuel consumption can be seen in many other countries. Many governments have chosen to promote new technologies to substitute fossil fuels with renewable fuels to reduce greenhouse gas emissions, adhere to environmental regulations, provide some security of supply, and reduce imports.

Bio-fuel is a type of fuel whose energy content is as a result of CO_2 conversion to organic compounds by living organisms. Bio-fuels are renewable and clean and can be used as alternatives to fossil fuels or can be used in combination with them. Another advantage of using bio-fuels relates to the economical interests of the agricultural sector. In addition, bio-fuels can be upgraded to value added chemicals for a variety of applications. Biomass is a main source of bio-fuels production which can be animal waste or plant residue such as forestry and agricultural residues. Throughout this thesis, biomass is assumed to be a plant residue. Biomass is a renewable resource and its conversion to energy releases no net CO_2 to the environment and in the case of an increase in the price of fossil fuels or depletion of their resources, biomass can be counted as a safe and reliable resource of energy.

A common method for the conversion of biomass to a gas, a liquid bio-oil or a solid bio-char is pyrolysis; *i.e.*, thermal cracking in the absence of oxygen. Fast pyrolysis, which is conducted under a high heat transfer rate and short reaction time gives better products than slow pyrolysis which can take several hours and is appropriate for bio-char production[4, 5]. Bio-char is a product that may have value and recent research is suggesting a varity of uses of bio-char (or, better, bio-carbon), ranging from soil amendment and fertilizer (bio-char) to energy (bio-coal and bio-coke) to advanced materials (catalysts, adsorbents, strengthening agents for composites, etc.). The gaseous product stream contains hydrogen, carbon monoxide, carbon dioxide, and light hydrocarbons such as methane, ethane and ethylene. These gases can be either recycled and combusted to supply required energy for the pyrolysis or collected and transported to another process that can use them. Bio-oil has great potential to be upgraded to supply either renewable energy resources or further chemicals. Similar to pyrolysis or gasification of biomass, the gasification of bio-oil also leads to the production of syngas (H_2+CO), CO_2, CH_4 and to some extent C_2H_4 and C_2H_6. Biomass is produced over wide areas; it is seasonal and not available at a constant rate, and its transportation is expensive because it has a low density, it is bulky and polluting. Conversion of biomass to syngas is, therefore, problematic and impractical as both biomass and syngas are not easily transportable. On the other hand, conversion into a high density easily transportable material (bio-oil) at the site of production of the biomass and at the time of its availability would make more sense. The bio-oil would then be gasified at a centralized processing plant where it will be utilized as a building block for production of high value chemicals.

Syngas, which is also called producer gas, town gas, and blue water gas, can be produced from different resources such as natural gas, naphtha, residual oil, petroleum coke, coal, and biomass. The H_2/CO ratio depends on the feedstock and the applied technology [6]. Syngas is a very valuable chemical mixture representing a key building block in petrochemical industries, and many chemicals and fuels can be produced from this mixture. Figure 1.1 illustrates different processes through which syngas can be converted into new products.

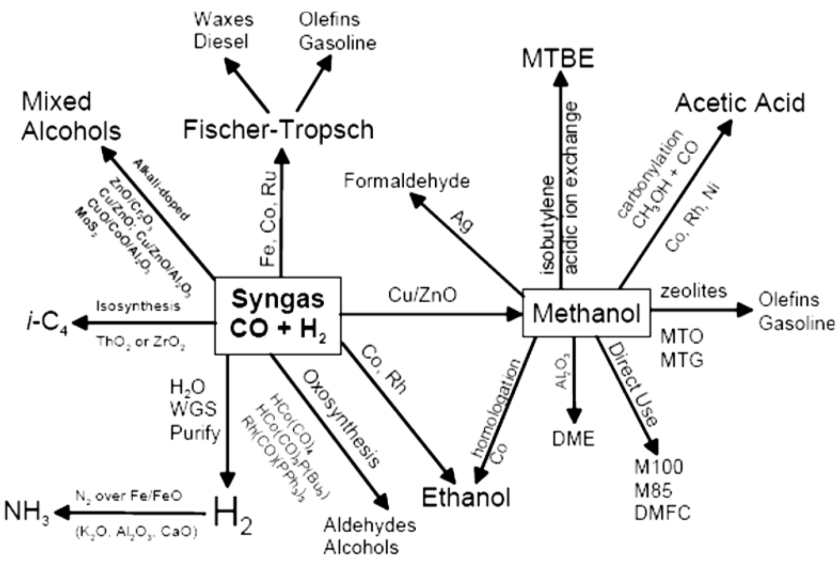
Waxes
Diesel
Olefins
Gasoline
MTBE
Mixed Alcohols
Fischer-Tropsch
Acetic Acid
Alkali-doped
ZnO/Cr$_2$O$_3$
Cu/ZnO; Cu/ZnO/Al$_2$O$_3$
CuO/CoO/Al$_2$O$_3$
MoS$_2$
Fe, Co, Ru
Formaldehyde
Ag
isobutylene
acidic ion exchange
carbonylation
CH$_3$OH + CO
Co, Rh, Ni
Syngas
CO + H$_2$
Cu/ZnO
Methanol
zeolites
Olefins
Gasoline
MTO
MTG
i-C$_4$
Isosynthesis
ThO$_2$ or ZrO$_2$
H$_2$O
WGS
Purify
HCo(CO)$_4$
HCo(CO)$_3$P(Bu$_3$)
Rh(CO)(PPh$_3$)$_3$
Oxosynthesis
Co, Rh
homologation
Co
Al$_2$O$_3$
DME
Direct Use
M100
M85
DMFC
NH$_3$
N$_2$ over Fe/FeO
(K$_2$O, Al$_2$O$_3$, CaO)
H$_2$
Aldehydes
Alcohols
Ethanol

Figure 1.1. **Diagram of syngas conversion processes taken from [7]**

Hydrogen has many applications in industry; it is also considered as a clean and environmentally reliable source of energy in combination with fuel cells. Hydrogen, however, is mainly produced by steam reforming of natural gas according to the block flow diagram in Figure 1.2. Methane reacts with steam to produce hydrogen and carbon monoxide followed by the water-gas shift reaction:

$$CH_4 + H_2O \leftrightarrow 3H_2 + CO \qquad \Delta H = 49.3\,kcal/mol \tag{1.1}$$

$$CO + H_2O \leftrightarrow H_2 + CO_2 \qquad \Delta H = -9.8\,kcal/mol \tag{1.2}$$

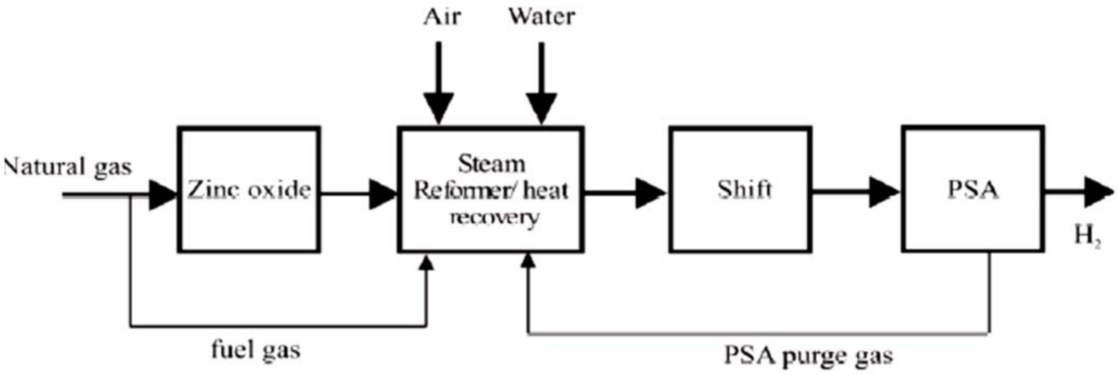
Air
Water
Natural gas
Zinc oxide
Steam
Reformer/ heat
recovery
Shift
PSA
H$_2$
fuel gas
PSA purge gas

Figure 1.2. **Block flow diagram of Hydrogen via Steam Methane Reforming taken from [6]**

Many researchers across the world are working on the development of reliable and economic processes to produce hydrogen from biomass and its fractions. Demirbas reviewed current technologies related to renewable biomass derived energy resources such as bioethanol, biodiesel, biomethanol and bio-oil [8, 9]. Balat reviewed different thermochemical routes reported in the literature from which hydrogen can be produced from biomass, such as pyrolysis, gasification and steam gasification of biomass as well as steam gasification of bio-oil. Yield of hydrogen versus cost of the process is briefly compared for each thermochemical process [10]. Digman *et al.* reviewed available pyrolysis and gasification technologies to convert biomass to energy value added products [11].

Production of hydrogen from biomass is not yet industrialized on a large scale, but according to the projections shown in Figure 1.3, hydrogen and biofuels can potentially play a significant role in fuel consumption in the transportation sector in the future. The hydrogen content of biomass is less than that of natural gas, so co-reforming of bio-oil and natural gas may be an economic option at the moment.

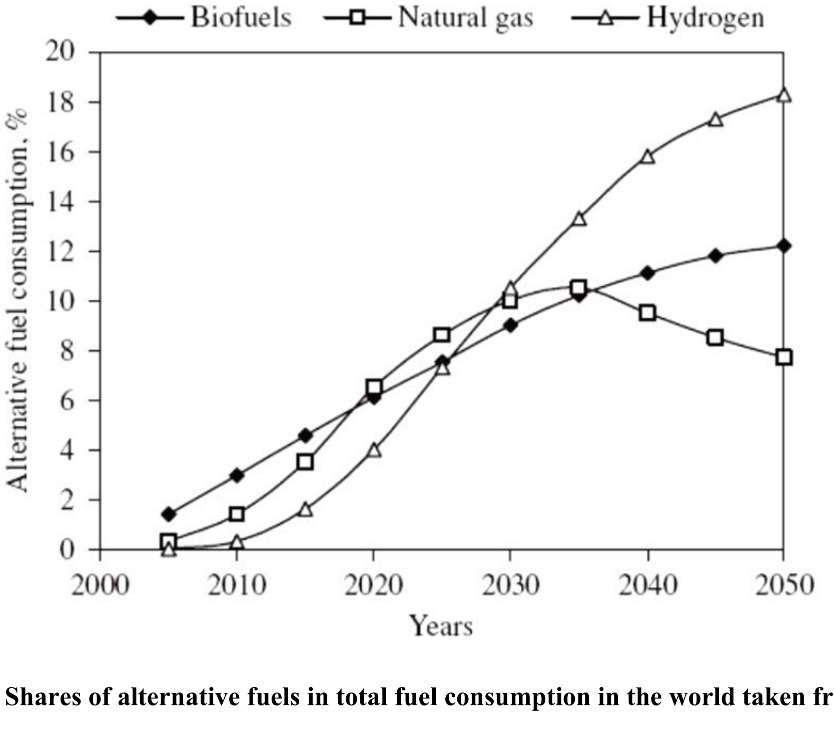

Figure 1.3. **Shares of alternative fuels in total fuel consumption in the world taken from [8]**

Recent literature about the direct production of syngas from biomass has been reviewed by several authors [12-18]. Another route of syngas production from biomass is the indirect process through which biomass is first converted to bio-oil and then the bio-oil is gasified to produce syngas with or without steam. However, there is not such a comprehensive review about these technologies available in literature to help future researchers perceive an overall image of the advances, challenges and future potentials to do with syngas production through the bio-oil gasification. This report tries to address this need.

Due to limitations caused by the lack of consistency, physical and chemical complexities of bio-oils produced from different feedstocks, production of syngas from representative model compounds of bio-oils haves been investigated more than than from actual bio-oils. However, Results of such research help narrowing on the optimal operating conditions, type of catalyst and design of the reactor for bio-oil gasification. There are many publications in literature dealing with steam reforming of bio-oil model compounds, but due to the fact that they have similar subjects and similar operating conditions, only some of them are reviewed in detail in this chapter. On the other hand, a limited number of reports are available in literature treating the subject of gasification/steam reforming of the whole bio-oil.

There are more severe challenges with gasification of whole bio-oil because it contains heavy molecules that are difficult to crack. For example, due to the physical and chemical properties of the lignin fraction of the bio-oil, cracking and gasification would require a higher temperature and more steam than what can be generated based on the water content of the bio-oil. Also, the composition of each bio-oil depends on the original biomass and operating conditions used for the pyrolysis process. In addition, bio-oil is a mixture of different oxygenates, organic compounds containing oxygen, with individual chemical and physical properties. Therefore, optimum operating conditions for a bio-oil can be different for another type of bio-oil. Furthermore, each bio-oil can have different interactions with a catalyst.

1.2. Bio-oil gasification reaction and kinetics

1.2.1. Biomass

Although hydrogen is a clean source of energy, for instance, during its combustion, it is currently mostly produced from sources such as natural gas, naphtha, and coal, with co-production of carbon dioxide. However, biomass is a renewable and alternative source for hydrogen that results in no net greenhouse gas emissions.

Biomass is a general term which is used to define any kind of solid renewable organic residue, like animal waste or plant residue such as forestry and agricultural residues, when its major elemental composition includes carbon, hydrogen and oxygen. Analysis of the molecular structure of the plant biomass shows that it consists of water, cellulose, hemicellulose and lignin [19].

1.2.2. Bio-oil

Bio-oil is the valuable liquid product obtained from biomass fast pyrolysis. It may be either combusted to generate carbon-neutral electricity, upgraded to value added chemicals, or converted to syngas, from which high value chemicals or clean advanced fuels can be produced.

Constituents of bio-oils are different in their chemical composition depending on the original biomass, pyrolysis conditions, and whether or not a catalyst was used to produce the bio-oil. However, all bio-oils usually have a series of characteristic and similar constituents. Bio-oils contain organic/ligning phase, which insoluble in water, and aqueous phase; depending on the original biomass and the pyrolysis process, these phase could be either mixed homogenatly or separate and distinguishable. Table 1.1 depicts four samples of bio-oils with the composition of their constituents.

Table 1.1. **Composition of different bio-oils (Yields in wt % of dry biomass). Adapted from [20]**

	Fluidized bed (University of Waterloo)			Vortex (NREL)
	Poplar (504°C)	Maple (508°C)	Spruce (500°C)	Oak (~500°C)
Acetic acid	5.4	5.8	3.9	5.0
Formic acid	3.1	6.4	7.2	3.3
Hydroxyacetaldehyde	10.0	7.6	7.7	4.3
Glyoxal	2.2	1.8	2.5	3.0
Methylglyoxal	-	0.65	-	-
Formaldehyde	-	1.2	-	2.2
Acetol	1.4	1.2	1.2	1.8
Ethylene glycol	1.1	0.6	0.9	-
Levoglucosan	3.0	2.8	4.0	3.8
1.6-anhydroglucofuranoze	2.4	-	-	-
Fructose	1.3	1.5	2.3	-
Xylose	-	-	-	0.9
Glucose	0.4	0.6	1.0	-
Cellobiosan	1.3	1.6	2.5	-
Oligosaccharides	0.7	-	-	-
Pyrolytic lignin	16.2	20.9	20.6	24.9
Unidentified	11.9	17.1	12.9	5.8
Oil	65.8	67.9	66.5	55.3
Water	12.2	9.8	11.6	10.4
Char	7.7	13.7	12.2	12.4
Gas	10.8	9.8	7.8	12.2
Mass closure	96.5	101.2	97.7	90.3

According to Basagiannis and Verykios [21] and Takanabe *et al.* [22] major components of bio-oils are oxygenates belonging to the following groups: acids, aldehydes, alcohols, ketones and substituted furans derived from cellulose and hemi-cellulose, and phenolic and cyclic oxygenates derived from lignin. About 300 different molecules have been identified in an aqueous fraction of bio-oil, which contains components with low molecular weight like acids, aldehydes and alcohols. Lignin-derived products contribute to 25– 30% of the whole bio-oil. A typical composition of wood oil includes water (20–30%), lignin fragments (15–30%), aldehydes (10–20%), carboxylic acids, carbohydrates (5–10%), and phenols (2– 5%) [23].

Direct usage of bio-oil as a fuel has been reported to be difficult because of the physico-chemical properties of bio-oils, especially, their high thermal instability [23]. Bio-oil is stable at room temperature, but it polymerizes after being heated up even to moderate temperatures (around 80°C). Bio-oil is decomposed to a new structure of molecules at higher temperatures. Even at low temperatures, some of the molecules of bio-oil may not be stable and composition of bio-oil can be influenced by aging phenomena [21, 22]. Chaala *et al.* [24] worked on the identification of colloidal properties of a bio-oil produced from softwood bark. They identified a multiphase complex colloidal system composed of solid particles, three-dimensional structures, and droplets. It was realized that the main colloidal properties of bio-oil are due to an upper layer of bio-oil containing dispersed droplets which includes waxy materials, like fatty and resin acids, as well as water-insoluble compounds. Bio-oil has high viscosity and non-Newtonian behavior at low temperatures, because of the presence of waxy materials. When these materials reach their melting point, bio-oil no longer has high viscosity and non-Newtonian properties.

The dependence of bio-oil physical and chemical properties on temperature is a challenge for storage and transportation. In addition, challenges arise during the injection of bio-oil into themal processing units, such as gasifiers, because the temperature of injection nozzles is typically high enough to influence the bio-oil stability and reactivity even before it is sprayed into the reactor. Consequently, bio-oil tends to solidify and plug the nozzles. This issue has been tackled by using a specially designed gas atomized nozzle [25].

Czernik *et al.* [26] developed a conceptual process to produce syngas from the aqueous fraction of bio-oil; i.e. during the fast pyrolysis of biomass, bio-char, bio-oil and product gases are being produced. By adding water to bio-oil it can be separated to two phases: a lignin fraction can be used for phenol substitution and an aqueous fraction which mainly contains hydrocarbons can be used for hydrogen production. Figure 1.4 illustrates the process of syngas production from aqueous fraction of bio-oil.

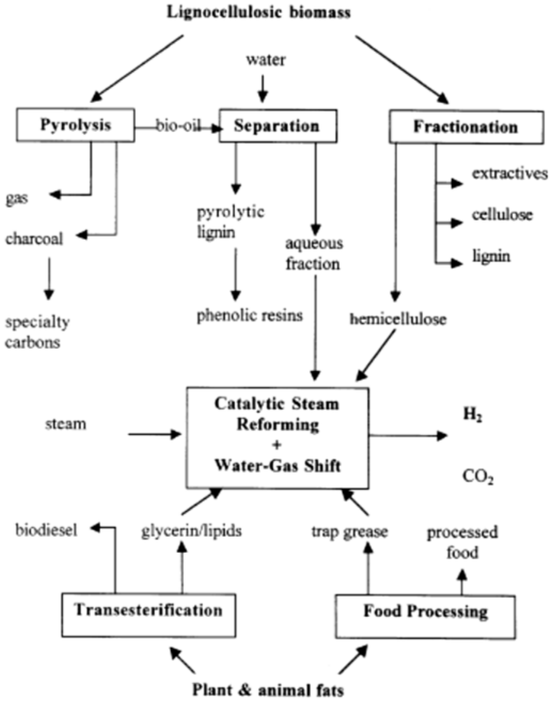
Lignocellulosic biomass
water
Pyrolysis
bio-oil
Separation
Fractionation
gas
charcoal
specialty carbons
pyrolytic lignin
phenolic resins
aqueous fraction
extractives
cellulose
lignin
hemicellulose
steam
Catalytic Steam Reforming + Water-Gas Shift
H₂
CO₂
biodiesel
glycerin/lipids
trap grease
processed food
Transesterification
Food Processing
Plant & animal fats

Figure 1.4. **Syngas production from an aqueous fraction of bio-oil taken from [26]**

1.2.3. Steam reforming reactions of bio-oil and its model compounds:

Although bio-oils contain 20 to 30 wt% water, almost all researchers used additional steam to increase bio-oil conversion and yield of hydrogen production. Due to the fact that carbon, hydrogen and oxygen are abundant elements of bio-oil, a general formula like $C_nH_mO_k$ is usually considered for a bio-oil.

The steam reforming reaction of any oxygenated organic compound proceeds according to the reaction 1.3 [26]:

$$C_nH_mO_k + (n-k)H_2O \rightarrow nCO + \left[\left(n + \frac{m}{2} - k\right)\right]H_2 \tag{1.3}$$

In other words, 1+m/2n-k/n moles of hydrogen are obtained from one mole of carbon.

Another main reaction during steam reforming reactions is a water gas shift reaction, in which carbon monoxide reacts with steam and produces carbon dioxide and hydrogen:

$$nCO + nH_2O \leftrightarrow nCO_2 + nH_2 \tag{1.4}$$

Steam reforming reactions (like reaction 1.3) are very endothermic, but the water gas shift reaction is an exothermic reaction which releases heat inside the reactor. For example, consumed and released heat during steam reforming of methane can be evaluated according to the reactions 1.5 and 1.6:

$$CH_4 + H_2O \leftrightarrow CO + 3H_2 \quad \Delta H = +251\ kJ/mol \tag{1.5}$$

$$CO + H_2O \leftrightarrow CO_2 + H_2 \quad \Delta H = -42\,kJ/mol \tag{1.6}$$

Therefore, an optimum temperature should be found for the reaction at which a required ratio of H_2/CO can be obtained.

According to reaction 1.7, as soon as bio-oil is sprayed into the reactor, bio-oil is partially decomposed to other forms of oxygenated molecules ($C_xH_yO_z$), some permanent gases and coke [26]. Besides, since CO, CO_2 and coke are available inside the reactor, the Boudouard reaction (reaction 1.8) is another important reaction which can affect the CO/CO_2 ratio in the final product gases.

$$C_nH_mO_K \leftrightarrow C_xH_yO_z + gases\left(H_2, H_2O, C, CO_2, CH_4, \ldots\right) + coke \tag{1.7}$$

$$2CO \leftrightarrow CO_2 + C \tag{1.8}$$

Acetic acid, one of the typical bio-oil model compounds, has been used by many investigators for syngas production. Basagiannis *et al.* [21] described all possible reactions during acetic acid steam reforming (reactions 1.9-1.17). These reactions can take place during steam reforming of any other oxygenated feedstock, but with different stoichiometric multipliers.

Complete steam reforming:

$$CH_3COOH + 2H_2O \rightarrow 2CO_2 + 4H_2 \tag{1.9}$$

Steam reforming:

$$CH_4 + H_2O \leftrightarrow CO + 3H_2 \tag{1.10}$$

Thermal decomposition:

$$CH3COOH \rightarrow 2CO + 2H_2 \quad (1.11)$$

$$CH_3COOH \rightarrow CH_4 + CO_2 \quad (1.12)$$

$$CH_3COOH \rightarrow C_2H_4, C_2H_6, C_3H_4, coke,... \quad (1.13)$$

Ketonization:

$$CH_3COOH \rightarrow (CH_3)_2CO + H_2O + CO_2 \quad (1.14)$$

Water–gas shift:

$$CO + H_2O \leftrightarrow CO_2 + H_2 \quad (1.15)$$

Methanation:

$$CO + 3H_2 \leftrightarrow CH_4 + H_2O \quad (1.16)$$

$$CO_2 + 4H_2 \leftrightarrow CH_4 + 2H_2O \quad (1.17)$$

Takanabe *et al.* [22] reported that methane formation by the hydrogenation of carbon monoxide (forward direction of reaction 1.16) is kinetically much slower than the methane consumption (backward direction of reaction 1.16). Thus, observed methane during the catalytic steam reforming of acetic acid is an initial product that resulted from acetic acid decomposition, not from secondary hydrogenation of carbon monoxide.

Acetone is another model compound which has been used for steam reforming studies [22]:

$$CH_3COCH_3 + 5H_2O \rightarrow 3CO_2 + 8H_2 \quad (1.18)$$

Carbon deposition on the surface of a catalyst is a key issue in bio-oil steam reforming, which should be controlled to enhance total efficiency of the gasification process. Davidian *et al.* [23] proposed a two-step strategy of continuous cracking and regeneration reactors to decrease carbon deposition on the catalyst surface (reactions 1.19 and 1.20).

Cracking $CH_4 \xrightarrow{catalyst} C + 2H_2$ (1.19)

Regeneration $C + O_2 \rightarrow CO_2$ (1.20)

In order to operate this process, there should be at least two parallel reactors, so that in one reactor cracking reaction occurs while in another reactor the regeneration process is carried out. In addition, it is required to have a switching possibility between reactors from the cracking mode to the regeneration mode and vice versa, or to move the catalyst between reactor and regenerator. Through the cracking step, coke is deposited on the surface of catalysts as a result of cracking a molecule of hydrocarbons like CH_4, or an oxygenated compound to carbon and hydrogen. However, at the same time and in the regenerating reactor, the deposited carbon on the surface of a catalyst is burned by a flow of air and then the catalyst can be used for further gasification reactions on its surface. This cyclic process has been used already in butane dehydrogenation in the fluidized bed reactors [23].

Wang *et al.* [27] claimed that coke formation during catalytic steam reforming of acetic acid is due to the adsorbed acetate molecules that decarboxylate to form the coke precursor $(CH_{1-3})_{abs}$.

Solid carbon formation on the surface of a catalyst may be whiskers, encapsulating deposits (polymers) and pyrolytic carbon. In addition, sulfur content of the feedstock is poisonous for the catalyst and can deactivate it, but due to small traces of sulfur in bio-oil compared to that in hydrocarbons, there is no need to use a desulphurization unit before bio-oil gasification [20].

Czernik *et al.* [26] pointed out one major property of bio-oil that facilitates more carbon deposition on the catalyst; there are carbon-oxygen bonds in bio-oil which make the molecules of bio-oil more reactive when compared to hydrocarbons. Thus, some components like furans, phenols and carbohydrates which are unstable at high temperatures contribute to carbon deposition.

1.2.4. Thermodynamics of gasification

Cracking reactions of oxygenate molecules are irreversible, but reactions between permanent gases such as hydrogen, CO, CO_2, CH_4, H_2O and carbon are reversible. Therefore, there is always a potential for these gases to reach thermodynamic equilibrium inside the gasification reactor.

Wang *et al.* [20] used ASPEN plus software to model the equilibrium yield of hydrogen from different oxygenated feeds versus temperature and molar S/C ratio. According to data in Table 1.2, which presents the equilibrium yield of hydrogen from water free poplar bio-oil with general formula of $CH_{1.33}O_{0.53}$, the yield of hydrogen is increased by temperature. In addition, additional steam looks to be very influential to maximize the yield of hydrogen which indicates the importance of having a separate water-gas shift reactor after the gasification reactor.

Table 1.2. **Stoichiometric yield of H_2 at equilibrium from steam reforming of a water free poplar bio-oil with formula of $CH_{1.33}O_{0.53}$. Adapted from [20]**

Operating temperature, °C	% yield of H_2	
	S/C= 5	S/C= 10
500	57.0	76.3
600	76.9	90.4
700	84.6	92.8
800	84.7	91.7
900	82.8	89.9

Vagia and Lemonidou [28] investigated the equilibrium yields of steam reforming of major components of bio-oil such as acetic acid, ethylene glycol and acetone, within a temperature range between 400K and 1300K, molar steam to carbon ratio of 1to 3, and pressure range of 1-20 atm. The equilibrium model was contructed by the Aspen plus software based on the minimum Gibbs free energy of the system. Hydrogen, carbon monoxide, carbon dioxide, methane and solid carbon were assumed as the final products at equilibrium.

In the case of acetic acid, their results showed that around 400K acetic acid was decomposed to only methane and carbon dioxide. However, hydrogen reached maximum mole fraction at 900K while methane fraction at this temperature was around zero. CO was also increased versus temperature while CO_2 was decreased.

In the case of acetone and ethylene glycol steam reforming, results were similar to the case of acetic acid. At lower temperatures (400K) methane was the predominant product, while it decreaseed to zero at higher temperatures. Hydrogen reached its maximum fraction at temperatures above 900K, CO production rose with temperature while CO_2 declined.

Regarding the steam to carbon ratio, in the case of acetic acid, the mole fraction of hydrogen grew at all temperatures with increasing molar S/C ratio. The CO mole fraction was not affected by the molar S/C ratio below 700K, but at higher temperatures, it decreased when molar S/C ratio increased. Methane was only affected by this ratio between 400K-900K and its mole fraction decreased with increasing molar S/C ratio. The CO_2 mole fraction declined with a rise in molar S/C ratio up to 800K, and then the trend was reversed. It is interesting that the solid carbon product was almost zero at high molar S/C ratios.

In the case of acetone and ethylene glycol steam reforming, the only difference with respect to the acetic acid equilibrium data was that the CO_2 mole fraction first rose with increasing molar S/C ratio where it reached a maximum amount at temperatures about 600K-700K, and then declined.

The effect of pressure of ethylene glycol steam reforming showed that the hydrogen mole fraction was higher at low pressures (1 atm) rather than at high pressures (20 atm). This effect on CO and CO_2 was negligible, but methane formation was larger at higher pressures.

As illustrated in Table 1.3, Vagia and Lemonidou [28] suggested the optimum operating conditions estimated by the equilibrium model for steam reforming of acetic acid, acetone and ethylene glycol.

Table 1.3. **Estimated optimum conditions for steam reforming of model compounds. Adapted from [28]**

Operating variable	Acetic acid SR	Acetone SR	Ethylene glycol SR
S/F ratio (S/C ratio)	6/1 (3/1)	9/1 (3/1)	6/1 (3/1)
Reactor Temperature, K	900	900	900
Reactor pressure, atm	1	1	1
Conversion, %	100	100	100
Yield, % (based on carbon)			
H_2 (based on stoichiometric H_2)	84.76	79.46	84.44
CO	24.01	32.23	27.34
CO_2	74.37	62.14	69.77
CH_4	1.62	5.63	2.89

1.2.5. Gasification kinetics

In the literature there are no reports about the kinetic studies of reactions involved in bio-oil gasification. Yet, there are many reports about the kinetic study of biomass pyrolysis and gasification, coal gasification and methane steam reforming and kinetic models are reported for the reactions involved in such processes.

Hajaligol *et al.* [29] worked on the effect of temperature, residence time and heating rate on the rapid pyrolysis of cellulose, and reported Arrhenius kinetic data for first order formation of pyrolysis products. Nunn *et al.* [30] reported kinetic data for the generation of the major products of rapid pyrolysis of sweet gum hardwood under conditions of constant residence time and heating rate but temperature was varied between 600K-1400K. Muhlen *et al.* [31] worked on steam gasification of char in the presence of hydrogen, carbon monoxide and carbon dioxide and derived an empirical model to describe carbon conversion rate as a function of temperature. Neogi *et al.* [32] studied thermal gasification of coal with steam and developed a predictive model for a reaction network of devolatilization of coke, char gasification and water-gas shift reactions. Brown *et al.* [33] developed a mathematical model to simulate an entrained flow gasification process which was used to convert four types of coal to syngas. Boroson *et al.* [34] worked specifically on the cracking of tar and reported kinetic data to predict the generation of product gases. Their proposed kinetic model is a first order kinetic equation which is similar to models by Hajaligol *et al.* [29] and Nunn *et al.* [30]. This kinetic model is helpful as it is a good tool to predict the yield of gases produced due to tar cracking.

Xu and Froment [35] worked on catalytic steam reforming of methane. They used Ni/$MgAl_2O_4$ as the catalyst and considered possible reactions in methane steam reforming; then proposed a mechanism of catalytic reactions to derive the rate of methane steam reforming, methanation and water-gas shift reactions. These models are very useful for catalytic reactions, but they need to be modified according to the operating conditions and the type of catalyst. Donnot *et al.* [36] used decarbonated and recarbonated dolomites as well as some commercial catalysts to find the highest yield of cracking of tar produced from wood pyrolysis. They developed kinetic models and then found activation energy, rate constants and unit volume of catalysts. Adjaye and Bakhshi [37] studied catalytic conversion of bio-oil over HZSM catalyst in a fixed bed reactor. They proposed kinetic data for conversion of volatile and nonvolatile parts of oil as well as kinetic data for the formation of gas, coke and residue; however, their model does not predict the distribution of product gases. Biggs and Agarwal [38] developed a mathematical model for a combustion fluidized bed in which char particles react with oxygen, and then they studied the effect of CO/CO_2 ratio on the process. Encinar *et al.* [39] pyrolyzed maize, sunflower, grape and tobacco residues for different residence times and temperatures and then proposed a kinetic model for the production of gases. Fletcher *et al.* [40] developed a computational fluid dynamics model for a biomass combustion system. They assumed that biomass was totally converted to the gas phase, so only reactions between char, methane, hydrogen, steam, carbon monoxide and carbon dioxide were considered. Di Blasi and Branca [41] used the thermogravimetric technique to estimate the kinetic parameters of wood pyrolysis primary products. Fagbemi *et al.* [42] worked on pyrolysis of wood, coconut shell and straw and compared the product yield of these three types of biomass. They also developed a kinetic model for tar thermal cracking. Fiaschi and Michelini [43] used a two phase one dimensional model for biomass gasification in a bubbling fluidized bed to predict the concentration of gases along the reactor. They considered the effect of mass transfer between the bubble phase and dense phase along with kinetic reactions. Hamel and Krumm [44] also developed a mathematical model which predicts gasification of lab scale and industrial scale gasification processes of coal and biomass. Among reactions that they considered, they assumed that tar reacts with oxygen and steam and produces hydrogen, carbon monoxide, carbon dioxide and methane.

Wurzenberger *et al.* [45] developed a comprehensive model for biomass gasification. They considered biomass drying step, homogeneous and heterogeneous reactions of biomass and tar cracking to make sure any kind of reaction has been assumed in the model. Then they solved derived equations out of momentum, heat and mass transfer relations. Liu and Gibbs [46] developed a model for a circulation biomass gasification process. They considered emissions of NH_3 and HCN which are produced in the process. Having considered a reaction network of 40 reactions, they used all kinetic models from literature but tried to modify some of them according to their model. Kersten *et al.* [47] reported their review of available kinetic models for biomass pyrolysis in literature. They point out that there is not such a good compromise between models and engineering cases. Corella and Sanz [48] developed their rigorous model for biomass circulation fluidized bed gasifiers. They tried to include in their model as many available reactions as possible and to consider heat and mass transfer effects. They reported that it was difficult to consider the process hydrodynamics because biomasses are very different and make it hard for the model to be flexible for any biomass.

Radmanesh *et al.* [49] worked on biomass pyrolysis and gasification. They simulated a bubbling fluidized bed reactor by considering hydrodynamics of the process. Their model predicts the concentration of gasification products in bed and in freeboard. Lee *et al.* [50] estimated the yield of product gases of biomass pyrolysis through the combination of thermodynamic and kinetic models. They used a soft ware which generates all chemical equilibrium reactions to measure the equilibrium yield of gases. Then they used latter results as kinetic limitations to apply to their kinetic models in which they considered all elementary reactions between final gaseous products of pyrolysis. Patel and Oant [51] developed kinetic models for catalytic steam reforming of methanol over $Cu/Zn/Al_2O_3$ catalyst. Yu *et al.* [52] developed a comprehensive model which predicts syngas production from coal in an entrained flow gasifier. They considered heat and mass transfer effects on the gasification process. They modified kinetic models by Xu and Froment [35] according to the calcium catalyst that they used.

Other than reaction 1.7 which considers the thermal decomposition of bio-oil upon its injection into the reactor, gasification reactions are similar to those in biomass, coal and methane gasifiers and their available kinetic models should be applicable to the kinetic study of bio-oil gasification.

Similar to bio-oil evaporation, an initial thermal decomposition reaction (reaction 1.7) takes place inside the pyrolysis and gasification reactors for any kind of feedstock with a $C_mH_nO_k$ general formula such as biomass and tar. Fortunately, some kinetic models have been estimated for biomass and tar thermal decomposition. Hajaligol *et al.* [29], Nunn *et al.* [30] and Boroson *et al.* [34] proposed a single first order reaction kinetic model for the production of gases due to thermal decomposition of biomass, but for different biomasses (cellulose, sweet gum hardwood and wood respectively):

$$\frac{\mathrm{dV_i}}{\mathrm{dt}} = \mathrm{k_{0i}} \exp\left(-\frac{\mathrm{E_i}}{\mathrm{RT}}\right)(\mathrm{V_i^*} - \mathrm{V_i}), \mathrm{i: tar}, \mathrm{CO}, \mathrm{CO_2}, H_2, CH_4, H_2O, \ldots \qquad (1.21)$$

V_i^* is the ultimate attainable yield of each component at the longest residence time and highest temperature. E and k_0 are activation energy and reaction constant of the arhenius kinetic equation. In Table 1.5, kinetic data reported in literature are listed.

***Table 1.5.* Kinetic data for thermal decomposition of biomass and tar**

	Log k_{0i}, s^{-1}			E_i, kcal/mol			V^*, wt%		
Reference	[29]	[30]	[34]	[29]	[30]	[34]	[29]	[30]	[34]
Biomass weight loss	8.30	16.5	-	31.79	4.53	-	94.08	92.97	-
Total gases	-	11.8	-	-	2.88	-	-	41.01	-
Tar	-	-	4.98	-	-	99.3	-	-	5.79
H_2	6.17	-	6.64	27.29	-	129	1.16	-	1.09
CO	11.75	14.6	4.66	52.74	3.36	87.9	21.64	17.05	36.33
CH_4	13.0	16.6	4.89	60.04	3.79	94.2	2.41	1.91	5.83
CO_2	5.39	14.3	2.55	23.42	3.77	49.0	3.08	5.97	13.2
H_2O	6.71	11.5	-	24.62	3.35	-	8.04	5.14	-

Wurzenberger *et al.* [45] assumed tar is cracked into CO, CO_2, CH_4, H_2 and inert tar into the gas phase:

$$tar \rightarrow \nu_{CO}\,CO(g) + \nu_{CO2}CO_2(g) + \nu_{CH4}CH_4 + \nu_{H2}H_2(g) + \nu_{inert\ tar}tar_{inert} \quad (1.22)$$

Regarding the relative stoichiometry of each component compared to the tar feed, the rate of formation of each component was suggested to be estimated by equation 1.23:

$$r_i = \vartheta_i . 10^{4.98} . \exp(-99.3/RT) . \left(W_{g,tar} . \rho_g\right) \quad (1.23)$$

$W_{g,tar}$ is the mass fraction of tar and ($W_{g,tar}.\rho_g$) is the mass of tar per volume of reactor in the gas phase. This equation has been deduced from models developed by Hajaligol *et al.*, Nunn *et al.* and Boroson *et al.*

Similar models have been reported for tar cracking during coal gasification. For example, Yu *et al.* [52] considered cracking of tar produced during coal gasification according to reaction 1.24 and used kinetic model proposed by Brown *et al.* [33]:

$$Tar \rightarrow \nu_{CO}\,CO(g) + \nu_{CO2}CO_2(g) + \nu_{CH4}CH_4 + \nu_{H2}H_2(g) + \nu_{C2H6}C_2H_6 + \nu_{C2H4}C_2H_4 + \nu_{H2S}H_2S + \nu_{NH3}NH3 + \nu_{inert\ tar}tar_{tar} \quad (1.24)$$

$$r_i = \vartheta_i . 3.7 \times 10^5 \exp\left(-\frac{25018}{T}\right) . (tar)^{0.2} \quad (1.25)$$

The most important operating parameters in bio-oil gasification are temperature, molar steam to carbon ratio (S/C), residence time and catalyst to feed ratio. Since steam reforming is an endothermic reaction and needs more heat, high temperature and excess steam (regarding equilibrium conditions of the reaction) favorably shifts the direction of the reaction towards increasing the rate of hydrogen production. A catalyst to feed ratio in a continuous flow reactor is explained by gas hourly space velocity (GHSV), which is defined as the ratio between feed flow rate and volume of the catalyst. This parameter helps to compare catalyst activity per unit carbon in the complex feedstocks like bio-oil. Some researchers changed GHSV by changing the mass of the catalyst while some researchers changed the flow of the feed by keeping the mass of the catalyst untouched.

1.3. Review of experimental results from gasification of bio-oil and its model compounds

1.3.1. Experimental objectives and setups

1.3.1.1. Bio-oil model compounds

Wang *et al.* [20] worked on catalytic steam reforming of oxygenated liquids which represent different constituents of bio-oil such as acids, ketones, alcohols, aldehydes, phenols and furans. They investigated the effects of temperature, molar S/C ratio, gas hourly space velocity and residence time on the conversion of the model compounds and yield of hydrogen. Experiments were carried out in a vertical, dual-bed quartz reactor. The mass of the catalyst is not reported, but the catalyst was mixed with chips of quartz if its mass had to be less than 0.25g.

Marquevich *et al.* [53] investigated catalytic steam reforming of acetic acid as an acid, m-cresol and dibenzyl ether as two aromatic compounds, and xylose, glucose and sucrose as sugar compounds. Experiments were carried out in two fixed bed reactors: a larger reactor (2.64cm I.D. and 41cm length) packed with 100g catalyst and a smaller reactor (1.27cm O.D. and 28cm length) packed with 10g catalyst. The larger reactor had a nozzle injector to spray from the top of the reactor high boiling point or thermally unstable compounds, in particular, sugars,. Water and oxygenated liquids were pumped by two HPLC metering pumps, while water was superheated to 300°C-400°C and model compounds were vaporized and mixed with steam and nitrogen at the reactor inlet at the top.

Rioche *et al.* [54] studied steam reforming of acetic acid, phenol, acetone, ethanol and bio-oil at the temperatures between 650°C and 950°C with catalysts synthesized by Pt, Pd and Rh as active metals supported on alumina and ceria–zirconia sample. The bio-oil was produced from beech wood with a general formula of $CH_{1.32}O_{0.54}$ with 29 wt% water content. Bio-oil and water were injected through two syringe pumps from the top of the reactor. The needle of the bio-oil pump was cool enough to prevent bio-oil polymerization before contact with catalysts. The fixed bed reactor consisted of a quartz tube with 1.8cm O.D., 1.5 cm I.D. and 30cm height. The catalytic bed contained 100-200mg of catalyst and 1000mg of the inert cordierite filler.

Galdamez *et al.* [55] investigated non catalytic and catalytic steam reforming of acetic acid in a fluidized bed reactor. Molar steam to carbon ratio was 5.58 and total mass of bed material was 200g (sand and catalyst) in all experiments, while mass of catalyst was 2g in catalytic experiments. Non catalytic tests were carried out over 450°C-700°C and their catalytic experiments were conducted at 650°C. The internal cross section area of the fluidized bed reactor was 13.14cm^2. The solution of acetic acid in water (representing molar S/C ratio of 5.58) was fed into the reactor by a HPLC metering pump with a flow rate of 5ml/min.

Basagiannis and Verykios [21] investigated catalytic steam reforming of acetic acid and its reaction network as a model compound of bio-oil between 200°C and800°C. Their reactor consisted of a quartz cell with 8 mm O.D in between two 6 mm O.D. quartz tubes as the inlet and the outlet tubes. The total length of the reactor was 32 cm.

Takanabe *et al.* [56] investigated deactivation of the Pt/ZrO_2 catalyst during steam reforming of acetic acid. About 50-200mg of the catalyst were placed in the fixed bed reactor (dimension is not reported). The aqueous solution of the feed (molar S/C=5) was injected to the reactor by a micro feeder equipped with a syringe. The GHSV of 40000h^{-1} was supplied by a flow of argon in the inlet and temperature was 875K. Deposited coke on the surface of catalyst was detected by burning the coke in a thermogravimetry system.

Ramos *et al.* [57] studied non catalytic and catalytic steam reforming of acetol with experimental setup and operating conditions similar to that reported in [55].

Medrano *et al.* [58] investigated the effects of catalyst calcination temperature and additional oxygen to increase the conversion of acetic acid during its catalytic steam reforming in a fluidized bed reactor at 650°C with Ni/Al catalysts. The catalytic bed was a mixture of sand and catalyst with an equal size distribution of 160μm-320μm forming the height of 7cm so that mass of catalyst was 1.1 g. The solution of acetic acid and water (molar S/C= 5.58) was injected to the bottom of the reactor with a peristaltic pump through a cooled spray nozzle with GHSV of 6800h^{-1}.

Vagia *et al.* [59] studied catalytic and non catalytic steam reforming of acetic acid and acetone in a fixed bed reactor over 550°C-750°C. The molar steam to carbon ratio was 3 for all experiments. They used quartz particles for the non catalytic tests. 0.05g of catalyst was diluted with 0.1g of quartz particles for the catalytic runs. The O.D. of the reaction zone was 10mm and the O.D. of the pre and post reaction zones was 6mm. Solutions of acetic acid and acetone in water were prepared to represent required molar S/C ratio of 3 and were fed into the reactor by a HPLC pump with flow rates of 6 and 4.5 cm^3/h for acetic acid and acetone, respectively.

Davidian *et al.* [60, 61] worked on catalytic cracking of acetic acid with their proposed sequential cracking/regeneration cycles in their reactor system in the absence of steam. According to Figure 1.5, they proposed a system of two parallel acetic acid cracking/regeneration cycles which includescracking/purging/regeneration/purging steps for time intervals of 15/2/10/3 minutes in each reactor. Although less hydrogen is produced by cracking of the acetic acid compared to steam reforming of the acetic acid, less energy input is required in the cracking reactor according to their calculations. It has been claimed that catalytic activity loss on the proposed process is prevented because of the presence of the regeneration step.

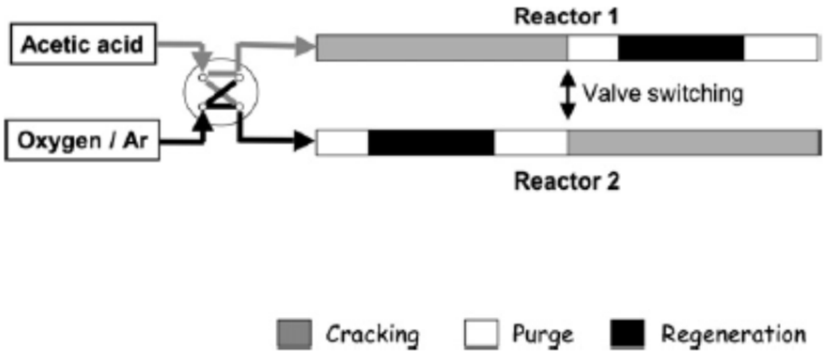

Figure 1.5. **Sketch of the two parallel reactors performing acetic acid cracking/regeneration sequences in opposition for continuous hydrogen production taken from [60]**

1.3.1.2. Bio-oil

Garcia *et al.* [62] studied catalytic steam reforming of aqueous fraction of bio-oil. The original bio-oil was produced from poplar wood and contained 46.8wt% carbon, 7.4wt% hydrogen and 45.8 wt% oxygen, while its water content was 19wt%. To separate the aqueous fraction from the lignin fraction, water was added to bio-oil with mass ratio of 2 so that the final obtained aqueous fraction contained 22.9wt% organics with a general formula of $CH_{1.34}O_{0.81}$ and 77.1wt% water presenting a molar S/C ratio of 4.92. The experiments were conducted in a dual bed reactor made of quartz with I.D. of 0.785 cm. The feed was injected by a syringe pump into the fixed bed reactor.

Czernik *et al.* [26] worked on catalytic steam reforming of the aqueous phase of bio-oil produced from pine sawdust in a fluidized bed reactor. They also investigated co-steam reforming of bio-oil and natural gas. Elemental composition of the bio-oil was 47.7wt% carbon, 7.4wt% hydrogen and 44.8wt% oxygen with 26.7wt% water content. Water was added to the bio-oil with a mass ratio of 2 to separate aqueous fraction from the lignin fraction of bio-oil; the resulted aqueous solution contained 21.8% organics with general formula of $CH_{1.25}O_{0.55}$ and 78.2% water (molar S/C=7). An aqueous solution of bio-oil was injected by a water cooled injector into the reactor and steam was flowing into the reactor though the distributor as both fluidization medium and reactant. Reactions were conducted at temperatures 800°C and 850°C, and with molar S/C ratio of 7-9 as well as GHSV in the range of 700 to1000 h^{-1}. The commercial steam reforming catalyst,C11-NK, from Sud-Chemie was crushed to reach average size of 300µm-500µm suitable for a fluidized bed. The bubbling fluidized bed reactor with 2 inch diameter made of inconel was used for the following reasons:

- In the fluidized bed reactor, there is very good mixing between the feed and the catalyst particles.
- In the fluidized bed reactor, deposited carbon is more exposed to steam to be gasified, so the regeneration time for the catalyst is shorter.

Panigrahi *et al.* [63] investigated the effect of residence time on gasification of bio-oil in the absence of catalyst to produce syngas and high Btu gaseous fuel, like methane and olefins. The bio-oil was produced at Dynamotive Technologies Inc. Vancouver (Table 1.6).

Table 1.6. **Properties of Dynamotive's bio-oil. Adapted from [63]**

Property of bio-oil	Value
C, wt%	43.6
H, wt%	8.5
N, wt%	0.5
O, wt% (by difference)	47.9
pH	2.5
Water content, wt%	21.5
Lignin content, wt%	25.0
Ash content, wt%	0.16
Density, g/cm^3	1.8-1.24
Calorific value, MJ/kg	17.5-19.1
Kinematic viscosity, cSt at 20°C	110
Kinematic viscosity, cSt at 80°C	45.6

Experiments were conducted at temperatures between 650°C and 800°C in a vertical fixed bed downward flow micro reactor with an I.D. of 12.7 mm and 500 mm high. About 5g of quartz chip were placed in between the quartz wool to maintain a good temperature and flow distribution and prevent a large pressure drop. Bio-oil was pumped by a syringe pump towards the reactor top and then was carried by a nitrogen flow to be atomized to the reactor. Each experiment took about 30-45 minutes. After any experiment the reactor was weighed to measure the coke yield.

Panigrahi *et al.* [64] investigated non-catalytic gasification of bio-oil with CO_2 (CO_2/N_2), H_2 (H_2/N_2) and steam (H_2O/N_2) in the absence of hydrogen at 800°C in a similar experimental setup. Flow rate of carbon dioxide and hydrogen varied between 0 and 18 ml/min, but the total flow rate of each gas plus nitrogen was set at 30ml/min. During steam reforming tests, the flow rate of nitrogen was 30ml/min while flow rate of steam was 2.5 to10 g/h. Flow rate of bio-oil was 5g/h in all experiments.

Kechagiopoulos *et al.* [65] worked on catalytic steam reforming of bio-oil model compounds and also aqueous fraction of bio-oil in a fixed bed reactor. The fixed bed reactor had a length of 71.2 cm and I.D. of 1.25cm. Experiments with an equimolar mixture of acetone, acetic acid and ethylene glycol were conducted at 650°C-750°C, molar S/C ratio of 3-6 and GHSV of 1500 h^{-1}. Water was added to the bio-oil, which was produced from catalytic fast pyrolysis of beech wood, with a mass ratio of 2 to separate aqueous fraction from the lignin fraction. The resulted aqueous fraction, representing molar S/C ratio of 8.2, contained 16 wt% organics with general formula of $CH_{2.48}O_{0.94}$. Liquid feeds and water were injected to the reactor by two syringe pumps.

Davidian *et al.* [23] developed the idea of having a continuous sequential catalytic gasification process having one reactor in which bio-oil was cracked during the cracking step and then catalyst was regenerated during the regeneration step (similar to their proposed process in [60, 61]). The bio-oil studied was made from beech wood residues with a general formula of $CH_{2.3}O_{1.04}N_{0.01}$ including 28.8wt% water content with some impurities like chlorine, sulphur and traces of metals like K, Mg and Ca. A double envelop reactor (the configuration of the reactor has not been reported) was used equipped with a water cooled capillary nozzle through which bio-oil pumped by a syringe pump (5 ml/h) was injected to the top of the catalyst bed. An automated two position switching valve was used to inject the bio-oil to the reactor during the cracking step and to a collector tank during the regeneration step. An inert gas was used to purge out the gases inside the reactor during cracking and regeneration steps. The catalysts were reduced with hydrogen at 650°C before start up of the experiments.

Czernik *et al.* [66] used a fluidized bed reactor (with 5cm diameter) to produce hydrogen by catalytic steam reforming of Dynamotive bio-oil. They had added 10 wt% methanol to the bio-oil to reduce its viscosity, so the elemental composition of the final mixture was 36.5 wt% carbon, 8.4 wt% hydrogen and 55.0 wt% oxygen. The experiments were carried out at 850 °C while mass of the catalytic bed was 250 g , molar S/C ratio was 5.8 and the methane-equivalent space velocity was 920 h^{-1}.

Van Rossum *et al.* [67] worked on non catalytic and catalytic steam gasification of bio-oil in a fluidized bed reactor. Their goal was to convert the whole bio-oil to produce a clean syngas free of hydrocarbons and with the lowest tar content. They used bio-oils produced from pine wood and beech wood at the BTG in Netherlands. Elemental composition and water content of the bio-oils are listed in Table 1.7.

***Table 1.7.* Elemental analysis and water content of BTG bio-oils. Adapted from [67]**

(wt%)	Beech wood bio-oil	Pine wood bio-oil
C	30.4-37.7	38.1-39.9
H	7.6-7.9	7.9-8.3
O	54.4-61.7	51.6-53.7
N	<0.01-0.27	0.13-0.16
S	<0.01	<0.01
H_2O	32.5-43.7	29.7-30.4

The fluidized bed reactor had an I.D. of 10.8cm and a height of 72cm, and 4-9 kg of the bed material was loaded inside. There was also an additional free board with a 19.6cm I.D. and 33cm height to minimize loss of the bed material. However, less than 0.2wt% of sand was elutriated from the bed at each run and this value was higher when catalyst was the bed material (no number is reported). Instead of using a perforated plate, the lower section of the reactor was conical to provide spouting behavior while bio-oil, steam and other gases were being introduced upward from the bottom. Before atomizing the bio-oil into the reactor by nitrogen, the temperature of the bio-oil line was kept at 80°C to avoid any thermal decomposition of the bio-oil before reaching the bed material inside the reactor.

Van Rossum *et al.* [68] developed the idea of using a staged gasification setup consisting of a fluidized bed reactor with inert bed material, to initially gasify/vaporize the bio-oil, followed by a fixed bed of nickel based steam reforming catalysts (K23 and K46 supplied by the Johnson Matthey) above the fluidized bed to produce a syngas stream with no methane, C_2-C_3 and tar content (Figure 1.6).

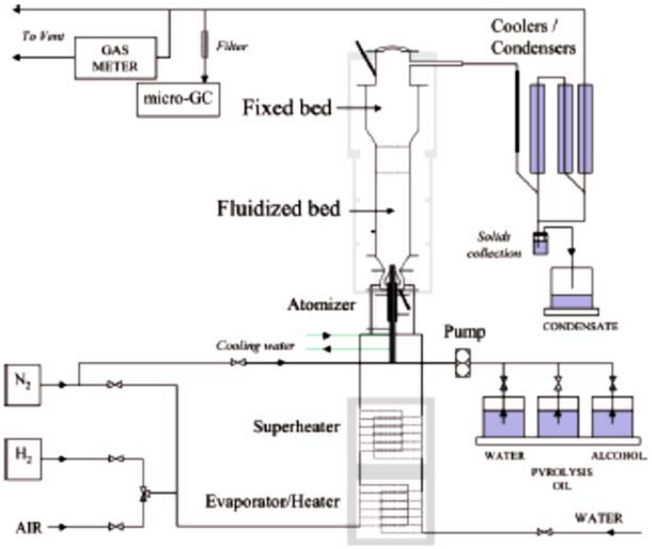
To Vent
GAS METER
Filter
micro-GC
Coolers / Condensers
Fixed bed
Fluidized bed
Solids collection
CONDENSATE
Atomizer
Cooling water
Pump
N$_2$
H$_2$
AIR
Superheater
Evaporator/Heater
WATER
ALCOHOL
PYROLYSIS OIL
WATER

Figure 1.6. **Schematic overview of the staged setup; taken from [68]**

Wu *et al.* [69] developed the idea of hydrogen production from the sawdust bio-oil via steam reforming in a two stage catalytic fixed bed reactor. In order to reduce deactivation of the nickel based catalysts, the dolomite, calcined at 950°C for 5h, was used in the first fixed bed reactor for a primary steam reforming of bio-oil. A commercial Ni/MgO catalyst, reduced by 5vol% hydrogen flow at 500°C for 8h, was used in the second fixed bed reactor in which further catalytic steam reforming reactions between product gases of the previous stage took place, to increase conversion of hydrocarbons and yield of hydrogen.

Marda *et al.* [70] investigated non-catalytic partial oxidation (NPOX) of the bio-oil produced from the poplar wood. Additional oxygen was introduced to an empty tubular reactor while the bio-oil was sprayed from the top through an ultrasonic nozzle. The elemental composition of the bio-oil was 48.2wt% carbon, 7.2wt% hydrogen and wt44.6% oxygen including its 17% water content ($CH_{1.32}O_{0.46}.0.23H_2O$). No additional steam was used. Their idea was to maximize conversion of the carbon content of the bio-oil to gaseous products through the NPOX process, and then to increase the yield of hydrogen in a catalytic reactor where lower temperature and less load of catalyst is required. The poplar bio-oil had been stored since 1997 at a temperature of

4°C. Due to the aging issues, they had to add methanol for a 50:50 mass ratio to be able to pump the bio-oil by a syringe pump and then spray it through the ultrasonic nozzle.

Sakaguchi *et al.* [71] investigated non-catalytic and catalytic steam gasification of bio-oil and bio-oil/bio-char slurry in a fluidized bed reactor. The bio-oil and the bio-char were products of the fast pyrolysis plant of the Dynamotive Energy Systems Corporation of Canada. Water content of the bio-oil was 25.2 wt%. Elemental composition of these feedstocks is listed in Table 1.8:

***Table 1.8.* Elemental analysis of Dynamotive's bio-oil and bio-char. Adapted from [71]**

Sample	C, wt%	H, wt%	N, wt%	S, wt%	O, wt%
Bio-oil	42.5	7.2	<0.3	<0.3	49.7
Bio-char	76.5	3.7	<0.3	<0.3	19.2

The fluidized reactor had an I.D. of 7.79cm and a height of 80cm. The steam generated by a steam generator was used to fluidize the bed material through a perforated plate. The bed material occupied 0.6L of the reactor volume. The feed was pumped by a peristaltic pump and atomized into the reactor from the side by an atomizer nozzle. The temperature on the surface of the nozzle was kept at 80°C to prevent the bio-oil to be thermally decomposed inside the nozzle and plug it. The gasification experiments were carried out at temperatures of 747°C to 803°C, molar steam to carbon ratios of 2.7-7.5, and GHSV between 210 and 400 h^{-1}.

Following their research on catalytic steam reforming of bio-oil in a fluidized bed reactor with the Ni/MgO catalyst [72], Lan *et al.* [73] conducted catalytic steam reforming of bio-oil in a fixed bed reactor and in a fluidized bed reactor. The dimensions of the reactor are not reported. The bio-oil was produced from rice husk with 40.71 wt% water content (Table 1.9).

***Table 1.9.* Elemental composition of rice husk bio-oil. Adapted from [73]**

Water content, wt%	Kinematic viscosity (20°C), mm^2s^{-1}	C, wt%	H, wt%	O, wt%	N, wt%	S, wt%
40.71	6.45	56.64	7.97	33.06	1.69	0.64

A mixture of bio-oil and steam was transferred by a syringe pump to the top of the fixed bed reactor. In the fluidized bed reactor bio-oil was pushed by an electromagnetic drive pump and then mixed with steam through a nozzle at the bottom. Experiments were conducted at 650°C-950°C in the fixed bed reactor and 500°C-800°C in the fluidized bed reactor for 1 hr. Although they compared the results of fixed bed and fluid bed reactors, operating conditions were not similar. For example, molar S/C ratio changed between 3 and 15 in the fixed bed reactor, while it was between 8 and 20 in the fluidized reactor. Also, the mass of the catalyst was 1g in the fixed bed and 100g in the fluid bed.

Medrano *et al.* [74] continued their work on catalytic steam reforming of bio-oil model compounds with Ni/Al catalysts in a fluidized bed reactor for aqueous phase of bio-oil at 650°C. Either 0.5g or 1.1g catalyst were mixed with a 7 cm height of sand in a quartz fluidized bed with 2.54cm I.D. ($u/u_{mf} = 10$). They added water to the bio-oil produced from pine wood by mass ratio of 2 to separate the aqueous phase of the bio-oil from its lignin phase. The solution contained 84 wt% water, representing a steam to carbon ratio of 7.64 in the reactor (Table 1.10).

Table 1.10. **Elemental composition of pine wood bio-oil. Adapted from [74]**

	Bio-oil	Aqueous solution of bio-oil
C, wt%	36.1	7.4
H, wt%	8.4	10.8
N, wt%	0.1	0.0
O, wt%	55.4	81.8
pH	2.6	2.5
Water content, wt%	36	84

Seyedyn-Azad *et al.* [75] worked on catalytic steam reforming of bio-oil in a tubular fixed bed reactor to investigate the effect of catalyst composition, molar S/C ratio, temperature and GHSV. I.D. and height of the reactor were 1cm and 43cm, respectively. The bio-oil was produced by Biomass Technology Group (BTG) in the Netherlands (Table 1.11).

Table 1.11. **Bio-oil characteristics supplied by the BTG. Adapted from [75]**

C,wt%	H,wt%	N.wt%	O,wt%	Water,wt%	pH	Density, kg/m^3	HHV,MJ/kg
45.83	7.15	0.87	46.15	23.1	2.1	1225.00	17.5

Droplets of bio-oil and water were fed from the top of the reactor by two syringe pumps and capillary tubes. The flow rate of bio-oil was 2.3ml/h and flow rate of water changed between 1.2 and 13.8 ml/h to supply the desired molar S/C ratio. The GHSV varied between 9 and 26 hr^{-1}.

1.3.1.3. Summary

Different setups of fixed bed and fluidized bed reactors have been used to gasify bio-oil and its model compounds.Fluidized bed reactors have been shown to be more efficient in term of less coke deposition on the catalyst. However, catalyst loss is a problem in fluidized bed reactors.

In order to inject bio-oil and its model compounds continuously into the reactor, several injectors have been developed.

Acetic acid has been the most common bio-oil model compound used. On the other hand, bio-oils produced from different biomasses, and therefore, with different elemental composition, have been gasified. In addition, tested operating parameters such as molar S/C ratio, temperature, residence time and feed flow rate as well as the catalysts type and mass were different. Therefore, it is not easy to sort out the experimental results in literature versus bio-oil types and operating parameters. However, an accurate image of the overall effect of catalyst mass and type as well as operating parameters on the syngas yield and bio-oil conversion can be achieved.

1.3.2. Composition and effect of the catalysts

1.3.2.1. Bio-oil model compounds

Composition of the synthesized and commercial nickel based catalysts and the Cu/Zn shift catalyst used by Wang *et al.* [20] for the steam reforming of model compounds are listed in

Table 1.12. All catalysts were crushed and sieved for the size of 250µm-355µm. Nickel catalysts were reduced at 600°C and the shift catalyst was reduced at 350°C by a 20% flow of hydrogen.

***Table 1.12.* Catalysts used in screening tests. Adapted from [20]**

ID	Catalyst name	Manufacturer	Composition
A	S.U.	Sherbrook Univ.	NiO, Al_2O_3, Cr_2O_3, La_2O_3, MgO
B	UCI G-90C	United catalysts Inc.	15% Ni, ceramic carrier (70-76% Al_2O_3, 5-8% CaO)
C	ICI 25-4M	Imperial Chemical Industries	15% NiO, 70% Al_2O_3, 13% CaO, 1.5% K_2O promoted
D	ICI 46-1	Imperial Chemical Industries	10-25% NiO refractory carrier, 1.5% K_2O promoted
E	UCI G-90B	United Catalysts Inc.	11% Ni, ceramic carrier (76-82% Al_2O_3, 6-9% CaO)
F	UCI C18HC	United Catalysts Inc.	42% CuO, 47% ZnO, 10% Al_2O_3
G	BASF g1-25S	BASF	15% Ni, ceramic carrier
H	ICI 46-4	Imperial Chemical Industries	NiO, CaO, Al_2O_3, ZrO_2
I	UCI G-91	United Catalysts Inc.	11% Ni, ceramic carrier (76-82% Al_2O_3, 6-9% CaO), K_2O promoted
J	Ni-Mg	Univ. of Zaragoza	NiO, MgO, Al_2O_3

Catalysts were screened for steam reforming of some model compounds such as methanol, acetic acid, hydroxyacetaldehyde, and ADP/methanol mixture at 700°C, molar S/C=5, GHSV=6725h^{-1} and residence time 0.01s. According to Table 1.13, conversions higher than 99.5% were achieved for all feeds, except for ADP/methanol mixture where conversion of ADP with ICI 46-1 catalyst was about 96%. Regarding the yield of hydrogen, catalysts did not show any significant differences, so that an average hydrogen yield of 89% was achieved with all the tested catalysts. It is reported that the shift catalyst was not suitable for steam reforming tests especially for temperatures above 400°C.

***Table 1.13.* Conversion (%) of model compounds by catalytic steam reforming. Adapted from [20]. Experimental conditions: 700°C, S/C= 5, GHSV= 6725 h^{-1} and t= 0.01s**

Catalyst ID	MeOH	AA	HAA	ADP/MeOH		MeOH repeat
				ADP	MeOH	
A	99.5	99.85	99.95	99.95	99.7	99.95
E	99.95	99.95	99.8	99.6	99.7	99.92
G	99.91	99.95	99.95	99.7	99.95	99.8
D #1	99.95	99.95	99.95	98.0	99.4	99.95
D #2	99395	99.95	99.95	95.9	98.3	99.88
C #1	99.95	99.95	99.95	99.95	99.95	99.95
C #2	99.5	99.9	99.7	99.3	99.5	99.5
B #1	99.95	99.95	99.95	99.95	99.95	99.95
B #2	99.95	99.95	99.90	99.8	99.95	99.95
B #3	99.95	99.95				

Rioche *et al.* [54] conducted catalytic steam reforming of model compounds with noble metal containing synthesized catalysts and summarized the general activity trend of the catalysts. Although having different activities, the catalysts were effective to increase carbon conversion and yield of hydrogen. In comparison with their non-catalytic results, methane formation was significantly reduced by using the catalysts; this shows that catalysts were effective to steam reform the methane to hydrogen and carbon monoxide. In addition, each catalyst resulted in different yields of hydrogen, CO/CO_2 ratio and methane for each model compound. For example, in the case of the 1% Rh-$CeZrO_2$ catalyst, production of methane was about 1-2% during steam reforming of acetic acid, acetone and ethanol, but it was about 5-8% during steam reforming of phenol. Also, the CO/CO_2 ratio was higher than 1 for steam reforming of acetic acid, acetone and ethanol, but this ratio for phenol steam reforming was close to zero. Tables 1.14 and 1.15 present general yield range of product gases resulted from steam reforming of the model compounds versus the synthesized noble catalysts obtained at applied operating conditions.

***Table 1.14.* Activity of various catalysts for steam reforming of model compounds in term of CO_x yield; adapted from [54]: (-) 20-40%; (0) 40-60%; (+) 60-80%; (++) >80%**

Catalyst	CO+CO_2 yield (%)			
	Acetic acid	Acetone	Ethanol	Phenol
1% Pt-Al_2O_3	+	+	-	++
1% Rh-Al_2O_3	++	++	++	++
1% Pd-Al_2O_3	+	++	++	+
1% Pt-ZrO_2	+	++	+	++
1% Rh-ZrO_2	+	++	++	++
1% Pd-ZrO_2	0	++	0	++

***Table 1.15.* Activity of various catalysts for steam reforming of model compounds in term of hydrogen yield; adapted from [54]: (--) <20%; (-) 20-40%; (0) 40-60%; (+) 60-80%; (++) >80%**

Catalyst	Hydrogen yield (%)			
	Acetic acid	Acetone	Ethanol	Phenol
1% Pt-Al_2O_3	-	-	-	++
1% Rh-Al_2O_3	0	+	+	++
1% Pd-Al_2O_3	-	-	0	0
1% Pt-ZrO_2	+	+	0	++
1% Rh-ZrO_2	+	+	+	++
1% Pd-ZrO_2	0	0	-	++

In general they concluded that ceria-zirconia based catalysts are more active than alumina based catalysts and result in larger conversion of model compounds and yield of hydrogen so that the trend of efficient catalysts was: 1% Rh-$CeZrO_2$ > 1% Pt-$CeZrO_2$ ≈ 1% Rh- Al_2O_3 > 1% Pd-$CeZrO_2$ > 1% Pt-Al_2O_3 > 1% Pd-Al_2O_3.

They investigated the effect of their synthesized catalysts on bio-oil steam reforming at 860°C with molar S/C ratio of 10.8 and GHSV of 3090h^{-1}; again, zirconium based catalysts showed better activities than alumina based showed. However, Pt, in comparison with Rh, on zirconium resulted in a higher yield of hydrogen and carbon conversion; also, CO/CO_2 ratio, although less than 1, was larger. In addition, the yield of hydrogen was decreased versus time from about 78% to about 62% after 2h by 1% Rh-$CeZrO_2$ while it was constant at about 70% by the 1% Pt-$CeZrO_2$ catalyst. To test the durability of the optimum catalyst at 830°C with molar S/C ratio of 5 and GHSV of 3090h^{-1}, it was observed that the yield of hydrogen production was decreased from 60% to 50% after 9 hours by the 1% Pt-$CeZrO_2$ catalyst.

Galdamez *et al.* [55] carried out catalytic steam reforming of acetic acid with catalytic beds of reduced and non reduced fresh catalysts (reduction by hydrogen). The catalyst was synthesized by a Ni/Al molar ratio of ½. The reduced catalyst was reduced with a flow of H_2/N_2 (1:10) at 650°C for 1h. During catalytic tests with either of the reduced and non reduced catalysts, in comparison to data of non catalytic tests, the yield of hydrogen and CO_2 was increased whereas the yield of CO, methane and C_2 hydrocarbons declined. In other words, water gas shift reaction led to the production of hydrogen and CO_2 and also some steam reacted with hydrocarbons to produce more hydrogen and CO (although the net CO production had a reducing trend). However, when the catalyst was reduced, the composition of product gases was very close to the predicted equilibrium compositions (Figures 1.7 and 1.8). Also, catalytic deactivation was not observed after 1h period of each test.

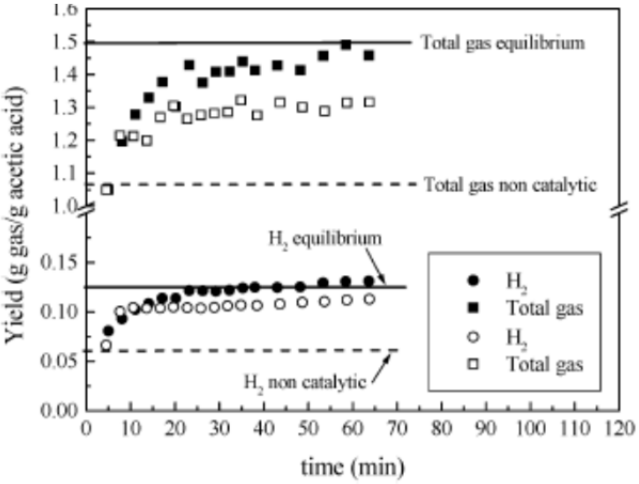

Figure 1.7. **H_2 and total gas yields obtained with and without previous reduction of the catalyst. Bold symbols correspond to yields with reduction and open symbols correspond to yields without reduction taken from [55]**

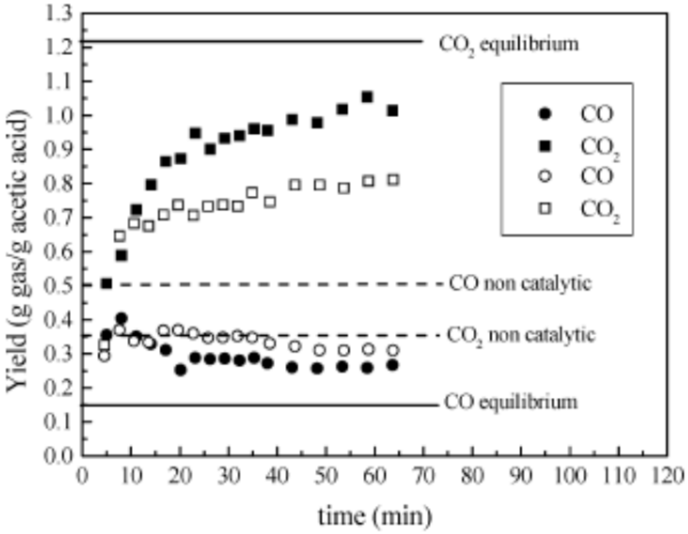

Figure 1.8. CO and CO_2 yields obtained with and without previous reduction of the catalyst. Bold symbols correspond to yields with reduction and open symbols correspond to yields without reduction taken from [55]

Galdamez *et al.* [55] investigated also the effect of lanthanum in their catalyst formulation with 8wt% and 12wt% mass fractions (Table 1.14). Although lanthanum has been proven to have a promoter role in decreasing the amount of coke formation on the catalyst, their results showed that the catalyst with a larger amount of this promoter (12wt%) caused lower total gas production, yield of hydrogen and CO_2, while the yield of methane and C_2 increased. The trend of CO was not clear. This could be because dispersion of Ni and Al becomes limited by the excess presence of lanthanum. Also, according to TPR analysis, the catalyst with a larger mass of La experiences a lower reduction by hydrogen under similar reduction conditions. Investigation on the effect of mass of catalyst revealed that a lower mass of catalyst decreases total gas production, hydrogen and CO_2 yields, but the yield of methane and C_2 are increased while the yield of CO is almost unaffected by mass of the catalyst (Table 1.16).

***Table 1.16.* Results of Catalytic Steam Reforming: Influence of Catalyst Composition and W/m_a Ratio. Adapted from [55]**

Catalyst	Ni-Al-La (12%) #1	Ni-Al-La (12%) #2	Ni-Al-La (8%) #1	Ni-Al-La (8%) #2	Ni-Al #1	Ni-Al #2	Ni-Al #3	Ni-Al #4
Temperature, °C	650	650	650	650	650	650	650	650
S/C (mol/mol)	5.58	5.58	5.58	5.58	5.58	5.58	5.58	5.58
Catalyst weight, g	1.29	0.78	1.29	0.80	1.29	0.80	0.50	0.28
g catalyst/g acetic acid	3.12	1.93	3.02	1.89	3.19	2.02	1.23	0.67
GHSV, h^{-1}	13354	21588	13796	22044	13061	20626	33873	62185
Liquid feeding rate, g/min	1.80	1.76	1.86	1.85	1.77	1.73	1.79	1.8
Time, min	56.3	55.6	64	55.1	59.1	55.5	55.6	55.3
Total acetic acid, g	23.3	22.5	27.4	23.4	24	22.9	22.9	22.9
Yields, g/g								
Total gas/ (AA+water)	0.2211	0.2510	0.2684	0.2705	0.3166	0.312	0.2982	0.2463
Total gas/acetic acid	0.9614	1.0911	1.1670	1.1759	1.3767	1.3566	1.2951	1.0710
Gas yields, g/g acetic acid								
H_2	0.077	0.060	0.090	0.078	0.136	0.120	0.084	0.057
CO	0.296	0.313	0.293	0.316	0.352	0.299	0.349	0.372
CO_2	0.484	0.547	0.651	0.617	0.805	0.854	0.716	0.475
CH_4	0.097	0.153	0.126	0.151	0.083	0.100	0.138	0.149
C_2	0.007	0.018	0.007	0.013	0.002	0.004	0.009	0.018

Basagiannis and Verykios [21] prepared different catalysts such as Al_2O_3, La_2O_3, Al_2O_3/ La_2O_3, and Ni/Al_2O_3/ La_2O_3 for catalytic steam reforming of acetic acid. The nickel based catalyst was reduced by hydrogen at 500 °C for 2h. Generally, they found that at intermediate temperatures (between 300°C and 500°C) thermal decomposition reactions are the dominant reactions which favor production of CH_4 and other hydrocarbons, while at higher temperatures, hydrogen, carbon monoxide and carbon dioxide are the main products. They also studied carbon deposition with different catalysts and concluded that catalyst composition affects the amount of coke formation; for example, alumina which has more acidity properties makes more carbon deposition compared to lanthana. In addition, they reported that disregarding the composition of the catalyst, less coke was deposited on the catalyst at higher temperatures (Table 1.17).

Table 1.17. **Carbon deposition with respect to the catalyst composition and temperature. Adapted from [21]; Ratio of H_2O/AA= 3**

Catalysts	Percentage of carbon deposited	
	T= 500°C	T= 700°C
Quarz bed	2.2/5.1[a]	1.6/3.2[a]
Al_2O_3	27.4	47.2
La_2O_3	7.8	1.32
$Ni/La_2O_3/Al_2O_3$	6.7	0.43
$Ni/La_2O_3/Al_2O_3$	9.5[b]	-

[a] In the absence of water in reactant mixture

[b] Ratio of H_2O/AA= 1.5

Takanabe *et al.* [56] synthesized the Pt/ZrO_2 catalyst and reduced it by a flow of 5% hydrogen in nitrogen at 925 K for 1h. Earlier experiments of acetic acid steam reforming which were carried out for 5h showed that, although conversion of acetic acid was about 100% and yield of hydrogen was more than 80% during the initial 3h of the operation, conversion of acetic acid and hydrogen started to drop dramatically until they reached 50% and 45% respectively after 5h of the operation. In the meantime, it was observed that acetone formation started after 2h of operation, reached a maximum yield of 8% after 3h of the operation and disappeared completely after 5h. Therefore, the researchers realized that there must be a relation between the catalyst deactivation and the acetone presence in the system, so they studied steam reforming of acetic acid and acetone and compared their conversion and yield of product gases. According to Figure 1.9, deactivation of the catalyst by acetone steam reforming occurred sooner than that by acetic acid steam reforming which proves the negative effect of acetone on the catalyst deactivation. It is known that acetone can be converted to mesityl oxide, ketene and isobutene which can be converted to larger hydrocarbons and some aromatics which deposit on the acidic catalysts like the Pt/ZrO_2 catalyst [76].

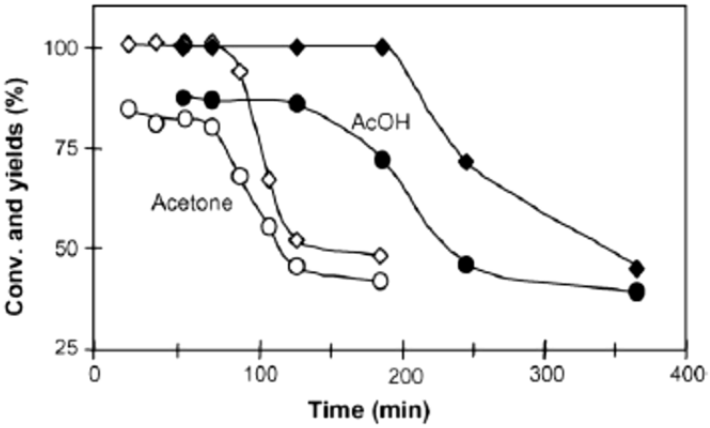

Figure 1.9. **Comparison of conversion and H_2 yields between steam reforming of acetic acid and acetone over Pt/ZrO_2 catalyst (875K, S/C=5, GHSV=40000h^{-1}; diamond: coversion; circle: yield; taken from [56]**

Based on the facts observed during steam reforming of acetic acid and acetone, researches proposed a pathway through which catalyst deactivation occurs as shown in the Figure 1.10: towards the right hand side of the figure, undesirable dehydrogenation reactions take place; for example, acetic acid loses H_2O to form acetone, and acetone loses another H_2O to form mesityl oxide, so finally C-C bonds in the form of oligomers and coke appear on the surface of the catalyst. Hence, the researchers concluded that this route should be minimized by enhancing the activation of water to overcome dehydration reaction in order to enhance catalyst life.

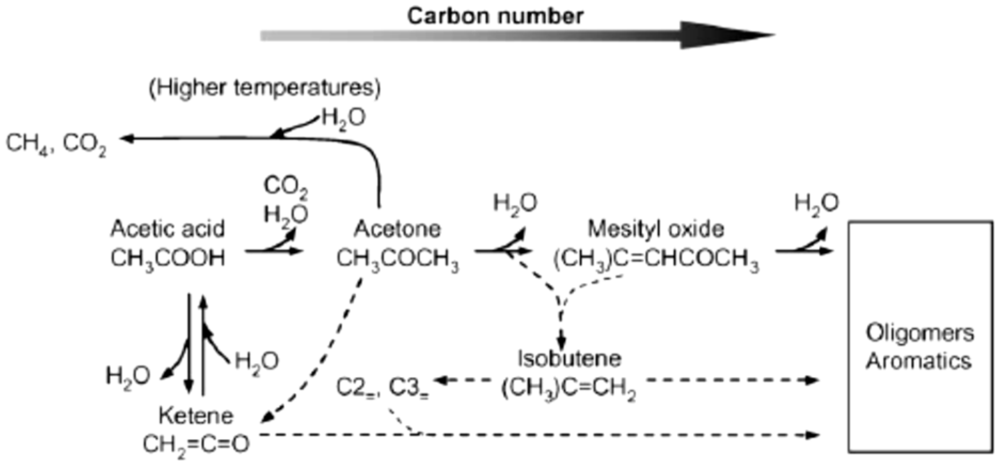
Carbon number
(Higher temperatures)
H₂O
CH₄, CO₂
CO₂
H₂O
Acetic acid
CH₃COOH
Acetone
CH₃COCH₃
H₂O
Mesityl oxide
(CH₃)C=CHCOCH₃
H₂O
H₂O
H₂O
Ketene
CH₂=C=O
C2₌, C3₌
Isobutene
(CH₃)C=CH₂
Oligomers
Aromatics

Figure 1.10. **Diagram for the possible reactions of acetic acid (and acetone) over ZrO_2 catalyst taken from [56]**

Ramos *et al.* [57] prepared Ni-Al catalysts with promoters of La (4 and 8 wt%) and Co (molar Co/Ni ratios of 0.25 and 0.025) to investigate the composition effect of the catalyst on catalytic steam reforming of acetol. Their investigation of the effect of the catalyst mass with Ni-Al at 650°C and molar S/C=4.6 showed that when the mass ratio of Ni/Al changed from 2.27 to 8.57, carbon conversion increased from 87.06% to 100%. Also, composition of the product gases during catalytic tests became very close to the equilibrium conditions; i.e. in comparison with non catalytic data, yield of H_2 and CO_2 increased while yields of CO, CH_4 and C_2 were decreased. In other words, the catalysts helped the steam reforming reactions of hydrocarbons as well as the water gas shift to proceed toward production of more hydrogen. Their investigations on the catalyst composition and effect of the promoter was carried out at 650°C and molar S/C =4.6. According to the data in Table 1.18, more loads of Lanthanum on Ni-Al-La catalysts resulted in more carbon conversion (from 81.58% to 92.75%) and larger productions of CH_4, CO_2 and C_2 but less production of hydrogen. In contrast, cobalt contents in Ni-Al-Co catalyst resulted in lowest carbon conversions (82.22% and 82.96%); however, cobalt increased the yield of hydrogen and the highest hydrogen production was detected by the catalyst with Co/Ni ratio of 0.025.

***Table 1.18.* Results of Acetol Catalytic Steam Reforming: Influence of Catalyst Composition at 650°C. Adapted from [57]**

Catalyst	Ni-Al	Ni-Al-La[a]	Ni-Al-La[b]	Ni-Al-La[c]	Ni-Co-Al[d]	Ni-Co-Al[e]	equ
Temperature, °C	650	650	650	650	650	650	650
S/C (mol/mol)	4.6	4.6	4.6	4.6	4.6	4.6	
Catalyst weight, g	1.2	1.2	1.2	1.2	1.2	1.2	
g catalyst/g acetol	3.41	3.41	3.41	3.41	3.41	3.41	
GHSV, h^{-1}	14860	14860	14860	14860	14860	14860	
Liquid feeding rate, g/min	1.53	1.53	1.53	1.53	1.53	1.53	
Time, min	65	65	65	65	65	65	
Total acetol fed, g	22.9	22.9	22.9	22.9	22.9	22.9	
Carbon conversion, %	87.22	81.58	95.18	92.75	82.96	82.22	100
Yields, g/g							
Total gas/ (acetol+water)	0.292	0.277	0.311	0.317	0.281	0.295	0.416
Total gas/acetol	1.268	1.203	1.354	1.378	1.221	1.284	1.81
Gas yields, g/g acetol							
H_2	0.134	0.121	0.120	0.118	0.126	0.0134	0.171
CH_4	0.082	0.080	0.100	0.087	0.081	0.072	0.001
CO	0.427	0.348	0.423	0.360	0.358	0.311	0.254
CO_2	0.609	0.638	0.689	0.796	0.638	0.761	1.381
C_2	0.016	0.016	0.022	0.017	0.018	0.006	0

[a] 4wt% La_2O_3, [b] 8wt% La_2O_3, [c] 12wt% La_2O_3, [d] Co/Ni= 0.025, [e] Co/Ni= 0.25

Medrano *et al.* [58] calcined their synthesized Ni/Al catalysts by air at 750°C, 850°C and 900°C before reduction by hydrogen. Then, the catalyst was reduced in situ by a flow of 10% hydrogen at 650°C for 1h. The highest calcination temperature resulted in the lowest carbon conversion (i.e. 87.15% for calcinations at 900°C compared to 98.87% for calcinations at 750°C) and yield of hydrogen (i.e. 0.106 g/g of acetic acid for calcinations at 900°C compared to 0.130 g/g of acetic acid for calcinations at 750°C). Results from experiments conducted for 2h showed that yield of product gases and total carbon conversion were similar and almost constant versus time with the catalysts calcined at 750°C and 850°C; however, with the catalyst calcined at 900°C, although they were initially similar to the yields obtained by other two catalysts, yields of hydrogen and carbon dioxide were decreased versus time from 0.13 g/g to 0.07 g/g and from 1.2g/g to about 0.9 g/g, respectively whereas yield of CO was increased versus time from 0.10g/g to about 0.25g/g and then was decreased to a stable yield of 0.18g/g. In addition, total carbon conversion was dropped versus time from 100% to about 80%. These observations indicate that the catalyst calcined at 900°C was not as active as the other two catalysts to drive the water gas shift reaction to increase production of hydrogen and CO_2 because less free Ni metals were likely available on the surface of the catalyst due to high calcinations temperature.

Following their research on steam reforming of acetic acid and acetol in a fluidized bed reactor with Ni/Al catalysts, Medrano *et al.* [77] investigated the effect of magnesium and calcium as promoters on the Ni/Al catalyst. They realized that loading these promoters improves attrition resistant of the catalyst in the fluidized bed reactor. When the molar ratio of magnesium over aluminum content on the catalyst was more than 0.12, no catalyst deactivation was observed. The Mg/Al molar ratio of 0.26 resulted in maximum yield of hydrogen (0.1158g/g) and carbon conversion (99.85%) during 2h steam reforming of acetic acid. However, presence of Ca on the catalyst increased production of CO and methane and caused less carbon conversion and hydrogen yield for both acetic acid and acetol. For example, during steam reforming of acetic acid, with molar Ca/Al ratio of 0.26, yield of hydrogen was 0.086 g/g and carbon conversion was 78.73%.

Vagia and Lemonidou [59] synthesized a variety of catalysts with 5wt% nickel and 0.5wt% noble metals (Rh and Ir) on two supports of calcium aluminates ($CaO.2Al_2O_3$ and $12CaO.7Al_2O_3$) to investigate the effect of the active metal and the support composition on hydrogen yield and coke deposition for steam reforming of the acetic acid and acetone. The catalysts were reduced at 750°C for 1hr with 25% hydrogen flow after synthesis and calcination with air at 600°C and 900°C for 4hr and 6hr, respectively. Results of steam reforming with the calcium aluminate support (without active metals on the support) at 750°C with molar S/C ratio of 3 showed that conversion of acetic acid was raised to about 45% at the first hour, but it declined to about 20% at the third hour. For the case of acetone, the conversion was 90% initially, but it was about 70% after three hours. In general, a decreasing trend versus time was observed for the production of gases. Yield of hydrogen was between 10% and 2% for acetic acid (14% in thermal cracking) and between 40% and 25% for acetone (9% in thermal cracking).

CO_2 and CH_4 were the main product gases of acetic acid steam reforming and CH_4 and CO were the main gases of the acetone steam reforming.

Steam reforming of acetic acid between 550°C and750°C with molar S/C ratio of 3 with 5wt% and 10wt% loads of nickel on the $CaO.2Al_2O_3$ and 12CaO.7Al2O3 supports revealed that conversion of acetic acid and yield of hydrogen was higher with larger mass of nickel, especially, when the support is the $CaO.2Al_2O_3$ (conversion of acetic acid was 100% and yield of hydrogen was 90% at 650°C and 750°C). During 1h of each test, no catalyst deactivation was observed. The lower observed activity of the catalyst with the support of $12CaO.7Al_2O_3$ was due to the less reducibility of Ni^{+2} because more nickel particles were incorporated in the bulk of the $12CaO.7Al_2O_3$. It was notable that CO_2/CO ratio increased by load of nickel which shows its influence on the water gas shift reaction. Estimation of coke formation (mol/mol of C in acetic acid) was conducted by CHN elemental analyzer. Although nickel catalysts led to the highest conversion of acetic acid, more coke was also produced even compared to thermal cracking results in which acetic acid is partly decomposed to solid carbon (0.28, 0.1, 0.18 and 0.03 for 10wt%Ni/Ca2Al, 5wt%Ni/Ca2Al, 5wt%Ni/12Ca7Al and quartz, respectively).

Steam reforming of acetone at 550°C-750°C with molar S/C ratio of 3 with 5wt%Ni/$Ca2Al_2O_3$ and 0.5wt%Rh/ $Ca2Al_2O_3$ resulted in 100% conversion of acetone at 750°C. However, Ru showed better catalytic activity to increase yield of hydrogen: considering much lower load of the Ru than that of the Ni, yield of hydrogen was 82% with Rh while it was about 70% with Ni. Composition of methane was about 10% with nickel but it was about 1% with Ru. However, a similar amount of coke was formed with two catalysts (0.03 mol/mol of C in acetone).

Davidian *et al.* [60,61] used two nickel based catalysts and some noble metal based (Pt, Rh, Ru and Pd) catalysts for catalytic gasification of acetic acid on their proposed cracking/regeneration system without injecting steam: a laboratorial 10wt% Ni/Al_2O_3 catalyst and a commercial 4wt%Ni.2wt% K/La_2O_3-Al_2O_3 catalyst as well as catalysts with 1 wt% of the noble metal supported on Al_2O_3. The nickel based catalysts were reduced with a flow of 30% hydrogen (100ml/min) at 650°C for 1h. The reduction temperature for the noble based catalysts was 350°C while flow and composition of hydrogen was similar. During the experiments, mass of the catalyst was 200mg and flow rate of the acetic acid was 100ml/min (5vol% acetic acid in argon). Their initial tests of activity evaluation of the catalysts showed that conversion of acetic acid increased and yield of hydrogen was closer to equilibrium condition with the nickel based catalysts over the temperature range of 600°C-800°C compared to noble based catalysts.

Experiments with catalytic cracking/regeneration cycles of acetic acid at 700°C using the commercial nickel catalyst revealed that after 18 minutes of the cracking step, production of CH_4 was increased and a trace of acetone was detected among the product gases, which was an indication of catalyst deactivation after that period of time. So, they set cracking step to be conducted for 15 minutes, then after purging the gases by argon, regeneration step started in the reactor by a flow of oxygen. Comparison of the product gases composition at different temperatures with the Ni/Al_2O_3 catalyst showed that less hydrogen and a larger ratio of CO/CO_2 was obtained at higher temperatures. This could be due to a lack of required steam to drive the water gas shift reaction towards hydrogen production. They reported that carbon deposition on the surface of the Ni/Al_2O_3 catalyst which was measured by the amount of CO and CO_2 produced during the regeneration step was less at higher temperatures. The nickel based catalysts showed a satisfactory level of stable activity over investigated temperatures because production of gases was reproducible at each cycle of the cracking/regeneration. However, the commercial catalyst had more selectivity towards hydrogen and better resistance against coke formation which should be due to the presence of K and La promoters on the commercial catalyst. Due to less Ni content on the commercial catalyst compared to the synthesized one, a little more methane was seen with the commercial catalyst.

They investigated the required amount of oxygen for the regeneration steps by using inert gas flows containing 5% to 20% of oxygen. Larger content of oxygen led to faster regeneration, a higher CO_2/CO ratio and greater temperature increase; however, regeneration step took less than 1 minute for all tested oxygen mixtures.

Davidian *et al.* [60, 61] also studied reduction and oxidation of the nickel catalysts comprehensively during cracking/regeneration cycles of the catalytic acetic acid cracking at 700°C. Their experimental results had shown that the production rate of gases at each cracking step was similar. Whereas, the catalyst was expected to be less active after each regeneration step due to conversion of Ni^0 on the catalyst to NiO. They conducted transient isotopic experiments on their cracking/regeneration system and used $^{18}O_2$ instead of $^{16}O_2$. They prepared samples of the fresh, coked, regenerated and re-reduced laboratorial 10wt% Ni/Al_2O_3 and commercial 4wt%Ni.2wt% K/La_2O_3-Al_2O_3 catalysts to screen and measure Ni^0 and NiO on their surfaces at different conditions. The results of their screening process revealed that there was a larger fraction of Ni^0 present on the catalysts at the end of the cracking step compared to a freshly reduced catalyst (49wt% vs 16% for Ni/Al_2O_3 and 92% vs 79% for $Ni.K/La_2O_3$-Al_2O_3) which means the nickel in the bulk spinal is extracted progressively during cracking steps. Also, they found out that there is an in-situ reduction mechanism for Ni during each cracking step because the deposited carbon and CO react with NiO at the beginning of the cracking step like an in-situ reduction of Ni during each cracking step:

$$C_{(s)} + 2NiO \rightarrow CO_2 + Ni \tag{1.26}$$

$$CO + NiO \rightarrow CO_2 + Ni \tag{1.27}$$

In addition, initial produced hydrogen reduces NiO by reacting with its oxygen and converting to H_2O. It is noteworthy that during the regeneration step, the catalyst is fully oxidized and there is an abundance of NiO on the catalysts while there is a very low fraction of Ni^0 on the surface of both commercial and laboratorial catalysts. The mechanism of reduction/oxidation of the nickel catalysts during the cracking/regeneration process of the acetic acid cracking is summarized in Figure 1.11:

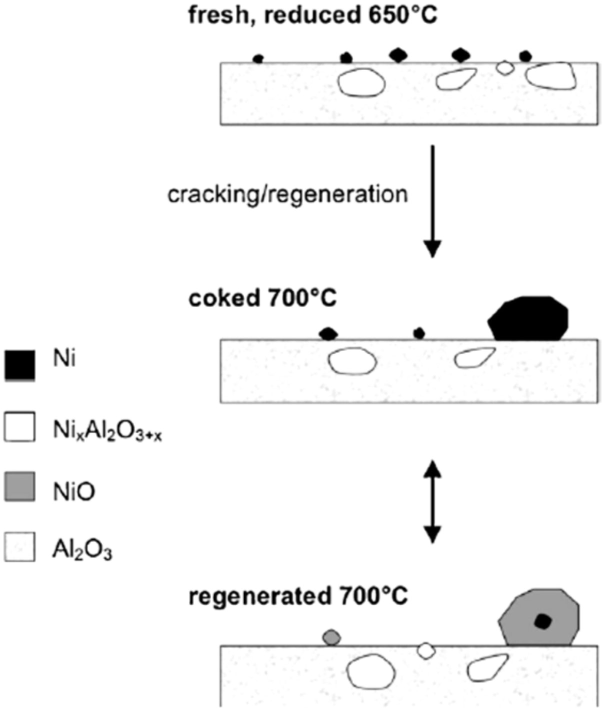

Figure 1.11. **Schematic structural evolution of Ni/Al_2O_3 catalyst during repeated cracking/regeneration sequences taken from [60]**

1.3.2.2. Bio-oil

Garcia *et al.* [62] performed catalytic experiments of the aqueous fraction of bio-oil with nickel based commercial and synthesized catalysts supported with α-Al_2O_3 (Table 1.19).

The synthesized catalysts contained magnesium, lanthanum, cobalt and chromium other than nickel because:

- Magnesium has the advantage of enhancing steam adsorption on catalyst and minimizing the catalyst sintering.
- Lanthanum decreases carbon formation on the surface of catalyst and improves stability of the catalyst.
- Chromium improves stability of Ni/Al_2O_3 catalyst, but does not increase activity of the catalyst
- Cobalt has more activity than nickel and helps to resist against deactivation of the Ni/Al_2O_3 catalysts by reducing the formation of the filamental carbon on the catalyst.

***Table 1.19.* Commercial and laboratory catalysts and surface areas. Adapted from [62]**

Catalyst	Surface area, (m^2/g)
Carrier G-90 (α-Al_2O_3)	2.5
G-91	16.0
ICI 46-1	12.8
ICI 46-4	11.8
C11-NK	17.7
Ni/Al_2O_3	2.7
Ni/MgO-Al_2O_3	3.1
Ni/MgO-La_2O_3-Al_2O_3	3.6
Ni-Co/MgO-La_2O_3-Al_2O_3	4.1
Ni-Cr/MgO-La_2O_3-Al_2O_3	4.9
MgO-Al_2O_3	2.9
MgO-La_2O_3-Al_2O_3	3.1

To measure the effectiveness of the synthesized catalysts and commercial nickel based catalysts, similar steam reforming reactions were carried out with the Ni/Al_2O_3 catalyst as the reference catalyst. Yield of hydrogen versus time as a function of the catalyst composition is illustrated in Figure 1.12 for commercial and synthesized catalysts during 25 minutes. Deactivation of catalyst versus time is very clear because the yield of hydrogen has a reducing trend. However, the reference catalyst caused the lowest yield of hydrogen. Therefore, it was concluded that modifications to the reference catalyst had a significant effect to reduce the deactivation of the catalyst over the time. After 25 minutes of the operation, hydrogen yield was decreased from about 80%-90% to 65% and 55% by commercial catalysts and research catalysts, respectively. This difference which is a measure for the effectiveness of the catalysts was claimed to be due to the larger surface area and lower Ni/Al ratio on the surface of commercial catalysts because either of these reasons increases steam adsorption on the catalyst, then steam reacts with carbon deposits on the catalyst surface. In between the synthesized catalysts, the Ni-Co/MgO-La_2O_3-Al_2O_3 and Ni-Cr/MgO-La_2O_3-Al_2O_3 catalysts showed the best performance regarding the yield of hydrogen.

Effectiveness of the commercial and synthesized catalysts on the conversion of bio-oil to total CO and CO_2 was found to be similar to the trend observed for the yield of hydrogen.

Since catalysts were not capable of being stable for a long enough production time, researches suggested regeneration-reduction of the catalysts must be carried out frequently during the operation.

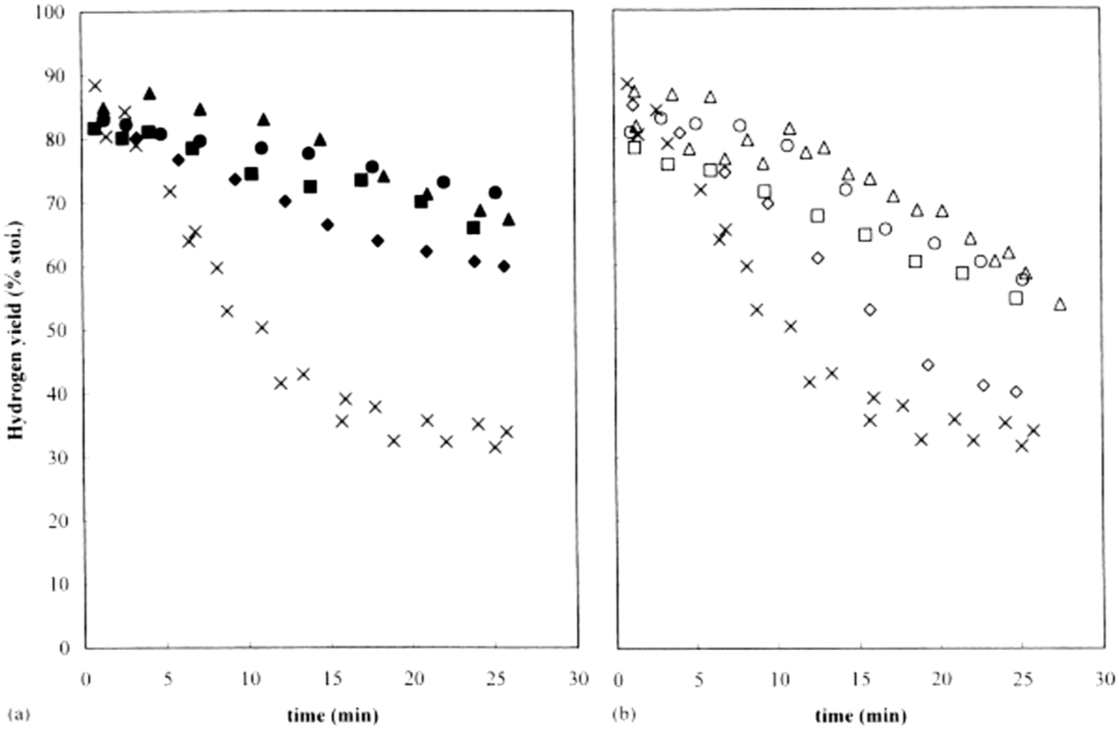

Figure 1.12. **Hydrogen yield obtained by catalytic steam reforming of bio-oil aqueous fraction. Reference catalyst: ×; (a) commercial catalysts; (b) research catalysts; T=825°C, S/C= 4.92, $G_{C1}HSV= 126000\ h^{-1}$. Taken from [62]**

Due to the fact that production of hydrogen from natural gas is more efficient than that from biomass in term of economy, Czernik *et al.* [26] investigated co-reforming of bio-oil and natural gas which can be beneficial from an environment point of view. The aqueous phase of bio-oil mixed with water (molar S/C=4.6) and compressed natural gas were fed with rates of 45 L/min (STP) and 120 g/h, respectively at 850°C over 56 hours. As illustrated in Figure 1.13 that shows yield of hydrogen versus time, the operation mode was alternated between bio-oil steam reforming mode and co-feeding steam reforming mode. During the bio-oil steam reforming mode, the catalyst started to be deactivated because of excess steam, but after injecting natural gas during the co-feeding mode, activation of the catalyst was restored because of its reduction by high content of hydrogen in natural gas. The average yield of hydrogen was 80% of the stoichiometric value. It was claimed that 23% of the produced hydrogen was from bio-oil fraction and the rest was from natural gas.

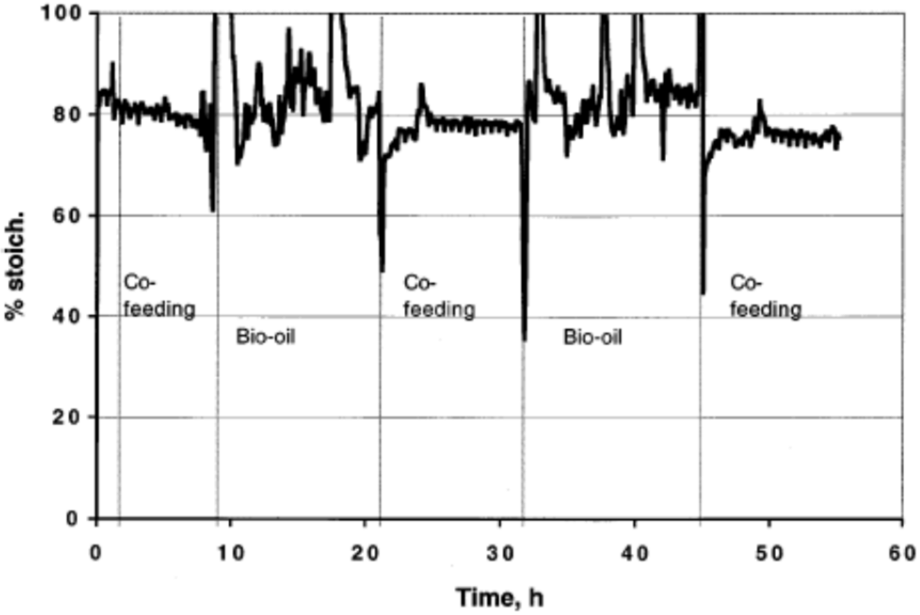

Figure 1.13. **Yield of hydrogen from co-reforming of bio-oil fraction with natural gas at 850°C, S/C=4.6 and $G_{C1}HSV=1000\ h^{-1}$. Taken from [26]**

Kechagiopoulos *et al.* [65] used the commercial nickel based catalyst (C11-NK) supplied from Sud-Chemie for catalytic steam reforming of bio-oil aqueous fraction and also catalytic steam reforming of an equimolar mixture of acetic acid, acetone and ethylene glycol. The catalyst was crushed and sieved to the size distribution of 180µm-500µm and then was reduced by hydrogen in-situ at 750°C for 1 h before starting the reaction. TGA-DSC was used to examine deposited coke on the catalyst. Catalysts were also burned in-situ by air at 700°C to estimate the amount of coke by measuring the released CO and CO_2. Steam reforming of the model compounds mixture resulted in product gases with compositions very close to the equilibrium composition. The yield of hydrogen was above 80% of the stoichiometric value at all temperatures and molar S/C ratios. CO/CO_2 ratio was increased versus temperature whereas this ratio was decreased versus molar S/C ratio which presents effect of water gas shift reaction. According to Figure 1.14, an extended run of steam reforming of the model compounds mixture showed that the catalyst was stable for the first 4h as the hydrogen yield was constant, but then the catalyst started to be deactivated until its activity was lost after 17h. As shown in Figure 1.14, although carbon to gas conversion was reduced over time, the molar concentration of the gases did not change.

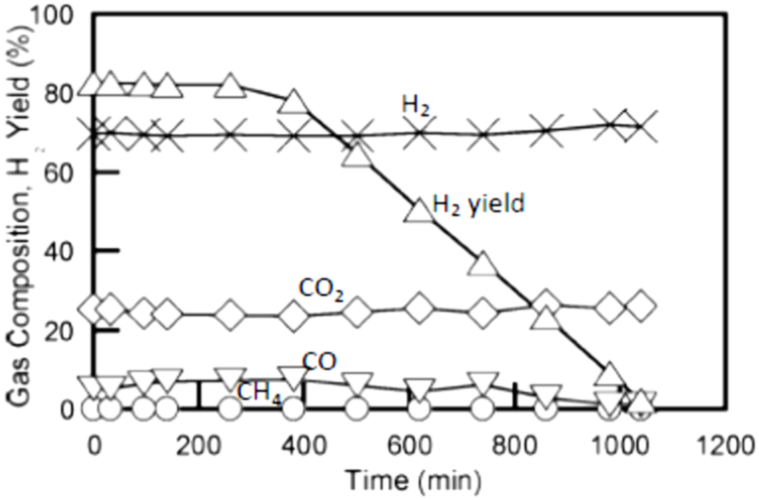

Figure 1.14. **Time-dependent concentration profiles (% mole fraction) and H_2 yield (% stoichiometric) during reforming of the three component mixture at 750°C and $H_2O/C=6$. Taken from [65]**

Non-catalytic gasification of the bio-oil solution at temperatures between 650°C-900°C resulted in carbon conversion from 12% at 650°C to 60% at 850°C and about 12%-20% of the inlet carbon was deposited inside the reactor. Hydrogen production was very low and could not be detected by the used GC. According to Figure 1.15, the maximum attainable hydrogen yield during the catalytic gasification of bio-oil solution was about 60% of the stoichiometric value which was far from the equilibrium yield (90%). Due to the fact that the yield of hydrogen during the catalytic steam reforming of the model compounds mixture was at equilibrium, this difference was claimed to be because of increased coke deposition, 30wt%, on the surface of the catalyst during catalytic gasification of bio-oil solution. In addition, analyses of the deposited cokes on the catalyst samples revealed that structure of the coke from bio-oil solution gasification was aromatic while the structure of the coke from gasification of the model compounds mixture was graphitic.

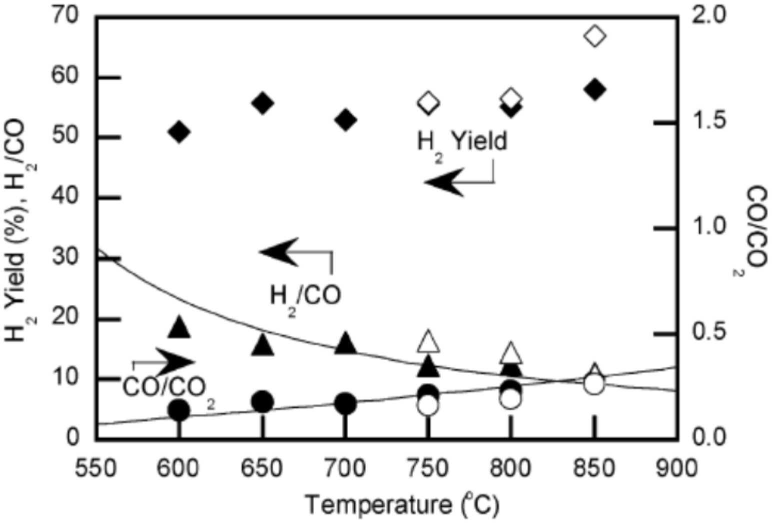

Figure 1.15. **Effect of reaction temperature on H_2 yield and gas proct compositions. Black symbols for GHSV=300 h^{-1} and White symbols for GHSV=600 h^{-1} .Taken from [65]**

It was commented by the researchers that their fixed bed reactor favored formation of the coke due to its limitations, in particular, for complex bio-oils. Thus, there should be a good and quick contact between molecules and catalysts to reduce the coke formation. Therefore, using a well-designed fluidized bed which facilitates internal gasification of coke with steam and carbon dioxide will be important. However, the catalyst must be capable of dealing with conditions inside a fluidized bed.

Davidian *et al.* [23] used 600mg of a synthesized 10 wt% Ni/Al_2O_3 catalyst and of the commercial 4wt%Ni-2wt%K/La_2O_3-Al_2O_3 catalyst from Johnson Matthey for the catalytic gasification of bio-oil in their cyclic cracking/regeneration system.

Figure 1.16 shows the rate of formation of product gases as a function of time during one sequence of the proposed process of bio-oil gasification with Ni-K/La_2O_3-Al_2O_3 catalyst. They suggested that the operating condition could be adjusted so that there would be an equal timing between the cracking and the regeneration steps; then it would be feasible to use two parallel reactors where the cracking step would be conducted in one reactor while a catalyst could be regenerated in another reactor and vice versa.

Bio-oil cracking data at 700°C showed that the composition of hydrogen obtained by the commercial catalyst (49.2%) was higher than that by the synthesized catalyst (about 40%). In addition, a larger amount of CO and less amount of methane and CO_2 was produced by the commercial catalyst. Furthermore, the concentration of product gases obtained by the commercial catalyst was very close to the predicted equilibrium compositions. TPO analysis on the catalysts showed that although a similar amount of coke deposition was formed on both catalysts measured by TGA, the type of the carbons are different: bi-dimensional carbon covered the surface of the commercial catalysts whereas stable graphitized carbon whiskers were formed on the surface of the laboratorial catalyst.

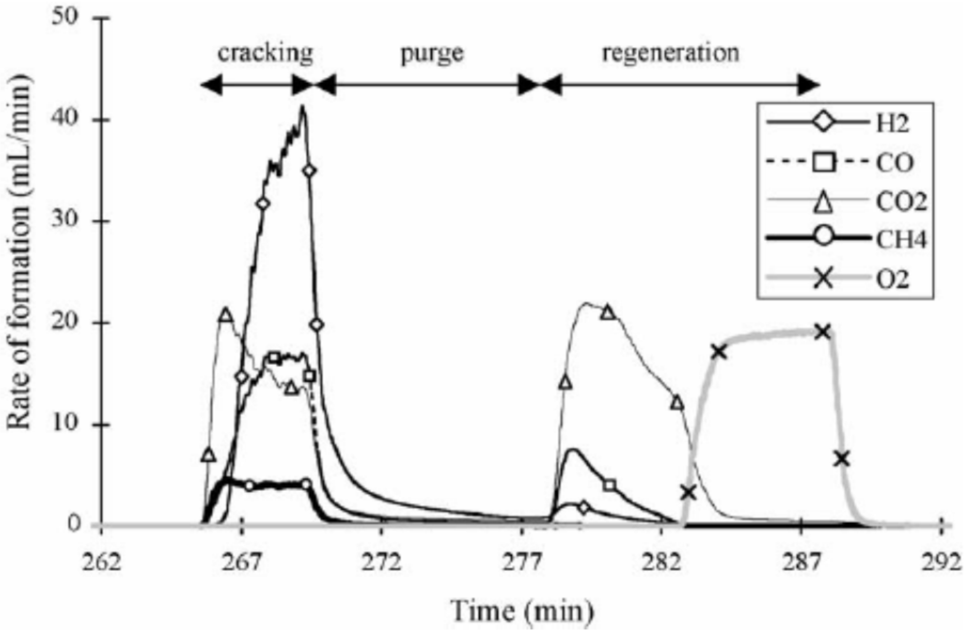

Figure 1.16. **Gaseous product formation during a single cracking/regeneration sequence on Ni-K/La_2-O_3-Al_2O_3 (600 mg catalyst, T= 700°C). Taken from [23]**

The heat of the cracking and regeneration steps were estimated with simulation of bio-oil composition ($CH_{2.3}O_{1.04}$) using model compounds: endothermic heat of the cracking step and exothermic heat of the regeneration step were estimated to be +1.22 kJ and -1.32 kJ; therefore, it was concluded that the heat released by combusting the carbon deposits can be used for reforming/cracking step to provide an autothermal process.

They also tested thermal cracking of bio-oil by injecting the bio-oil into a blank reactor to see the effects of a catalyst on syngas production:

Catalytic reactions compete with thermal cracking reactions and finally a product stream with higher hydrogen, CO and CO_2 and less methane is formed compared to when no catalyst is used.

Conversion of bio-oil to product gases is more when a catalyst is used while a significant portion of bio-oil is converted to coke/soot during the thermal cracking.

Regarding the regeneration of the catalyst, they have reported that NiO is formed on the surface of the catalyst, but after bio-oil is injected to the reactor, the catalyst is reduced by initial thermal decomposition products quickly (Ni^0 is formed on the surface) and then the catalyst works as a fresh catalyst in the process similar to their report for catalytic gasification of acetic acid [61].

Comparing the laboratorial catalyst and commercial steam reforming catalyst, both catalysts showed stable catalytic activity, but some Ni was lost from the surface of the laboratorial catalyst. They have reported the following reasons:

- Presence of K and La on the commercial catalyst prevents Ni to be sintered
- Load of Ni on the laboratorial catalysts was more, so not enough Ni^0 is probably formed after reduction.

The researchers proposed a reaction network of catalytic bio-oil gasification to syngas according to Figure 1.17: At first, bio-oil is decomposed thermally to the CO_2, H_2, CO, CH_4 , light hydrocarbons and soot-type carbon which can be 20% of the carbon in bio-oil, then due to water content of bio-oil and presence of CO_2, steam reforming, dry reforming and water gas shift reactions take place on the surface of the catalyst resulting in higher production of hydrogen and carbon monoxide. The type of the deposited carbon versus the type of catalyst was investigated: the Ni/Al_2O_3 catalyst forms whisker deposits while $Ni\text{-}K/La_2O_3\text{-}Al_2O_3$ catalyst forms amorphous deposits. Amorphous carbon is more active and can be removed by combustion at lower temperatures.

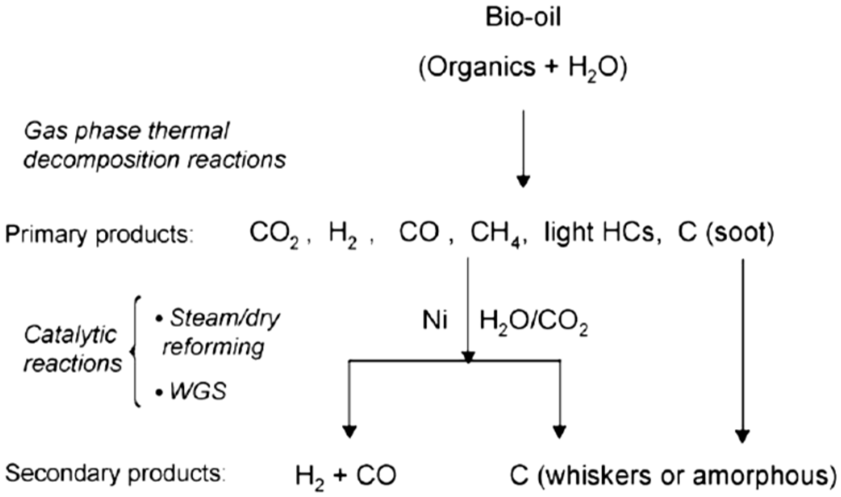
Bio-oil
(Organics + H_2O)
Gas phase thermal decomposition reactions
Primary products: CO_2, H_2, CO, CH_4, light HCs, C (soot)
Catalytic reactions
• Steam/dry reforming
• WGS
Ni
H_2O/CO_2
Secondary products: H_2 + CO
C (whiskers or amorphous)

***Figure 1.17.* Proposed reaction network during the bio-oil cracking . Taken from [23]**

Czernik *et al.* [66] used commercial and synthesized catalysts for catalytic steam reforming of bio-oil in a fluidized bed reactor. The naphtha steam reforming catalyst produced by Sud-Chemie (C11-NK) was crushed to the size distribution of 300µm-500 µm to be used in the fluidized bed reactor. They also synthesized four nickel based catalysts to compare their activity with the commercial one, but they did not report the composition of the catalysts. The catalyst bed was reduced by a flow of H_2/N_2 at the reaction temperature for 2 h before reforming.

The C11-NK catalyst showed great reforming results after 18 h because composition of the main products H_2, CO and CO_2 did not change significantly, 95% of the bio-oil carbon content was converted to the gases and the yield of hydrogen was about 94% of the stoichiometric value. However, due to attrition of the catalyst, catalyst loss of 1.1 wt%/h was observed.

The synthesized catalysts showed less activity compared to the C11-NK catalyst: the catalysts started to be deactivated faster and composition of the main product gases was not constant during 10 h runs. Also, yield of hydrogen was 70-80% of the stoichiometric value. They admitted that less nickel and the lower surface area of the synthesized catalysts compared to the C11-NK catalyst was the main reason to get less yield of hydrogen. On the other hand, the catalyst loss was 0.15 wt%/h which shows their synthesized catalyst has a superior attrition resistance.

Van Rossum *et al.* [67] used two nickel based catalysts for catalytic steam reforming of bio-oil and sand for non catalytic tests. The commercial nickel based catalysts were supplied by Johnson Matthey (K23 for methane reforming and K46 for naphtha reforming) and a fluidizable catalyst developed through an EU project (FB) which was composed of Ni-K/La on alumina were used for catalytic runs. The size distribution of the bed material was 200µm-300 µm. When the catalyst was the bed material, a flow of N_2/H_2 was maintained in the bed for 2hr at 500°C to activate the catalyst by reduction. After each experiment, alcohol was flushed to the reactor to clean the internal line of the feed nozzle and then a flow of steam or air was used to burn the deposited carbon on the surface of the bed material.

Results of the non-catalytic cracking of pine wood bio-oil showed that the composition of CO was larger than the composition of hydrogen, CO_2, CH_4 and C_2-C_3 hydrocarbons. However, concentrations of CH_4 and C_2-C_3 gases were considerably high. The carbon to gas conversion of 65% was achieved at 790°C and molar S/C ratio of 1.9. Their investigation showed that molar S/C ratio was not very effective to increase the carbon conversion. However, they realized that injecting additional oxygen into the reactor increases the carbon to gas conversion so that compositions of hydrogen and methane are lowered while those of CO and CO_2 are increased.

More production of hydrogen and CO_2 and less production of CH_4 and C_2-C_3 gases were achieved when catalysts were used as the bed material. Activity loss of the FB catalyst was the issue during the catalytic cracking experiments; the catalyst had initial activity, but its activity dropped by time until it reached stability after 1hr. Table 1.20 compares results of a catalytic cracking of bio-oil when a catalyst was fresh and when a catalyst was used after 1hr.

***Table 1.20.* Effect of catalytic activity on the concentration of product gases. Adapted from [67]**

	H_2	CO	CH_4	CO_2	C_2-C_3
Fresh catalyst	62.7%	14.3%	1.9%	20.9%	0.2%
Catalyst after 1hr	54.5%	11%	7.5%	23.7%	1.1%

After each experiment, steam was added to the bed of the catalyst to partly gasify the deposited carbon and then air was used to burn off the carbonaceous materials completely and to reactivate the catalyst. Although the catalyst was reactivated, its activity dropped again after a while. After many reactivation cycles, the catalyst reached an equilibrium activity after which its initial activity did not drop after reactivation. The problem of initial activity loss was also observed with commercial steam reforming catalysts (K43 and 46), but it was very gradual by time. Having the equilibrium catalyst of FB, conversion of bio-oil to product gases increased by temperature. Also, C_2-C_3 gases were decreased significantly. However, the catalyst was unable to minimize production of methane and secondary and tertiary tars. They changed the mass of the catalyst between 4 and 9 kg, but results were similar. As a result, they have proposed a fixed bed reactor should be used loaded by active commercial steam reforming catalysts after the fluidized bed gasification reactor to convert methane and tars to permanent gases and obtain a clean syngas with the lowest amount of tars.

Sakaguchi *et al.* [71] used a commercial naphtha steam reforming catalyst, RK-212, supplied from Haldor-Topsoe for catalytic experiments and silica sand for non-catalytic experiments of bio-oil and bio-oil/bio-char slurry. Size distribution of the solid particles was 180µm-355µm. Compositions of the catalyst and sand are listed in the Table 1.21.

Table 1.21. **Metal Analysis of the Catalyst (RK-212) and the Sand. Adapted from [71]**

	RK-212	sand	unit
Al2O3	60.99	0.64	wt%
CaO	3.36	0.04	
Fe2O3	0.15	0.15	
K2O	1.32	0.27	
MgO	13.98	0.02	
MnO	<0.01	<0.01	
Na2O	0.85	0.08	
P2O5	0.04	0.01	
SO3	0.14	0.01	
SiO2	2.50	98.14	
TiO2	0.01	0.05	
Ni	140200	41	ppm(wt)
Ba, V, Cr, Sr	569	187	
LOI at 1000°C	2.00	0.26	wt%
SUM	99.36	99.67	wt%

According to Figure 1.18a and 1.18b, the maximum carbon conversion for the production of CO, CO_2, CH_4, and C_2-C_4 in the thermal cracking runs was less than 70% at 832°C while carbon conversion of about 90% was achieved in the catalytic experiments at 725°C. In addition, composition of produced CO at thermal cracking experiments was significantly larger than composition of CO_2 whereas CO_2 constituted the largest carbonaceous product gas at the catalytic runs. Production of hydrogen compared to other hydrogen containing gases (CH_4, C_2-C_4) was not significantly different at thermal cracking experiments conducted at temperatures between 747°C and 832°C, but it was almost 4 times as high as that during catalytic experiments at temperature of 773°C.

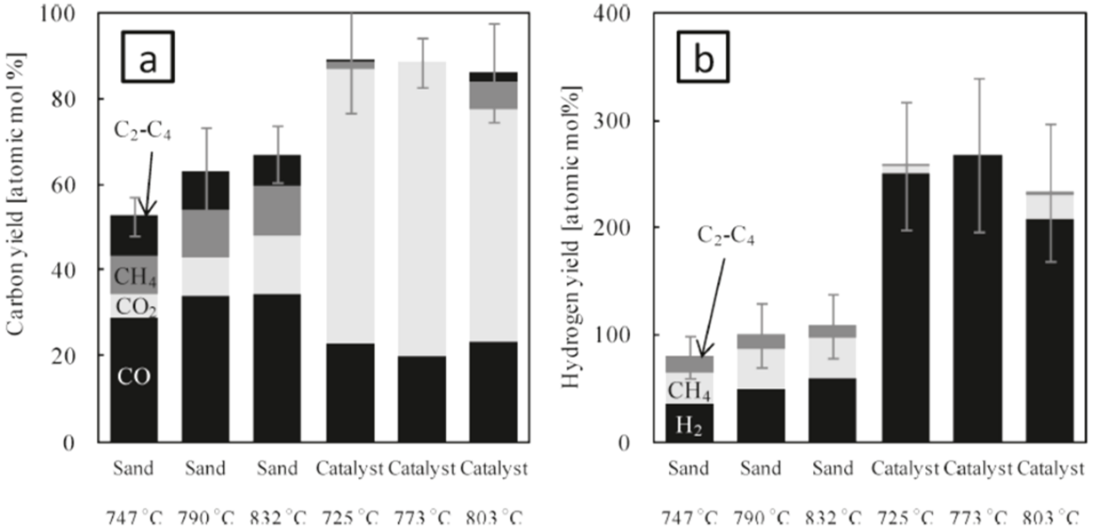

Figure 1.18. **Effect of catalysis on (a) carbon yield (mol %, atomic) as CO, CO_2, CH_4, and hydrocarbons (C_2-C_4) and (b) hydrogen yield (mol %, atomic) as H_2, CH_4, and hydrocarbons (C_2-C_4) on the dry feed stock basis; under steam gasification, $H_2O/C \approx 5.5$, and GC1HSV ≈ 340 h^{-1}. Taken from [71]**

Comparison of the gasification results of the bio-oil and of the bio-oil/bio-char slurry (Figure 1.19a and 1.19b) shows that bio-oil is converted to product gases more than the bio-oil/bio-char mixture is during catalytic cracking experiments. However, the catalyst also had a significant role to increase conversion of the bio-oil/bio-char mixture compared to similar operating conditions of the thermal cracking of the bio-oil/bio-char slurry.

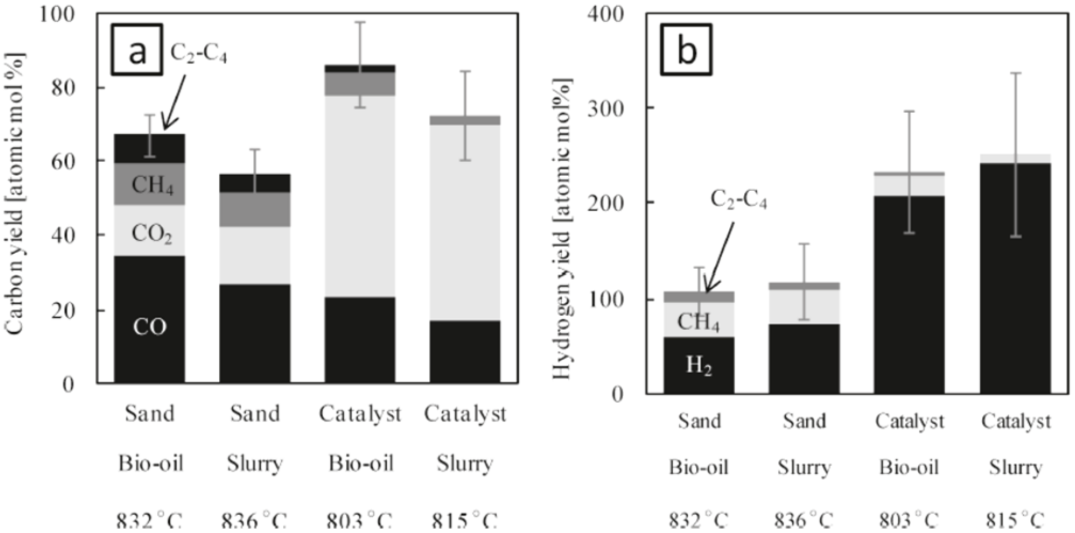

Figure 1.19. **Comparison of feedstock under catalytic and noncatalytic steam gasification on (a) carbon yield (mol %, atomic) as CO, CO_2, CH_4, and hydrocarbons (C_2-C_4) and (b) hydrogen yield (mol %, atomic) as H_2, CH_4, and hydrocarbons (C_2-C_4) at $H_2O/C \approx 5.6$ and GC1HSV ≈ 320 h^{-1}. Taken from [71]**

They reported 3% catalyst loss and 1% sand loss from the reactor after 1 hr. Regarding the catalyst activity, they found out that carbon conversion was decreased from about 95% at 842°C to about 90% at 847°C after 250 min of run although the deposited coke was burned four times by air after each run. Also, CO/CO_2 increased and yield of hydrogen declined to about 37%. In other words, regeneration of the catalyst by air was not enough after each run, and deactivation of the catalyst decreased the impact of the water gas shift reaction, so the catalyst must have been reduced by flow of hydrogen after regeneration by air.

Lan *et al.* [73] synthesized a catalyst with formulation of 18wt%Ni/10wt%MgO-10wt%La_2O_3-Al_2O_3 for catalytic gasification of the rice husk bio-oil in the fixed bed and in the fluid bed reactors. The catalyst was reduced by a 5 vol% flow of hydrogen at 700°C before starting the tests. Yields of hydrogen, CO and CO_2 were increased in both reactors with temperature while the yield of CH_4 was decreasing. The maximum yield of hydrogen and carbon to gas conversion were about 50% and 80% at 950°C in the fixed bed reactor (molar S/C=5) while they were about 60% and 95% at 800°C in the fluid bed (molar S/C=15). In other words, the fluidized bed reactor provided better mixing and catalytic contact to gain higher yield at lower temperatures. The carbon content on the surface of the catalyst was estimated by thermogravimetry. The carbon deposition was decreased by temperature; however, at similar temperatures, the amount of the produced coke in the fluid bed reactor was less than that in the fixed bed reactor. For example, at 650°C, carbon content of the catalyst was about 2.35 wt% in the fixed bed reactor and about 0.7 wt% in the fluid bed.

Medrano *et al.* [74] prepared Ni/Al catalysts with Mg (Mg/Al molar ratio of 0.26) and Ca (Ca/Al molar ratios of 0.12) promoters for catalytic steam reforming of pine wood bio-oil. The catalysts were calcined at 750°C for 3hr and then reduced by 10vol% hydrogen at 650°C for 1 h.

The magnesium added Ni/Al catalyst resulted in the highest carbon to gas conversion (81.01%) compared to the Ni/Al catalyst (73.5%) and the Calcium added Ni/Al catalyst (65.78%) at 650°C. The yield of hydrogen had similar trends with the catalysts: 0.1065, 0.0965 and 0.0774, respectively (g/g of oil). Although the Ca/Ni/Al catalyst showed the poorest gasification activity, the lowest carbon deposition was formed in comparison with the Ni/Al and Mg/Ni/Al catalysts: 141, 174 and 162, respectively (mg of C/g of catalyst).

Regardless of the type of catalyst, the production rate of the gases was not constant versus time: yield of hydrogen and CO_2 had a reducing trend while yield of CO and CH_4 had an increasing trend. However, the trend of carbon deposition was almost constant. This trend of catalyst activity loss shows the effect of the carbon deposition on the catalyst surface.

They increased the mass of magnesium catalyst twice as high as initial tests: the carbon conversion did not significantly increase (from 81.01% to 83.26%). On the other hand, the yield of hydrogen and CO_2 were raised a little bit: from 0.1056 to 0.1328 for hydrogen and from 0.8961 to 1.1469 for CO_2 (g/g of oil) while the yields of CO, methane and C_2 were decreased. Therefore, the additional mass of the catalyst favored a water gas shift reaction and steam reforming of the hydrocarbons. Also, carbon deposition was reduced from 162 to only 149 (mg of C/g of catalyst). The trends of production rate of the gases were moderated by using additional catalysts; however, they were not still constant versus time.

Seyedeyn-Azad *et al.* [75] synthesized Ni/Al_2O_3 catalysts containing nickel between 0 and 18 wt% for catalytic steam reforming of bio-oil. Before each experiment, the catalyst was reduced by a 400STP ml/min flow of 50 vol% hydrogen at 850°C for 1hr. Due to slow pulsed mechanism of the feed injection, composition of the product gases versus time was very fluctuating, so they had to consider the average value of their data to compare the effect of tested parameters. Testing the catalyst at 850°C and molar S/C=5 for a period of 1hr showed that the catalyst with 14.1 wt% nickel was the best catalyst in terms of higher total carbon to gas conversion, production of hydrogen and CO_2 and lower production of CO and hydrocarbons. The maximum carbon to gas conversion at such operating conditions though was about 70%-75%. Tests with longer runs revealed that the best catalyst tended to become significantly deactivated after 1 h.

1.3.2.3. Summary

Hydrogen yield and carbon conversion increases drastically in the presence of an appropriate catalyst in the reactor. Nickel based catalysts have been the most common used catalysts, in particular, with the alumina based supports in steam reforming/gasification of the bio-oil and its model compounds. However, formation of coke on the surface of such catalysts, which causes catalyst deactivation, is a major issue. The type of the coke differs depending on the type of feed, catalyst composition and reactor (fixed bed or fluidized bed). Reports from steam reforming of the bio-oil model compounds reveal that promoters such as Mg, Ca, La and Co help to minimize the coke deposition and to stabilize performance of the catalyst; on the other hand, each promoter has a different effect. Noble metals also showed very good activities with less mass compared to nickel in terms of less coke deposition and larger hydrogen yield and carbon conversion; however, they are expensive. Other than the active metal, the type of the catalyst support can also influence the yield of syngas and the carbon conversion.

The mass fraction of the active metal is important to increase activity of the catalyst; for instance, a large mass fraction of the active metal can prevent its sufficient reducibility, which is required to become an activate catalyst.

Although different catalysts have been synthesized in the labs to maximize hydrogen yield and carbon conversion and minimize coke deposition and production of hydrocarbons, the commercial catalysts have shown better activities than the laboratorial catalysts. Despite some success in development of stable catalysts, stability of the synthesized catalysts have been poor for the long experimental runs.

1.3.3. Effect of temperature

1.3.3.1. Bio-oil model compounds

According to Wang *et al.* [20], generally, it was observed that catalytic conversion of model compounds can reach 99% at temperatures above 600°C.

Rioche *et al.* [54] also reported that carbon conversion and yield of hydrogen increase with temperature, but in the absence of catalyst, yields are very low. They used inert cordierite fillers for non-catalytic tests for steam reforming of model compounds. As an example for non catalytic tests, highest conversion of acetic acid at 688°C and 779°C was 2% and 21% when molar S/C ratio was 5 and GHSV was $860h^{-1}$. Non catalytic ethanol conversion between 677°C and 770°C was constant at about 3% for molar S/C ratio of 3 and GHSV of $880h^{-1}$. It was also noticeable that methane was the main product gas of non catalytic tests. In other words, temperature increased conversion of the model compounds, but it is not enough to gain full conversions.

Non catalytic steam reforming of acetic acid conducted by Galdamez *et al.* [55] showed that although 100% carbon to gas conversion is achieved above 650°C, the composition of product gases was very far from the equilibrium conditions and yield of hydrogen was very low (0.052 g/g of AA compared to 0.120 g/g of AA at equilibrium at 700°C). It was noticeable that non catalytic conversion of acetic acid at 450°C was 8.05%. Composition of hydrogen and CO was increased versus temperature while composition of CO_2 and CH_4 had decreasing trends versus temperature; in other words, steam reforming of methane was favored at higher temperatures to produce hydrogen and CO.

Ramos *et al.* [57] carried out non catalytic steam reforming of acetol at 450°C-650°C with molar S/C=4.6. Conversion of acetol to product gases increased versus temperature from 36.9% at 450°C to 87.09% at 650°C. Interestingly, although the yield of product gases (g/g of acetol) increased versus temperature, the overall concentration of gases was almost similar: H_2 52%,

CH_4 10.5%, CO 32%, CO_2 3.5% and C_2 2%. Also, the concentrations were very far from predicted equilibrium conditions.

1.3.3.2. Bio-oil

Garcia *et al.* [62] conducted catalytic steam reforming of aqueous fraction of bio-oil at 825°C and 875°C, but they reported that temperature did not have an effect on the trend of yield of product gases obtained from different compositions of the tested catalysts.

Czernik *et al.* [26] found that, at 800°C, the yield of hydrogen decreased from 85% to 77% after 12 hours continuous reforming of bio-oil showing that catalyst particles were being deactivated by deposits of carbon. At 850°C and over 90 hours of steam reforming process, it was found that the yield of hydrogen had improved and reached 80% which is significant compared to the latter temperature. In addition to hydrogen, CO, CO_2 and small traces of methane and ethylene were produced. Methane formation was increased to 2.5% and then leveled off over the time showing that the catalyst was losing its activity. 90% of the feed carbon was converted to gas. The deposited carbon on the catalyst was minimal.

Van Rossum *et al.* [68] investigated different temperature configurations in their staged non catalytic fluid bed-catalytic fixed bed gasification setup to find optimum temperatures inside the reactor for maximum bio-oil conversion. The catalysts were not crushed. Their initial investigations showed that K23 and K46 catalysts had similar activities. They found out there should be enough load of catalyst in the fixed bed (5kg in their reactor) to completely convert the methane and C_2-C_3 to syngas. Therefore, three different temperature configurations in their reactor setup were investigated:

Fluid bed temperature and fixed bed temperatures at about 800 °C: the carbon content of the bio-oil is converted to coke, permanent gases and tars (primary, secondary and tertiary tars) in the fluid bed. Permanent gases and tars are converted to syngas in the catalytic fixed bed. At these conditions, a clean flow of syngas was produced.

Fluid bed temperature > 630°C and fixed bed temperature between 670°C and 830°C: the fixed bed temperature varied to find an optimum temperature at which carbon contents are fully converted to syngas. The optimum required temperature for this purpose was realized to be 800°C or higher. Concentration of product gases after the fixed bed was at equilibrium and no methane and C_2-C_3 were detected.

Fluid bed temperature between 430°C and 500°C and fixed bed temperatures between 530°C and 690°C: instead of converting to permanent gases, the bio-oil is initially converted mainly to a vapor containing primary tars in the fluidized bed reactor. Due to higher reactivity of the tars than hydrocarbons, they investigated an optimum low temperature in the fixed bed reactor. When the temperature of the fluidized bed was 496°C and the temperature of the fixed bed was 690°C, carbon to gas conversion and yield of hydrogen were obtained at larger values compared to when the fluid bed was 788°C and the fixed bed was 828°C. Although a very low production of methane was detected (0.1 vol%), the produced syngas was C_2-C_3 free. Table 1.22 illustrates the composition of the product gases according to the temperatures applied inside the reactors.

***Table 1.22*. Gasification results done at different temperatures of the staged system. Adapted from [68]**

Feed type	Pine	Pine
Liquid feed, kg/h	0.51	0.62
Bed type, sand fluid, kg	5.0	5.0
Inert fied, kg	3.6	3.6
K46 fixed, kg	5.0	5.0
K23 fixed, kg	0.0	0.0
T fluid bed, C	496	788
T fixed bed, C	690	828
S/C	2.6	2.2
Carbon to gas, %	70	61
H_2 yield, %	64	58
Gas production, Nm^3/kg		
H_2	1.28	1.16
CH_4	0.00	0.00
CO	0.28	0.25
CO_2	0.39	0.33
C_2-C_3	0.00	0.00
Gas composition, vol%		
H_2	63.8	62.7
CH_4	0.1	0.0
CO	14.0	13.7
CO_2	19.3	18.0
C_2-C_3	0.0	0.0

Seyedeyn-Azad *et al.* [75] conducted catalytic bio-oil steam reforming over temperatures between 650°C and 955°C with the 14.1wt% Ni/Al_2O_3 catalyst. Their result showed that yield of hydrogen and CO_2 increased by temperature which indicates an effect of the catalyst on the water gas shift reaction. Carbon to gas conversion of about 80% was reached at 955°C; however, traces of methane (2%-5%) were observed at all temperatures.

1.3.3.3. Summary

Hydrogen yield and carbon conversion increase with temperature; however, the extend of the effect depends on the presence of catalyst and on additional flows, such as steam. For instance, in addition to the effect of temperature, variation of CO/CO_2 ratio through the water gas shift reaction is highly influenced by the presence of catalyst and steam.

1.3.4. Effect of residence time and GHSV

1.3.4.1. Bio-oil model compounds

Wang *et al.* [20] varied residence time from 0.04s to 0.15s at 600°C and constant GHSV 1680 h^{-1} with UCI G-90C catalyst. Their result showed that residence time has no net effect on mole fraction of hydrogen in the product stream.

Medrano *et al.* [77] investigated the effect of gas hourly space velocity on catalytic steam reforming of acetol by increasing the mass of the Ni/Al catalyst. According to the data in Table 1.23, when GHSV decreased, carbon conversion of acetol increased from 26.36% to 100%. In addition, yield of hydrogen and CO_2 were increased while yield of CO and hydrocarbons were decreased. In other words, more mass of the catalyst which provided more catalyst-gas contact surface was very influential on activating the steam reforming of hydrocarbons and the water gas shift reaction in favor of higher production of hydrogen and CO_2.

***Table 1.23.* Experimental results of acetol steam reforming at 650 °C with Ni/Al catalyst, S/C=5.58, 2 h reaction time. Adapted [77]**

Run #	9	10	11	12	13
g catalyst min/g acetol	0	0.985	1.982	3.464	6.144
GHSV, h^{-1}	∞	51459	25561	14628	8247
Liquid feeding rate, ml/min	0.51	0.51	0.51	0.50	0.50
Carbon conversion, %	26.36	78.56	94.57	100.79	101.96
Total gas/ (acetol+water), g/g	0.047	0.216	0.299	0.343	0.352
Gas yields, g/g acetol					
H_2	0.0047	0.0822	0.1342	0.1624	0.1664
CO	0.1575	0.2950	0.2864	0.2685	0.2556
CO_2	0.0022	0.6047	1.0265	1.2739	1.3367
CH_4	0.0270	0.0378	0.0258	0.0180	0.0162
C_2H_4	0.0434	0.0631	0.0357	0.0119	0.0080
C_2H_6	0.0032	0.0105	0.0093	0.0051	0.0036
Gas composition, %					
H_2	20.53	58.32	64.58	66.85	67.02
CO	49.56	15.07	9.88	7.90	7.36
CO_2	0.44	19.51	22.44	23.84	24.48
CH_4	14.87	3.41	1.57	0.93	0.82
C_2H_4	13.61	3.20	1.23	0.35	0.23
C_2H_6	0.93	0.50	0.30	0.14	0.10

1.3.4.2. Bio-oil

To investigate the effect of residence time, Panigrahi *et al.* [63] changed the nitrogen flow rate as the carrier gas between 18 and 54 ml/min, while the bio-oil flow rate was 4.5g/h, In accordance with Table 1.21, at most tested temperatures, conversion of bio-oil increased with the nitrogen flow rate up to 30 ml/min while this trend was descending between 30ml/min and 42 ml/min. Flow rate of bio-oil between 42ml/min and 54 ml/min did not have significant effect on the bio-oil conversion. On the other hand, production of gases increased versus nitrogen flow rate at each temperature. For example, volume of product gases was raised from 400ml to 980ml at 600°C and from 900ml to 1780ml at 800°C (Table 1.24).

Table 1.24. **Conversion of bio-oil and Volume of Product Gas Formed over a Period of 30 min at different Temperatures and Nitrogen Flow Rates at bio-oil Flow Rate of 4.5 g/h. Adapted from [63]**

N2, ml/min	18		30		42		54	
Temp, °C	Conv., %	Prod.gas, ml	Conv., %	Prod.gas, Ml	Conv., %	Prod.gas, ml	Conv., %	Prod.gas, ml
650	48	500	57	730	60	740	62	980
700	60	820	75	900	60	950	59	1020
750	72	880	79	1020	68	1010	69	1200
800	76	900	83	1040	81	1140	80	17800

Interesting results were also reported for the effect of residence time (nitrogen flow rate) on the yield of the gases at 800°C: total concentration of syngas increased from 22% to 65% versus nitrogen flow rate from 18ml/min to 54ml/min. Production of methane at the longest residence time (nitrogen flow rate of 18ml/min) was about 30% while it reached about 22% at the shortest residence time. Production of ethylene and propylene was also reduced versus flow rate of nitrogen: 31.8% and 3.8% to 6.8% to 0.1% for ethylene and propylene, respectively; this can be due to secondary thermal decomposition of cellulosic and lignin fractions of bio-oil at the longest residence time at 800°C.

Sakaguchi *et al.* [71] investigated the effect of the GHSV on the thermal cracking of bio-oil. As it can be seen on Figures 1.20a and 1.20b, variation of the gas hourly space velocity did not significantly affect the yield of product gases during thermal cracking of bio-oil. They have not reported the effect of the $G_{C1}HSV$ on catalytic cracking experiments.

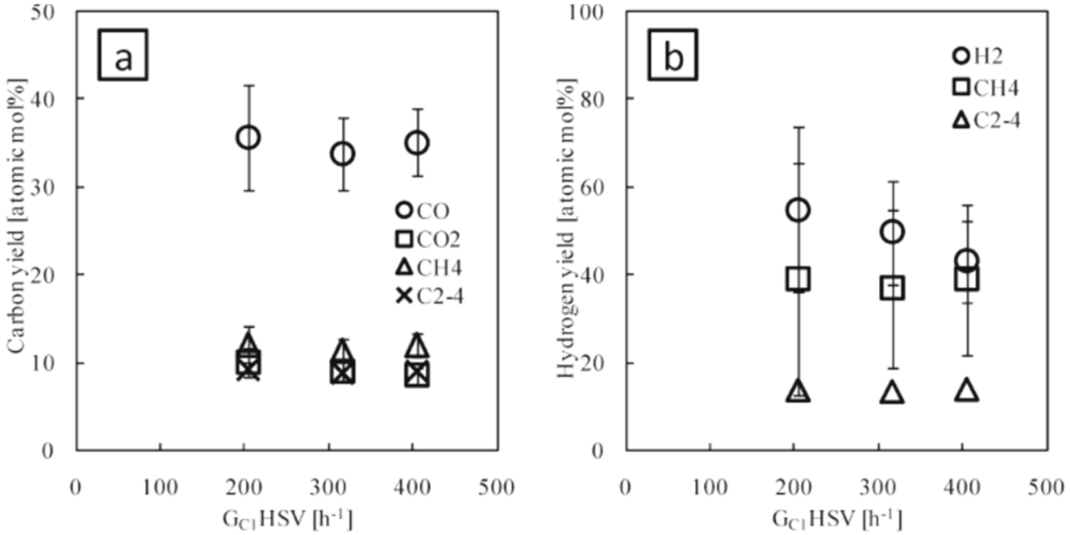

Figure 1.20. **Effect of space velocity on (a) carbon yield (mol %, atomic) as CO, CO_2, CH_4, and hydrocarbons (C_2-C_4) and (b) hydrogen yield (mol %, atomic) asH_2, CH_4, and hydrocarbons (C_2-C_4) on the dry feed stock basis at T ≈ 800°C and GHSV ≈ 320 h^{-1} under noncatalytic steam gasification. Taken from [71]**

Lan *et al.* [73] investigated the effect of the bio-oil flow rate on the gasification yield of the rice husk bio-oil: T=800°C and molar S/C=9 in the fixed bed reactor and T= 750°C and molar S/C=18 in the fluid bed reactor. According to the Figures 1.21a and 1.21b, due to effect of the bio-oil flow rate on shortening the residence time, in general, when flow rate is added up, yields of hydrogen and CO_2 were decreased, yield of CO was decreased and then became stable, yield of methane was raised and total carbon to gas conversion had a reducing trend.

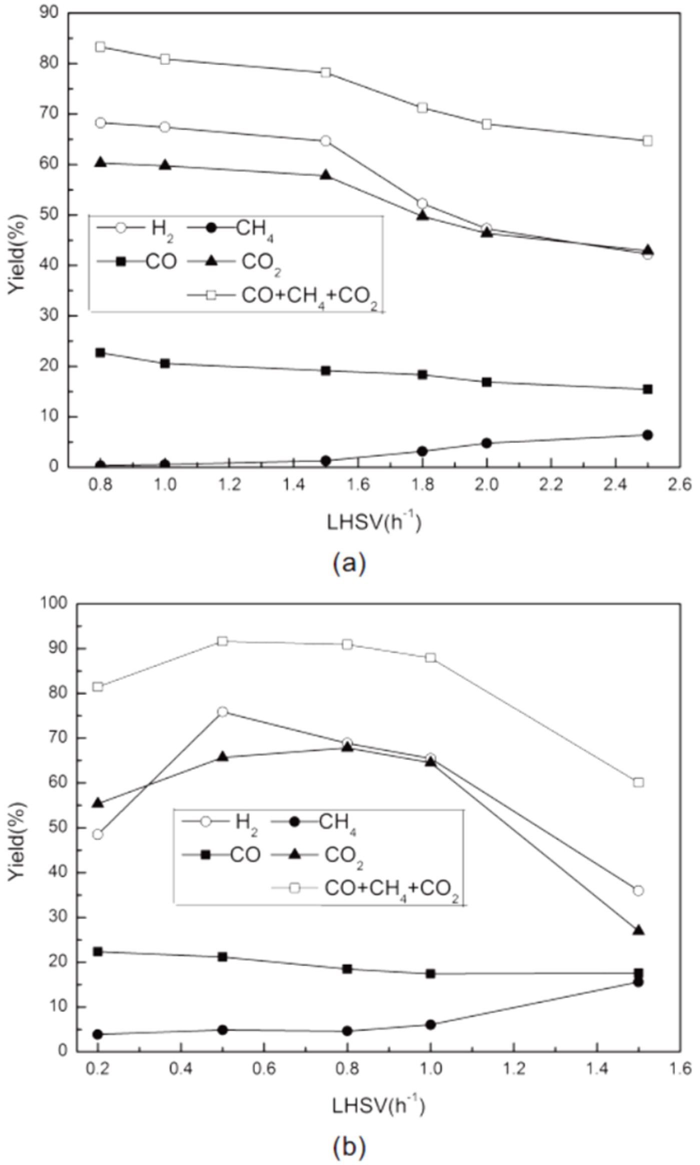

***Figure 1.21.* Steam reforming of bio-oil at different LHSV. (a) Fixed bed, experimental conditions: 1 g catalyst, T = 800 °C, S/C = 9.8, reaction time = 60 min. (b) Fluidized bed, experimental conditions: 100 g catalyst, T = 750 °C, S/C = 18, reaction time = 60 min. Taken from [73]**

Investigations by Seyedeyn-Azad *et al.* [75] for catalytic steam reforming of bio-oil showed that lowering the mass of catalyst caused a decrease in production of hydrogen and CO_2 as well as carbon to gas conversion; in addition, deposited coke on the surface of the catalyst was increased.

1.3.4.3. Summary

Different concepts of residence have been defined in literature: (1) flow rate of the total gas flow rate divided by volume of the reactor and (2) flow rate of feed divided by volume of the bed (catalyst or inert material) which is also definition of the GHSV.

Based on the first definition, there are very limited reports in literature which indicate either syngas yield and bio-oil conversion were not affected by residence time or they increased with shorter residence time.

Based on the second definition, larger gas hourly space velocity (either larger feed flow rate or less catalyst mass) causes less production of syngas and carbon conversion and rate of coke deposition is increased.

1.3.5. Effect of excess steam, hydrogen and CO_2

1.3.5.1. Bio-oil model compounds

Wang *et al.* [20] changed molar S/C ratio from 4.5 to 7.5 at 600°C and constant GHSV 1680 h^{-1} with UCI G-90C catalyst, but they found that molar S/C ratio has no net effect on mole fraction of hydrogen in product stream.

Marquevich *et al.* [53] showed that model compounds of bio-oil depending on their molecular structure and physical properties need different molar S/C ratios to be completely converted to product gases.

Catalytic tests of acetic acid were conducted between 500°C-750°C, molar S/C of 3 and 6 and GHSV of 67mol.h^{-1}.L^{-1} in the larger reactor and 244 and 232 67mol.h^{-1}.L^{-1} in the smaller reactor. Commercial nickel based UC G-90C catalyst manufactured by United Catalyst Inc was used for steam reforming of the acetic acid and aromatics and commercial nickel based ICI 46-1 catalyst manufactured by ICI Katalco was used for steam reforming of sugars. The catalysts were crushed and sieved for size distributions of 2.4mm-4.0mm or 1.0mm-2.0mm depending on the size of reactor. The catalysts were reduced in-situ at 600°C for 4h with a constant 0.8SLM flow of 50% hydrogen. Before each test of catalytic steam reforming of the sugars, the catalytic bed was regenerated by steam for 4h (12-15 g/min) to gasify deposited coke on the surface of catalysts from previous tests, and then it was reduced by flow of hydrogen with composition and flow similar to that used for fresh catalysts for 3h. When molar S/C ratio was 6, carbon conversion was 73% at 500°C but it was almost 100% at temperatures above 600°C in the larger reactor. However, maximum carbon conversion in the smaller reactor was about 95% at 750°C. Yield of hydrogen was increased versus temperature in both reactors but it was less than 80%. When molar S/C ratio was 3, carbon conversion was about 86% at all temperatures. This lower conversion can be attributed to the activity of the catalyst which could not reform all acetic acid because partial pressure of steam was lower. It is reported that concentration of gases at all operating conditions were very close to equilibrium concentrations.

m-Cresol catalytic steam reforming were carried out in the small reactor at 725°C, 800°C and 875°C with molar S/C ratio of 3 and 6 and GHSV of 8650h^{-1}. Carbon conversion was between 97% and 100% at all temperatures and molar S/C ratios. Stoichiometric yield of hydrogen was between 74%-77% for molar S/C ratio of 6 but it was between 67%-71% for molar S/C ratio of 3. On the other hand, concentrations of all gases were found to be very close to equilibrium at all operating conditions.

Benzyl ether experiments were conducted at operating conditions similar to those for m-Cresol but GHSV was 11800h^{-1}. Carbon conversion was 100% and stoichiometric yield of hydrogen was about 83% and 67% for molar S/C ratios of 6 and 3, respectively. Gas concentrations were close to equilibrium for molar S/C ratio of 6, but when molar S/C ratio was 3, concentrations of hydrogen and CO_2 were below the equilibrium while concentration of CO was above the equilibrium.

Catalytic steam reforming of sugars were conducted at high molar S/C ratios because they are pyrolysed upon injection into the reactor and char is formed, so high enough ratio of molar S/C which favors gasification of char was needed. Operating condition and results of steam reforming of glucose, xylose and sucrose are presented in Table 1.25. Glucose conversion at molar S/C ratio of 7 was 78% and it reached 98% with molar S/C ratio of 47. Xylose was converted to gases completely at all tested molar S/C ratios. However, Sucrose was very difficult to be converted to gas because its conversion was 88% at 835°C with molar S/C ratio of 34.

Table 1.25. **Steam Reforming of Mono- and Disaccharides Using the ICI 46/1 Catalyst; Experimental Conditions, Carbon Balance, and Hydrogen Yields. Adapted from [53]**

Sugar	S/C ratio, mol/mol	GHSV, h^{-1}	T, °C	Carbon balance, % of feed	H_2 yield, % of stoichiometric H_2
Glucose	47	717	843	98	82
	32	717	860	102	89
	17	627	897	92	80
	7	538	869	78	67
Xylose	37	806	787	100	84
	27	739	806	103	89
	14	739	860	105	90
Sucrose	34	851	835	88	72

Takanabe *et al.* [22] studied mechanism of steam reforming reactions of acetic acid on the Pt/ZrO_2 catalyst in a fixed bed reactor. The synthesized catalyst was reduced by a flow of 5% hydrogen in nitrogen at 775 K for 1h. Aqueous samples of acetic acid and acetone (molar S/C=5) were prepared for experiments at 625K .

They injected pulses of acetic acid with and without steam to find the role of steam in acetic acid reforming. It was discovered that steam has a clear role to react with and gasify the deposits on the surface of catalyst from the previous pulses; hence, the yield of hydrogen was almost similar for each pulse of injection whereas when pulses of acetic acid without steam was injected, the yield of hydrogen was reducing consequently at each pulse.

In order to investigate selective removal of carbon deposits on different catalysts, duration of catalysts activity, formation of hydroxyl groups by steam on the catalyst and probable secondary reactions, pulse injections of acetic acid and continuous steam reforming of acetic were conducted on different combination of catalysts (Pt/ZrO_2, and ZrO_2). Then, the nature of the deposited carbon was detected by TPO (temperature-programmed oxidation) measurements, and then it was burnt by oxygen to estimate the coke quantitatively. Finally, a bifunctional mechanism was proposed for steam reforming of the acetic acid on the Pt/ZrO_2 catalyst:

As illustrated in Figure 1.22, acetic acid is decomposed to acetate and acyl groups on the Pt. Then, these two groups are decomposed to CO_2, CO and CH_3 so that methyl groups adsorb hydrogen to form CH_4. Methyl groups, in addition, may be graphitized and oligomerized to block surface of Pt. On the other hand, steam gasifies methyl groups on Pt to form hydrogen and carbon dioxide because steam becomes activated on the surface of ZrO_2 to form hydroxyl groups; then, these groups react with methyl groups on the boundary between Pt and ZrO_2. Therefore, it was concluded that the boundary of catalyst is very important and in order to regenerate the catalyst, carbon removal from the boundary between Pt and ZrO_2 must be taken into account.

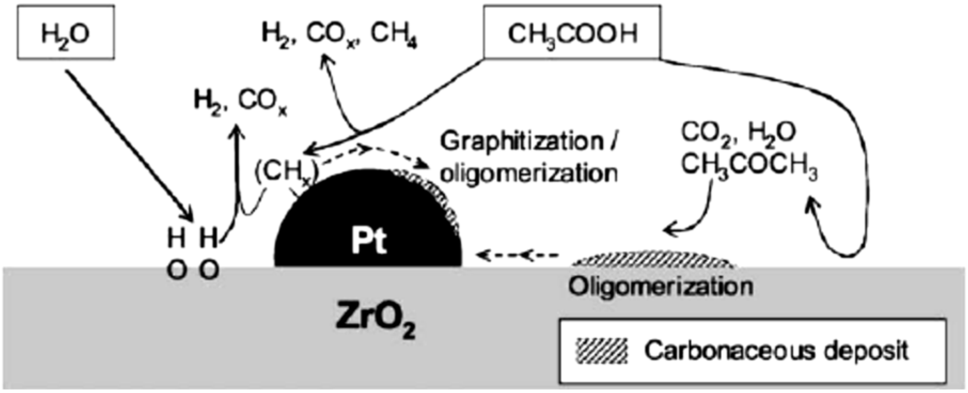

Figure 1.22. **Pathway for the steam reforming of AcOH involving bi-functional catalysts of Pt/ZrO_2 . Taken from [22]**

Ramos *et al.* [57] changed the molar S/C ratio from 1.3 to 6 for catalytic steam reforming of acetol at 650°C with Ni-Al catalyst. As it can be seen in the Table 1.26, carbon conversion was increased from 75.88% to 93.5%. Also, larger molar S/C ratio increased production of hydrogen and CO_2 , but yield of CO fluctuated between 0.474 and 0.380. Although it is expected to see that yields of hydrocarbons were decreased versus molar S/C ratio, yields of CH_4 and C_2 were almost constant.

Table 1.26. **Results of Acetol Catalytic Steam Reforming: Influence of S/C Ratio at 650°C Using Ni-Al Catalyst. Adapted from [57]**

Run #	13	7	14	15	16	17	18
Temperature, °C	650	650	650	650	650	650	650
S/C (mol/mol)	6	4.6	3.3	3.3	2	1.3	1.3
Catalyst weight, g	1.2	1.2	1.52	1.2	1.2	2.7	1.2
g catalyst/g acetol	4.22	3.41	3.40	2.68	1.90	3.40	1.51
GHSV, h^{-1}	12008	14860	14904	18908	26670	14904	33558
Liquid feeding rate, g/min	1.53	1.53	1.54	1.54	1.55	1.56	1.56
Time, min	65	65	65	65	65	65	65
Total acetol fed, g	18.46	22.9	29.06	29.06	41.02	51.54	51.54
Carbon conversion, %	93.50	87.22	86.68	81.46	75.24	72.33	75.88
Yields, g/g							
Total gas/ (acetol+water)	0.256	0.292	0.350	0.337	0.429	0.518	0.510
Total gas/acetol	1.379	1.268	1.208	1.161	1.057	1.022	1.007
Gas yields, g/g acetol							
H_2	0.134	0.134	0.113	0.112	0.094	0.095	0.090
CH_4	0.093	0.082	0.099	0.082	0.074	0.060	0.080
CO	0.384	0.427	0.415	0.396	0.388	0.407	0.474
CO_2	0.749	0.609	0.562	0.555	0.488	0.448	0.351
C_2	0.019	0.016	0.019	0.016	0.013	0.012	0.012

Vagia and Lemonidou [59] carried out non catalytic gasification of acetic acid and acetone at 750°C for 1h with and without steam with residence time of 4.5ms. Conversion of acetic acid and acetone were, respectively, 23% and 65% with steam and 29.7% and 70.6% without steam. It was commented that the lower gained conversion at the presence of steam was probably due to the stabilization effect of steam and lower partial pressure of acetic acid and acetone. Higher conversion of acetone than that of acetic acid, in general, indicated higher instability of acetone at 750°C. They have reported that conversion of acetone in the absence of steam was reduced from 70% to 40% during the third hour of the experiment while the conversion rate was stable in the presence of steam.

1.3.5.2. Bio-oil

Panigrahi *et al.* [64] reported interesting results to do with effect of inlet CO_2, hydrogen and steam on non catalytic gasification of bio-oil. Bio-oil conversion was reduced from 83 wt% to 68 wt%, while total volume of product gases was increased from about 2100 ml/h to about 2400 ml/h when the concentration of CO_2 was increased from 0 to 0.6 in the inlet CO_2/N_2 mixture. As presented in Table 1.27, the concentrations of hydrogen and CO are increased by increasing the inlet CO_2 concentration whereas the concentration of hydrocarbons drops significantly. In other words, inlet CO_2 favors CO_2 reforming and partial oxidation reactions of the hydrocarbons.

Table 1.27. **Product Gas Composition as a Function of CO_2 Concentration in a Feed Gas Mixture of N_2 and CO_2 at a bio-oil Flow Rate of 5.0 g/h at 800 °C. Adapted from Panigrahi *et al.* [64]**

Component, mol%	N_2: 30ml/min	N_2: 24ml/min CO_2: 6ml/min	N_2: 18ml/min CO_2: 12ml/min	N_2: 12ml/min CO_2: 18ml/min
H_2	12.8	15.0	37.4	54.6
CO	7.7	51.9	25.2	23.6
CO_2	2.6	0.01	0.02	0.01
CH_4	27.4	15.2	17.1	12.5
C_2H_4	31.1	10.1	13.4	7.4
C_2H_6	5.5	2.2	2.8	1.0
C_3H_6	3.1	1.8	2.0	0.06
C_3H_8	0.6	0.1	0.5	0.0
C_4+	9.2	3.3	1.2	0.5

The presence of hydrogen in the inlet nitrogen did not change the conversion of bio-oil, but the total volume of product gases, in general, was increased. According to data in Table 1.28, a higher concentration of hydrogen in the inlet flow of nitrogen led to a larger production of hydrogen (it is not reported if the inlet hydrogen was included) and carbon monoxide so that syngas mole fraction increased from 20% to 83% while production of hydrocarbons was significantly lowered which means hydrogen facilitated conversion of hydrocarbon to produce hydrogen and CO.

***Table 1.28.* Product Gas Composition as a Function of H_2 Concentration in a Feed Gas Mixture of N_2 and H_2 at a bio-oil Flow Rate of 5.0 g/h and at 800 °C. Adapted from [64]**

Component, mol%	N_2: 30ml/min	N_2: 4ml/min H_2: 6ml/min	N_2: 18ml/min H_2: 12ml/min	N_2: 12ml/min H_2: 18ml/min
H_2	12.8	33.3	59.2	47.8
CO	7.7	29.0	24.6	32.1
CO_2	2.6	4.9	3.4	4.0
CH_4	27.4	17.0	10.9	13.9
C_2H_4	31.1	14.0	1.3	1.6
C_2H_6	5.5	0.7	0	0.1
C_3H_6	3.1	0.2	0	0.1
C_3H_8	0.6	0.0	0	0
C_4+	9.2	0.9	0.6	0.4

Regarding steam reforming reactions, conversion of bio-oil increased from 67 wt% to 81 wt% versus steam flow rate from 2.5 g/h to 10 g/h. In addition, syngas was increased from 20 to 79 mol% in product stream. Since methane and other hydrocarbons react with steam, it was seen that the yield of hydrocarbons decreased with increasing steam flow rate (Table 1.29).

***Table 1.29.* Product Gas Composition as a Function of Steam Flow Rate at a Nitrogen Flow Rate of 30 mL/min and BDO Flow Rate of 5.0 g/h at 800 °C. Adapted from [64]**

Component, mol%	Steam flow rate, g/h				
	0	2.5	5	7.5	10
H_2	12.8	47.0	47.3	47.3	49
CO	7.7	26.6	27.0	29.5	30.2
CO_2	2.6	5.9	4.0	4.4	0.4
CH_4	27.4	16.2	13.6	12.8	13.4
C_2H_4	31.1	3.0	5.6	5.1	5.4
C_2H_6	5.5	0.2	0.3	0.2	0.2
C_3H_6	3.1	0	0	0	0
C_3H_8	0.6	0	0	0	0
C_4+	9.2	1.3	2.2	0.7	1.4

Wu *et al.* [69] conducted staged catalytic steam reforming of bio-oil in the two fixed bed reactors at temperatures between 700°C and 900°C and molar S/C ratio from 1 to 16. Although yield of product gases increased by temperature, the effect of temperature at the lowest values of molar

S/C ratio was not significant. The maximum yield of hydrogen was observed at molar S/C ratios higher than 16 at 850°C (57.2% of the potential hydrogen). Molar S/C ratio did not influence production of CO at temperatures lower than 800°C, but at higher temperatures, production of CO was decreased by molar S/C ratio. Opposite to the production of CO, the yield of CO_2 was raised by molar S/C ratio indicating the effect of the catalyst on driving the water gas shift reaction. CH_4 was observed at all conditions. Production of CH_4 increased by temperature, but low values of methane was obtained at higher molar S/C ratios.

In order to see the effect of dolomite in the first fixed bed reactor on the ultimate yield of the product gases, inert porcelain chips were used instead at similar conditions. It was realized that presence of dolomite influenced higher yield of hydrogen and CO_2 and decreased yield of CO, but yield of methane was similar.

Sakaguchi *et al.* [71] investigated the effect of molar S/C ratio on thermal cracking of bio-oil. Although steam was used in the gasification runs, only about 3% of the inlet steam was converted in thermal cracking experiments at 836°C while steam conversion was about 15% at 803°C in catalytic experiments. As a result, molar S/C ratio did not affect bio-oil conversion and yield of product gases during thermal cracking experiments. They have not reported the effect of molar S/C ratio on catalytic cracking experiments.

Lan *et al.* [73] investigated the effect of molar S/C ratio at 800°C in the fixed bed reactor and at 750°C in the fluid bed reactor for catalytic steam reforming of the rice husk bio-oil. Their results showed that when this ratio is raised, yields of hydrogen and CO_2 are raised while yields of CO and CH_4 decline. However, a higher yield of hydrogen and carbon to gas conversion was observed in the fluid bed at lower temperatures compared to those in the fixed bed reactor (Figures 1.23a and 1.23b).

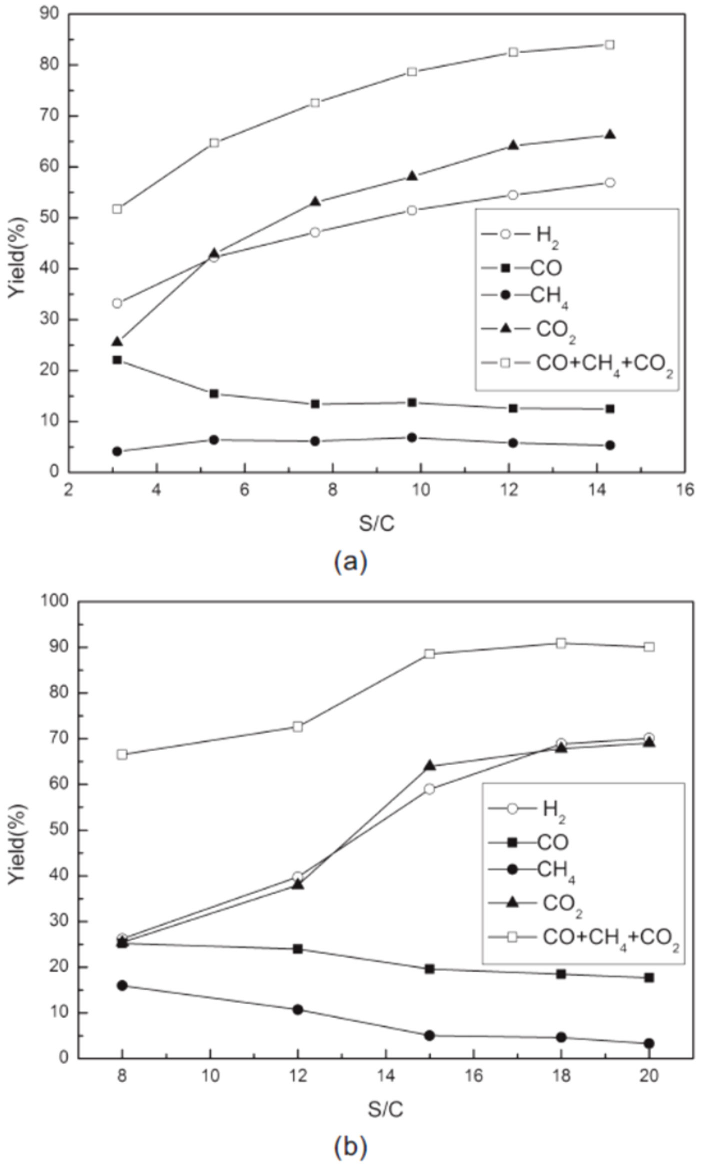

Figure 1.23. **Steam reforming of bio-oil at different rates of steam to carbon. (a) Fixed bed, experimental conditions: 1 g catalyst, T = 800 °C, LHSV = 1.8 h^{-1}, reaction time = 60 min. (b) Fluidized bed, experimental conditions: 100 g catalyst, T = 750 °C, LHSV = 0.8 h^{-1}, reaction time = 60 min. Taken from [73]**

Seyedeyn-Azad *et al.* [75] changed molar S/C ratio between 2 and 5 at 850°C for catalytic bio-oil steam reforming with the 14.1wt% Ni/Al_2O_3 catalyst. A lower yield of hydrogen and CO_2 and a higher yield of CO were observed at molar S/C ratio less than 2, indicating that the steam was not enough for the water gas shift reaction and the majority of the available steam was being used for steam reforming reactions. A maximum carbon to gas conversion was obtained at molar S/C ratios between 2 and 5 and the yield of hydrogen did not change beyond molar S/C=5.

1.3.5.3. Summary

For the case of catalyst absence in the reactor, there are different reports about the effect of steam on the yield of syngas and on conversion of bio-oil and its model compounds: steam can either have stabilization effects and decrease the carbon conversion, can have negligible effects, or can increase yield of syngas and carbon conversion depending on the molar S/C ratio, type of bio-oil or its model compound and temperature.

In general, in the presence of sufficient steam in a catalytic process at a given temperature and for the specific feed, yield of hydrogen and CO_2 as well as carbon conversion increase. The optimum amount of steam should be investigated for a type of bio-oil for a given catalyst and temperature.

Additional CO_2 and hydrogen as inlet streams to the reactor would have positive effect to increase yield of hydrogen and carbon conversion of bio-oil.

1.3.6. Effect of oxygen

1.3.6.1. Bio-oil model compounds

Rioche *et al.* [54] investigated auto thermal conditions for bio-oil steam reforming at 830°C with molar S/C ratio of 10.8 and GHSV of $3090h^{-1}$ with the 1% Pt-$CeZrO_2$ catalyst while O/C ratio varied between 0.54, 0.69, 0.92 and 1.31. It was found that the yield of hydrogen decreased from 70% (without excess oxygen) to 30% (O/C= 1.31). In addition, it was found that the catalyst was deactivated 50% faster when oxygen was used in the reactor although the rate of the carbon deposition on the catalyst decreased significantly. So, deactivation of the catalyst can be due to sintering of Pt on the catalyst because less coke was deposited on the catalyst in presence of oxygen.

Medrano *et al.* [58] studied the effect of additional stoichiometric oxygen in the reactor for 2h on the yield of product gases from acetic acid steam reforming with the Ni/Al catalyst primarily calcined at 750°C (Table 1.30). It was realized that burning the feed with above the 8% of the stoichiometric oxygen will lead to less production of hydrogen and CO_2 while production of CO and CH_4 is raised. Optimum oxygen for the period of 6h tests was found to be 4% because the yield of hydrogen remained almost constant at 0.12 g/g over the time while less coke was deposited on the catalyst. However, it was noticed that carbon conversion with 4% additional stoichiometric oxygen was decreased from 100% and remained almost constant at about 92%.

***Table 1.30.* Experimental results at 650°C, with a catalyst weight of 1.1 g of Ni/Al catalyst calcined at 750°C with oxygen addition. Adapted from [58]**

Run #	1	5	6	7	8	9
Reaction time, h	2	2	2	2	6	6
O_2 addition, %	0	2	4	8	0	4
Liquid feeding rate, ml/min	0.76	0.76	0.77	0.75	0.75	0.74
g catalyst min/g AA	6.152	6.096	6.026	6.179	6.205	6.246
GHSV, h^{-1}	6772	6835	6914	6743	6715	6670
Total gas/ (AA+water), g/g	0.343	0.344	0.344	0.330	0.339	0.351
Liquid yield, g/g	0.672	0.620	0.667	0.693	0.689	0.688
Recovery	1.014	0.964	1.011	1.024	1.028	1.039
Carbon conversion, %	98.87	99.83	100.27	100.52	98.09	102.64
Gas yields, g/g AA						
H_2	0.1303	0.1224	0.1203	0.1096	0.1255	0.1233
CO	0.1533	0.1595	0.1704	0.2467	0.1546	0.1775
CO_2	1.2053	1.2134	1.2028	1.0764	1.1908	1.2246
CH_4	0.0014	0.0000	0.0000	0.0037	0.0017	0.0007
Gas composition, %						
H_2	66.42	64.78	64.30	62.07	65.75	64.28
CO	5.58	6.03	6.50	9.97	5.78	6.65
CO_2	27.92	29.19	29.20	27.70	28.36	29.03
CH_4	0.09	0.00	0.00	0.26	0.11	0.05

1.3.6.2. Bio-oil

Marda *et al.* [77] conducted non-catalytic partial oxidation (NPOX) of the poplar wood bio-oil at temperatures varied from 625°C to 850°C and molar oxygen to carbon ratio (O/C) changed between 0.7 and 1.6. They realized that at low O/C ratios, the conversion of bio-oil was dependent on the temperature, so that higher conversion was achieved at higher temperature. However, the trend of conversion did not change with temperature at O/C ratios of 1.5 and 1.6.

Conversion of bio-oil to the permanent gases, such as hydrogen, CO, CO_2 and CH_4 accounted for 85-95% at the highest O/C ratio. Residual carbon and aromatic gases like benzene constituted the remaining balance. Their results showed that production of CO was way more than production of hydrogen, CO_2 and CH_4 indicating that the water-gas shift catalytic reactor is required to condition this composition to favor hydrogen and CO_2.

Medrano *et al.* [74] tried introducing 4% of the stoichiometric oxygen to their fluid bed reactor containing the Mg/Ni/Al catalyst. It was revealed that, although there were slight differences in the concentration of the product gases, the carbon to gas conversion at 650°C increased from 83.26% to 85.23% and carbon deposition decreased from 149 to 73 mg of C/g of catalyst (Table 1.31).

***Table 1.31.* Experimental results of pyrolysis liquid aqueous phase steam reforming at 650 °C, u/u_{mf} =10, 2 h reaction time, catalyst MgAl 0.26. Adapted from Medrano *et al.* [74]**

Run #	2	4	5
g catalyst min/g organics	4.110	8.971	8.954
GHSV, h^{-1}	11809	8971	8954
Liquid feeding rate, ml/min	0.75	0.75	0.76
Carbon conversion, %	81.01	83.26	85.23
Total gas/ (liquid feed), g/g	0.201	0.227	0.229
Deposited carbon, mg C/g catalyst	162	149	73
Gas yields, g/g organics			
H_2	0.1056	0.1328	0.1284
CO	0.2250	0.1449	0.1774
CO_2	0.8961	1.1469	1.1297
CH_4	0.0276	0.0113	0.0121
C_2H_4	0.0185	0.0054	0.0046
Gas composition, %			
H_2	63.13	67.37	66.07
CO	9.65	5.26	6.56
CO_2	24.34	26.45	26.41
CH_4	2.07	0.72	0.79
C_2H_4	0.79	0.20	0.17

1.3.6.3. Summary

The addition of oxygen has been investigated to either supply some part of the required heat for the endothermic reactions through an auto thermal process, or increase conversion of bio-oil by burning some fractions of large molecules of bio-oil.

Oxygen helps to minimize coke deposition on the catalyst and increase carbon conversion of bio-oil and its model compounds. However, it might deactivate the catalyst and lower the syngas yield. Thus, an optimum O/C ratio must be investigated by which required production of syngas can be achieved with low detrimental effect on the catalyst activity.

1.4. Critical review

In general, it is perceived from the literature review that the gasification of model compounds has been much easier than that of bio-oil in terms of feeding operation and conversion rate. For example, some researchers had to separate and only operate with the aqueous phase of bio-oil [26, 62, 65]. Fortunately, the technique of injecting bio-oil through a water cooled nozzle has overcome the issue of bio-oil polymerization in the nozzle [23, 25, 67, 71].

Due to the fact that most tested bio-oil model compounds were light compounds, such as acetic acid, acetone, acetol and ethylene glycol, which are found in the aqueous fraction of bio-oil, complete conversion of these model compounds has been achieved by applying appropriate operating conditions in a catalytic bed reactor. On the other hand, with similar reactor setups, complete conversion of bio-oil was hard to achieve because of the heavy and complex compounds such as the lignin phase of bio-oil. According to Marquevich *et al.* [53], quite high steam to carbon ratios were needed to catalytically crack the sugar compounds of bio-oil. Therefore, some researchers proposed to use two reactors in series to increase the conversion of bio-oil and the yield of hydrogen. For example, Van Rossum *et al.* [68] suggested that bio-oil should be vaporized initially in a fluidized bed of sand to produce a stream of tars that would then be converted in a catalytic fixed bed reactor to a stream with high concentration of syngas and minimum concentration of hydrocarbons. As an another example, Wu *et al.* [69] proposed two fixed bed reactors that could be used so that bio-oil undergoes a primary gasification in the first fixed bed filled with dolomite and then the outlet gases are carried to the second fixed bed reactor filled with nickel catalysts for further catalytic steam reforming reactions.

Gasification results reveal that, although from a thermodynamic point of view bio-oil and its model compounds can be fully converted to permanent gases and the maximum yield of hydrogen and carbon monoxide can be achieved in equilibrium at temperatures above 700°C [20,59], conducting thermal steam gasification at high temperatures is not enough to reach complete conversion of the feed and maximize the yield of syngas [54-55,57,59, 63,65,71]. In other words, an appropriate catalyst is needed to expedite the conversion and to condition the composition of the permanent gases in order for the syngas to be produced at the desired rate.

A big portion of the research on the gasification of bio-oil and its model compounds has been dedicated to test laboratory and commercial catalysts to increase feed conversion and syngas yield. Nickel has been the most commonly used active metal on the surface of catalysts because it has been already been proven in natural gas steam reforming processes that this metal is very active for steam reforming reactions and, in particular, drives the water gas shift reaction towards the production of hydrogen and CO_2. Steam gasification of bio-oil model compounds has also shown that nickel based catalysts are very promising to maximize the conversion of the feed and the yield of hydrogen and CO_2 while the yield of hydrocarbons, CH_4 in particular, is minimized. The yield of CO has usually been less than the yield of CO_2 in the catalytic steam reforming reactors.

The catalysts were usually reduced by hydrogen to convert NiO to Ni^0 because nickel is active in its free metal form. Galdamez *et al.* [55] reported that the compositions of product gases from steam reforming of acetic acid, compared to results with the non reduced catalyst, were closer to the equilibrium compositions when a catalyst was initially reduced by hydrogen, and also, the catalyst activity was stable after 1h. Sakaguchi *et al.* [71] reported the issue of low activity of the commercial catalyst since it was not initially reduced by hydrogen.

A major problem observed with nickel based catalysts was the deactivation of the catalyst, especially, after long time runs due to the coke deposition. Formation of coke can be because of different reasons such as composition of the catalyst [21, 23, 28, 60-61], intermediate products [56] and composition of the bio-oil and its model compounds [65, 71]. In addition, coke can be formed with different structures which can directly affect the gasification yields. For instance, Davidian *et al.* [23] reported that the coke formed on commercial catalysts was bi-dimensional carbon while the coke on the laboratorial catalyst was stable graphitized carbon whiskers. Kechagiopoulos *et al.* [65] showed that, at similar operating conditions and catalyst, the conversion of bio-oil was less than the conversion of the mixture of the model compounds and the mass of the deposited coke was larger; in addition, the coke formed from bio-oil had aromatic compounds while the coke from model compounds was graphitic.

The reviewed literature indicates that the commercial nickel based catalysts have been more active and stable than synthesized catalysts [23, 62, 66, 67, 60] due to the presence of promoters on these catalysts. Therefore, researchers investigated the addition of some metal promoters like Mg, Co, La and Ca on the surface of the catalysts to improve the activity and stability of the catalysts to maximize feed conversion and hydrogen yield [55, 57, 62, 74]. Medrano *et al.* [77] reported that Mg and Ca strengthen the nickel based catalysts against attrition in the fluidized bed reactors, but the catalyst with Mg was more active that the catalyst with Ca. Medrano *et al.* [58] showed that the calcination temperature of the catalyst during its synthesis was effective on conversion of acetic acid and yield of hydrogen. Some researchers loaded different masses of nickel on their catalysts, but in contrast to their expectations, excess load of nickel make the catalyst less reducible by hydrogen and, as a result, activity of the catalyst was lower [23, 75]. Limitation of mass of the metal was also reported for the metal promoters [55]. Vagia and Lemonidou [59] implied that composition of the support can also make the active metal less reducible and therefore less active due to incorporation of the active metal in the bulk of support.

Davidian *et al.* [23, 60-61] proposed their cracking/regeneration system in which coke deposits are burned and catalyst is reactivated frequently and as a result conversion of bio-oil is increased.

Some researchers realized that the rate of coke formation in the fixed bed reactors is high and a fluidized reactor is required to enhance contact with the catalyst surface through effective agitation of the catalytic bed [65, 73]. Some researchers reported a catalyst loss in fluidized bed reactors because of attrition of the catalysts; actually, they used commercial nickel based catalysts which were designed originally for fixed bed reactors of natural gas steam reforming [65, 71]. Czernik *et al.* [65] developed four nickel based catalysts which were not as active as the commercial catalyst, but resisted attrition better and the rate of the catalyst loss from the fluidized bed reactor was low.

Noble metals have also been tested for gasification of bio-oil and its model compounds. Vagia and Lemonidou [59] reported that the catalyst with 0.5wt% Rh, in term of yield of hydrogen, was more active than the catalyst with 5wt% Ni in steam reforming of acetone although the coke deposition rates on these catalysts were similar. Rioche *et al.* [54] showed that their synthesized catalysts with 1wt% of noble metals were very active for the gasification of bio-oil model compounds. They also showed that the catalysts with a ceria-zirconium support were more active than catalysts with an alumina support. However, the catalysts were not stable as the yield of hydrogen was decreased from 60% to 90% during 9h steam gasification of bio-oil at 830°C with a steam to carbon ratio of 5 and a GHSV of $3090h^{-1}$ with the Pt-$CeZrO_2$ catalyst, which was the most active catalyst of the noble metal based catalysts. They have reported that sintering of the Pt was the main reason of the catalyst deactivation because coke deposition was not the issue on the catalyst. On the contrary, Davidian *et al.* [60] reported that their nickel based catalysts were more active than the noble metal based catalysts in terms of acetic acid conversion and yield of hydrogen.

Temperature is a key operating parameter in bio-oil gasification. Reaction 1.3 is endothermic and an increase in temperature drives this reaction towards the production of hydrogen and CO. In addition, the decomposition reaction 1.7 is more active at high temperatures towards the production of lighter compounds and permanent gases. So, assuming that there is enough steam, produced hydrocarbons can be steam reformed according to reaction 1.3. Reported results proved that bio-oil conversion and syngas yield increased with temperature. Nonetheless, it has been reported that non catalytic conversion of bio-oil is lower than catalytic conversion even at high temperature and steam to carbon ratio [54, 67, 71]. However, there have been some contradicting reports. For instance, Ramos *et al.* [57] claimed they accomplished a high conversion of 87.09% of acetol through thermal cracking at 650°C. Also, Galdamez *et al.* [55] reported that they could reach 100% conversion of acetic acid at temperatures above 650°C although compositions of the gases were far from equilibrium.

A sort of misunderstanding in the literature results the definitions of the gas hourly space velocity (GHSV) and residence time. GHSV is defined as the ratio between flow rate of the feed and volume of the bed whereas residence time is defined as the ratio between total flow rate of the gases and volume of the reactor. In a continuous reactor, feed is usually atomized through a nozzle to the reactor. Atomization is supplied by an inert gas like nitrogen and argon. Other than atomization gas, a carrier inert gas is also usually used to flush the product gases out of the reactor. Residence time is dependent on the flow of the atomization and carrier inert gases. It has been noticed that most researchers have not emphasized residence time in their reactor, but the GHSV has been well specified.

Wang *et al.* [20] conducted their catalytic steam reforming reactions at very short residence times (0.15 - 0.4 s), but they did not see any change on the composition of their product gases. Panigrahi *et al.* [63] reported an effect of flow rate of the carrier gas on bio-oil gasification yields, but the exact residence time was not reported. They claimed that bio-oil conversion decreased at longer residence times and then stabilized at longer residence times. In addition, composition of the syngas was decreased at shorter residence times. A decline of conversion at longer residence can be attributed to a lack of enough steam and a catalyst. Increase in syngas at shorter residence times might be justified by production of CO because CO can react with steam at longer residence times.

GHSV can be changed by either changing the mass of the catalyst or flow rate of the feed. Some researchers reported that conversion of the feed and yields of hydrogen and CO_2 increased with decreasing GHSV [71, 73, 77], but some researchers pointed out that they did not see any effect of the GHSV on their gasification results [71].

Steam is also a key reactant in bio-oil gasification as it plays a significant role in the steam reforming of hydrocarbons as well as in the water gas shift reactions; therefore, bio-oil conversion and hydrogen yield are expected to increase with increasing steam to carbon ratio. Review of the literature showed that most researchers managed to increase bio-oil conversion and hydrogen yield by increasing the steam flowrate, especially when an appropriate catalyst was present. The effect of the steam to carbon ratio was not greatly pronounced in non catalytic gasification tests [71]. Vagia and Lemonidou [59] found out that for non catalytic conversion of acetic acid and acetone, the presence of steam was less than when there was no steam in the reactor which can be because of the stabilization effect of steam and lower partial pressure of the model compounds.

Due to the fact that steam reacts with CO in the water gas shift reaction, the production of CO is limited in favor of the production of hydrogen. The CO/CO_2 ratio is not, however, only controlled by the water gas shift reaction because, for instance, the Boudouard reaction is also effective. Furthermore, the activity of the bed material and its influence on production of CO and CO_2 must be taken into account. During thermal cracking tests, in general, yield of CO has been more than yield of CO_2 while this trend was reversed during catalytic tests. This is because a water gas shift is not very active in the absence of a catalyst at thermal cracking experiments.

Some researchers used oxygen in the gasification reactor either to minimize the formation of the coke on the surface of the catalyst [55] or to increase conversion of bio-oil by burning heavy compounds of bio-oil [74, 77]. It is expected that the concentration of CO_2 should be increased by burning the bio-oil and its model compounds. According to Panigrahi *et al.* [64], CO_2 can react with hydrocarbons (dry reforming) for the production of CO and hydrogen. Medrano *et al.* [58] reported that burning acetic acid with oxygen at the presence of Ni/Al catalyst increased the yield of CO and CH_4 while the yields of hydrogen and CO_2 were decreased; this can be because initial high concentration of CO_2 derived the water gas shift reaction towards reverse direction in favor of CO production. Also, CO_2 may have reacted with solid carbon on the surface of catalyst according to the Boudouard reaction. Marda *et al.* [77] also, reported that the concentration of CO was higher than the concentration of other product gases.

1.5. Thesis objectives

The number of publications concerning syngas production, and, in particular, hydrogen production from bio-oil and its model compounds has increased significantly in the past decade; however, the number of such reports in literature is still limited. In addition, the research work on gasification/steam reforming using bio-oil model compounds greatly exceeds that utilizing bio-oil. Moreover, due to the physical and chemical properties of bio-oil, syngas production from the aqueous fraction of bio-oil hasattracted more interest. Therefore, there are very few publications dealing with the gasification of whole bio-oil, given the fact that the composition of bio-oil depends greatly on the primary biomass resource and the pyrolysis process from which bio-oil is produced. Furthermore, the reported experimental data have been generated from different operating setups.

Therefore, it is important to develop techniques and experimental setups to be able to systematically investigate the conversion of different bio-oils, in the form of whole bio-oil, as a function of different operating parameters, such as temperature, residence time and inlet steam to carbon ratio as well as composition and mass of the catalysts. Such experimental setup facilitates the evaluation of the effects of each operating parameter and catalyst as functions of the composition of bio-oils, and to identify the optimal conditions required to maximize the conversion of a given bio-oil for syngas production.

The main objective of this thesis was to design and develop fluidized bed reactors suitable to carry out thermal and catalytic gasification experiments to achieve optimal conversion of whole mass of a bio-oil and maximum production of syngas as functions of operating conditions, such as temperature, residence time and steam. Due to the fact that bio-oil supply is limited and in order to save operation costs and time, as the sub-objective of this thesis, a novel batch-wise micro fluidized bed reactor was designed and developed to test the effects of catalysts, in terms of mass and type, on bio-oil gasification. The advantage of such a unique setup is that the best catalyst and operating conditions can be investigated very quickly and at a minimal cost for different bio-oils; and then, these optimum findings can be re-tested in a continuous bench-scale reactor to study operating conditions in continuous processes such as gas hourly space velocity, optimum condition for a auto thermal process and stability of the optimum catalyst during long experimental runs.

References

[1] North American Transportation Statistics Database.
http://nats.sct.gob.mx/nats/sys/tables.jsp?i=3&id=14.

[2] World Bank. Fossil fuel energy consumption (%) in the countries.
http://data.worldbank.org/indicator/eg.use.comm.fo.zs

[3] Energy Department of the United States. http://energy.gov/science-innovation/energy-sources/fossil

[4] Briens C, Piskortz J, Berruti F. Biomass Valorization for Fuel and Chemicals Production- A Review. International Journal of Chemical Reactor Engineering. 2008;6.

[5] Xu R. Development of Advanced Technologies for Biomass Pyrolysis: UWO; 2010.

[6] Spath PL, Dayton DC. Assessment of Synthesis Gas to Fuels and Chemicals with Emphasis on the Potential for Biomass-Derived Syngas. December 2003.

[7] Hagey HL. Kinetic modeling of synthesis gas into hydrocarbons: UWO; 2001.

[8] Demirbas A. Progress and recent trends in biofuels. Progress in Energy and Combustion Science. 2007;33:1-18.

[9] Demirbas MF. Hydrogen from Various Biomass Species via Pyrolysis and Steam Gasification Processes. Energy Sources, Part A: Recovery, Utilization, and Environmental Effects. 2006;28:245-52.

[10] Balat M. Thermochemical Routes for Biomass-based Hydrogen Production. Energy Sources, Part A: Recovery, Utilization, and Environmental Effects. 2010;32:1388-98.

[11] Digman B, Joo HS, Kim D-S. Recent progress in gasification/ pyrolysis technologies for biomass conversion to energy. Environmental Progress and Sustainable Energy. 2009;28:47-51.

[12] Goransson K, Soderlind U, He J, Zhang W. Review of syngas production via biomass DFBGs. Renewable and Sustainable Energy Reviews. 2011;15:482-92.

[13] Guo Y, Wang SZ, Xu DH, Gong YM, Ma HH, Tang XY. Review of catalytic supercritical water gasification for hydrogen production from biomass. Renewable and Sustainable Energy Reviews. 2010;14:334-43.

[14] Puig-Arnavat M, Bruno JC, Coronas A. Review and analysis of biomass gasification models. Renewable and Sustainable Energy Reviews. 2010;14:X2841-51.

[15] Tanksale A, Beltramini JN, Lu GM. A review of catalytic hydrogen production processes from biomass. Renewable and Sustainable Energy Reviews. 2010;14:166-82.

[16] Kalinci Y, Hepbasli A, Dincer I. Biomass-based hydrogen production: A review and analysis. International Journal of Hydrogen Energy. 2009;34:8799-817.

[17] Saxena RC, Seal D, Kumar S, Goyal HB. Thermo-chemical routes for hydrogen rich gas from biomass: a review. Renewable and Sustainable Energy Reviews. 2008;12:1909-27.

[18] Corella J, Toledo JM, Molina G. A review on dual fluidized-bed biomass gasifiers. Industrial and Engineering Chemistry Research. 2007;46:6831-9.

[19] Reed TB. Biomass Gasification: principles and technology: Noyes Data Corporation; 1981.

[20] Wang D, Czernik S, Montane D, Mann M, Chornet E. Biomass to Hydrogen via Fast Pyrolysis and Catalytic Steam Reforming of the Pyrolysis Oil or Its Fractions. Industrial & Engineering Chemistry Research. 1997;36:1507-18.

[21] Basagiannis AC, Verykios XE. Reforming reactions of acetic acid on nickel catalysts over a wide temperature range. Applied Catalysis A: General. 2006;308:182-93.

[22] Takanabe K, Aika K, Inazu K, Baba T, Seshan K, Lefferts L. Steam reforming of acetic acid as a biomass derived oxygenate: Bifunctional pathway for hydrogen formation over Pt/ZrO2 catalysts. Journal of Catalysis. 2006;243:263-9.

[23] Davidian T, Guilhaume N, Iojoiu E, Provendier H, Mirodatos C. Hydrogen production from crude pyrolysis oil by a sequential catalytic process. Applied Catalysis B: Environmental. 2007;73:116-27.

[24] Ba T, Chaala A, Garcia-Perez M, Roy C. Colloidal properties of bio-oils obtained by vacuum pyrolysis of softwood bark. Storage stability. Energy and Fuels. 2004;18:188-201.

[25] Latifi M, Ferrante L, Briens C, Berruti F. Effect of temperature and residence time on the thermal cracking of bio-oil for syngas production. ECI Conference, Bioenergy II. Rio de Janeiro, Brazil2009.

[26] Czernik S, French R, Feik C, Chorine E. Hydrogen by Catalytic Steam Reforming of Liquid Byproducts from Biomass Thermoconversion Processes. Industrial & Engineering Chemistry Research. 2002;41:4209-12.

[27] Wang D, Montane D, Chorine E. Catalytic steam reforming of biomass-derived oxygenates: acetic acid and hydroxyacetaldehyde. Applied Catalysis A: General. 1996;143:245-70.

[28] Vagia E, Lemonidou A. Thermodynamic analysis of hydrogen production via steam reforming of selected components of aqueous bio-oil fraction. International Journal of Hydrogen Energy. 2007;32:212-23.

[29] Hajaligol MR, Howard JB, Longwell JP, Peters WA. Product compositions and kinetics for rapid pyrolysis of cellulose. Industrial & Engineering Chemistry Process Design and Development. 1982;21:457-65.

[30] Nunn TR, Howard JB, Longwell JP, Peters WA. Product compositions and kinetics in the rapid pyrolysis of sweet gum hardwood. Industrial & Engineering Chemistry Process Design and Development. 1985;24:836-44.

[31] Muehlen H-J, van Heek KH, Juentgen H. Kinetic Studies of Steam Gasification of Char in the Presence of H2, Co2 and Co. Fuel. 1985;64:944-9.

[32] Neogi D, Chang CC, Walawender WP, Fan LT. Study of coal gasification in an experimental fluidized bed reactor. AIChE Journal. 1986;32:17-28.

[33] Brown BW, Smoot LD, Smith PJ, Hedman PO. Measurement and prediction of entrained-flow gasification processes. AIChE Journal. 1988;34:435-46.

[34] Boroson ML, Howard JB, Longwell JP, Peters WA. Product yield and kinetic from phase ctacking of wood pyrolysis tars. AIChE Journal. 1989;35:120-8.

[35] Xu J, Froment GF. Methane steam reforming, methanation and water-gas shift: I. Intrinsic kinetics. AIChE Journal. 1989;35:88-96.

[36] Donnot A, Magne P, Deglise X. Kinetic parameters of the cracking reaction of tar from wood pyrolysis; comparison of dolomite with industrial catalysts. Journal of analytical and applied pyrolysis. 1991;22:47-59.

[37] Adjaye JD, Bakhshi NN. Catalytic Conversion of Bio-oil- Kinetics and Model prediction. Biomass and Bioenergy. 1995;8:265-77.

[38] Biggs MJ, Agarwal PK. The CO/CO2 product ratio for a porous char particle within an incipiently fluidized bed: a numerical study. Chemical Engineering Science. 1997;52:941-52.

[39] Encinar JM, Beltran FJ, Gonzalez JF, Moreno MJ. Pyrolysis of maize, sunflower, grape and tobacco residues. Journal of Chemical Technology and Biotechnology. 1997;70:400-10.

[40] Fletcher DF, Haynes BS, Christo FC, Joseph SD. A CFD based combustion model of an entrained flow biomass gasifier. Applied mathematical modeling. 2000;24:165-82.

[41] Di Blasi C, Branca C. Kinetics of Primary Product Formation from Wood Pyrolysis. Industrial & Engineering Chemistry Research. 2001;40:5547-56.

[42] Fagbemi L, Khazemi L, Capart R. Pyrolysis products from different biomasses: application to the thermal cracking of tar. Applied Energy. 2001;69.

[43] Fiaschi D, Michelini M. A two-phase one dimensional biomass gasification- kinetic model. Biomass and Bioenergy. 2001;21:121-32.

[44] Hamel S, Krumm W. Mathematical modeling and simulation of bubbling fluidized bed gasifier. Powder Technology. 2001;120:105-12.

[45] Wurzenberger JC, Wallner SW, Raupenstrauch H, Khinast JG. Thermal conversion of biomass: Comprehensive reactor and particle modeling. AIChE Journal. 2002;48:2398-411.

[46] Liu H, Gibbs BM. Modeling NH3 and HCN emissions from biomass circulating fluidized bed gasifiers☆. Fuel. 2003;82:1591-604.

[47] Kersten SRA, Wang X, Prins W, van Swaaij WPM. Biomass Pyrolysis in a Fluidized Bed Reactor. Part 1: Literature Review and Model Simulations. Industrial & Engineering Chemistry Research. 2005;44:8773-85.

[48] Corella J, Sanz A. Modeling circulating fluidized bed biomass gasifiers. A pseudo-rigorous model for stationary state. Fuel Processing Technology. 2005;86:1021-53.

[49] Radmanesh R, Chaouki J, Guy C. Biomass gasification in a bubbling fluidized bed reactor: Experiments and modeling. AIChE Journal. 2006;52:4258-72.

[50] Lee DH, Yang H, Yan R, Liang DT. Prediction of gaseous products from biomass pyrolysis through combined kinetic and thermodynamic simulations. Fuel. 2007;86:410-7.

[51] Patel S, Pant KK. Experimental study and mechanistic kinetic modeling for selective production of hydrogen via catalytic steam reforming of methanol. Chemical Engineering Science. 2007;62:5425-35.

[52] Yu L, Lu J, Zhang X, Zhang S, Wang X. Two fluid model using kinetic theory for modeling of one-step hydrogen production gasifier. AIChE Journal. 2008;54:2833-51.

[53] Marquevich M, Czernik S, Chornet E, Montane D. Hydrogen from Biomass: Steam Reforming of Model Compounds of Fast-Pyrolysis Oil. Energy & Fuels. 1999;13:1160-6.

[54] Rioche C, Kulkarni S, Meunier FC, Breen JP, Burch R. Steam reforming of model compounds and fast pyrolysis bio-oil on supported noble metal catalysts. Applied Catalysis B: Environmental. 2005;61:130-9.

[55] Galdámez JR, García L, Bilbao R. Hydrogen Production by Steam Reforming of Bio-Oil Using Coprecipitated Ni−Al Catalysts. Acetic Acid as a Model Compound. Energy & Fuels. 2005;19:1133-42.

[56] Takanabe K, Aika K, Seshan K, Lefferts L. Catalyst deactivation during steam reforming of acetic acid over Pt/ZrO2. Chemical Engineering Journal. 2006;120:133-7.

[57] Ramos MC, Navascués AI, García L, Bilbao R. Hydrogen Production by Catalytic Steam Reforming of Acetol, a Model Compound of Bio-Oil. Industrial & Engineering Chemistry Research. 2007;46:2399-406.

[58] Medrano J, Oliva M, Ruiz J, Garcia L, Arauzo J. Catalytic steam reforming of acetic acid in a fluidized bed reactor with oxygen addition. International Journal of Hydrogen Energy. 2008;33:4387-96.

[59] Vagia EC, Lemonidou AA. Hydrogen production via steam reforming of bio-oil components over calcium aluminate supported nickel and noble metal catalysts. Applied Catalysis A: General. 2008;351:111-21.

[60] Davidian T, Guilhaume N, Daniel C, Mirodatos C. Continuous hydrogen production by sequential catalytic cracking of acetic acid. Applied Catalysis A: General. 2008;335:64-73.

[61] Davidian T, Guilhaume N, Provendier H, Mirodatos C. Continuous hydrogen production by sequential catalytic cracking of acetic acid. Applied Catalysis A: General. 2008;337:111-20.

[62] Garcia L, French R, Czernik S, Chornet E. Catalytic steam reforming of bio-oils for the production of hydrogen: Effects of catalyst composition. Applied Catalysis A:General. 2000;201:225-39.

[63] Panigrahi S, Chaudhari ST, Bakhshi NN, Dalai AK. Production of synthesis gas/high-Btu gaseous fuel from pyrolysis of biomass-derived oil. Energy and Fuels. 2002;16:1392-7.

[64] Panigrahi S, Dalai AK, Chaudhari ST, Bakhshi NN. Synthesis gas production from steam gasification of biomass-derived oil. Energy and Fuels. 2003;17:637-42.

[65] Kechagiopoulos PN, Voutetakis SS, Lemonidou AA, Vasalos IA. Hydrogen production via steam reforming of the aqueous phase of bio-oil in a fixed bed reactor. Energy & Fuels. 2006;20:2155-63.

[66] Czernik S, Evans R, French R. Hydrogen from biomass-production by steam reforming of biomass pyrolysis oil☆. Catalysis Today. 2007;129:265-8.

[67] van Rossum G, Kersten SRA, van Swaaij WPM. Catalytic and Noncatalytic Gasification of Pyrolysis Oil. Industrial & Engineering Chemistry Research. 2007;46:3959-67.

[68] Van Rossum G, Kersten SRA, Van Swaaij WPM. Staged catalytic gasification/steam reforming of pyrolysis oil. Industrial & Engineering Chemistry Research. 2009;48:5857-66.

[69] Wu C, Huang Q, Sui M, Yan Y, Wang F. Hydrogen production via catalytic steam reforming of fast pyrolysis bio-oil in a two-stage fixed bed reactor system. Fuel Processing Technology. 2008;89:1306-16.

[70] Marda JR, DiBenedetto J, McKibben S, Evans RJ, Czernik S, French RJ, *et al.* Non-catalytic partial oxidation of bio-oil to synthesis gas for distributed hydrogen production. International Journal of Hydrogen Energy. 2009;34:8519-34.

[71] Sakaguchi M, Watkinson AP, Ellis N. Steam Gasification of Bio-Oil and Bio-Oil/Char Slurry in a Fluidized Bed Reactor. Energy & Fuels. 2010;24:5181-9.

[72] Xu Q, Lan P, Zhang B, Ren Z, Yan Y. Hydrogen production via catalytic steam reforming of fast pyrolysis bio-oil in a fluidized-bed reactor. Energy and Fuels. 2010;24:6456-62.

[73] Lan P, Xu Q, Zhou M, Lan L, Zhang S, Yan Y. Catalytic Steam Reforming of Fast Pyrolysis Bio-Oil in Fixed Bed and Fluidized Bed Reactors. Chemical Engineering & Technology. 2010;33:2021-8.

[74] Medrano JA, Oliva M, Ruiz J, García L, Arauzo J. Hydrogen from aqueous fraction of biomass pyrolysis liquids by catalytic steam reforming in fluidized bed. Energy. 2011;36:2215-24.

[75] Seyedeyn-Azad F, Salehi E, Abedi J, Harding T. Biomass to hydrogen via catalytic steam reforming of bio-oil over Ni-supported alumina catalysts. Fuel Processing Technology. 2011;92:563-9.

[76] Gayubo AG, Aguayo AT, Atutxa A, Aguado R, Bilbao J. Transformation of oxygenate components of biomass pyrolysis oil on a HZSM-5 zeolite. I. Alcohols and phenols. Industrial and Engineering Chemistry Research. 2004;43:2610-8.

[77] Medrano JA, Oliva M, Ruiz J, García L, Arauzo J. Catalytic steam reforming of model compounds of biomass pyrolysis liquids in fluidized bed reactor with modified Ni/Al catalysts. Journal of Analytical and Applied Pyrolysis. 2009;85:214-25.

CHAPTER 2:

Effects of Residence Time and Temperature on the Thermal Cracking of Bio-oil for Syngas Production

2.1. Introduction

Syngas can be produced from different resources such as natural gas, naphtha, residual oil, petroleum coke, coal, and biomass [1]. Syngas is an important chemical building block from which valuable products can be produced, such as methanol, ethanol, olefins, and paraffins. While biomass contains less hydrogen than resources such as natural gas, it is a renewable resource that releases net zero greenhouse gases to the atmosphere [2].

Biomass may be converted to syngas either directly, through a gasification process, or indirectly in two steps: biomass is first pyrolyzed to produce primarily liquid bio-oil, which is then gasified to syngas. The indirect route has several advantages. The bio-oil may be generated in decentralized production facilities or mobile plants in the vicinity of the biomass sources, and then shipped to a central facility for conversion to syngas, avoiding the expensive transportation of bulky and perishable biomass. Also, the syngas produced from bio-oil is cleaner because less tar compounds are produced in comparison with direct biomass gasification [37]; tar has detrimental effects in the downstream processes. Finally, valuable green chemicals may be extracted from the bio-oil before it is converted to syngas. For example, the lignin fraction of the bio-oil could be used in producing phenol-formaldehyde adhesives or high-octane gasoline-blending components [3].

A typical biomass consists of water, cellulose, hemicellulose and lignin. Bio-oil composition depends on the biomass from which it was pyrolyzed, the pyrolysis conditions and whether catalyst was used in the process. However, all bio-oils have usually similar constituents as they are generally oxygenated compounds like acids, aldehydes, alcohols, and ketones [5-8]. Bio-oil is reasonably stable at room temperature, but polymerizes even at moderate temperatures (around 80°C), and, at higher temperatures, it decomposes. Some of molecules of bio-oil may not even be stable at ambient temperatures [5,7,9].

The gasification of model compounds representing the major constituents of bio-oil has been studied to identify reaction mechanisms and the impact of reaction conditions and of the presence of various catalysts. Although these results do not represent real bio-oil gasification, they provide useful information [4-7,10-29].

Publications on the gasification or steam reforming of actual bio-oils are less numerous than for model compounds. Because of physical properties of bio-oil such as its quick solidification inside the hot injection nozzles, there had been challenges to gasify whole bio-oils, so aquoues fraction of bio-oil which was separated from the lignin fraction by adding excess water was tested for syngas production taking advantage of high water content in the solution [3,30-32].

During the recent years, utilization of whole bio-oil has been considered to produce syngas [33-42]. Most of the published literature so far dealt with catalytic steam reforming of the bio-oils. Thermal cracking of bio-oil was considered as a route to produce product gases with high heat values [33,34], but the limited publications about bio-oil thermal gasification reported low bio-oil conversion and syngas yield in the absence of catalyst [36,37,40].

As the first step of the experimental work of this thesis, thermal cracking of whole bio-oil was investigated. The objective of this work was to investigate a practical process for the conversion of whole bio-oil into syngas, using a fluidized bed of inexpensive, attrition-resistant silica sand, and operating at low pressure and temperatures (500°C to 700°C) with varied vapor residence time (8s to 28s) to understand whether it is possible to increase bio-oil conversion through a thermal cracking process. There was not any literature report of gasifying the whole bio-oil at the time, so this investigation included designing an efficient bio-oil feeder for long run continuous experiments and a downstream separation system to maximize separation of the condensable products in a condenser and separate the fine oil droplets from the stream of the permanent ptoduct gases which do not stay in the condenser. Results of this research enable us to identify strategies to improve the gasification process in terms of operating conditions, catalysis, and reactor configurations.

2.2. Pilot plant set-up

The Institute for Chemicals and Fuels from Alternative Resources (ICFAR) has recently designed and set up a fluidized bed reactor, operating in the bubbling regime, for the conversion of bio-oil to syngas. The reactor consists of a 0.076m I.D. bed column made of stainless steel, with an expanded freeboard, whose volume may be adjusted to vary the gas residence time. This reactor can be used to carry out either thermal cracking or catalytic cracking/reforming of bio-oil. Figure 2.1 shows a schematic diagram of the gasification pilot plant. In order to feed bio-oil at a continuous and fixed flow rate into the reactor, a special hydraulic pumping system is used in which there is a reciprocating piston inside a cylinder. Hydraulic oil is pumped by a fixed flow rate to push bottom of the piston upward so that bio-oil that is stored at top of cylinder is fed into the reactor. During normal operation of the pilot plant, the pressure supplied by the pump is about 60 psig. Figure 2.2 shows this hydraulic system.

A spray nozzle was designed to address two conflicting concerns: thermal degradation of the bio-oil and excessive cooling of the fluidized bed near the injection zone. An initial design of a water-cooled nozzle resulted in cooling not only of the nozzle but also of the fluidized bed, whose local bed temperature dropped by 20 to 30 °C. Experiments without cooling water showed the bio-oil temperature never rose past 200 ºC in the nozzle. On the other hand, thermal stability experiments showed that, in the presence of oxygen, bio-oil quickly degraded at temperatures as low as 100 ºC. However, there was no degradation of the bio-oil at 200 ºC under a nitrogen blanket. The spray nozzle was, therefore, used without water cooling and with nitrogen as atomization gas.

Either nitrogen or steam can be preheated by furnaces and then used as atomization and fluidization medium. In case of steam reforming, still water passes through the furnace and then is superheated up to 300 °C. In this work, nitrogen was only used as fluidization and atomization gas. Atomization nitrogen was not preheated and was mixed with bio-oil at the nozzle tip. Sugar solution with physical characteristics of density and viscosity similar to bio-oil was used to test flow rate of nitrogen versus quality of spray. The appropriate flow rate of nitrogen required to efficiently spray the sugar solution was about 5 standard liters per minute. Figure 2.2 shows how the nozzle was designed. The central tube of the nozzle through which bio-oil was pumped to reactor had an I.D. of 0.015m. Fluidizing nitrogen was heated up to reactor temperature inside reactor windbox and then passed through a grid to fluidize bed material. Feed injection point was 0.18m above the grid.

If bio-oil stays stagnant inside the nozzle, it can plug the nozzle easily because of two reasons: it either sticks to solid particles or it burns with air and then coke is formed along the tube of the feeding nozzle. In order to avoid having this problem, after each run the nozzle was flushed with an ethanol flow to wash the remaining bio-oil into reactor, followed by a flow of nitrogen. Also, before starting to pump bio-oil towards the nozzle, a continuous flow of nitrogen inside central tube of the nozzle prevented solids from entering and plugging the nozzle.

The reactor consisted of a cylindrical section with an I.D. of 0.078m and a height of 0.52m, topped by an expanded section whose diameter and height were varied to obtain different residence times of gases inside the reactor. Band heaters were used to heat up and keep the reactor at the desired reaction temperature and thermocouples were used to measure the reactor temperature at different levels. The reactor was surrounded by two 0.05m thick layers of insulation: an inner layer of FiberFrax and an external layer of covered glass wool.

Product gas entered a cyclonic condenser, immersed in an iced water tank, where water and bio-oil liquids including tars were condensed. Condenser was made of aluminum with I.D. of 0.076m and height of 0.91m. Since the condenser was immersed completely inside a cold water tank, its wall temperature was as cold as equilibrium temperature of the tank. Outlet vapors from reactor entered condenser from top through a short tube (0.01m I.D. and 0.05m downward from top bent with a 45° angle), therefore gases hit internal wall of the condenser at top and started a spiral flow until they arrived at the bottom of condenser. Non condensable gases would leave the condenser through another 0.01m I.D. tube which was hanged from top and its bottom had 0.013m distance from the bottom of condenser. This design helped fast condensation of gases and easy separation of liquid products from non-condensable gases (Figure 1.1). There was also one by-pass condenser which was used before running an experiment. After non-condensable gases exited the condenser, fine liquid droplets were recovered with an electrostatic precipitator (ESP). More details of the design of the ESP can be found elsewhere [43]. Gases exiting the ESP were further filtered and then either vented or collected in Tedlar gas sampling bags for subsequent analysis. An HP 5890 gas chromatograph with a thermal conductivity detector was used to analyze the product gas (H_2, CO, CO_2, CH_4 and N_2). Nitrogen was used as an internal standard gas to determine the flowrate of product gases. During experiments designed to investigate the effects of residence time on gasification yield, a 2 m long RESTEK Shin Carbon ST (micro packed) column with 0.001m ID and 0.0016 cm OD was used, with argon as the carrier ga--s, in the gas chromatograph. When studying the effect of temperature on thermal cracking of bio-oil, a molecular sieve column followed by a silica gel column in series was used, with helium as carrier gas, and an automatic Valco valve changed the direction of the gas flow through the columns to detect all gas components. The molecular sieve column was used for detecting H_2, N_2, CH_4 and CO while the silica gel column was used to detect CO_2. The Valco valve was programmed to switch the carrier gas flow from the the silica gel-molecular sieve direction to the moleculr sieve-silica gel direction direction after the CO was completely eluted.

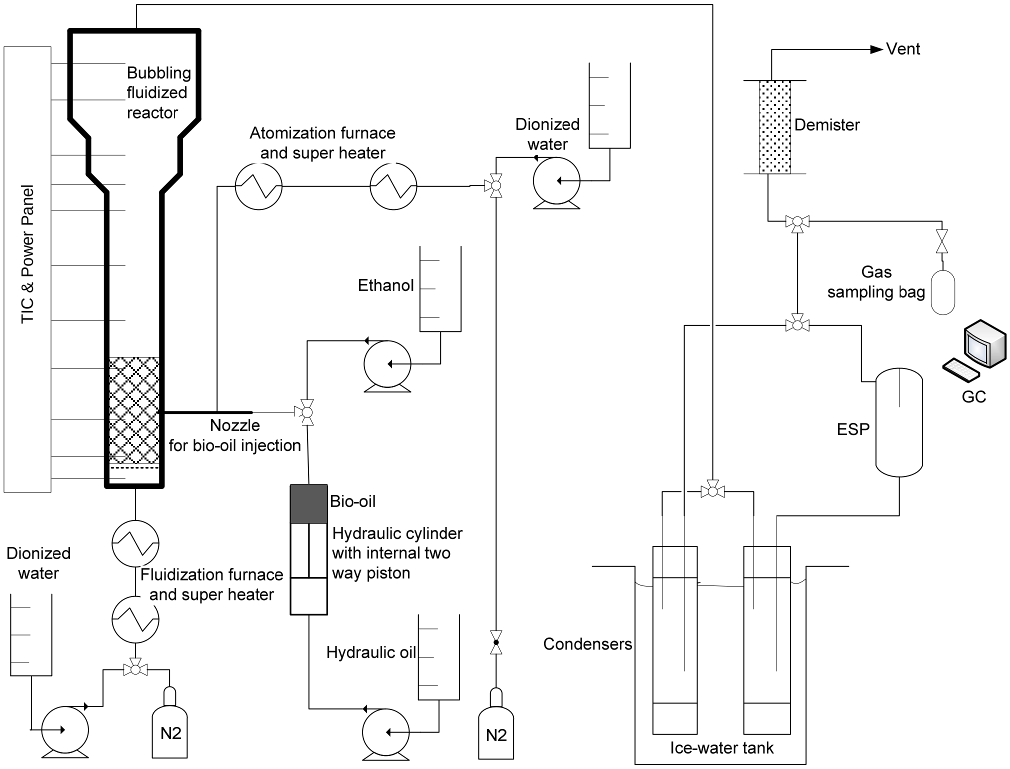
Bubbling fluidized reactor
TIC & Power Panel
Atomization furnace and super heater
Dionized water
Vent
Demister
Ethanol
Gas sampling bag
GC
ESP
Nozzle for bio-oil injection
Bio-oil
Hydraulic cylinder with internal two way piston
Dionized water
Fluidization furnace and super heater
Hydraulic oil
Condensers
N2
N2
Ice-water tank

Figure 2.1. **Schematic diagram of the bubbling fluidized bed set-up**

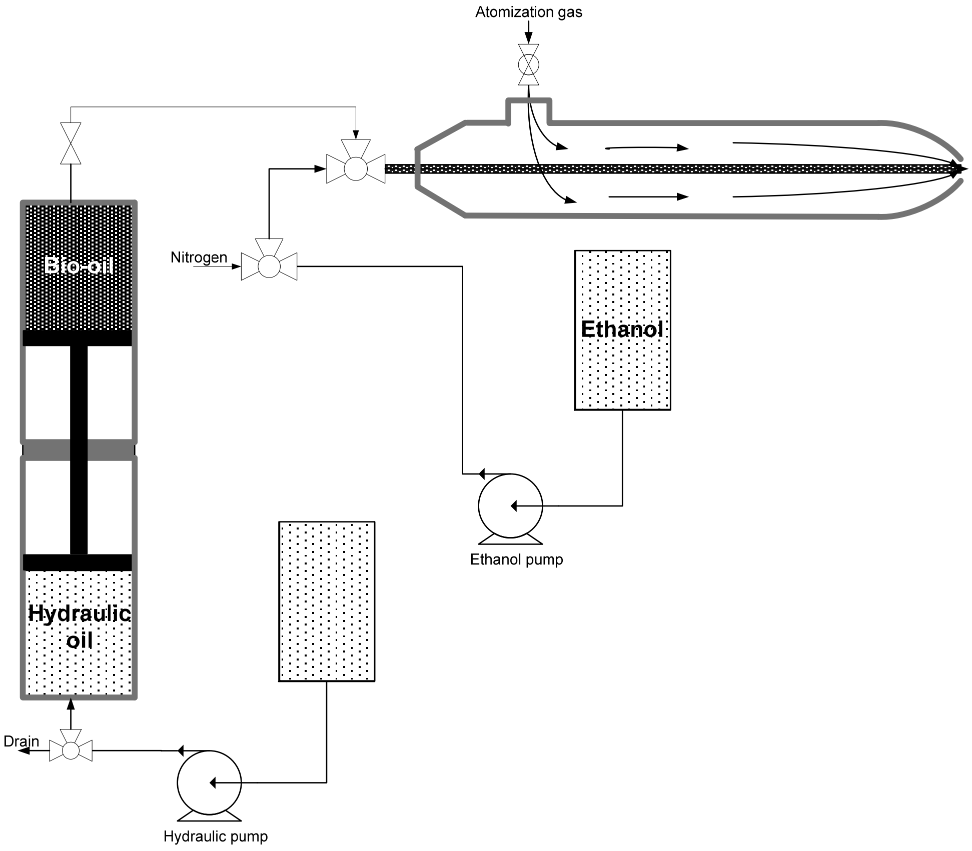

Figure 2.2. **Hydraulic pumping system and nozzle to feed bio-oil into reactor**

2.3. Experimental procedure

Nitrogen was used to fluidize reactor particles and to spray-atomize bio-oil into reactor bed. The nitrogen flowrate could be adjusted by mass flow meters. The fluidized bed provided very good contact of bio-oil droplets with hot solid particles to achieve high rates of heat and mass transfer; also solids backmixing within the bed ensured a uniform bed temperature. After each run, coke deposits on the bed particles could be easily burned off with air.

Silica sand (ρ_p=2650 kg/m^3) was used as the bed material. As per Geldart's solid particles classification, bubble properties within the fluidized bed, and, hence, heat and mass transfer are greatly different for groups A and B. Two different silica sands were, therefore, used to determine that there were no significant mass or heat transfer limitations: sand with a Sauter mean diameter of 80 μm representing group A particles and sand with a Sauter mean diameter of 200 μm representing group B particles.

A bed mass of 1.5 kg of silica sand was used for most experiments. Silica sand is not a porous solid and it is mainly used as inert bed material for good mixing and heat transfer purposes. To check for possible catalytic activity of the sand, some selected experiments were repeated with 3.0 kg of silica sand.

The thermal cracking experiments were conducted over the temperature range between 500°C and 700°C. The lowest temperature, 500°C, was the temperature that was used to produce the bio-oil from hardwood pyrolysis. The highest temperature, 700°C, corresponds to the maximum temperature that could be achieved with a reactor build of inexpensive steel. The reactor pressure was just above atmospheric pressure.

While the reactor was being heated up to the set-point temperature, air was used to keep the bed at the minimum fluidizing condition. Furthermore, to prevent plugging of the spray nozzle with solids, air flow was maintained through atomization and internal feeding tube of the nozzle. At the start of a run, all air streams were switched to nitrogen. While the by-pass condenser was in operation, injection of bio-oil started to avoid collecting liquids in the main condenser in case of likely malfunction of the bio-oil nozzle. After proper bio-oil injection was ensured, the product gas stream was switched from the by-pass condenser to the main condenser. After each experiment, the product stream was switched back to the by-pass condenser and bio-oil was replaced by ethanol to clean the feeding system.

2.4. Gasification reactions

Bio-oil is a complex mixture of oxygenated compounds, such as acids, alcohols, aldehydes, esters and ketones. Its water content varies between 20 and 30 wt%. Including its water content, bio-oil can be represented by a general formula such as CH_mO_k. Syngas production processes are also called steam reforming processes, because steam is added to the reactor to react with the feed at sufficiently high temperatures to produce hydrogen and carbon monoxide. To increase the steam concentration in the reacting gases, additional steam can be added as fluidization medium, beyond the water naturally contained in the bio-oil. In the current study, however, no additional steam flow was used and the only steam present in the reactor came from the water contained in the injected bio-oil.

In the presence of steam, bio-oil with general formula of CH_mO_k (neglecting the nitrogen content) can be converted to syngas (H_2+CO) according to reaction 2.1 which is an endothermic reaction:

$$CH_mO_k + (1-k)H_2O \rightarrow CO + \left(1 + {}^{m}/_{2} - k\right)H_2 \tag{2.1}$$

If there was enough steam in the reactor, the produced CO would react with steam through the water-gas shift reaction to produce more hydrogen:

$$H_2O + CO \leftrightarrow H_2 + CO_2 \tag{2.2}$$

Therefore, summing up reactions 2.1 and 2.2, the overall steam reforming of bio-oil can be expressed by reaction 2.3:

$$CH_mO_k + (2 - k)H_2O \rightarrow CO_2 + \left(2 + {}^{m}/_{2} - k\right)H_2 \tag{2.3}$$

There are a number of other reactions taking place after bio-oil is injected into the reactor. For example, As soon as bio-oil is entered into the reactor, it decomposes thermally to other forms of the oxygenated molecules (CH_yO_z) as well as some permanent gases (hydrogen, steam, CO, CO_2 and light hydrocarbons) and coke (reaction 2.4). Czernik et al (2002) claim that the carbon-oxygen bonds of bio-oil make it more reactive when compared to hydrocarbons. Thus, some components, like furans, phenols and carbohydrates, which are unstable at high temperatures, react with carbon deposition [3]. Besides, since CO, CO_2 and coke are available inside the reactor, the Boudouard reaction (reaction 2.5) is another important reaction which can affect the CO/CO_2 ratio in the final product gases.

$$CH_mO_k \rightarrow CH_yO_z + gases\ (H_2, H_2O, CO, CO_2, CH_4, \dots) + coke \tag{2.4}$$

$$2CO \leftrightarrow C + CO_2 \tag{2.5}$$

In addition, in the presence of steam, the produced hydrocarbons undergo steam reforming reactions towards production of hydrogen and carbon monoxide. For example, reactions 2.6 and 2.7 illustrate how methane can be converted to syngas:

$$CH_4 + H_2O \rightarrow CO + 3H_2 \tag{2.6}$$

$$CH_4 + 2H_2O \rightarrow CO_2 + 4H_2 \tag{2.7}$$

At higher temperatures methane production is decreased. Also, the partial pressure of steam affects the conversion of methane to syngas.

2.5. Results and discussion

Results presented here were obtained by thermal gasification of a bio-oil that was produced by pyrolysis of hardwood at moderate temperatures, in the absence of oxygen, at the Dynamotive Energy Systems Corporation in Canada. Table 1.1 lists elemental analysis, general formula and high heat value of this bio-oil.

Table 2.1. **Elemental analysis and HHV of bio-oil**

C, wt%	H, wt%	O, wt%	CH_mO_k	HHV, kJ/kg
41.67	7.20	51.13	$CH_{2.07}O_{0.92}$	15,696

The nitrogen flowrates were the same for atomization and fluidization, at 4.5 standard liters per minute at reactor conditions. In order to keep the same residence time for all experiments, the flowrate of nitrogen was adjusted according to the temperature of each run. The voltage applied to the ESP was 1.8 kV to collect all mists from the product gas.

Initial experiments were carried out to investigate the effect of vapors residence time on the yield of bio-oil gasification products. Then, once the most appropriate vapors residence time was identified, the effect of temperature on product yields was investigated.

2.5.1. Effect of residence time

The effect of residence time was studied by changing the freeboard volume. Three residence times were investigated: 7.8, 11.4 and 27.6 seconds. Flow rate of bio-oil was 2 ml/min. Experiments were conducted at 600°C and 700°C for 10 minutes and the product gas was sampled at the end of each test. The preliminary tests had shown that composition of the product gases did not change within the initial 10 minutes.

Figures 2.3 to 2.5 show that residence time plays an important role in syngas production. Total gas production (H_2, CO, CO_2 and CH_4) increases with longer residence times. The yield of (H_2+CO) at the longest residence time is almost doubled when compared to that achieved at the shortest residence time. Figure 2.5 shows that longer the residence time has also a very beneficial effect on the molar H_2/CO ratio. The effect of longer residence times at higher temperatures is even more significant. This means that there are more thermally unstable compounds at elevated temperatures and when they are staying longer inside reactor, the rate of thermal cracking increases in favor of hydrogen production.

As a result, the next series of experiments designed to investigate effect of temperature on bio-oil gasification were conducted at a residence time 27.6 seconds.

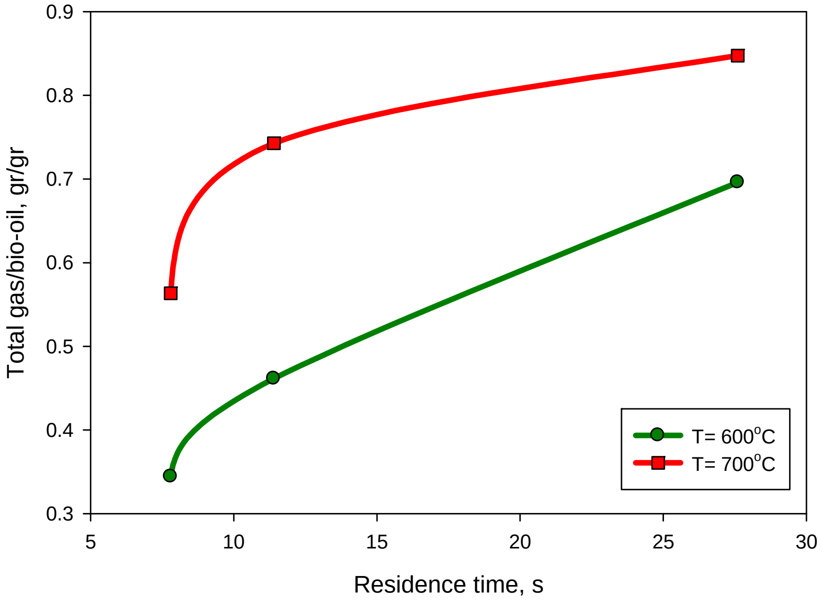

Figure 2.3. **Yield of total gas production versus versus residence time as moles produced per injected grams of bio-oil; Mass of the sand bed: 1.5kg, sauter mean diameter of the sand: 200µm**

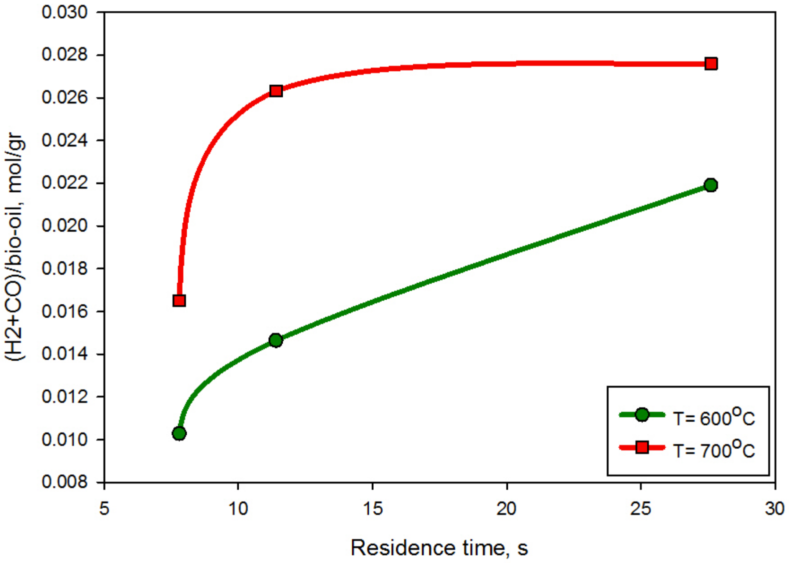

Figure2.4. **Yield of syngas production versus residence time as moles produced per injected grams of bio-oil; Mass of the sand bed: 1.5kg, sauter mean diameter of the sand: 200µm**

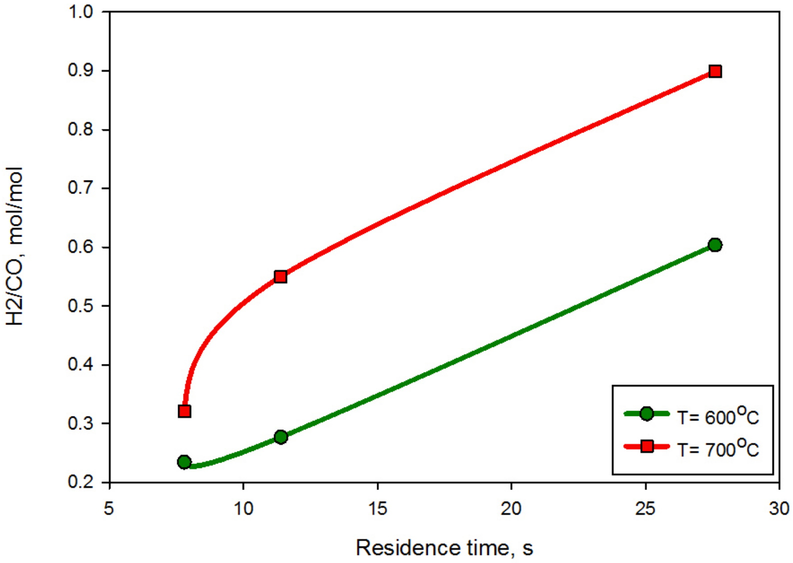

Figure 2.5. **Yield of molar H_2/CO versus residence time; Mass of the sand bed: 1.5kg, sauter mean diameter of the sand: 200µm**

2.5.2. Effect of temperature

Preliminary experiments have shown that the composition of product gas evolves with time during long runs. There are two possible reasons: the sand may have catalytic activity and becomes deactivated by coke deposits, or the coke deposits themselves may have a catalytic activity. It was, therefore, decided to run each test for one hour to clearly characterize the evolution in gas production and gas composition: bio-oil flow rate was 4 ml/min for these experiments. The product gas was sampled after 5, 30, and 60 minutes. Bed samples showed negligible coke deposits after 5 minutes while, after 60 minutes, the bed particles were completely covered with coke.

Figures 2.6 to 2.9 present the yield of permanent gases as produced moles of each component per grams of injected bio-oil over the temperature range of 500°C to 700°C during one hour of operation for group B (average size cut of 200µm) and group A (average size cut of 80µm) solids. The hydrogen yield is similar for group B and group A sands, confirming that there are no significant heat or mass transfer limitations. As suggested by equation 2.1, higher temperatures increase hydrogen production. At all temperatures, there is a dramatic drop of hydrogen production with time.

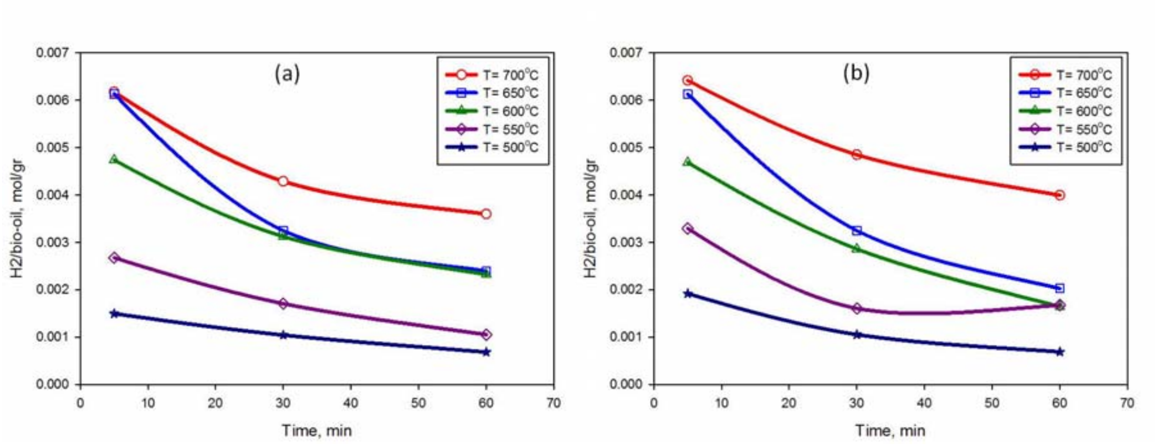

Figure 2.6. **Yield of hydrogen as moles produced per injected grams of bio-oil; Mass of the sand bed 1.5kg, sauter mean diameter of the sand: (a) 200µm, (b) 80µm**

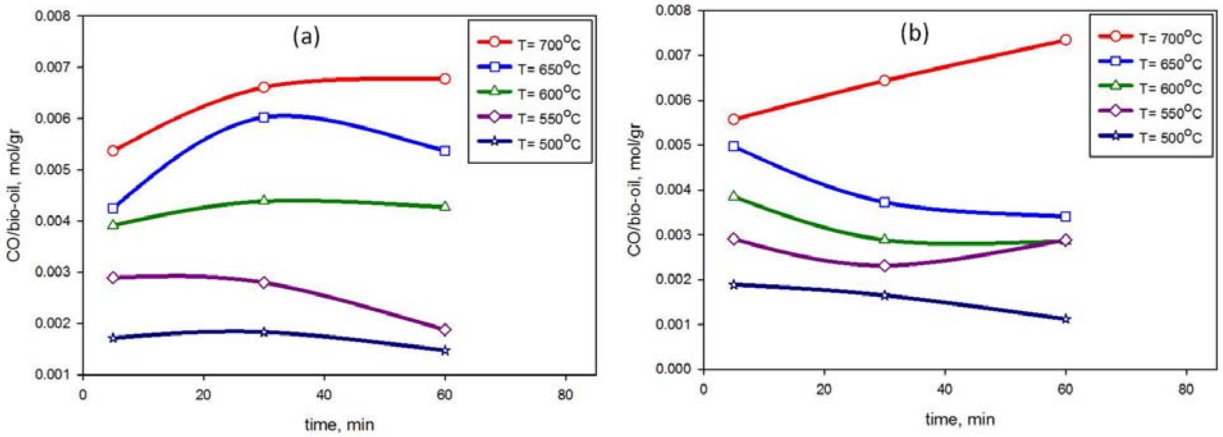

Figure 2.7. **Yield of CO as moles produced per injected grams of bio-oil; Mass of the sand bed 1.5kg, sauter mean diameter of the sand: (a) 200µm, (b) 80µm**

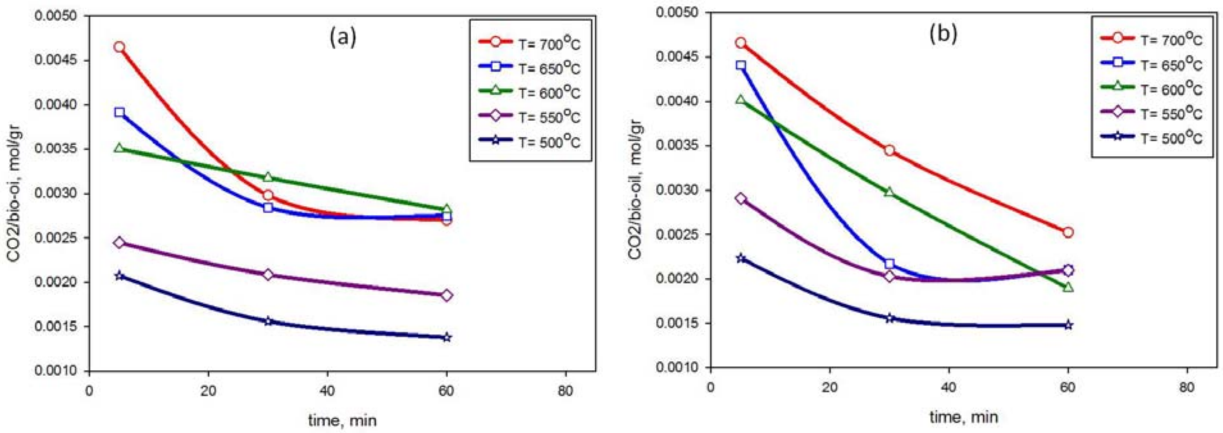

Figure 2.8. **Yield of CO2 as moles produced per injected grams of bio-oil; Mass of the sand bed 1.5kg, sauter mean diameter of the sand: (a) 200µm, (b) 80µm**

The yield of carbon monoxide also increases with temperatures (Figure 2.7). It seems difficult to determine how CO production evolves with time. Results show that at higher temperatures CO production increases with time while at lower temperatures, this trend is reversed. There is also a difference between group A and B solids at intermediate temperatures.

Carbon dioxide follows the same trends as hydrogen production (Figure 2.8). More carbon dioxide is produced at higher temperatures. Carbon dioxide production also drops dramatically with time.

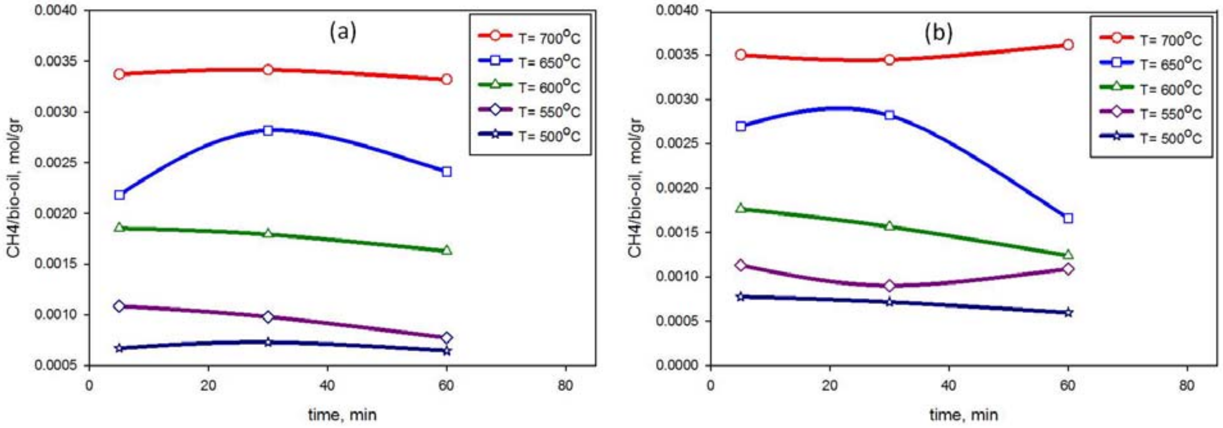

Figure 2.9. **Yield of CH_4 as moles produced per injected grams of bio-oil; Mass of the sand bed 1.5kg, sauter mean diameter of the sand: (a) 200µm, (b) 80µm**

Methane production increases with increasing temperature (Figure 2.9). There is no definitive evolution of methane production with time.

The positive effect of temperature on the production yield of all gases indicates that kinetics rather than thermodynamics control the reaction. For example, the water gas-shift reaction is exothermic, and, if there was thermodynamic control, increasing the temperature should reduce the production of CO and increase the production of H_2 and CO_2. The reverse results were observed. Results indicate complexity of kinetics of the chemical reaction requiring further investigation in the future.

Figure 2.10 depicts the total mass yield of the dry gases (H_2, CO, CO_2 and CH_4). The total gas production decreases with time, and increases with increasing temperature. The maximum yield is about 42 % for both solid sands at 700°C, the highest temperature, and it drops to 37-38 % after one hour.

After each experiment, condenser and ESP were weighed to measure the mass of liquid collected in one hour. More liquid was collected in the condenser than in the ESP, as shown in Figure 2.11. The condenser liquid is mainly aqueous and has a dark brownish color at lower temperatures and becomes lighter at higher temperatures, indicating the concentration of very heavy compounds decreases at higher temperatures. One the other hand, the ESP liquid is an oil phase. Figure 2.11 shows that similar results were obtained for group A and B beds, suggesting that liquid conversion was not significantly affected by any heat or mass transfer limitation.

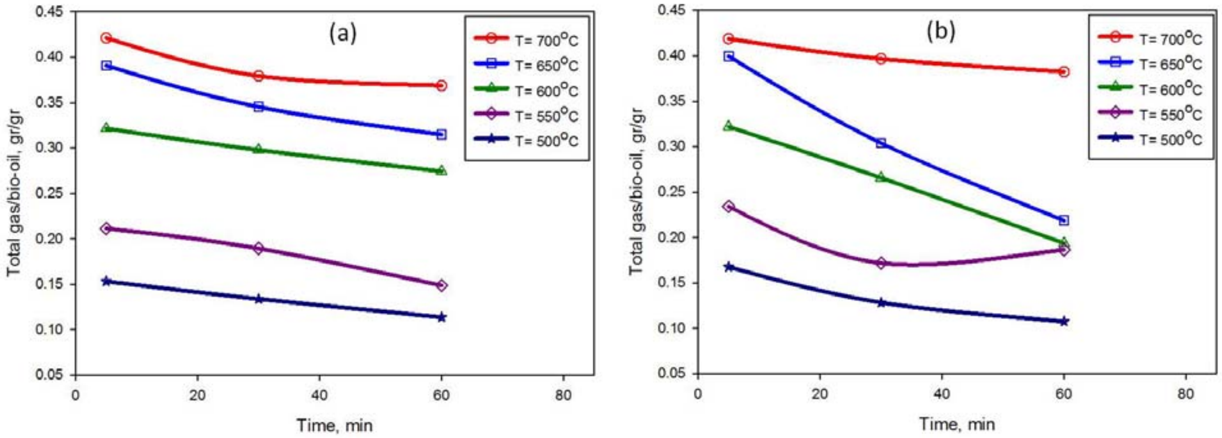

Figure 2.10. **Yield of total gas production as grams produced per injected grams of bio-oil; Mass of the sand bed 1.5kg, sauter mean diameter of the sand: (a) 200μm, (b) 80μm**

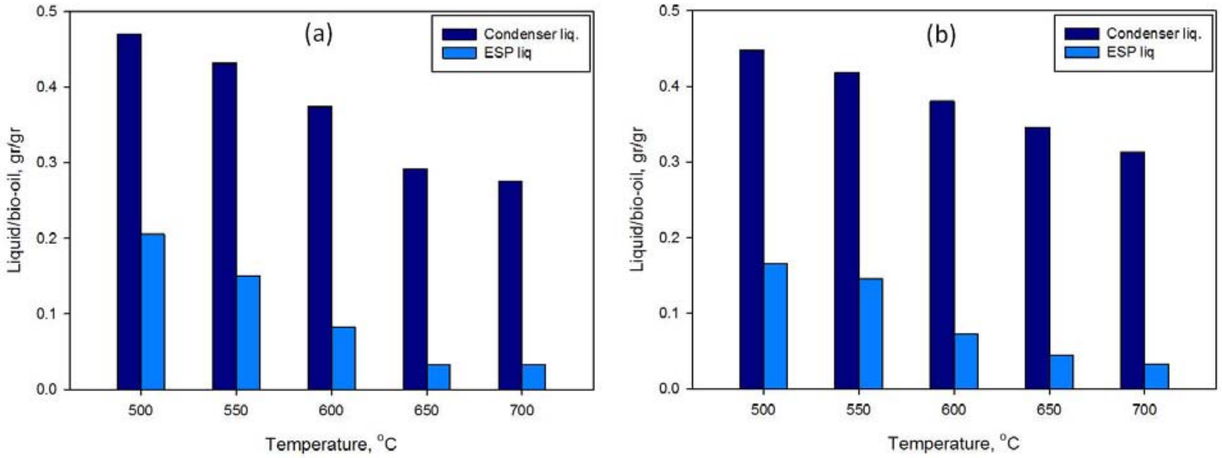

Figure 2.11. **Yield of liquid production as grams produced per injected grams of bio-oil; Mass of the sand bed 1.5kg, sauter mean diameter of the sand: (a) 200μm, (b) 80μm**

It has been estimated that between 20 wt% and 30 wt% of bio-oil injected is converted into coke. It can be concluded that coke formation is a main cause of the reduction with time of the yield of total gases.

2.5.3. Effect of bed mass

Because the freeboard temperature was the same as the bed temperature, thermal cracking occurred equally in the bed or the freeboard. Doubling the bed mass should, therefore, only affect catalytic cracking. Figures 2.12 to 2.16 show the results of gasification experiments performed at 600°C, 650°C and 700°C with a sand mass of 3.0 kg. The trends were the same as with the lower bed mass.

Doubling the bed mass did not greatly increase the total yield of dry gases. At 700 °C, for example, this total gas yield was only increased by around 3%. This confirms the results obtained with the two particle sizes, since increasing the specific surface of the sand particles by a factor of 2.5 did not greatly affect gas production. Therefore, the sand particles did not have a significant catalytic effect. Since fine coke particles were distributed through the freeboard, it is likely that the dramatic drop in reactor performance with time was caused by a detrimental catalytic effect of the coke particles.

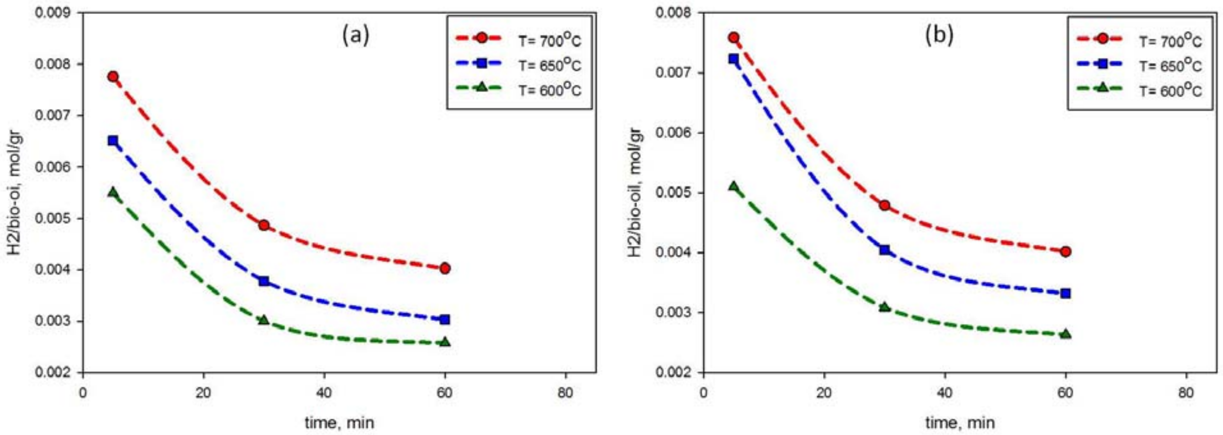

Figure 2.12. **Yield of hydrogen as moles produced per injected grams of bio-oil; Mass of the sand bed 3.0kg, sauter mean diameter of the sand: (a) 200µm, (b) 80µm**

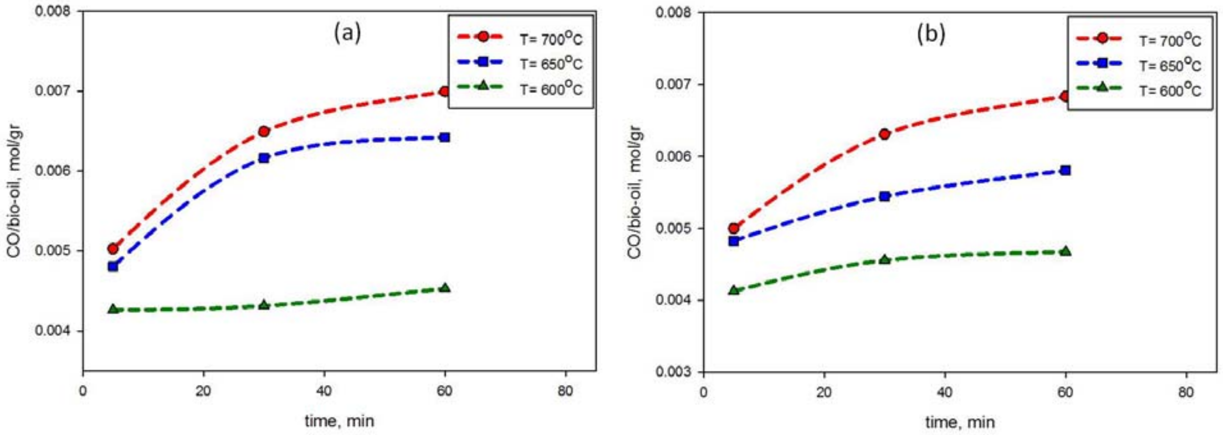

Figure 2.13. **Yield of CO as moles produced per injected grams of bio-oil; Mass of the sand bed 3.0kg, sauter mean diameter of the sand: (a) 200µm, (b) 80µm**

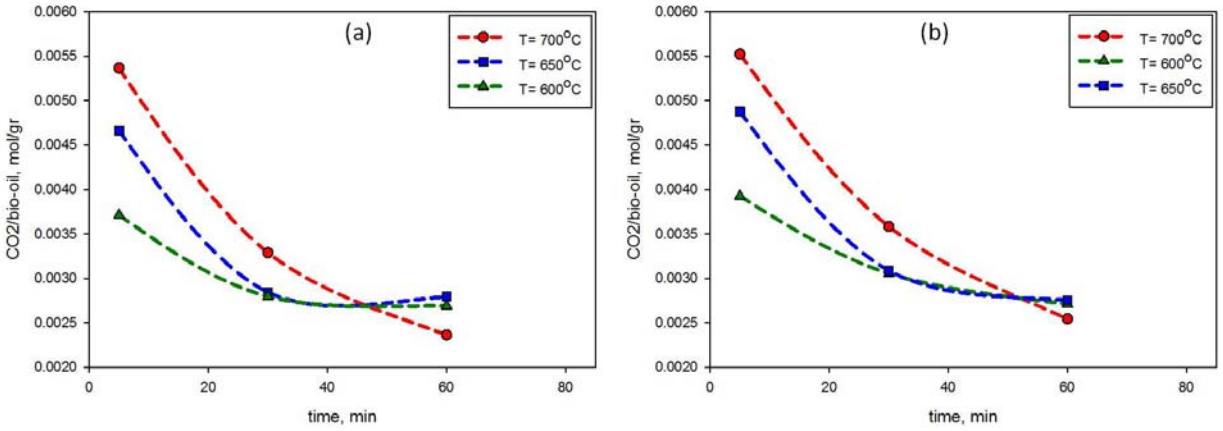

Figure 2.14. **Yield of CO_2 as moles produced per injected grams of bio-oil; Mass of the sand bed 3.0kg, sauter mean diameter of the sand: (a) 200µm, (b) 80µm**

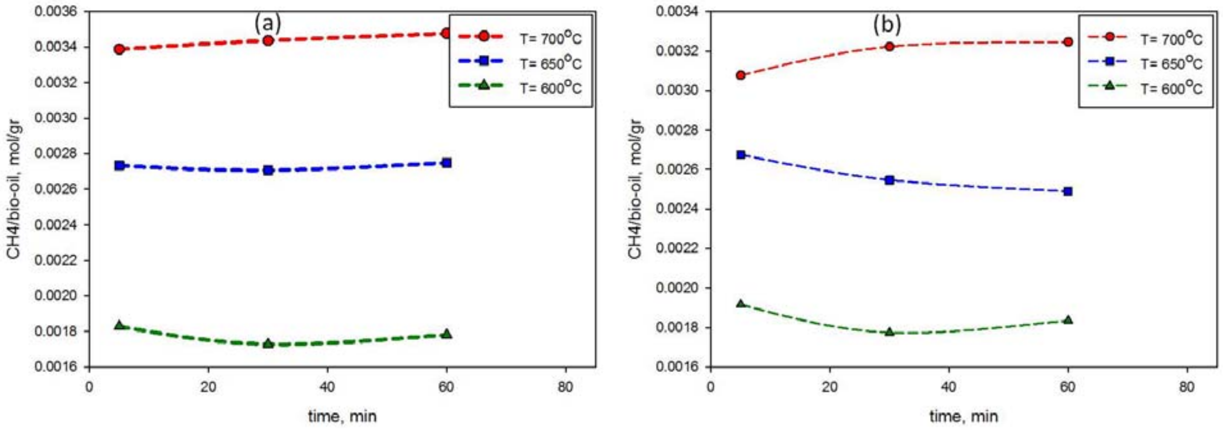

Figure 2.15. **Yield of CH_4 as moles produced per injected grams of bio-oil; Mass of the sand bed 3.0kg, sauter mean diameter of the sand: (a) 200µm, (b) 80µm**

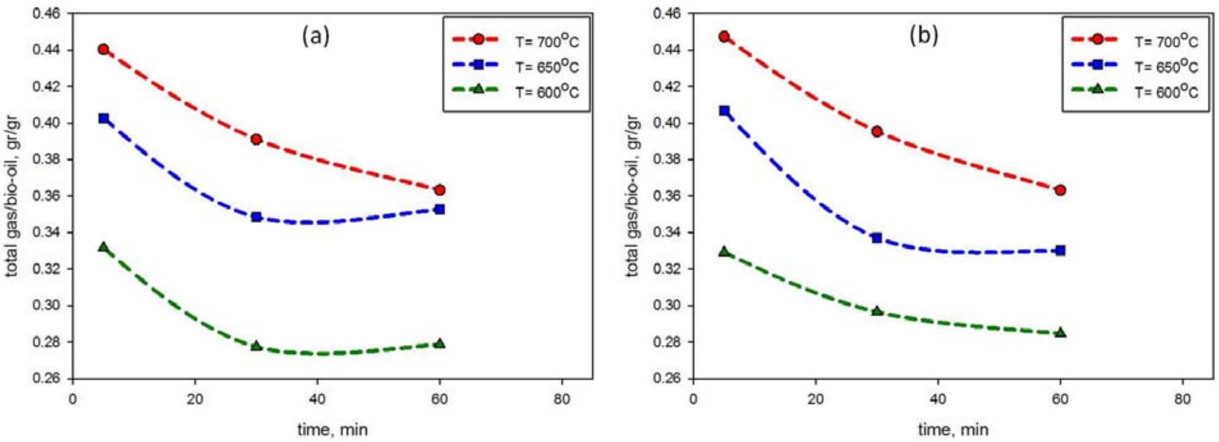

Figure 2.16. **Yield of total gas production as grams produced per injected grams of bio-oil; Mass of the sand bed 3.0kg, sauter mean diameter of the sand: (a) 200µm, (b) 80µm**

2.5.4. Effect of particle size

As discussed, two different solid sand sizes were used to determine whether there were significant heat or mass transfer limitations, since heat and mass transfer rates are much higher with the smaller particles [44]. Figure 2.17 compares the total initial gasification yield for all experiments with the two types of sand. Although there are minor differences, results obtained with group B and group A solids are very similar. Therefore, it can be concluded that there were no significant heat or mass transfer limitations.

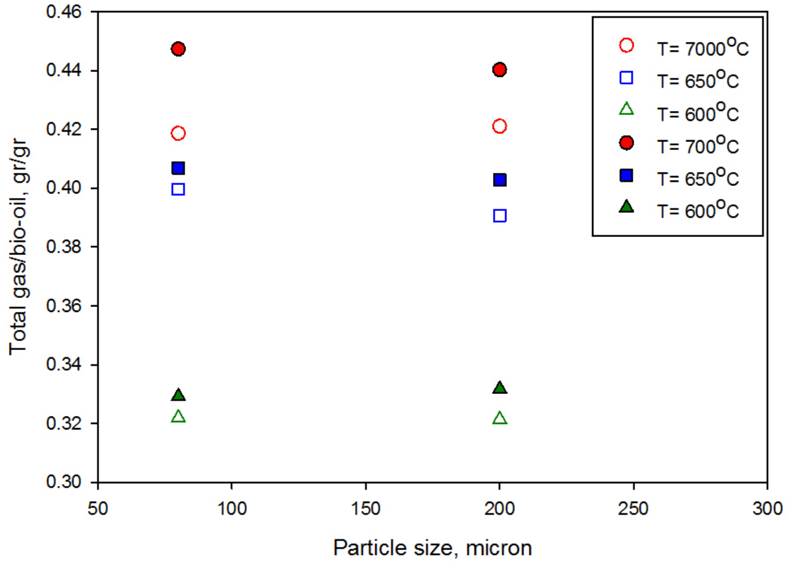

Figure 2.17. **Effect of sauter mean diameter of the sand on total yield of gasification. Empty symbols: mass of bed 1.5kg, bold symbols: mass of bed 3.0kg**

In addition, Figure 2.17 illustrates that, at the best condition, total conversion of bio-oil to gaseous products was less that 45%; therefore, in order to increase conversion of bio-oil to gaseous products, the effect of additional steam, of elevated temperatures and of appropriate catalysts must be investigated.

2.5.5. Syngas (H_2+CO) production

The two gases of economic interest for conversion to other products are hydrogen and carbon monoxide. This section reports the total production of these two gases and its quality, as determined by the molar H_2/CO ratio. Figure 2.18 shows that the rate of syngas production increases with increasing temperature. It also decreases moderately with time.

The molar H_2/CO ratio is usually an important parameter in reforming processes and all processes would require ratios higher than that obtained in this study. Figure 2.19 shows that this ratio dropped dramatically with time; as it was seen before, concentration of CO tends to increase by time while concentration of hydrogen reduces by time. Bed mass also had little effect on the molar H_2/CO ratio

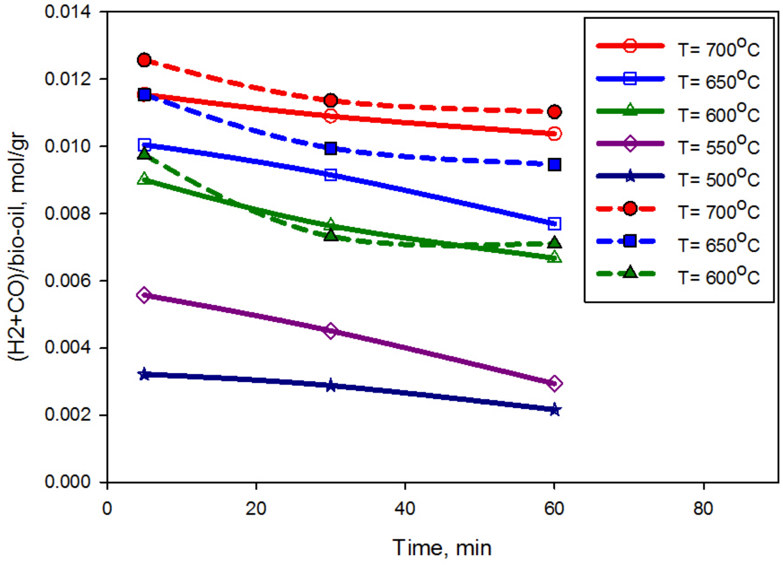

Figure 2.18. **Yield of syngas production as moles produced per injected grams of bio-oil; solid lines: mass of bed 1.5kg, dashed lines: mass of bed 3.0kg; sauter mean diameter of the sand: 200µm**

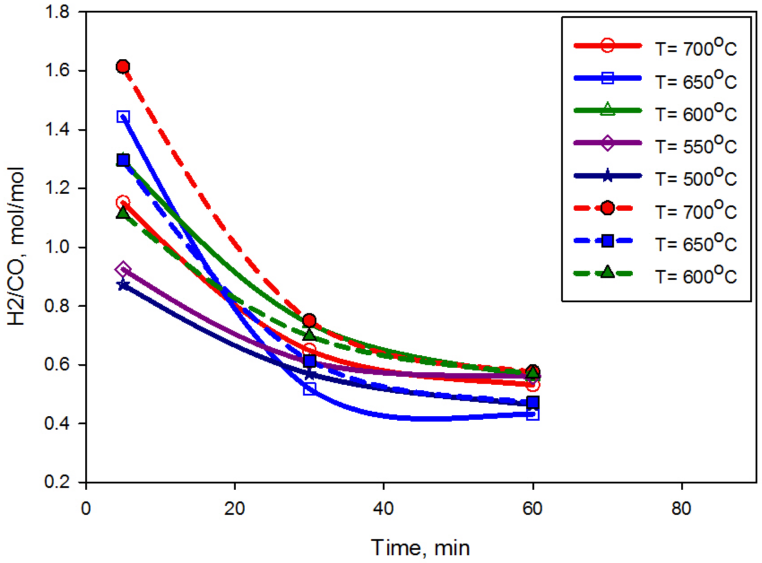

***Figure 2.19.* Yield of molar H2/CO ratio; solid lines mass of bed: 1.5kg, dashed lines mass of bed: 3.0kg; sauter mean diameter of the sand: 200µm**

2.6. Conclusions

Thermal cracking of whole of bio-oil was investigated in a bubbling fluidized pilot plant over temperature range of 500°C-700°C. The effects of gas residence time, temperature, bed mass and particle size on thermal cracking of bio-oil were studied. Longer residence times promote more cracking in the reactor and, as a result, more syngas is produced and the H_2/CO ratio is higher. Coke must have a detrimental effect on the kinetics of the gasification because higher yield of gasification was obtained at the beginning of experimental runs when deposition of coke in the bed was negligible, but, with time that coke is deposited on the surface of the sand, the yield of gasification declines. Higher temperatures always favor gasification yields, especially during the initial times of operation. In addition, liquid yields show that at low temperatures, bio-oil conversion is very poor. At the operating conditions studied, kinetics always control the thermal cracking reactions and the system is far from thermodynamic equilibrium. Total yield of gasification was increased, not significantly though, after the bed mass was doubled which is probably due to the fact that mass ratio of deposited coke to sand became less and, as a result, the detrimental effect of coke on the gasification kinetics was reduced. Results obtained using either group B and group A sand were very similar, indicating no heat and mass transfer limitations in the bed.

References

[1] Spath PL, Dayton DC; “Assessment of Synthesis Gas to Fuels and Chemicals with Emphasis on the Potential for Biomass-Derived Syngas”; December 2003

[2] Demirbas MF; “Hydrogen from Various Biomass Species via Pyrolysis and Steam Gasification Processes”; Energy Sources, Part A, (2006), 28:245–252

[3] Czernik S, French R, Feik C, Chorine E; “Hydrogen by Catalytic Steam Reforming of Liquid Byproducts from Biomass Thermoconversion Processes”; Ind. Eng. Chem. Res. 2002, 41, 4209-4215

[4] Wang D, Czernik S, Montane D, Mann M, Chornet, E; “Biomass to Hydrogen via Fast Pyrolysis and Catalytic Steam Reforming of the Pyrolysis Oil or Its Fractions” Ind. Eng. Chem. Res. 1997, 36, 1507-1518

[5] Basagiannis AC, Verykios XE; “Reforming reactions of acetic acid on nickel catalysts over a wide temperature range “;Applied Catalysis A: General 308 (2006) 182–193

[6] Basagiannis AC, Verykios XE; “Catalytic steam reforming of acetic acid for hydrogen production”; International Journal of Hydrogen Energy 32 (2007) 3343 – 3355

[7] Takanabe K, Aika K, Inazu K, Baba T, Seshan K, Lefferts L; “Steam reforming of acetic acid as a biomass derived oxygenate: Bifunctional pathway for hydrogen formation over Pt/ZrO2 catalysts”; Journal of Catalysis 243 (2006) 263–269

[8] Davidian T, Guilhaume N, Iojoiu E, Provendier H, Mirodatos C; “Hydrogen production from crude pyrolysis oil by a sequential catalytic process”; Applied Catalysis B: Environmental 73 (2007) 116–127

[9] Chaala A, Ba T, Garcia-Perez M, Roy C; “Colloidal Properties of Bio-oils Obtained by Vacuum Pyrolysis of Softwood Bark: Aging and Thermal Stability”; Energy & Fuels (2004), 18, 1535-1542

[10] Adjaye JD, Bakhshi, NN; “Production of hydrocarbons by catalytic upgrading of a fast pyrolysis bio-oil. Part II: Comparative catalytic performance and reaction pathways”; Fuel Processing Technology 45 (1995) 185-202

[11] Marquevich M, Czernik S, Chornet E, Montane D; “Hydrogen from Biomass: Steam Reforming of Model Compounds of Fast-Pyrolysis Oil”; Energy & Fuels (1999), 13, 1160-1166

[12] Rioche C, Kulkarni S, Meunier FC, Breen JP, Burch R; "Steam reforming of model compounds and fast pyrolysis bio-oil on supported noble metal catalysts"; Applied Catalysis B: Environmental 61 (2005) 130–139

[13] Vagia ECh, Lemonidou AA; "Thermodynamic analysis of hydrogen production via steam reforming of selected components of aqueous bio-oil fraction"; International Journal of Hydrogen Energy 32 (2007) 212 – 223

[14] Takanabe K, Aika K, Seshan K, Lefferts L; " Catalyst deactivation during steam reforming of acetic acid over Pt/ZrO2"; Chemical Engineering Journal 120 (2006) 133–137

[15] Yamazaki T, Matsuki K; " Steam reforming of biomass-derived substances over nanoporous Ru/ZrO_2 catalysts (part 1) steam reforming reaction of acetic acid"; Journal of the JJapan Petroleum Institute, 49 (5), 246-255 (2006)

[16] Basagiannis AC, Verykios XE; "Influence of the carrier on steam reforming of acetic acid over Ru-based catalysts"; Applied Catalysis B: Environmental 82 (2008) 77–88

[17] Davidian T, Guilhaume N, Daniel C, Mirodatos C; "Continuous hydrogen production by sequential catalytic cracking of acetic acid. Part I. Investigation of reaction conditions and application to two parallel reactors operated cyclically"; Applied Catalysis A: General 335 (2008) 64–73

[18] Davidian T, Guilhaume N, Daniel C, Mirodatos C; "Continuous hydrogen production by sequential catalytic cracking of acetic acid. Part II. Mechanistic features and characterization of catalysts under redox cycling"; Applied Catalysis A: General 337 (2008) 111–120

[19] Hu X, Lu G; "Steam Reforming of Acetic Acid to Hydrogen over Fe–Co Catalyst"; Chemistry Letters Vol.35, No.4 (2006)

[20] Wang D, Montané D, Chornet E; "Catalytic steam reforming of biomass-derived oxygenates: acetic acid and hydroxyacetaldehyde"; Appl. Catal. A. 143 (1996)

[21] Medrano JA, Oliva M, Ruiz J, Garcı´a L, Arauzo J; "Catalytic steam reforming of model compounds of biomass pyrolysis liquids in fluidized bed reactor with modified Ni/Al catalysts"; J. Anal. Appl. Pyrolysis 85 (2009) 214–225

[22] Guell BM, Babich I, Nicholas KP, Gardeniers JGE, Lefferts L, Seshan K; "Design of a stable steam reforming catalyst—A promising route to sustainable hydrogen from biomass oxygenates"; Applied Catalysis B: Environmenta, Volume 90, Issues 1–2, 25 July 2009, 38–44

[23] Hu X, Lu G; "Investigation of the steam reforming of a series of model compounds derived from bio-oil for hydrogen production"; Applied Catalysis B: Environmental 88 (2009) 376–385

[24] Hu X, Lu G; "Comparative study of alumina-supported transition metal catalysts for hydrogen generation by steam reforming of acetic acid"; Applied Catalysis B: Environmental 99 (2010) 289–297

[25] Hu X, Lu G; "Acetic acid steam reforming to hydrogen over Co–Ce/Al_2O_3 and Co–La/Al_2O_3 catalysts—The promotion effect of Ce and La addition"; Catalysis Communications 12 (2010) 50–53

[26] Vagia ECh, Lemonidou AA; "Investigations on the properties of ceria–zirconia-supported Ni and Rh catalysts and their performance in acetic acid steam reforming"; Journal of Catalysis 269 (2010) 388–396

[27] Thaicharoensutcharitthama S, Meeyoo V, Kitiyanan B, Rangsunvigit P, Rirksomboon T; "Hydrogen production by steam reforming of acetic acid over Ni-based catalysts"; Catalysis Today 164 (2011) 257–261

[28] Lu A, Changqing Dong LA, Yang Y, Lei He JZh; "The influence of Ni loading on coke formation in steam reforming of acetic acid"; Renewable Energy 36 (2011) 930e935

[29] Li Zh, Hu X, Zh L, Lu G; "Renewable hydrogen production by a mild-temperature steam reforming of the model compound acetic acid derived from bio-oil"; Journal of Molecular Catalysis A: Chemical; Volume 355, March 2012, 123–133

[30] Garcia1 L, French R, Czernik S, Chornet E; "Catalytic steam reforming of bio-oils for the production of hydrogen: effects of catalyst composition"; Applied Catalysis A: General 201 (2000) 225–239

[31] Kechagiopoulos PN,Voutetakis SS, Lemonidou AA, Vasalos IA;"Hydrogen production via steam reforming of the aqueous phase of bio-oil in a fixed bed reactor"; Energy & Fuels 2006, 20, 2155-2163

[32] Medrano JA, Oliva M, Ruiz J, Arauzo J; "Hydrogen from aqueous fraction of biomass pyrolysis liquids by catalytic steam reforming in fluidized bed"; energy 36 (2011) 2215-2224

[33] Panigrahi S, Chaudhari ST, Bakhshi NN, Dalai AK; "Production of Synthesis Gas/High-Btu Gaseous Fuel from Pyrolysis of Biomass-Derived Oil"; Energy & Fuels 2002, 16, 1392-1397

[34] Panigrahi S, Dalai AK, Chaudhari ST, Bakhshi NN; "Synthesis Gas Production from Steam Gasification of Biomass-Derived Oil"; Energy & Fuels 2003, 17, 637-642

[35] Czernik S, Evans R, French R; "Hydrogen from biomass-production by steam reforming of biomass pyrolysis oil"; Catalysis Today 129 (2007) 265–268

[36] Davidian T, Guilhaume N, Iojoiu E, Provendier H, Mirodatos C; "Hydrogen production from crude pyrolysis oil by a sequential catalytic process"; Applied Catalysis B: Environmental 73 (2007) 116–127

[37] Van Rossum G, Kersten SRA, van Swaaij WPM; "Catalytic and noncatalytic gasification of pyrolysis oil" Ind. Eng. Chem. Res. 2007, 46, 3959-3967

[38] Van Rossum G, Kersten SRA, Van Swaaij WPM; "Staged catalytic gasification/steam reforming of pyrolysis oil"; Ind. Eng. Chem. Res., 2009, 48, 5857-5866

[39] Wu C, Huang M, Sui M, Yan Y, Wang F; "hydrogen production via catalytic steam reforming of fast pyrolysis bio-oil in a two-stage fixed bed reactor system"; Fuel Processing Technology; 89 (2008) 1306-1316

[40] Sakaguchi M, Watkinson AP, Ellis N; "Steam gasification of bio-oil and bio-char slurry in a fluidized bed reactor"; Energy&Fuels, 2010, 24, 5181-5189

[41] Lan P, Xu Q, Zhou M, Lan L, Zhang S, Yan Y; "Catalytic steam reforming of fast pyrolysis bio-oil in fixed bed and fluidized bed reactors"; Chem. Eng. Technology, 2010, 33, No. 12, 2021-2028

[42] Seyedeyn-Azad F, Salehi E, Abedi J, Harding T; "Biomass to hydrogen via catalytic steam reforming of bio-oil over Ni-supported alumina catalysts"; Fuel Processing Technology 92 (2011) 563-569

[43] Bedmutha RJ, Ferrante L, Briens C, Berruti F, Inculet I; "Single and two-stage electrostatic demisters for biomass pyrolysis application'; Chemical Engineering and Processing 48 (2009) 1112–1120

[44] Briens C.; "Industrial Multiphase Reactor Design"; Department of Chemical and Biochemical Engineering; The University of Western Ontario, 2008

CHAPTER 3:

A Novel Fluidized and Induction Heated Micro Reactor for Catalyst Testing

3.1. Introduction

Gasification processes are conducted at very high temperatures [1] where the feedstock is cracked to produce hydrogen and carbon monoxide, which constitute a syngas, the key building block mixture for the production of many valuable chemicals in the petrochemical industry. Steam reforming of natural gas and coal are very common gasification processes. Recent developments of renewable energy resources, like biomass conversion, have opened up new pathways to produce syngas. For example, biomass can be directly converted to syngas. Also, bio-oil, which is the liquid product of biomass pyrolysis, can be gasified to syngas.

Gas-solid fluidized bed reactors offer some advantages when used for gasification reactions due to higher rates of mass and heat transfer when compared to fixed bed reactors. Bench scale and pilot plant scale reactors represent appropriate options to investigate the effect of some operating parameters [2] such as temperature, pressure, residence time, steam-to-carbon ratio and carbon-to-catalyst ratio. However, such reactors are not ideal to test new catalyst formulations for the gasification process, since they require relatively large amounts of catalyst. On the other hand, suitable micro reactors may help reducing the cost of testing various catalyst preparations under ideal conditions.

Currently, available micro reactors have some drawbacks. For instance, due to temperature gradients, poor mixing, and unrealistic catalyst on stream times, traditional fixed bed micro reactors may not be able to truly mimic the operating conditions of the industrial reactors. Similar drawbacks are associated with the very limited fluidized bed micro reactor technologies available in the market. For example, although the SCT-RT is a micro reactor which operates batch-wise, it is designed specifically to test catalysts of processes which require very short residence time like the FCC process [3]. The Berty-style recycle reactors suffer from axial coke profile due to high recycle rates [4]. The riser simulator developed by de Lasa's group [5], overcomes the problem of Berty-style reactors by intense gas-solid mixing provided by an internal impeller above the basket of catalysts. However, a major problem with such micro reactors is the heating method. Gasification processes are endothermic, so enough heat must be supplied to provide heat for the endothermic chemical reactions. In traditional reactors, an external heater is provided for this purpose, where heat is transferred through the wall of the reactor and then to the gases and solids inside the reactor. Therefore, the temperature on the wall of the reactor must be kept at a higher level than that in the core of the reactor. As a result, hot spots are formed next to the wall of the reactor. In addition, since heat is transferred from a wall to a gas, the heat transfer coefficient is low and, consequently, the wall temperature must be maintained significantly higher than the temperature of the core of the reactor. In addition, the volume of the catalyst bed in the riser simulator is much smaller than its total internal volume. Therefore, for a given residence time, a significant fraction of reactions proceed in the non catalytic, hot section of the reactor. Moreover, using an impeller operating at high temperature to provide mixing of the solids increases the potential of gas leakage through the mechanical seals.

Some heating techniques have been employed to attempt to gain information about the temperature profiles inside the test reactors which are similar to those in commercial reactors, such as single pulse shock-tube [6], light irradiation [7] and resistive heating [8]. The single pulse shock tube essentially works based on bursting a diaphragm located between a high pressure and a low pressure gas sections. Not only the apparatus should be large, but the shock tube system does not seem to be able to maintain the constant temperature for a long residence time i.e. more than a few milliseconds. Also, the burst diaphragm must be replaced each time with a new one. The light irradiation setup is designed for thermo gravimetric studies only in which a concentrated flux of light is beamed to a mass in the focal point of an elliptical mirror. Since each material has different reflectivity and absorptive properties, these optical parameters must be known to estimate the required flux of the light. Also, since small values of the flux are needed, the short duration of the light pulses must be very well controlled. An alternating current through a wire mesh supplies heat in the resistive heating method; however, this apparatus is also designed for thermo gravimetric studies of pyrolysis. A thermocouple is attached to the wire mesh, but the temperature difference between the wire mesh and the gases in the reactor is not reported.

Induction heating is a heating technique which has been utilized for several applications such as hardening, melting and welding of conductive materials. The advantage of this heating system is that it is clean, indirect, non-contact, very fast and precisely controllable.

Induction heating is used to heat up conductive materials with high frequency electrical power where an AC current passes through a copper coil attached to a power supply [9,10]. Due to the high frequency of the power, the direction of the produced magnetic field around the copper coil alternates very rapidly. The magnetic field induces current on the surface of the conductive material which is inside the coil. Varying the direction of the magnetic field also changes the direction of the induced current alternatively, which generates heat. Two types of current can be induced on the surface of the conductive material: the eddy current and hysteresis current. The alternating magnetic field induces eddy currents within the material, whether the material is ferromagnetic or paramagnetic. However, if the conductive material is ferromagnetic and its temperature is below its Curie point, a hysteresis current is also formed: the alternating magnetic field magnetizes and de-magnetizes the material crystals, and this rapid switching of magnetic properties causes considerable friction and heating inside the material. The size of the coil and position of the conductive material are important factors to make an effective induction couple to achieve maximum efficiency of the induction heating [11].

There are very few reports on the application of induction heating to chemical reactors. Rastogi *et al.* developed a batch micro reactor to study the kinetics of propane pyrolysis. To minimize the temperature gradient, ferromagnetic wires with different Curie temperatures were provided inside a magnetic field. These researchers demonstrated that the temperature of the micro reactor rapidly reached the Curie point of the corresponding ferromagnetic wire and then remained constant over the period of induction heating [12]. Tsai *et al.* used induction to heat up a tubular stainless steel reactor in which biomass pyrolysis was taking place. However, they did not report the temperature difference between the reactor wall and its contents [13].

Initial developments by Rohani *et al.* indicated that an external induction field can heat up vertical Inconel wires inside a fluidized bed. As a result, the heat is very rapidly generated inside the catalyst bed and efficiently and uniformly distributed throughout the solid particles which are being fluidized, thus avoiding the creation of hot spots and high temperature gradients [14]. To prevent shielding of the induction field, the body of reactor cannot be metallic and it must be made of ceramic.

An efficient heat and mass transfer can be achieved by mixing the catalytic bed in a gas fluidized bed reactor; however, such a reactor can not be used for a batch-wise reactor unless the fluidizing gas is circulated by a mechanical force. Rather than using a fluidizing gas, the catalyst particles can be fluidized mechanically [15, 16]. For example, the novel reactor presented in this study uses a linear pneumatic actuator to vertically mix the bed of solids. A major advantage of this method is that it is non-invasive. There are reports of some other applications of mechanical vibration used to enhance the performance of chemical reactors. Klusacek *et al.* achieved a CSTR condition in their reactor with a piston vibrating at 20Hz with a 3mm amplitude, which was generated by a commercial loud speaker and an amplifier [17]. Richter *et al.* used an electromotor attached to a shaft to vibrate their CSTR reactor, but they did not report the frequency and the amplitude of their vibrator [18]. The disadvantage of using an electromotor is that other than being expensive, it is not very flexible, since it is difficult to adjust its frequency and amplitude of the vibrations. Electromagnetic vibrators have also been used for some chemical reactor applications. Squires used an electromagnetic vibrator to investigate axial gas dispersion in laboratory gas-solid reactors [19]. Nelson *et al.* used an electromagnetic vibrator to fluidize titania-based catalysts for the photo catalytic oxidation of methanol [20]. Although it has been proven that vibrations are an effective technique for fluidization, due to the fact that electromagnetic vibrators operate at very high frequencies of about 20-40Hz and short amplitudes of 2-4mm, beds of solid catalyst do not expand entirely inside the reactor. Therefore, secondary reactions would take place in the catalyst-free portion of the reactor. In batch systems, it is desirable to fluidize the catalysts over the entire length of the reactor. It is, therefore, essential to adjust the amplitude and frequency of the vibrations to ensure that the catalyst moves between the two ends of the reactor. In addition, the frequency must be high enough to provide intense mixing of the catalyst with the gas phase and to avoid segregation of particles with different physical characteristics.

The objectives of the work described in this paper were the design, construction, operation and optimization of the fluidization dynamics of a novel mechanically mixed “jiggle bed” reactor suitable for gasification catalyst testing, and, secondly, the characterization of the performance of its heating system.

3.2. Equipment

3.2.1. The Jiggle Bed Reactor

The objective of the design of the new jiggle bed reactor (JBR) was to provide a well controlled reactor for testing gasification catalysts in a fluidized gas-solid system, where mixing of the catalysts was created by a vibrating motion and the required heat for the endothermic reactions was supplied by induction heating. The jiggle reactor includes three sections: the linear pneumatic actuator, the reaction zone, and the induction heating system. The main structure of the JBR is shown in Figure 3.1.

The gasification reactions take place batch-wise in the JBR. Before injecting the feed, inert gas flushes away any air from the reactor. The feed is then introduced in the reactor through an air lock. At the end of each run, the lower inlet valve and the outlet valve are opened (lower valve 1 and valve 9 in Figure 3.1), and the reaction products are flushed out by a flow of inert gas into a gas sampling bag.

Since induction heating is used to supply the required heat, the reaction chamber is made of a non-conductive material to prevent shielding of the magnetic field. In addition, it is necessary to ensure that it can withstand temperatures as high as 900 °C. Moreover, the material must be non-porous and strong enough to sustain the vibrating conditions. Therefore, a non-porous ceramic crucible made of 99.8% alumina is utilized. The crucible has an I.D. of 2.54 cm and a height of 7.3 cm (Figure 3.2a).

Catalyst particles are fluidized inside the ceramic crucible due to the alternating vertical motion of a linear pneumatic actuator installed below the crucible. This vibrating motion is transferred to the crucible through a scalloped shape stainless steel on top, three stainless steel threaded support rods and a round aluminum seat underneath the crucible, which is mounted directly on the air cylinder of the actuator.

As shown in Figure 3.2b, the heating element of the JBR is an assembly of eight Inconel wires with a 0.32 cm diameter and a 7.0 cm length, which are attached symmetrically to a round disk made of Inconel. This assembly is inserted from the top, inside the ceramic crucible. When a high frequency current is applied through the copper coil (item 11 in Figure 3.1), the associated magnetic field induces a current through the Inconel wires. Due to the high frequency of the magnetic field, the energy of the induced currents is lost rapidly in the form of heat which is uniformly transferred from the surface of the wires into the bed of catalyst particles.

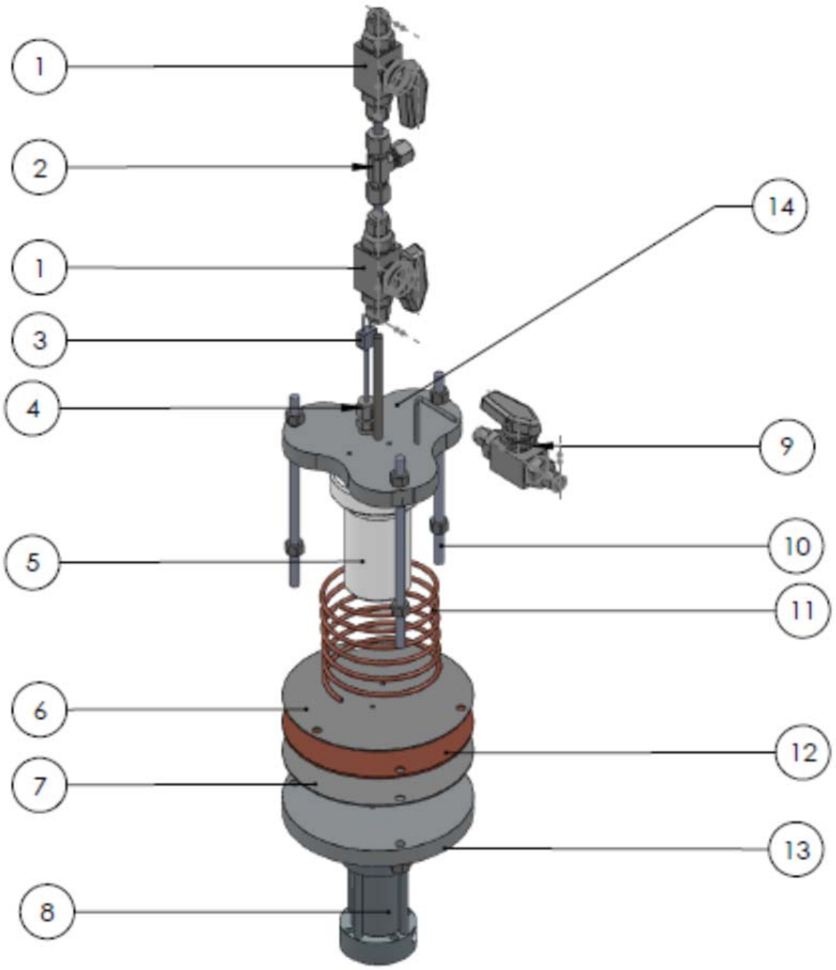

***Figure 3.1.* Diagram of the jiggle reactor: 1. on/off feed valves 2. Inlet of carrier gas 3. Thermocouple 4. Inlet of feed and carrier gas 5. Ceramic crucible with insulation 6. Insulation disk 7. Insulation disk 8. Linear pneumatic actuator 9. Outlet gas valve 10. Stainless steel support rods 11. Copper coil 12. Copper disk 13. Aluminum disk mounted on the actuator 14. Stainless steel scalloped disk**

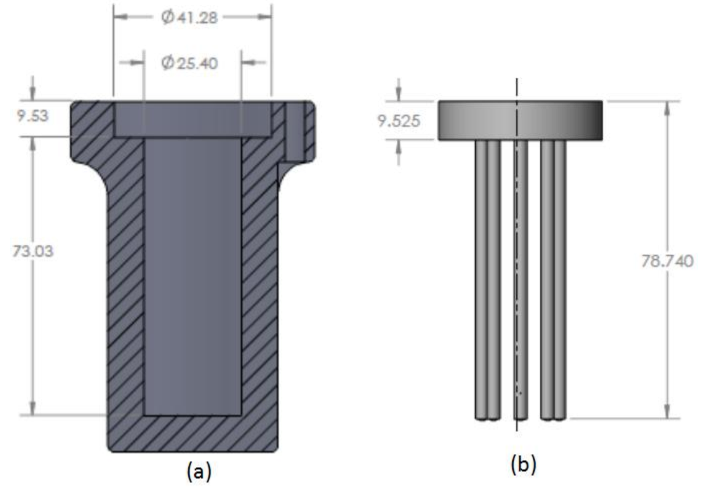

Figure 3.2. **Reaction chamber of the jiggle bed reactor: a) ceramic crucible b) heating element assembly (dimensions are in mm)**

3.2.2. The Motion system

In order to provide good mixing between the solids and gases over the entire length of the ceramic crucible, a linear pneumatic actuator was designed to vibrate the reaction chamber of the JBR with the appropriate frequency and amplitude. This reciprocating motion is transferred to the solid particles inside the ceramic crucible, fluidizing them. The linear pneumatic actuator consists of the following parts (Figure 3.3):

1. Compressed air line
2. A double acting BIMBA FLAT-II air cylinder with dual piston rods and a rod end block to ensure that the rods work in tandem.
3. Two BIMBA reed switches (RS) attached on the external surface of the air cylinder to control the motion of the piston.
4. A 2 position, 3 way solenoid valve to alternate the direction of the compressed air flow between extension and retraction modes.
5. Two air flow controllers to adjust the flow rate of the compressed air.
6. Tubing between the solenoid valve and the air cylinder.

7. A programmed logic controller (PLC) to start up and shut down the actuator and also to actuate the solenoid valve to alternate the direction of the compressed air flow between extension and retraction modes

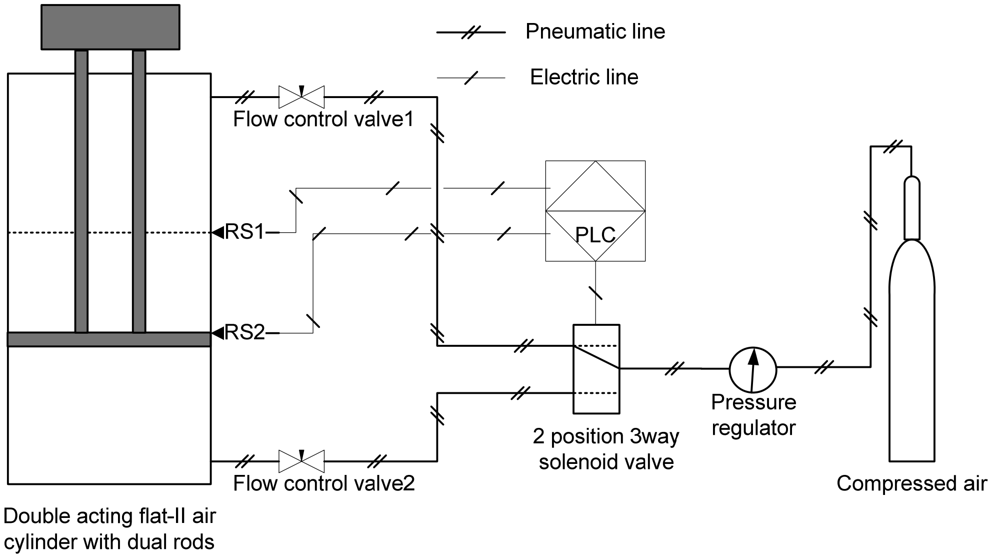
Pneumatic line
Electric line
Flow control valve1
RS1
RS2
PLC
Pressure regulator
2 position 3way solenoid valve
Flow control valve2
Compressed air
Double acting flat-II air cylinder with dual rods

***Figure** 3.3.* **Schematic of the linear pneumatic actuator**

Having dual piston rods in the air cylinder eliminated the need for an external guide to align the movement of the reactor and prevent torsion. A magnet was inserted on the piston so that the reed switches could sense the position of the piston inside the air cylinder.

To find the optimum size of the air cylinder which could produce vibrations of the desired frequency and amplitude, the effect of mass of the reaction zone of the JBR, distance between the reed switches (RSD) and bore size of the air cylinder were investigated (see appendix A). An air cylinder with a 2.7 cm bore size and a 10.16 cm stroke length was, thus, selected as the core of the pneumatic actuator.

3.2.3. The induction heating system

A 9 kW Ameritherm EASY HEAT 7590LI power supply was used to provide high frequency current through the copper coil. The power supply works with a voltage of 187-230 VAC and its normal achievable frequency is 140kHz-400 kHz, depending on the size of its capacitors as well as the size and design of the induction coil and of the type of conductive metals inside the coil. Cooling water flows through the coil and then discharges from the power supply to prevent the coil to be melted by the high frequency and amperage of the current that flows through it. A UP550 YOKOGAWA controller was used to adjust the output power of the power supply to maintain the desired temperature setpoint within the reactor, which is measured with a type K thermocouple.

The copper coil was made of 6 turns of a tube with 0.64 cm O.D.. Both coil diameter and height were 7.6 cm. An insulation sleeve for electricity was used to cover the external surface of the coil for safety reasons. A high temperature sleeve was used for the lower turn of the coil where it is in contact with very hot surfaces.

Although the JBR has a fast vibrating motion, the final design implemented included a coil that moved with the ceramic crucible, eliminating any motion between the coil and the internal Inconel wires. This design was selected to avoid any possible variability of the magnetic field which would lead to a non-uniform heating of the internal Inconel wires. Therefore, in order to deliver the electrical current from the power supply to the vibrating coil, two insulated, conductive flexible tubes with a 91cm length and a 0.64 cm I.D. connected the coil to the power supply.

3.3. Optimization of fluidization dynamics - Cold study

3.3.1. Particle mixing in the jiggle bed reactor

Mixing of the catalyst particles inside the ceramic crucible is induced by the vertical alternating motion of the linear pneumatic actuator. As a result of this motion, the catalyst bed alternately expands and contracts.

When the catalyst bed expands over the entire length of the crucible, the majority of the gas in the upper part of the crucible is displaced downward. When the bed contracts downward, the gas in the lower regions of the crucible is displaced upward. Thus, the alternating expansion/contraction of the catalyst bed induces intense axial and radial mixing of the gas and solid phases. It also promotes heat and mass transfer between the gas and the catalyst particles. Some sequences of the particles mixing are illustrated in Figure 3.4 when a transparent crucible was used.

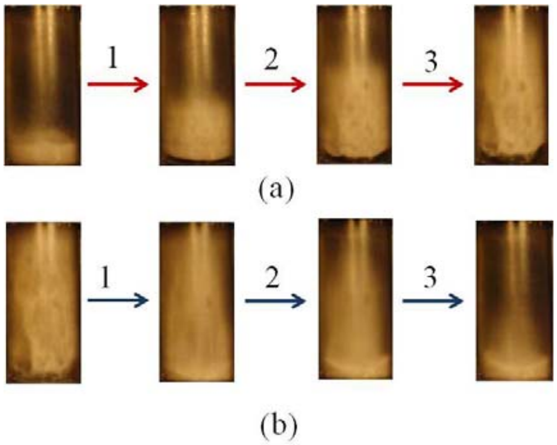

***Figure 3.4.* Sequences of mixing of catalyst particles in the jiggle bed reactor: (a) bed expansion during downward actuator retraction (b) bed contraction during upward actuator extension**

To achieve intense mixing, the actuator must be operating with a sufficiently high frequency and amplitude to mix the catalyst particles over the entire length of the ceramic crucible. A systematic study was, therefore, conducted to identify the operating conditions resultingin the catalyst bed expanding over the entire length of the crucible and, overall, in a good mixing throughout the micro reactor volume.

3.3.2. Experimental set-up

A visual set-up with a transparent crucible was developed to investigate the uniform distribution of catalyst particles over the entire length of the crucible as a function of the amplitude and frequency of the pneumatic actuator (Figure 3.5).

Sand particles with mass of 5 g, 10 g and 20 g and size distributions of 75-149 μm, 149-212 μm, and 212-355 μm were loaded in a transparent crucible with dimensions similar to those of the ceramic crucible, to form a bed of particles. The pressure of the air driving the actuator was varied between 138 kPa and 690 kPa to adjust the actuator frequency between 3 and 6Hz. The amplitude of the pneumatic actuator motion was varied between 6.4 and 8.9 cm.

A CASIO EX-FS10 high speed video recording camera, located in front of the transparent crucible (Figure 5) recorded the bed motion. The camera was attached to the crucible frame, so that there was no relative motion between the crucible and the camera. The recording rate of the videos was 210 frames per second. The distance between the camera and the crucible was 13.5 cm. To enhance the contrast of the video recordings, the back of the transparent crucible was wrapped in black tape to provide a dark background contrasting with the light colour of the sand particles. In addition, two 500 W lights illuminated the front of the transparent crucible to improve the video quality.

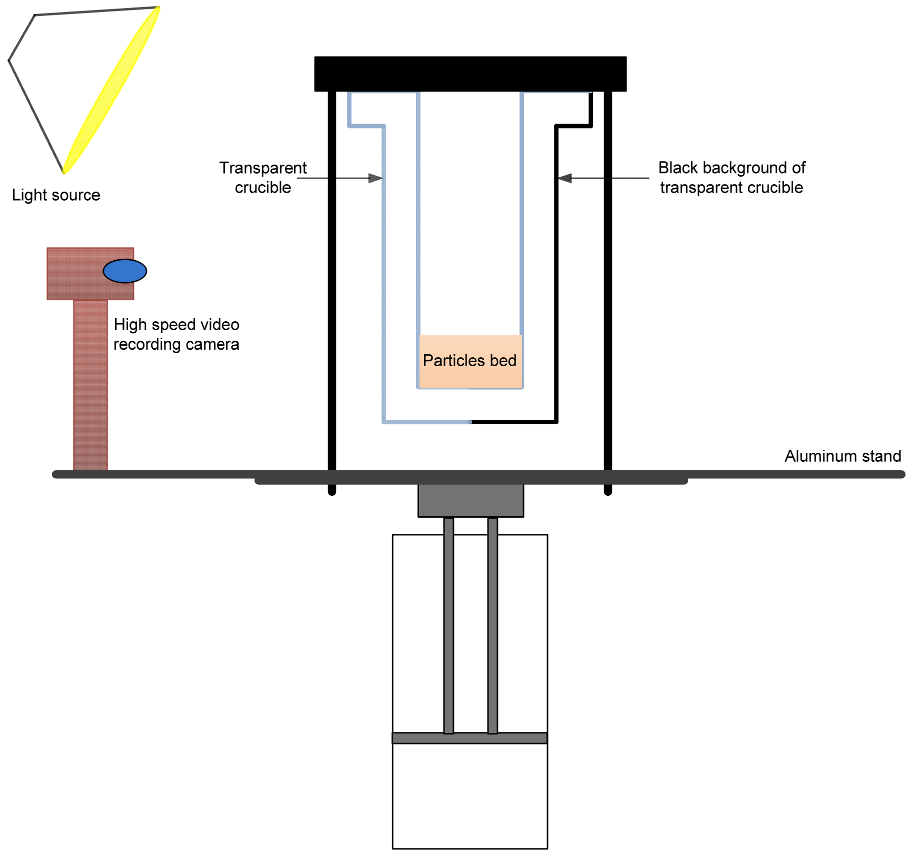
Light source
Transparent crucible
Black background of transparent crucible
High speed video recording camera
Particles bed
Aluminum stand

Figure 3.5. **Visual set-up to investigate mixing of sand particles in a transparent crucible**

Viewing the videos in slow motion shows that the catalyst bed reaches its minimum height when the actuator is in its full extension mode. On the other hand, the catalyst bed expands quickly in the crucible when the actuator is in retraction mode. This behavior is caused by the inertia of the catalyst particles. In addition, the videos show that the speed of the bed expansion-retraction does not follow the speed of the actuator so that particles are mixed faster.

3.3.3. Image processing methodology

A video to picture conversion software was used to convert the recorded videos, originally in AVI format, to a series of successive pictures, in JPEG format. Pictures showed the catalyst bed every 1/210th of a second.

A MATLAB program was developed to upload the pictures in the RGB (red, green and blue) color mode and then convert them to the gray mode. In the gray mode, a single pixel of the picture is described by one gray value between 1 and 256 levels, where 1 corresponds to black and 256 corresponds to white.

For each run, 3000 pictures of a test were uploaded and converted in MATLAB, which corresponds to about 15 seconds. To gain pictures containing the area of the crucible and its content of the sand particles only, a frame around the crucible was cropped from the first picture and then the same area was cropped from other pictures automatically by the program. Since the high speed camera was attached to the crucible stand and did not move relative to the crucible, the coordinates of the area of the cropped frames were the same. The program converted the cropped frame of each picture to a matrix.

In order to develop a methodology to interpret uniform distribution and fluidization enhancement of the sand particles by image processing, the coefficient of variation of the pixel gray values was obtained in both space and time coordinates:

$$CV_{space} = \left(\frac{\sigma}{\mu}\right)_{space} = \frac{\sqrt{\frac{1}{N_i}\sum_i\left(y_{i,j}-\frac{\sum_i y_{i,j}}{N_i}\right)^2}}{\frac{\sum_i y_{i,j}}{N_i}} \tag{3.1}$$

$$CV_{time} = \left(\frac{\sigma}{\mu}\right)_{time} = \frac{\sqrt{\frac{1}{N_j}\sum_j\left(y_{i,j}-\frac{\sum_i y_{i,j}}{N_j}\right)^2}}{\frac{\sum_j y_{i,j}}{N_j}} \tag{3.2}$$

where i is the index for space and j is the index for time.

To estimate CV_{space} of each cropped frame, the program first calculated CV_{space} for each column of the matrix corresponding to the cropped frame. Then, the average of CV_{space} for all the matrix columns was considered as the CV_{space} of the related frame.

Preliminary tests showed that CV_{time} is a useful indicator of local mixing versus time, but it does not seem to be related to the fluidization of the solid particles along the reactor. On the other hand, CV_{space} is a useful indicator to quantify the motion of the catalyst bed along the length of the crucible. As the catalyst bed moves, CV_{space} fluctuates and its minimum value $CV_{space,min}$ corresponds to the maximum bed expansion. Values of $CV_{space,min}$ larger than 0.15 were obtained when the catalyst bed does not expand over the entire length of the crucible. On the other hand, when the catalyst bed reaches the top of the crucible, $CV_{space,min}$ becomes smaller than 0.15.

Figures 3.6a and 3.6b present digitized gray pictures of the sand particles with a mass of 10 g and size distribution of 149-212 μm at two extremes: when the bed is retracted to its minimum height (Figure 3.6a) and when the bed is expanded over the entire length of the crucible (Figure 3.6b). Figure 3.6c presents the corresponding vertical profiles of the horizontal average of pixel gray values. Figure 3.6c shows the uniform distribution of solids over the crucible length when the bed is fully expanded, while, when the bed is retracted, the sharp drop in pixel gray value from 120 to below 60 corresponds to the volume above the dense bed.

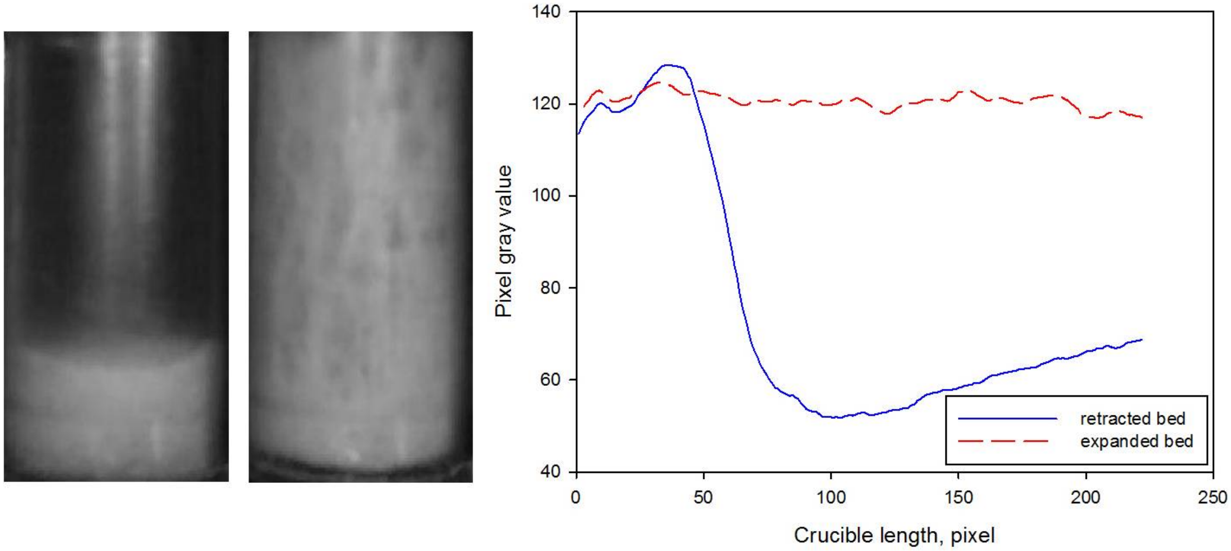

(a) (b) (c)

Figure 3.6. **Digitized gray pictures for a bed of the sand particles with 10 g mass and size distribution of 149-212 µm. Actuator frequency 4Hz: a) Retracted bed b) Expanded bed c) Variation of the horizontally averaged gray value along the crucible length.**

The variation of CV_{space} with time is illustrated in Figure 3.7 for 10 g of sand particles with size distribution of 149-212 µm and actuator frequency of 4Hz. The variation with time of CV_{space}, therefore, makes it possible to monitor the motion of the catalyst bed.

Therefore, a signal processing program, using the Fourier transform, was used to obtain the power spectrum from the variation with time of CV_{space}, at different amplitudes and frequencies. The power spectrum of the bed motion versus frequency of the bed motion, which was calculated from the variation with time of CV_{space}, is shown for different pneumatic air pressures in Figure 3.8. For each pressure, there is a clear dominant frequency. The dominant frequency provided the frequency of the catalyst bed motion. The power for the dominant frequency indicated the fluidization intensity. It can be seen that, although the frequency of the bed motion increases as the actuator air pressure is increased, the maximum power does not follow this trend and there is an optimum actuator air pressure (representing an actuator frequency) at which the maximum power, and hence the mixing intensity, can be achieved.

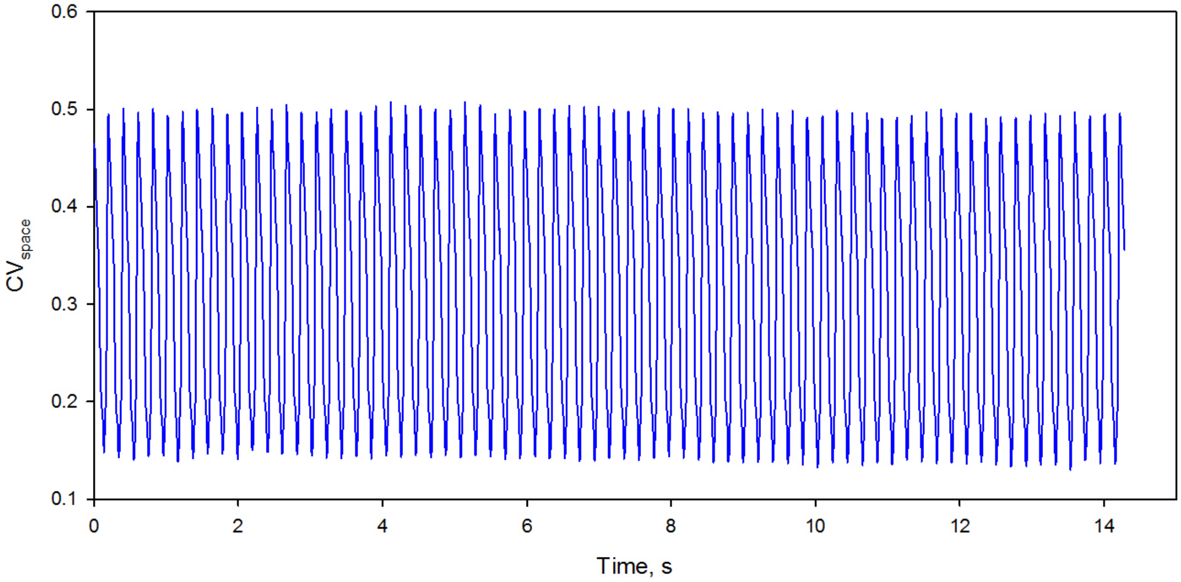

Figure 3.7. **Variation of CV_{space} versus time; sand particles 10 g, size distribution of 149-212 µm, air pressure of 345 kPa**

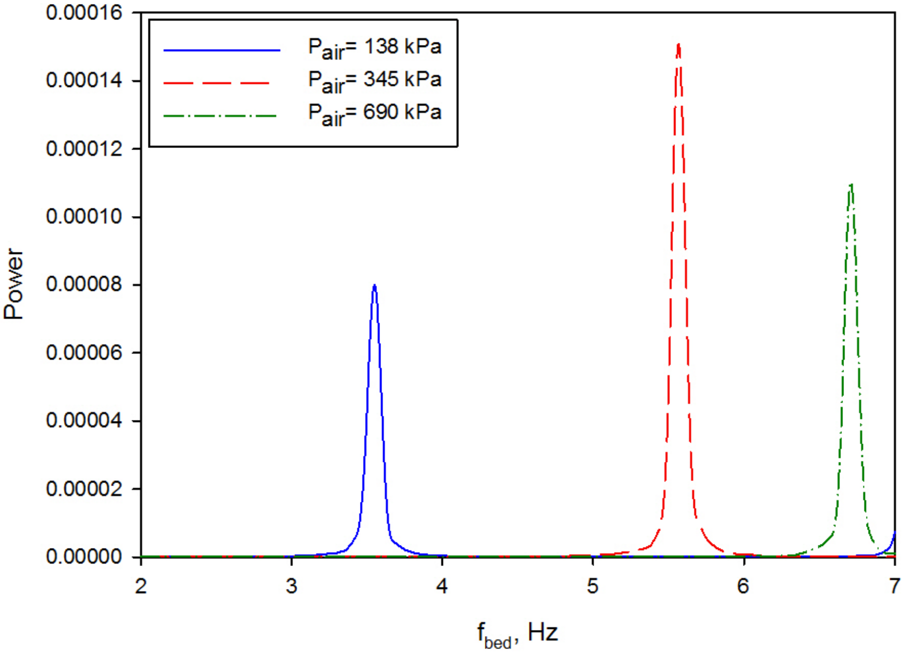

Figure 3.8. **Power spectrum of the bed motion; sand particles 10 g, size distribution of 149-212 µm; amplitude 6.4 cm**

3.3.4. Results and discussion

3.3.4.1. Relation between the air pressure and the frequency of the actuator

To estimate frequency of the alternating motion of the pneumatic actuator, the cycles were identified from the produced frames, and the frequency was estimated using Equation 3.3:

$$f_{actuator}(Hz) = \frac{No.of\ complete\ cycles}{No.of\ frames} \times \left(\frac{frame}{second}\right) \tag{3.3}$$

Figure 3.9 shows variation of the frequency with the air pressure applied to the actuator piston, at amplitudes of 6.4, 7.6 and 8.9 cm. As is expected, at a given air pressure, the frequency is lower for a longer amplitude. The frequency initially increases sharply with increasing air pressure and then plateaus at higher pressures. For the largest amplitude (8.9 cm), the frequency even decreases when the air pressure is increased beyond 600 kPa.

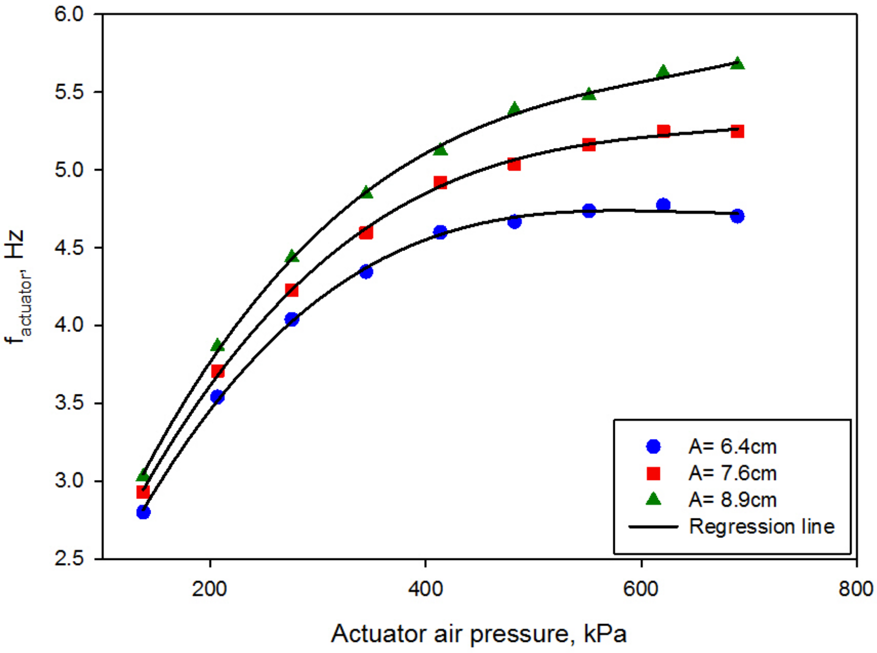

Figure 3.9. **Variation of frequency of the pneumatic actuator versus air pressure.**

3.3.4.2. Frequency of the actuator versus frequency of the bed

The dominant frequency of the bed, which is its significant frequency, is compared with the frequency of the actuator in Figure 3.10. As is shown, the bed vibrates with larger frequency than the frequency of the actuator at a given air pressure. In addition, there is a linear relation between the two frequencies. However, it is surprisingly noticeable that, despite some insignificant differences, the relation between the frequency of the bed and the frequency of the actuator is independent of the mass and size distribution of the particles inside the reactor according to the results displayed in Figures 3.10a and 3.10b.

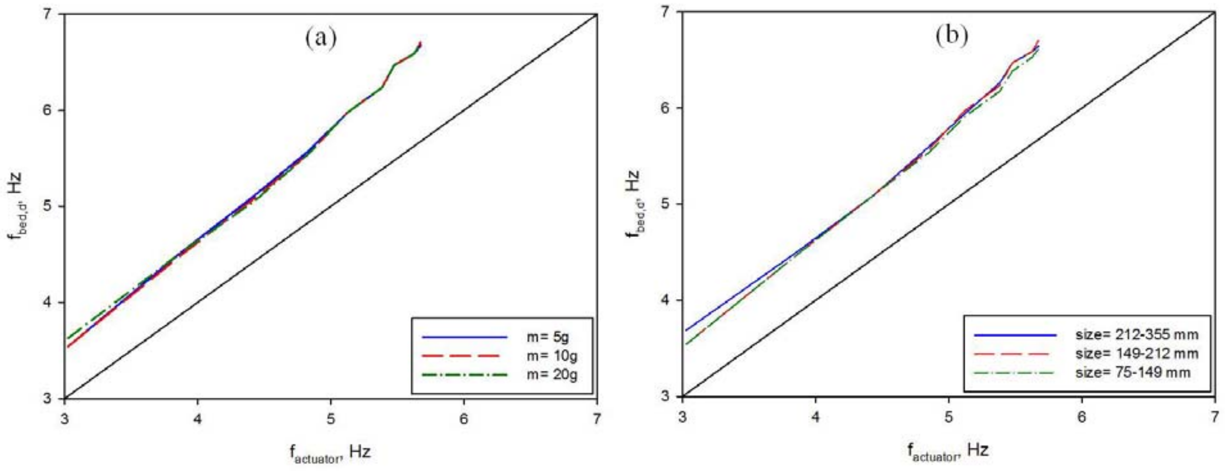

Figure 3.10. **Frequency of bed of the sand particles versus frequency of the actuator; (a) effect of mass; size 149-212 µm (b) effect of size distribution; mass 10g**

3.3.4.3. Effect of amplitude of the pneumatic actuator motion on fluidization

Figure 3.11 shows that $CV_{space,min}$ becomes less than 0.15 when the air pressure applied to the actuator piston is increased beyond 140 kPa, for all the tested amplitudes and frequencies. This indicates that there is good mixing of the particles as long as the air pressure was above 140 kPa.

Figure 3.12 compares the variation of the power of the CV_{space} signal with air pressure, for different amplitudes. As the pressure is increased, this power at first increases, peaks and then decreases. As the amplitude is increased, the pressure at which the power peaks increases, while the peak power decreases. This suggests that moderate amplitudes may be best to ensure intense mixing.

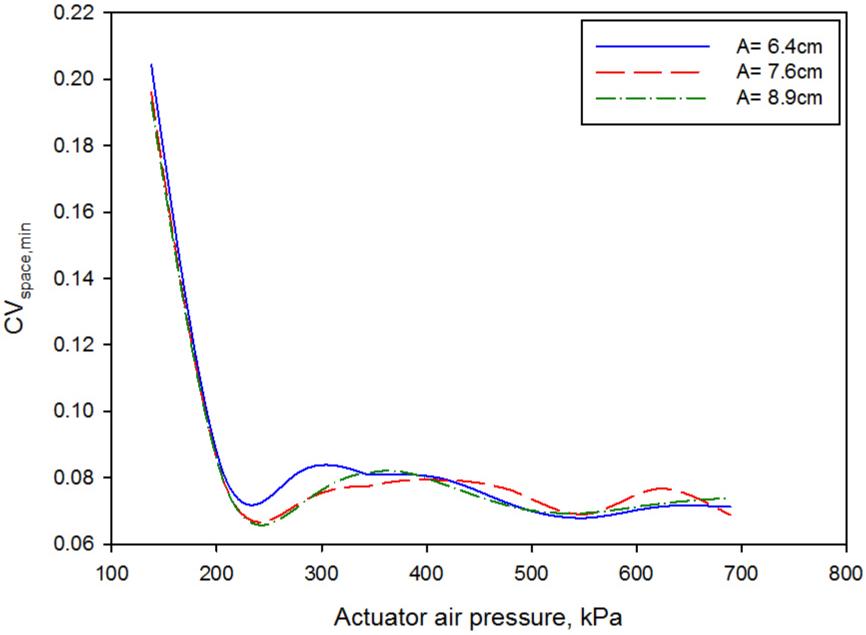

Figure 3.11. **Effect of amplitude on variation of $CV_{space,min}$ versus air pressure; sand particles: mass 10 g and size 149-212 µm**

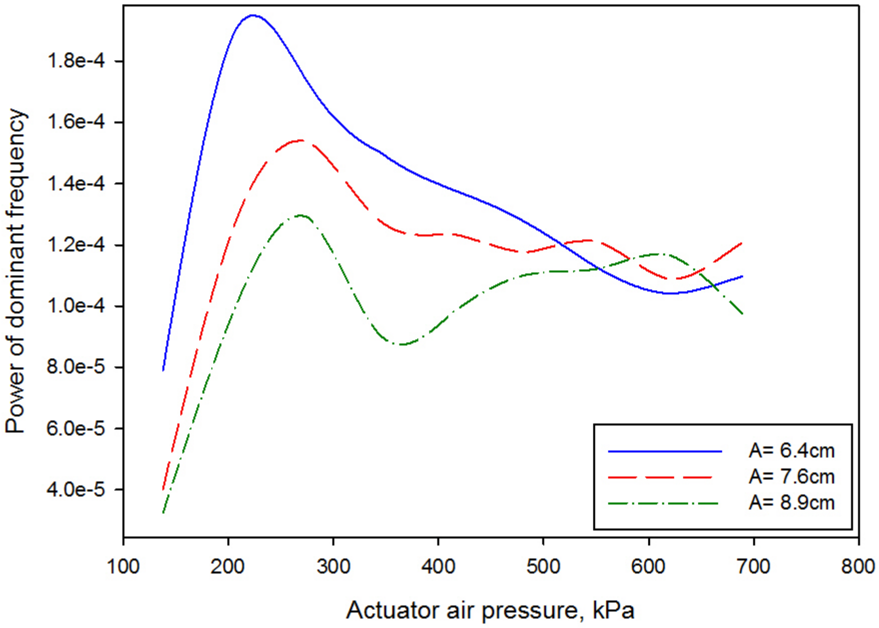

Figure 3.12. **Comparison of power of dominant frequencies versus air pressure and amplitude; sand particles: mass 10 g and size 149-212 µm**

3.3.4.4. Effect of mass and size distribution of the catalyst particles

Samples of the sand particles were prepared with size distributions of 75-149 µm, 149-212 µm and 212-355 µm and were filled in the crucible with masses of 5, 10 and 20 g. The amplitude of the pneumatic actuator was set at 7.0 cm and its frequency was adjusted by varying the air pressure.

There was no significant effect of bed mass of the sand particles on the variation of $V_{space,min}$ with the air pressure applied to the actuator piston. This means that the results of Figure 3.11 are valid for all the tested bed masses.

However, the bed mass had a significant impact on the fluidization dynamics, as shown in Figure 3.13. The power of the CV_{space} signal at its dominant frequency changed dramatically with the bed mass. This variation was non monotonic, with the highest power being achieved for the intermediate bed mass of 10 g, for all particle size distributions.

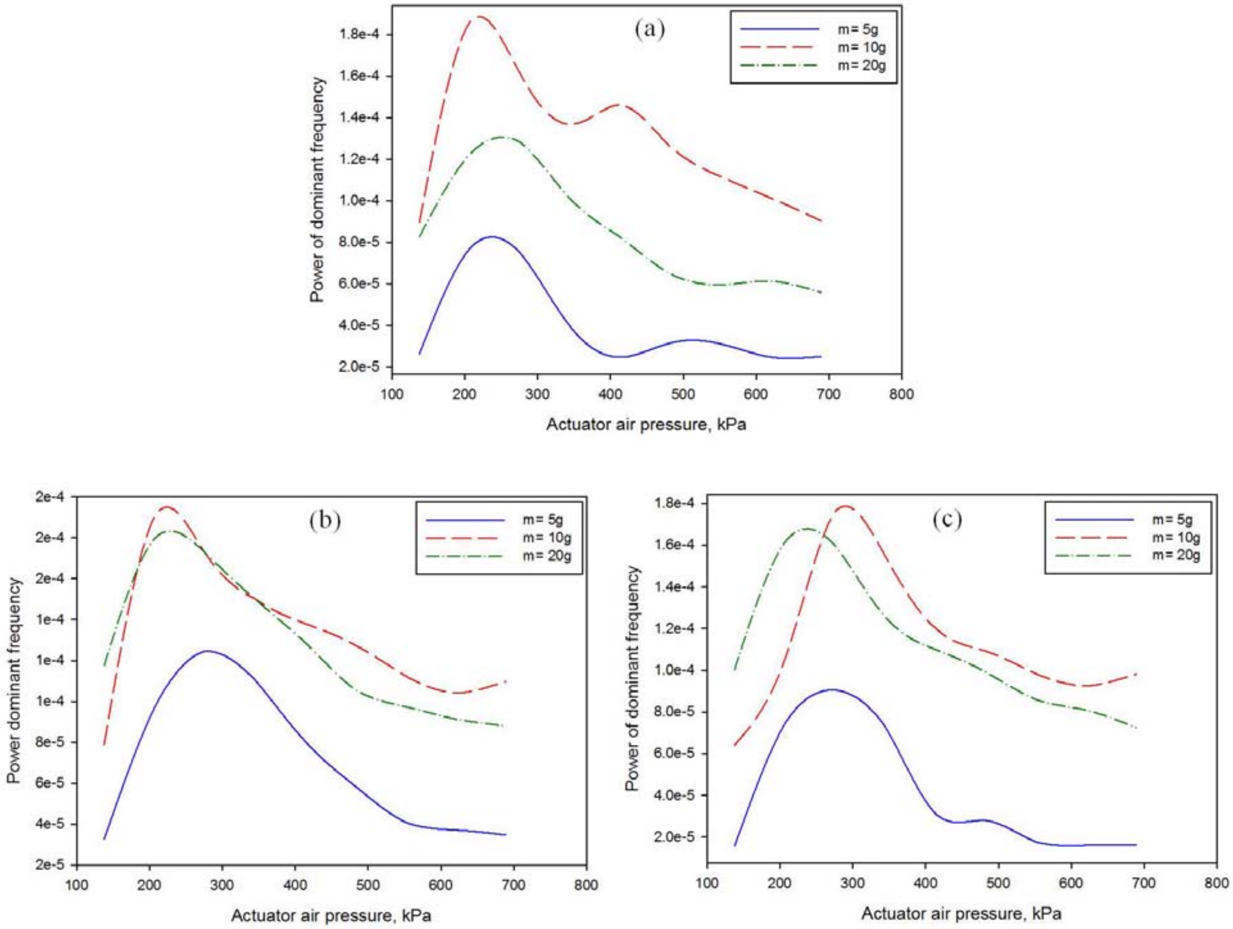

***Figure 3.13.* Effect of mass of the particles on dominant frequency power of the particle mixing; sand particles with size of (a) 212-355 µm, (b) 149-212 µm and (c) 75-149 µm**

The size distribution of the bed particles also had a significant impact on the fluidization dynamics, as shown in Figure 3.14. The power of the CV_{space} signal at its dominant frequency varied with size distribution of the bed particles. The highest power was obtained for the intermediate particle size distributions of 149 – 212 µm.

The conclusions that can be drawn from the results illustrated in Figures 3.13 and 3.14 is that it is best to use a bed of 10 g with a 149 – 212 µm particle size distribution. It is also preferable to operate the actuator piston with an air pressure slightly above 200 kPa.

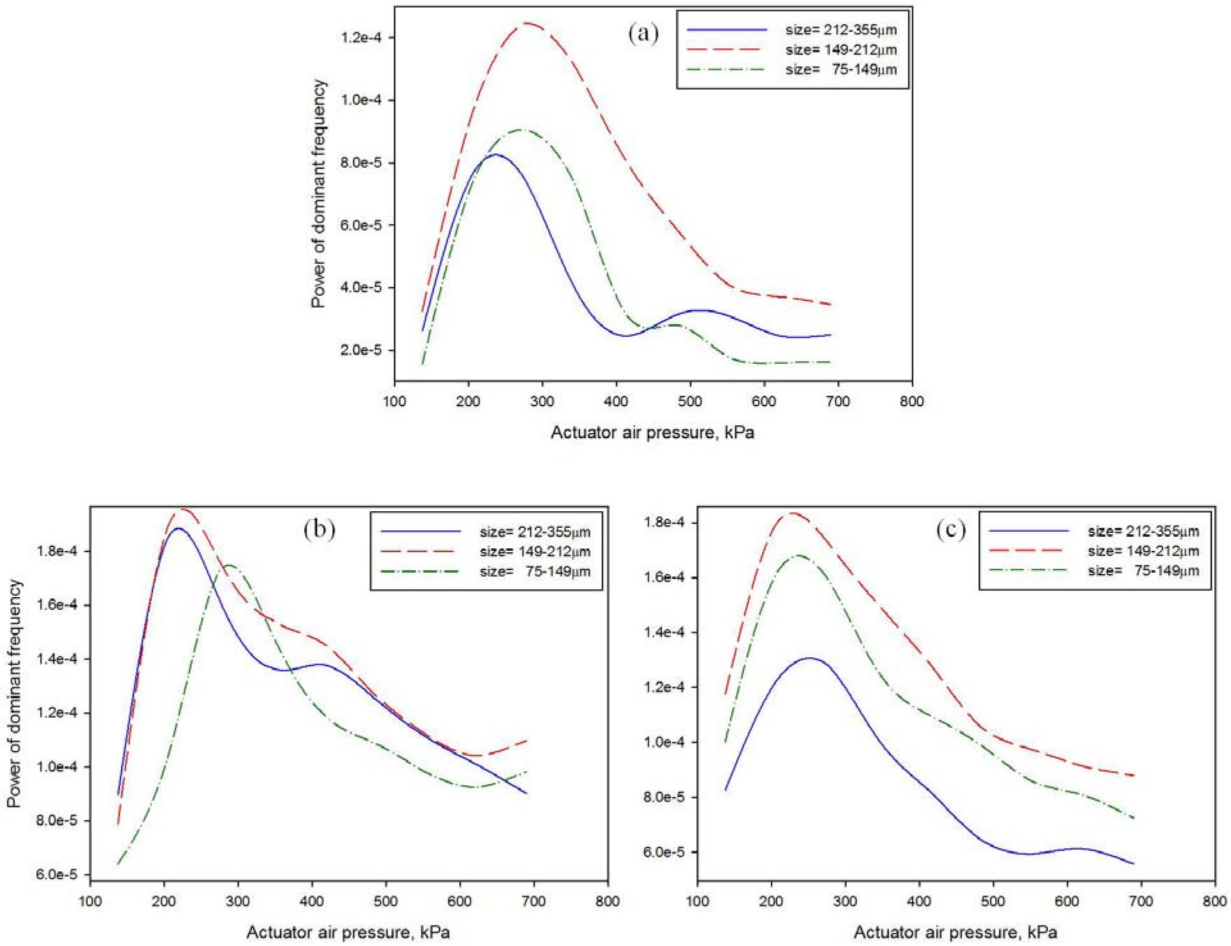

Figure 3.14. **Effect of size distribution of the sand particles on dominant frequency power of the particle mixing; mass of sand particles: (a) 5 g, (b) 10 g and (c) 20 g**

3.4. Optimization of fluidization dynamics- Heat transfer study

One of the main problems of the micro reactors that are currently used to test catalysts is that, with endothermic reactions, poor heat transfer results in metal heat transfer surfaces that are at a much higher temperature than the catalyst bed, causing undesirable parasitic thermal cracking reactions. It is, therefore, important to check that in the JBR, the temperature difference between the heating surfaces and the catalyst bed is minimized without compromising the ability to transfer the heat.

The ceramic crucible was loaded with 10 g of silica sand with a size distribution of 149-212 µm. The actuator was operated at air pressures of 138, 207 and 276 kPa and reactor was heated up to 800 °C by induction heating. The power supply was then switched off to let JBR cool down while the air cylinder was still vibrating.

3.4.1. Heat transfer modeling

When the power supply is switched off, the temperature of the catalyst bed drops quickly due to heat loss from the reactor:

$$m_s C_{P,s} \frac{dT_s}{dt} = -h_o A_o (T_s - T_\infty) \tag{3.4}$$

The temperature of the sand particles can be estimated by integrating Equation 3.4:

$$\frac{dT_s}{h_o A_o (T_s - T_\infty)} = -\frac{1}{m_s C_{P,s}} dt \tag{3.5}$$

$$\frac{dT_s}{(T_s - T_\infty)} = \frac{h_o A_o}{m_s C_{P,s}} dt \tag{3.6}$$

Setting a $= \frac{h_o A_o}{m_s C_{P,s}}$, Equation 3.6 is integrated:

$$\int_{T_{s,0}}^{T_s} \frac{dT_s}{(T_s - T_\infty)} = -\int_{t_0}^{t} a dt \tag{3.7}$$

Therefore,

$$\frac{T_s - T_\infty}{T_{s,0} - T_\infty} = exp\left(-a(t - t_0)\right) \tag{3.8}$$

During heating up of the catalyst bed in the JBR, the metal wires are heated by induction and heat is then transferred from the wires to the bed, where P is the power transferred to the bed. Heat is lost through the reactor wall, as during cooling:

$$m_s C_{P,s} \frac{dT_s}{dt} = P - h_o A_o (T_s - T_\infty) \tag{3.9}$$

Estimation of T_s during the heating step can be achieved by integrating Equation 3.9:

$$\frac{dT_s}{P-h_oA_o(T_s-T_\infty)} = \frac{1}{m_sC_{P,s}}dt \tag{3.10}$$

$$\frac{dT_s}{\frac{P}{h_oA_o}-(T_s-T_\infty)} = \frac{h_oA_o}{m_sC_{P,s}}dt = a\ dt \tag{3.11}$$

Setting $b = \frac{P}{h_oA_o}$, Equation 3.11 can be rearranged and integrated to form Equation 3.12:

$$\int_{T_{s,0}}^{T_s} \frac{d(T_s-T_\infty-b)}{(T_s-T_\infty-b)} = -\int_{t_0}^{t} adt \tag{3.12}$$

Therefore,

$$T_s = T_\infty + b + (T_{s,0} - T_\infty - b)exp(-a(t-t_0)) \tag{3.13}$$

Parameters a and b can be estimated by regression of the temperature data during cooling and heating steps. Parameters h_o and P can then be found from a and b. The heat transfer coefficient, h_w, from the heating wires to the bed can be estimated from the power transferred from the wires to the bed with Equation 3.14:

$$P = h_wA_w(T_w - T_s) \tag{3.14}$$

A_o and A_w are calculated with Equations 3.15 and 3.16:

$$A_o = \pi\frac{d_o^2}{4} + \pi d_o l_o \tag{3.15}$$

$$A_w = 8 \times \left(\pi\frac{d_w^2}{4} + \pi d_w l_w\right) \tag{3.16}$$

To calculate the heat transfer coefficient h_w, however, the temperature difference between the wires and sand particles must be known. A label temperature indicator whose color turns into black color at a rated temperature was applied to one of the wires, and the reactor was heated up to temperatures below the rated temperature of the label, changing the reactor temperature with one degree Celsius intervals between successive experiments. Experiments were conducted until the label color turned black. The difference between the achieved reactor temperature and the rated temperature of the wire label was used in Equation 3.14 to calculate the heat transfer coefficient between the heating wires and the catalyst bed.

3.4.2. Results and discussion

3.4.2.1. Effect of the delivered power

Induction heating is a very fast heating method. However, if the power supply delivered its full power to the induction coil, the internal wires of the reactor could reach a very high temperature after a few seconds, resulting in a large temperature difference between the wires and the sand particles inside the reactor. To minimize the thermal stress on the reactor, especially, the ceramic crucible, reduced power should be delivered to heat up the reactor to reach the desired temperature.

Figure 3.15 shows how quickly the catalyst bed could be heated, starting from an initial temperature of 100°C. The controller was set in the open loop mode to see the effect of the power outlet of the power supply on heat transfer inside the ceramic crucible. The power level was varied between 10 and 20 % of the maximum power. The reactor was vibrated at actuator air pressure of 207 kPa with an amplitude of 6.4 cm. Figure 3.15 indicates that reaching a reactor temperature of 800 °C requires a power of about 20% of maximum power.

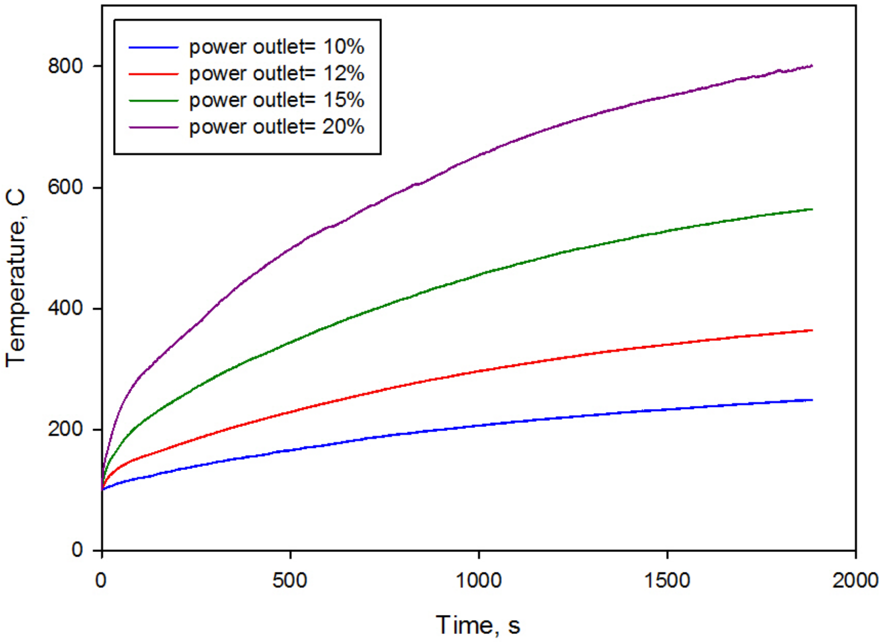

Figure 3.15. **Effect of power outlet of the power supply on rate of heating of the sand particles; mass 10 g, size 149-212 µm, air pressure 207kPa, amplitude 6.4cm**

Table 1 lists the heat capacity and mass of bed of sand particles as well as the dimensions of the heating surfaces. Regarding the 8 wires inside the crucible, it can be concluded from the data in Table 3.1 that the total surface area of the wires is less than the external surface area of the crucible.

Table 3.1. **Required data for heat transfer calculations**

Sand particles		$A_o(m^2) = 0.023$		$A_w(m^2) = 0.00614$	
$C_{P,s}\left(\frac{J}{Kg.°C}\right)$	830	$d_o(m)$	0.0635	$d_w(m)$	0.0032
$m_s(kg)$	0.01	$l_o(m)$	0.083	$l_w(m)$	0.0762

Table 3.2 shows the measured temperatures of the catalyst bed and of the surface of the heating wires for various power levels. The temperature difference between the wires and the bed was

quite small, indicating that heat transfer was very effective. Surprisingly, the temperature difference between the wires and the bed decreased as the power level was increased. This may be caused by the controller scheme. When the power level is 10%, the induction system does not deliver a constant power of 10% of its maximum power; instead, it delivers full power for 10% of the time. The intermittent nature of the power delivery is, therefore, exacerbated when the nominal power level is low. Since the method used in this study measured the maximum temperature reached by the wires over a whole run, the wire temperature will be overestimated by a larger margin as heating becomes more intermittent.

Table 3.2. **Measured temperatures on the surface of wires and inside the reactor**

Power level (%)	T_s (°C)	T_w (°C)	$(T_w - T_s)$ (°C)
10	198	204	6
12	205	210	5
15	246	249	3
20	247	249	2

Figure 3.16 shows that there is a linear relationship ($R^2 = 0.9962$) between the power level, i.e. the power supplied to the induction coil, and the power actually transferred from the heating wires to the catalyst bed. This confirms that the model and calculation procedure used to estimate the power transferred from the wires to the bed gave consistent results.

The heat transfer coefficients for the heat losses and between the heating wires and the bed were calculated from the experimental data for various power levels, using the method described earlier (Table 3.3). As expected, the heat transfer coefficient for the heat losses is independent of the power level.

The heat transfer coefficient between the heating wires and the bed increased dramatically with the power level (Table 3.3). As discussed earlier, the wire temperature would be overestimated by a larger margin at lower power levels, which would then result in an erroneous heat transfer coefficient. The heat transfer coefficient obtained at the higher power level of 20% is more realistic and is more relevant to this study, since it provided a steady state temperature of around 800 °C, a typical temperature for gasification reactions. According to the correlation from Molerus et al [21] for heat transfer between a tube and a fluidized bed, the heat transfer coefficient obtained at a power level of 20% would correspond to a ratio of fluidization velocity to minimum fluidization velocity of about 30, which is typical of a well-bubbling fluidized bed. This confirms the excellent quality of the fluidization achieved with the JBR.

Table 3.3. **Consumed power, heat loss heat transfer coefficient and heat transfer coefficient between wires and bed; air pressure 207 kPa, sand particles 10 g**

Power level (%)	$h_0\left(\frac{w}{m^2.\,°C}\right)$	$P\ (w)$	$h_w\left(\frac{w}{m^2.\,°C}\right)$
10	0.265	1.671	45
12	0.257	2.462	80
15	0.270	4.063	220
20	0.269	6.058	493

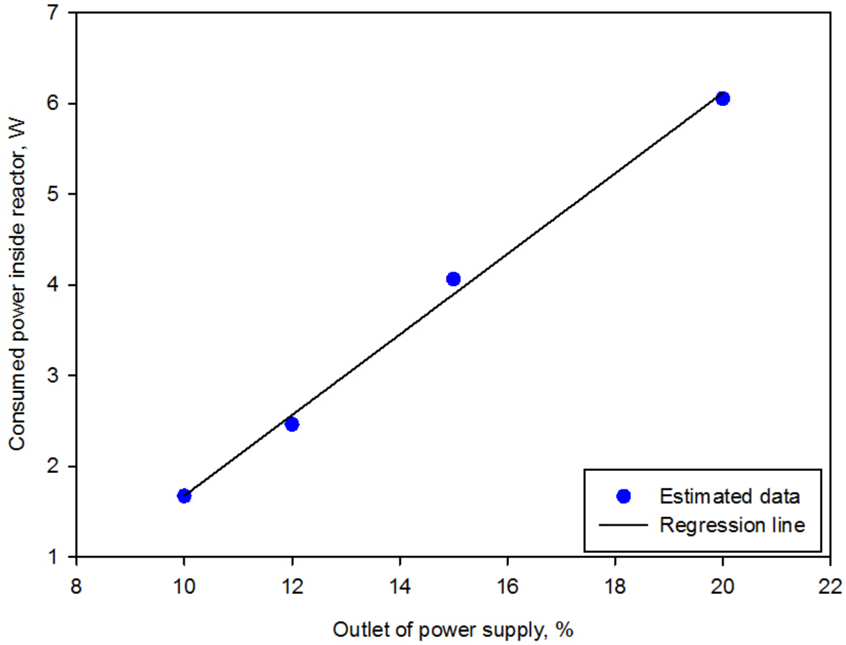

Figure 3.16. **Consumed power inside the reactor versus partial power outlet of the power supply**

3.4.2.2. Effect of frequency of the pneumatic actuator

Figure 3.17 shows how quickly the bed temperature increased for different air pressures applied to the actuator piston. The temperature rose more slowly at higher air pressures. Since, as shown in Figure 3.9, the frequency at which the bed level fluctuated increased with the air pressure, this suggests that operating with a lower frequency of bed pulsations would maximize heat transfer between heating wires and bed.

The results shown in Figure 3.17 are confirmed in Table 3.4, which shows that the heat transfer coefficient between the wires and the bed decreased slightly as the air pressure and, hence, the bed frequency increased. Interestingly, this means that the heat transfer coefficient between the wires and the bed is at its maximum when the bed agitation is maximized: Figure 3.13b shows that for the bed mass and particle size distribution used in the heat transfer experiments, bed agitation was obtained at an air pressure of just above 200kPa.

On the other hand, Figure 3.18 shows that the air pressure had little effect on the rate at which the bed temperature dropped once heating had been switched off. This indicates that, as expected, the heat losses are controlled by the external heat transfer between the outer crucible wall and the ambient air, and are practically independent of the heat transfer coefficient between the bed and the inner crucible wall.

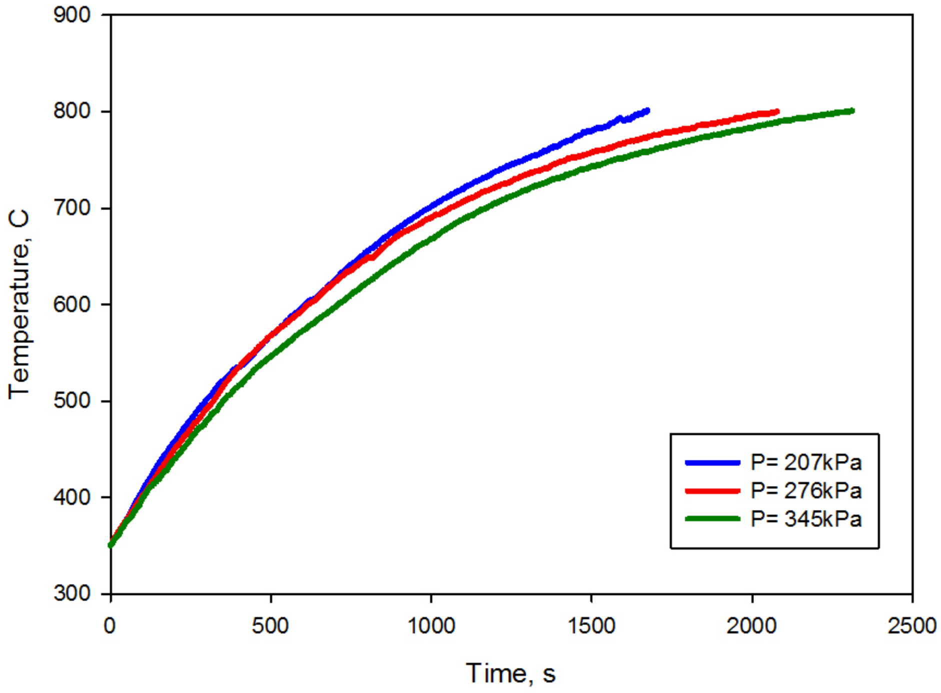

Figure 3.17. **Effect of the actuator air pressure on the rate of temperature rise inside the reactor during the heating step; power outlet 20%, mass of sand particles 10 g, amplitude 6.4 cm**

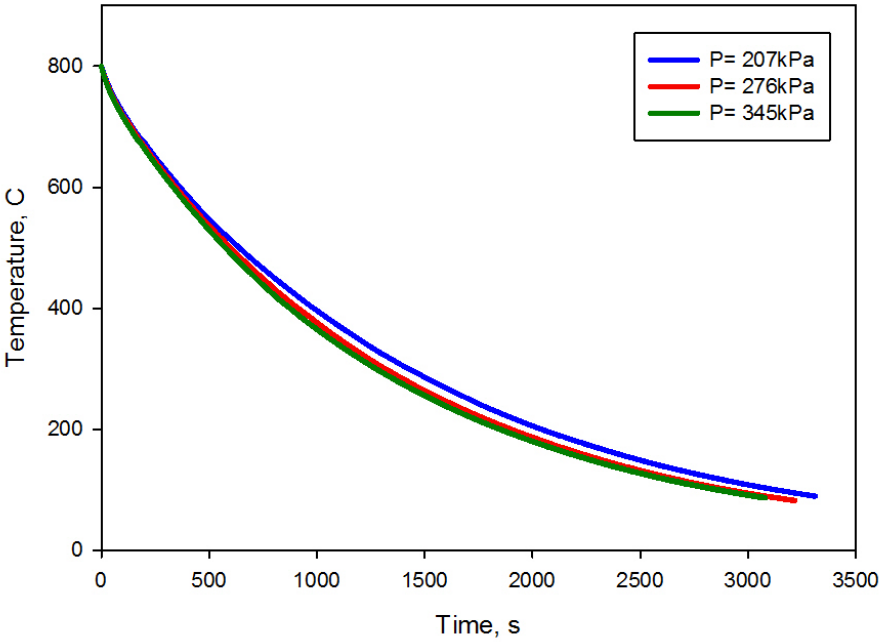

Figure 3.18. **Effect of air pressure of the actuator on rate of temperature drop inside the reactor during the cooling step; power outlet 20%, mass of sand particles 10 g, amplitude 6.4 cm**

Table 3.4. **Consumed power, heat loss heat transfer coefficient and heat transfer coefficient between wires and sand particles; power outlet 20%, sand particles 10 g, amplitude 6.4 cm**

Air pressure (kPa)	$h_o \left(\frac{w}{m^2.\,°C}\right)$	P (w)	$h_w \left(\frac{w}{m^2.\,°C}\right)$
207	0.269	6.058	493.27
276	0.290	6.054	492.91
345	0.299	5.969	486.06

In order to investigate whether the induction heating system implemented on the JBR is effective and rapid enough to compensate the heat consumed by the endothermic reactions, water injection was used for testing, since its vaporization is endothermic, 4 mg droplets of water were injected into the reactor to simulate heat consumption by the endothermic reactions. As shown on Figure 3.19, the bed temperature dropped by less than 2°C each time water was injected and then it took less than 5 seconds for the bed to recover its initial temperature. The negligible temperature drop and the fast recovery observed prove that the developed induction heating technique is very effective for the study of gasification reactions.

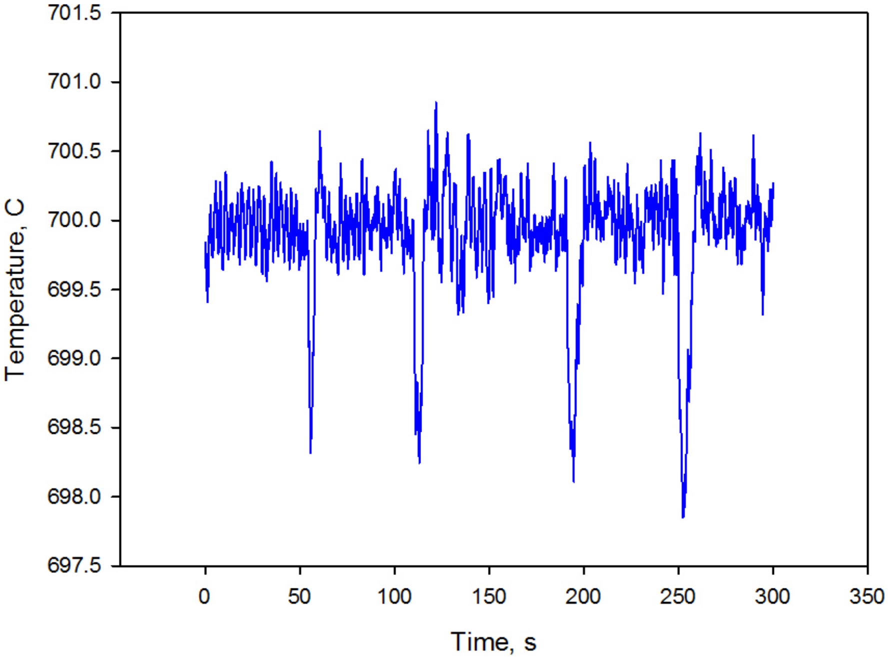

Figure 3.19. **Temperature recovery for endothermic reactions taking place in the JBR**

3.5. Conclusions

The jiggle bed reactor (JBR) is a batch micro reactor with performance characteristics that make it suitable to test gasification catalysts. A linear pneumatic actuator was successfully designed to achieve fluidization conditions in the reaction zone of the JBR, without using any fluidization gas. A new induction heating system was designed and implemented to provide a uniform distribution of heat to the bed with a very small temperature difference between the heating surface and the bed. Fluidization and heating of the catalyst bed can, thus, be achieved in a completely non-invasive manner.

A new image processing technique was developed to monitor the fluidization dynamics of the catalyst bed. A signal processing technique was used to optimize amplitude and frequency of the pneumatic actuator to achieve the best fluidization conditions. The size distribution and mass of the catalyst particles was also optimized to enhanced fluidization.

Heat transfer studies showed that induction heating provides a minimum temperature difference between the heating wires and the catalyst bed. The maximum fluidization intensity of the bed corresponds to the highest heat transfer coefficient between the heating wires and the catalyst bed.

Acknowledgments

The authors gratefully acknowledge the financial support of the Natural Sciences and Engineering Research Council of Canada (NSERC), of the Minister of Research and Innovation of Ontario and Agriculture and AgriFood Canada.   The authors would also like to thank Dr. Marcel Schlaf of the University of Guelph for suggesting that JBR could also stand for “James Bond Reactor”, since the reactor is “shaken, not stirred”.

Nomenclature

A: amplitude (cm)
A_o: external surface area of the ceramic crucible (m^2)
A_P: cross section area of the piston (m^2)
A_{rod}: cross section area of one rod (m^2)
A_w: surface area of an internal inconel wire (m)
$a_{P,ext}$: acceleration of the piston during extension mode $(\frac{m}{s^2})$
$a_{P,ret}$: acceleration of the piston during retraction mode $(\frac{m}{s^2})$
$C_{P,s}$: specific heat of the sand particles $\left(\frac{J}{kg.°C}\right)$

CV_{space}: coefficient of variation of colour change of pixels on picture i at time j
CV_{time}: coefficient of variation of colour change of pixel i on all pictures during the time period of j
$CV_{space,min}$: Maximum uniform distribution of the particles in the entire length of the reactor
d_o: O.D. of the ceramic crucible (m)

d_w: diameter of an internal inconel wire (m)
F: force (N)
$f_{actuator}$: frequency of the actuator(Hz)
f_{bed}: frequency of the bed(Hz)
$f_{bed,d}$: dominant frequency of the bed(Hz)
g: 9.806 acceleration constant of the ground $(\frac{m}{s^2})$
h_o: heat transfer coefficient of heat loss through wall of the ceramic crucible $\left(\frac{w}{m^2.^\circ\mathrm{C}}\right)$
h_w: heat transfer coefficient between internal inconel wires and bed of the sand particles $\left(\frac{w}{m^2.^\circ\mathrm{C}}\right)$
Δh: distance between the reed switches
l_o: external length of the ceramic crucible (m)
l_w: length of an internal inconel diameter (m)
m : mass of sand particles (g)
m_R: mass of the reaction zone (kg)
m_s: mass of bed of the sand particles (kg)
N_i: number of pixels in picture i
N_j: number of pictures in time period j
P: power consumed to heat up internal inconel wires
P_{air}: pressure of compressed air (Pa)
$\bar{P}_{air}$: average pressure of the compressed air during the piston brake (Pa)
T_s: temperature of bed of the sand particles $(^\circ\mathrm{C})$
T_w: temperature of surface of the internal inconel wires$(^\circ\mathrm{C})$
T_∞: room temperature $(^\circ\mathrm{C})$
$v_{P,ext}$: velocity of the piston during extension mode $(\frac{m}{s})$
$v_{P,ret}$: velocity of the piston during retraction mode $(\frac{m}{s})$
Δx_{ext}: brake length at the end of extension mode (m)
Δx_{ret}: brake length at the end of retraction mode (m)
$y_{i,j}$: color value of a pixel in picture i at time j

Greek notations

σ: standard deviation of color value
μ: average of color value

References

[1] Latifi M, Briens C, Berruti F; Development of a Thermodynamic Model to predict the Equilibrium Concentration of Gases from Bio-oil Gasification with Sand or Olivine Catalyst. 2012, Ph.D. Thesis, Chapter 6

[2] Latifi M, Ferrante L, Briens C, Berruti F. Effect of temperature and residence time on the thermal cracking of bio-oil for syngas production. ECI Conference, Bioenergy II, Rio de Janeiro, Brazil, March 2009

[3] Imhof P, Baas M, Gonzales JA. Fluid Catalytic Cracking Catalyst Evaluation: The Short Contact Time Resid Test. Catalysis Reviews, 46(2), 151 (2004).

[4] Berty JM. Testing Commercial Catalysts in Recycle Reactors. Catalysis Reviews - Science and Engineering, v 20, n 1, p 75-96, 1979

[5] Kraemer DW, de Lasa HI . Catalytic Cracking of Hydrocarbons in a Riser Simulator. Ind. Eng. Chem. Res. 27, 2002 (1988).

[6] Ozturk Z, Merklin JF. Rapid Pyrolysis of Cellulose with Reactive Hydrogen Gas in a single-Pulse Shock Tube. Fuel, 74(11), 91 (1995).

[7] Boutin O, Ferrier M, Lede J. Radiant Flash Pyrolysis of Cellulose – Evidence for the Formation of Short Life Time Liquid Species. Journal of Analytical and Applied Pyrolysis, 47, 14 (1998).

[8] Drummond AF, Drummond IW. Pyrolysis of Sugar Cane Bagasse in a Wire-Mesh Reactor. IndustrialEngineering and Chemistry Research, 35, 1263 (1996).

[9] Tudbury CA. Basics of induction heating. Vol1, New York, 1960

[10] Davies EJ. Conduction and Induction Heating. London, U.K.: P. Peregrinus Ltd., 1990

[11] Zhiming L, Shengrui X,Jincheng Z,Yongming C,Jingyu N,Xiaowei Z, Yue H. Finite element analysis of the temperature field in a vertical MOCVD reactor by induction heating . Journal of Semiconductors, v 30, n 11, 2009

[12] Rastogi A, Svrcek WY, Behie LA. Novel Microreactor with Quench System for Kinetic Study of Propane Pyrolysis. AIChE Journal, 34(9), 1417 (1988)

[13] Tsai WT, Lee MK, Chang YM. Fast Pyrolysis of rice straw, sugarcane bagasse and coconut shell in an induction-heating reactor. J. Anal. Appl. Pyrolysis, 76, 230 (2006).

[14] Rohani S, Latifi M, Ferrante L, Briens C, Berruti F. A novel induction heating microreactor for gasification catalyst-testing. 2nd GPE-EPIC conference, 14-17 june 2009 - Venice (Italy)

[15] Kastens ML, Hurst LL, Dressler RG. An American fischer tropsch plant. Industrial and engineering chemistry, v 44, n 3, p 450-466, 1952

[16] Vorontsov AV, Kozlov DV, Smirniotis PG, Parmon VN. TiO_2 Photocatalytic Oxidation: III. Gas-Phase Reactors. Kinetics and Catalysis, Vol. 46, No. 3, 2005, pp. 437–444.

[17] Klusacek, K.; Schneider, P. . Stationary Catalytic Kinetics via Surface Concentrations from Transient data. Chemical Engineering Science, v 37, n 10, p 1523-1528, 1982

[18] Richter M, Mrkwitschka G, Ohlmann G. An all-glass vibration mixed reactor for gas/solid catalyzed reactions. React. Kinet. Catal. Lett., Vol. 34, No. I, 21-27 (1987)

[19] Squires AM. Chemical process opportunities for vibrated powders 1. In the laboratory. Powder Technology, v 147, n 1-3, p 1-9, 2004

[20] Nelson RJ, Flakker CL, Muggli DS. Photocatalytic oxidation of methanol using titania-based fluidized beds.Applied Catalysis B: Environmental 69 (2007) 189–195

[21] Molerus O, Burschka A, Dietz S. Particle migration at solid surfaces and heat transfer in bubbling fluidized beds - II. Prediction of heat transfer in bubbling fluidized beds. Chemical Engineering Science, v 50, n 5, p 879-885, Mar 1995

Appendix A. Sizing the air cylinder

The frequency of the pneumatic actuator is a function of internal volume of the air cylinder, flow rate of the air, alternation timing of the solenoid valve and weight of the reaction zone at given amplitude. In addition, amplitude of the pneumatic actuator must be long enough for the solid particles to be fluidized in the entire length of the ceramic crucible. Maximum achievable amplitude is, however, limited by two ends of the air cylinder which is determined by the maximum possible distance between the reed switches. It has been seen in practice that, in contrary to general expectation, distance between the reed switches must be way less than the desired length of the amplitude so that the piston does not hit the air cylinder. In other words, although the piston is supposed to be stopped where a reed switch senses the magnet on the piston, due to fast speed of the piston and delay time of the alternation action by the solenoid valve, the piston tends to keep moving farther beyond the point in front of the reed switch until it either faces the opposite entering compressed air or hits the cylinder. We call this action “the piston brake” and the extra distance travelled beyond the reed switch is called “the brake length” (Figure 3.A1) which is an important design parameter to size the air cylinder. Therefore, it is crucial to know the distance between the reed switches on the external surface of the air cylinder to control the amplitude of vibration.

The brake length at the end of extension mode and retraction mode can be estimated from the equations below:

$$\Delta x_{ext} = -\frac{v_{P,ext}^2}{2a_{P,ext}} \tag{3.E1}$$

$$\Delta x_{ret} = \frac{v_{P,ret}^2}{2a_{P,ret}} \tag{3.E2}$$

v_P is estimated from the thermodynamics' first law (assuming weight of the piston is negligible) when the stagnant piston in front of a reed switch is pushed or pulled and then travels the length between the reed switches (Δh):

$$m_R g \Delta h + \frac{1}{2} m_R v_P^2 = F \Delta h \tag{3.E3}$$

Where at extension mode:

$$F = P_{air} A_P - m_R g \tag{3.E4}$$

While at retraction mode:

$$F = P_{air}\left(A_p - 2A_{rod}\right) + m_R g \tag{3.E5}$$

During the piston brake, pressure of air reduces dramatically until it becomes zero because its flow is stopped. Applying the Newton's second law for the brake length, a_P can be estimated as below:

At extension mode:

$$(P_{air} A_P - m_R g)dt = m_R dv_{p,ext} \tag{3.E6}$$

Assuming $\overline{P}_{air}$ as the average value of the reducing pressure of compressed air,

$$a_{P,ext} = \frac{\overline{P}_{air} A_P - m_R g}{m_R} \tag{3.E7}$$

Similarly, at retraction mode:

$$(P_{air}(A_P - 2A_{rod}) + m_R g)dt = m_R dv_{p,ret} \tag{3.E8}$$

$$a_{P,ret} = \frac{\overline{P}_{air}(A_P - 2A_{rod}) + m_R g}{m_R} \tag{3.E9}$$

Finally, if we assume that $\overline{P}_{air}$ is almost zero in equations 3.E7 and 3.E9 which is a true assumption, the brake lengths will be calculated from the equations below:

$$\Delta x_{ext} = -\frac{(P_{air}A - m_R g)\Delta h - m_R g \Delta h}{m_R g} \tag{3.E10}$$

$$\Delta x_{ret} = \frac{(P_{air}(A - 2A_{rod}) - m_R g)\Delta h - m_R g \Delta h}{m_R g} \tag{3.E11}$$

Equations 3.E10 and 3.E11 illustrate that the brake lengths are dependent on mass of the reaction zone, distance between the reed switches and bore size of the air cylinder at a given pressure of the compressed air. Effect of these parameters on the brake lengths were investigated to find the optimum size of the air cylinder.

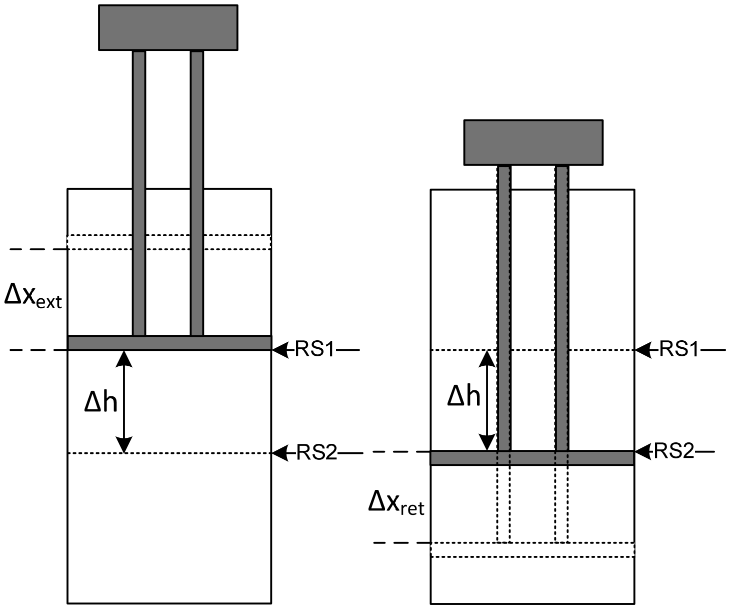

Figure 3.A1. **Schematic of the flat air cylinder with the dual rods presenting position of the reed switches (RS) and the brake length (Δx) at the end of extension (left) and retraction (right) modes**

CHAPTER 4:

Non-catalytic and Catalytic Steam Reforming of Acetic Acid in the Jiggle Bed Reactor

4.1. Introduction

Since bio-oil contains C-H-O compounds, it is a potentially attractive feedstock for syngas production. However, it is crucial to find the required operating parameters to maximize bio-oil conversion and syngas yield. For example, gasification of bio-oil in a bubbling fluidized bed reactor in the absence of catalyst gave a poor bio-oil conversion to gas and a low hydrogen yield [1]. Before testing different catalysts in such a large scale reactor, it would be beneficial having an appropriate micro reactor to carry out small scale testing of the catalysts to find out the optimum catalyst for bio-oil conversion and syngas production. The jiggle bed reactor (JBR) is a novel micro reactor that was designed and developed at the Institute for Chemical and Fuels from Alternative Resources (ICFAR) to test catalysts for endothermic reactions such as bio-oil gasification. This is a batch reactor in which catalyst particles are fluidized by vibration and the required heat is supplied by induction [2].

Fluidization dynamics and heat transfer in the jiggle bed reactor were studied earlier [2]. Such study demonstrated that excellent fluidization and mixing of the solid particles can be achieved with the appropriate frequency and amplitude of the linear actuator which is providing the required level of agitation. In addition, the induction heating mechanism provides fast response and supplies the heat required by endothermic reactions in the jiggle bed reactor with a heating surface temperature that is only a few degrees higher than the bed temperature, thus avoiding undesirable thermal cracking reactions.

The next step in the development of the jiggle bed reactor was to test with a model reaction that is representative of typical gasification reactions. Since acetic acid is a model compound of bio-oil, its non-catalytic and catalytic steam reforming was performed in the jiggle bed reactor for a wide range of operating variables such as temperature, residence time, molar S/C ratio, bed material, and mass of catalyst.

Catalytic steam reforming of bio-oil model compounds, which has been studied by many researchers, is a standard procedure to examine the effect of the operating parameters as well as the type of the catalyst which are important factors in conversion of bio-oil for production of syngas. Although setups with different configurations have been used for steam reforming reactions, all setups have been continuous systems. Also, catalysts with different compositions were tested.

Wang *et al.* worked on the catalytic steam reforming of oxygenated liquids that represent different constituents of bio-oil such as acids, ketones, alcohols, aldehydes, phenols and furans in a dual-bed quartz reactor. They investigated the effects of temperature, molar S/C ratio, gas hourly space velocity and residence time on the conversion of the model compounds and the yield of hydrogen [3]. Marquevich *et al.* investigated catalytic steam reforming of acetic acid as an acid, m-cresol and dibenzyl ether as two aromatic compounds and xylose, glucose and sucrose as sugar compounds in fixed bed reactors [4]. Rioche *et al.* studied steam reforming of acetic acid, phenol, acetone, ethanol and bio-oil at the temperatures between 650°C–950°C with catalysts synthesized by Pt, Pd and Rh as active metals supported on alumina and ceria–zirconia sample [5]. Galdamez *et al.* investigated catalytic steam reforming of acetic acid in a fluidized bed reactor at 450°C-700°C [6]. Basagiannis and Verykios investigated catalytic steam reforming of acetic acid and its reaction network as a model compound of bio-oil between 200°C-800°C. Their reactor consisted of a quartz cell with 8 mm O.D in between two 6 mm O.D. quartz tubes as the inlet and the outlet tubes. The total length of the reactor was 32 cm [7]. Takanabe *et al.* investigated deactivation of the Pt/ZrO_2 catalyst during steam reforming of acetic acidat temperature 875K [8]. Ramos *et al.* studied non catalytic and catalytic steam reforming of acetol in a bubbling fluidized bed reactor [9]. Medrano *et al.* investigated the effects of catalyst calcination temperature and additional oxygen to increase the conversion of acetic acid during its catalytic steam reforming in a fluidized bed reactor at 650°C with Ni/Al catalysts [10]. Vagia *et al.* studied steam reforming of acetic acid and acetone in a fixed bed reactor over 550°C-750°C [11]. Davidian *et al.* worked on catalytic cracking of acetic acid with their proposed sequential cracking/regeneration cycles in their reactor system in the absence of steam [12, 13]. Medrano *et al.* eveloped Ni/Al catalysts modified with Ca and Mg with different Ca/Al and Mg/Al ratios for steam reforming of acetic acid and acetol in a fluidized bed reactor at 650°C with a S/C ratio of 5.58. They have reported that the magnesium modified catalysts showed better activities in terms of highest hydrogen yield and carbon conversion when compared to the calcium modified catalysts [14]. Guell *et al.* carried out steam reforming of acetic acid with Pt/ZrO_2 and Pt/CeO_2 catalysts. They also measured the effect of additional oxygen on catalyst activity. They have proposed that using a catalyst with redox properties as well as additional oxygen in the reactor can help minimize coke deposition on the catalyst [15]. Hu and Lu carried out steam reforming of acetic acid, ethylene glycol, acetone, ethyl acetate, m-xylene, and glucose at temperatures from 300°C to 800°C with molar S/C ratios of 1 to 9 with a Ni/Al_2O_3 catalyst with 30wt% nickel content. They have reported that coke formation on the catalyst surface can depend on the feedstock [16]. Hu and Lu compared the activity of catalysts synthesized with transitional metals (Ni, Co, Fe or Cu) supported by Al_2O_3 in acetic acid steam reforming at temperatures between 300°C and 600°C with molar S/C ratio of 7.5 [17]. They also studied whether promoters such as Ce and La can increase the activity of the Co/alumina catalyst which had shown good selectivity for hydrogen production. Both promoters increased conversion of acetic acid and stability of the catalyst against metallic oxidation and coke formation [18]. Vagia and Lemonidou investigated presence of Ni and Rh on catalysts with Ceria-zirconia supports to maximize hydrogen production in steam reforming experiments of acetic acid at 550°C-750°C with molar S/C ratio of 3. They also investigated effect of such metals on the type of coke formed on the catalyst surface [19]. Thaicharoensutcharitthama *et al.* synthesized nickel based catalysts with different nickel loadings on different supports such as α-Al_2O_3, $Ce_{0.75}Zr_{0.25}O_2$, and MgO at 650°C with molar S/C ratios of 1, 3 and 6 in steam reforming of acetic acid. They have reported that the catalyst with 15 wt% nickel on the $Ce_{0.75}Zr_{0.25}O_2$ support had the highest activity in term of carbon conversion and such catalyst support showed the best stability against the coke formation [20]. Lu *et al.* developed Ni/γ-Al_2O_3 catalysts with different nickel loadings to investigate coke deposition and its structure during steam reforming of acetic acid at 600°C and molar S/C ratio of 2 [21]. Li *et al.* developed Ni/La_2O_3 catalysts with different nickel loadings and used them in steam reforming of acetic acid to find the operating catalyst and operating conditions that maximize the hydrogen yield [22].

The main goal of acetic acid steam reforming in the jiggle bed reactor was to investigate functionality of the reactor to change in operating conditions such as temperature, residence time and molar S/C ratio while reliable and reproducible data are generated.

4.2. Experimental setup and procedure

To investigate the relative effects of the catalyst, non-catalytic experiments were initially performed. Since, according to the literature data, the nickel based catalysts are promising for steam reforming reactions, a commercial nickel based steam reforming catalyst (called catalyst X in this chapter) was used for the catalytic steam reforming of acetic acid in this research. Molar S/C ratios of 0, 3 and 6 were tested. Temperature was varied between 650°C, 700°C and 750°C and the residence time ranged from 10s to 90s for non-catalytic experiments; the longest residence time was tested to investigate whether acetic acid conversion and hydrogen yield can be maximized in the absence of catalyst. Catalytic experiments were carried out at 700°C and residence times between 10s and 30s.

The jiggle bed reactor is a batch fluidized bed micro reactor where the required heat is supplied by induction heating. Solid particles including the catalyst are fluidized in a ceramic crucible by vibration that is provided by a linear pneumatic actuator. The actuator frequency is 3 Hz and its amplitude is 10 cm. There is a copper coil around the ceramic crucible. A high voltage current through the coil provides a magnetic field; as a result, hysteresis and eddy currents are induced on the surface of wires inside the crucible. Direction of the magnetic field and the induced currents are alternated with a frequency of about 250 kHz; therefore, energy is released in the form of heat. Solid particles can be easily fluidized in the jiggle bed reactor and induction heating provides heat for the endothermic reactions while with a very small temperature difference between heating surface and reactor bed, preventing parasitic thermal cracking reactions on the heating surface [2].

The original design of the jiggle bed reactor was utilized for hydrodynamic studies [2]. Such design had to be modified to carry out the gasification experiments. For example, the ceramic crucible was attached to the top lid with a suitable high temperature gasket to prevent any leak at gasification temperatures. In addition, an in-situ system for reduction and regeneration of the catalytic bed was set up. The new design of the ceramic crucible replaces sharp edges with smooth edges and its top flange is flatter to provide for a bigger gasket between the crucible and the top lid. The metal heating wires were welded directly to the top lid. Figure 4.1 shows new design and dimensions of the ceramic crucible which was manufactured by the KYOCERA group. Ceramic material can withstand temperatures of up to 1500°C.

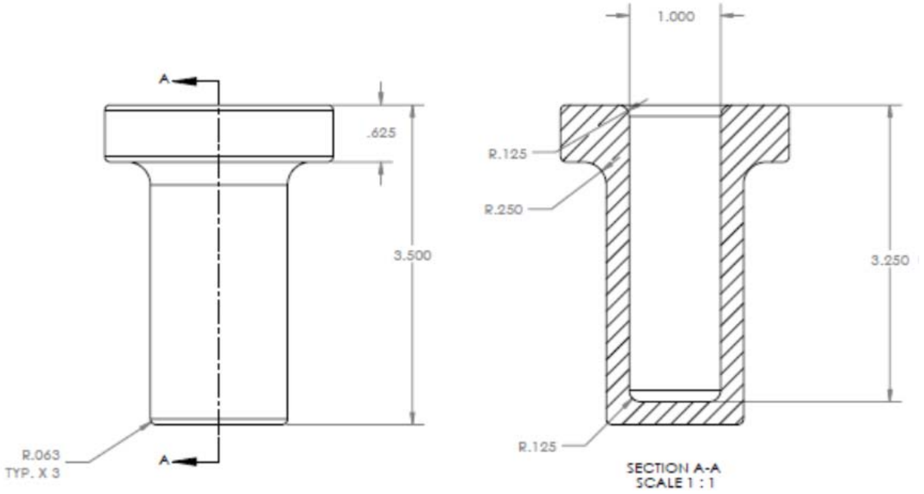

Figure 4.1. **Design and dimensions of the ceramic crucible**

A stainless steel clamp was designed to hold the ceramic crucible and its metal lid together. A high temperature gasket was placed between the upper surface of the flange and the metal lid and one another gasket was placed between the clamp and lower surface of the flange to avoid breaking the ceramic with the applied torque required for tightening the bolts. A torque wrench was used to equally tighten the bolts. Two different gaskets, Thermiculite and Garlock, were tested and performed well. Figure 4.2 shows how the ceramic crucible is held by the clamp on the metal lid.

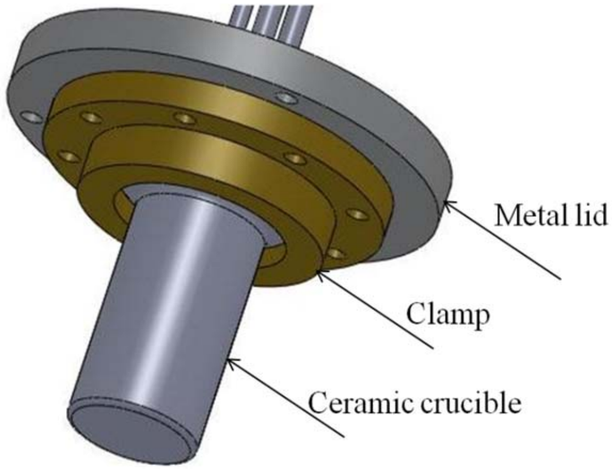

Figure 4.2. **Configuration of the ceramic crucible and clamp on the jiggle bed reactor**

One of the main advantages of the jiggle bed reactor is its ability to perform in-situ reduction and regeneration of the catalytic bed, which saves time. In other words, instead of reducing the catalyst sample with hydrogen and passivating it with oxygen in a separate unit, a tube reaching the bottom of the ceramic crucible is used to introduce the desired gas into the catalyst bed. The catalyst bed can, thus, be easily regenerated and reduced after each test in preparation for the next test. This tube is also used to flush all air from the reactor, which is essential. Figure 4.3 shows the location of the tube as well as the configuration of the welded heating wires inside the ceramic crucible.

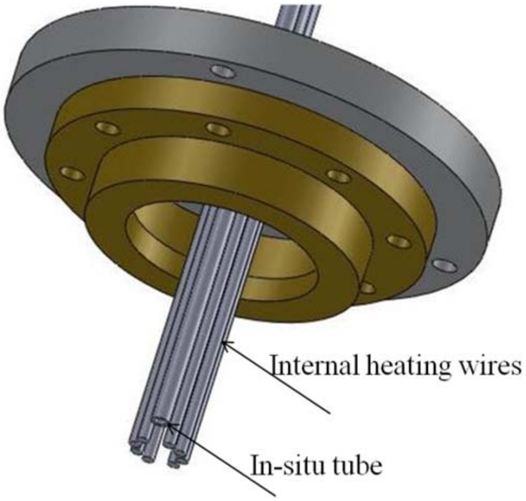

***Figure 4.3.* Position of the in-situ tube and internal heating wires in the jiggle bed reactor**

A schematic of the experimental setup is shown in Figure 4.4. There is an aluminum extrusion on which the jiggle bed reactor setup is mounted. The setup is comprised of moving and stationary parts. The moving part includes the ceramic crucible setup (as shown in Figure 4.2), the surrounding copper coil as well as the valves V_1, V_2 and V_3. The copper coil is insulated with an electrical insulation sleeve. Fiberfrax thermal insulation covers the whole ceramic crucible. As cooling water flows through the copper coil, the Fiberfrax insulation was placed between the ceramic crucible and the copper coil. The stationary part includes the induction heating power supply, the temperature controller, the pneumatic actuator, the coil style condenser, the gas sampling bag, the flow meters and the valves V_4 and V_5. Flexible tubes and wires connect the moving and stationary parts. The air cylinder of the pneumatic actuator which vibrates the ceramic crucible setup with a frequency of 3 Hz and amplitude of 10 cm is attached to the aluminum extrusion.

Solutions of acetic acid and water representing a molar steam to carbon ratios of 0, 3 and 6 were prepared for the gasification tests. Since the jiggle bed reactor is a batch setup for injecting micro liters of the liquid feed, the Drummond capillary tubes with a 4µl volume were used to inject precise amounts of solution into the reactor.

Due to very small volume of the liquid feed injection, presence of air in the reactor may lead to combustion of the gasification products, so it is very crucial to make sure that air is completely purged before each experiment. Because of its larger molecular weight, argon was introduced from valve V_2 to the reactor as inert carrier gas to flush air out through valves V_1 and V_3 alternatively. In other words, all gasification reactions took place in an argon environment. Before injection of the liquid feed, valves V_2 and V_3 are open and while there is a flow of argon outwards, the vacuumed gas sampling bag is connected to the condenser. Then, valve V_3 is closed and valve V_1 is opened to drop the capillary tube containing the liquid feed into the reactor; then, valves V_1 and V_2 are closed. Once the desired residence time is reached, valve V_3 and then valve V_2 are open to sweep away all the product gases with argon and collect them in the gas sampling bag.

A Varian micro GC CP4900 instrument was used to analyze the product gases H_2, CH_4, CO, CO_2, C_2H_4 and C_2H_6. This micro GC was equipped with three columns 10m MS5A, 10m PPU and 8m 5CB. Helium was used as the carrier gas in the micro GC. Since the product gases were diluted with argon in the gas sampling bag, their concentration was very low. Therefore, the sensitivity of the TCD was set at a high level and the sampling time was set at 500 ms to be able to observe peaks of the product gases. GC runs were conducted for 3 minutes.

In order to calculate the number of moles of the product gases and the total carbon conversion, an external standard gas with known volume was needed in the mixture of the product gases. Although it would have been ideal to use an inert gas such as N_2, it was impossible because there were minute amounts of air contaminating the gas bag through the fittings when the bag was connected to the micro GC. Therefore, 500µl of normal C_4H_{10} was injected into the vacuumed gas sampling bag with a gas tight syringe as the external standard gas. Despite the fact that the product gases are mixed with the external standard gas during the gas collection in the gas sampling bag after the test, the gas sampling bag was also squeezed manually for several times to ensure good mixing between the standard and product gases. Several tests were conducted to verify that normal C_4H_{10} was never produced during the gasification tests. Experiments were repeated for 3 times to check out data reproducibility.

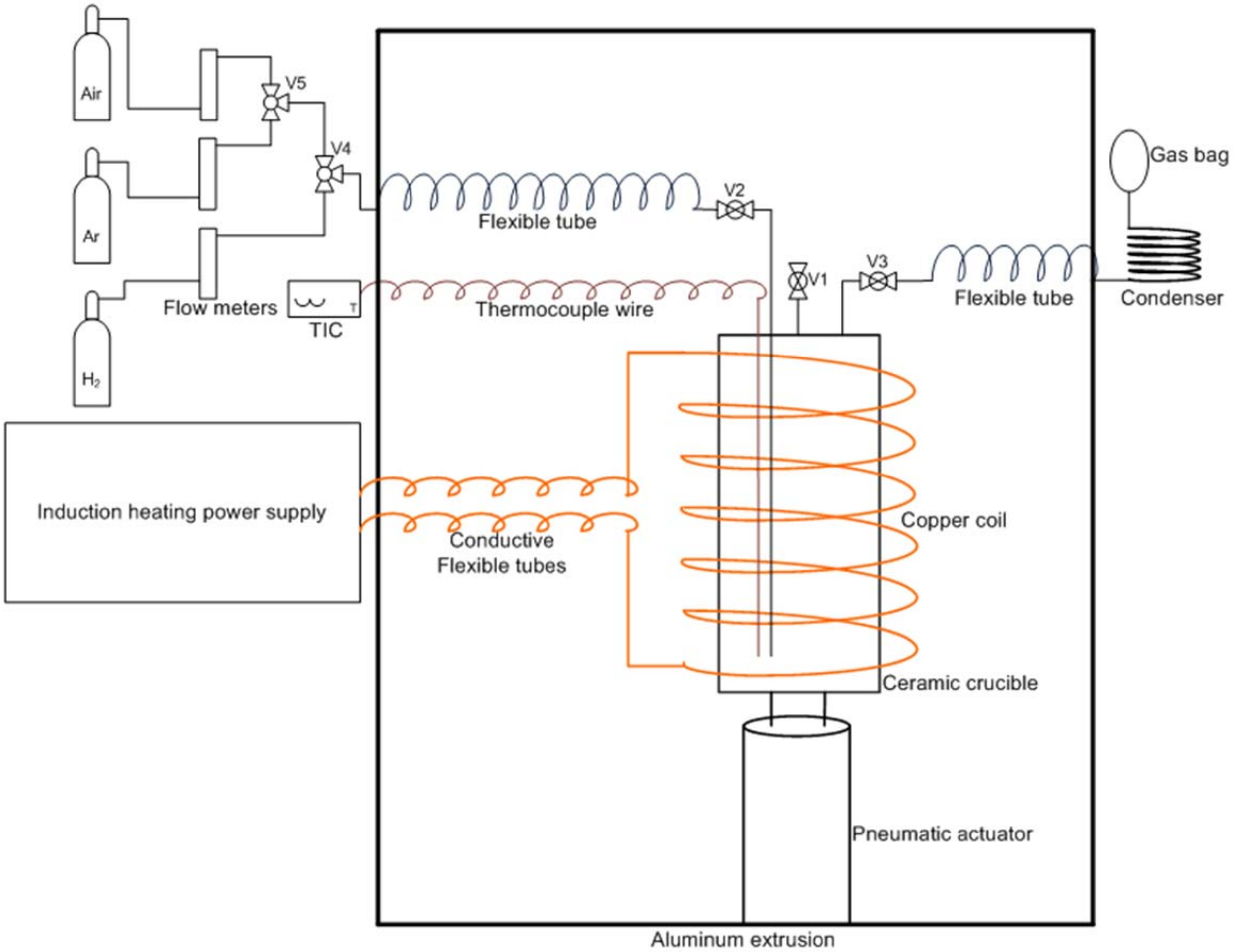
Air
Ar
H₂
V5
V4
Flow meters
TIC
Flexible tube
V2
Thermocouple wire
V1
V3
Flexible tube
Gas bag
Condenser
Induction heating power supply
Conductive
Flexible tubes
Copper coil
Ceramic crucible
Pneumatic actuator
Aluminum extrusion

Figure 4.4. **Schematic of the JBR experimental setup for the catalytic gasification tests**

4.3. Catalyst preparation

A nickel-based steam reforming catalyst for steam reforming of light hydrocarbons, catalyst X, was used. Pellets of the catalyst were crushed and sieved to obtain particles between 220 and 350µm. Since the fresh catalyst is provided in the non-reduced form, a 10 g batch of the catalyst was initially reduced in-situ in the JBR setup with a flow of 100 ml/min of pure hydrogen at 600 °C for 6 hours. Since the reduced catalyst is pyrophoric, the catalytic bed was exposed to steam for an hour before discharge to get passivated; the prepared passivated catalyst was then kept inside the desiccators.

The desired mass of the prepared catalyst was mixed with silica sand with size distribution of 106μ-220μ for the gasification tests in the reactor so that the total mass of the solid particles was 10g for all experiments. Before starting the experiments, the catalytic bed was reduced in-situ again with a 100 ml/min flow of pure hydrogen at the reaction temperature for 1 hour to make sure that nickel on the surface of catalyst are in the form of free nickel (Ni^0) with no NiO on the surface. A larger size distribution of the catalyst particles was chosen to be able to separate them from the silica sand particles after the experiments. Although silica sand and catalyst particles were with different size distributions, segregation was not observed after mixing these solids together.

4.4. Catalyst characterization

Surface area analysis of the fresh catalyst was carried out with the instrument ASAP 2010 through adsorption of N_2 at 77.35 K. According to Table 4.1, the BET surface area of the catalyst is 15.37m^2/g, the average pore size is 130.05 A° and the total pore volume is 0.05 cm^3/g.

Table 4.1. **Surface and pore analysis of the catalyst X**

Catalyst	BET surface area, m^2/g	Average pore size$^{\times}$, A°	Total pore volume^{+}, cm^3/g
Fresh catalyst	15.375	130.049	0.0502

$^{\times}$Adsorption Average Pore Diameter (4V/A° by BET)

$^{+}$Single Point Adsorption Total Pore Volume of pores less than 775.52 A° Diameter at P/P_0= 0.974

X-Ray Fluorescence (XRF) analysis of the fresh catalyst is presented in Table 4.2. Estimated nickel content of the catalyst that is supported on calcium aluminate is 11.61 wt%. However, TPR-TPO analysis on the fresh catalyst was carried out by the AutoChem II 2920 to measure how much nickel is present on the surface of the catalyst for the catalytic gasification reactions: A sample of the fresh catalyst was oxidized completely with air to convert all the elemental nickel to nickel oxide. Then the TPR analysis was started with a flow of hydrogen of 50 cm^3 STP/min with the rate of 10 °C/min until 750 °C when the catalyst was completely reduced. In the next step, the TPO analysis was performed on the reduced catalyst with a flow of oxygen of 50 cm^3 STP/min until 410 °C when the catalyst was completely oxidized. At the end of the TPR analysis, NiO on the surface of catalyst is converted to Ni^0 according to reaction 4.1:

$$NiO + H_2 \rightarrow Ni^0 + H_2O \tag{4.1}$$

Also, at the end of the TPO analysis, Ni^0 on the surface of the catalyst is converted to NiO according to reaction 4.2:

$$Ni^0 + \frac{1}{2}O_2 \rightarrow NiO \tag{4.2}$$

Knowing the consumption of hydrogen and oxygen during the TPR and TPO analyses, respectively, it was estimated that the nickel content of the catalyst on its surface available for the catalytic reactions was between 4.05 wt% and 5.31 wt% (Table 4.3). Similarly, the TPR-TPO analyses were conducted on the reduced catalyst. As presented in Table 4.3, the nickel content on the surface of the reduced catalyst was between 4.35 wt% and 5.46 wt%. In other words, other than activating the catalyst, reduction of the catalyst caused a little amount of the elemental nickel in the bulk of the catalyst to move to the surface.

Table 4.2. **XRF analysis data of the steam reforming catalyst X**

Compound	Mass, wt%	Element	Mass, wt%
Al_2O_3	63.66	Al	33.69
NiO	14.78	Ni	11.61
CaO	12.66	Ca	9.05
SiO_2	1.06	Si	0.494
MgO	0.492	Mg	0.297
P_2O_5	0.0574	Px	0.0250
Fe_2O_3	0.0472	Fe	0.0330
La_2O_3	0.0251	La	0.0214
Sc_2O_3	0.0039	Sc	0.0025

Table 4.3. **TPR-TPO analysis results on the fresh and reduced catalyst X**

Catalyst	Available Ni^0 on the catalyst surface, wt%
Fresh catalyst	4.05-5.31
Reduced catalyst	4.35-5.46

X-Ray powder Diffraction (XRD) of the fresh and reduced samples of the catalyst is shown in Figure 4.5. Phases of the NiO have disappeared on the reduced catalyst except at 2θ of 43.29°, which can be due to oxidation of the nickel on the surface because of its exposure to the room air. It is noteworthy that phases of Ni^0 appeared on the surface of the catalyst after its reduction with hydrogen which shows this catalyst has become active for the catalytic reactions. Other than peaks of the NiO and Ni^0 phases, structures of the other phases on both fresh and reduced catalysts are similar, but it is clear that after reduction, intensity of the peaks has become larger and the catalyst has gain a better crystal shape.

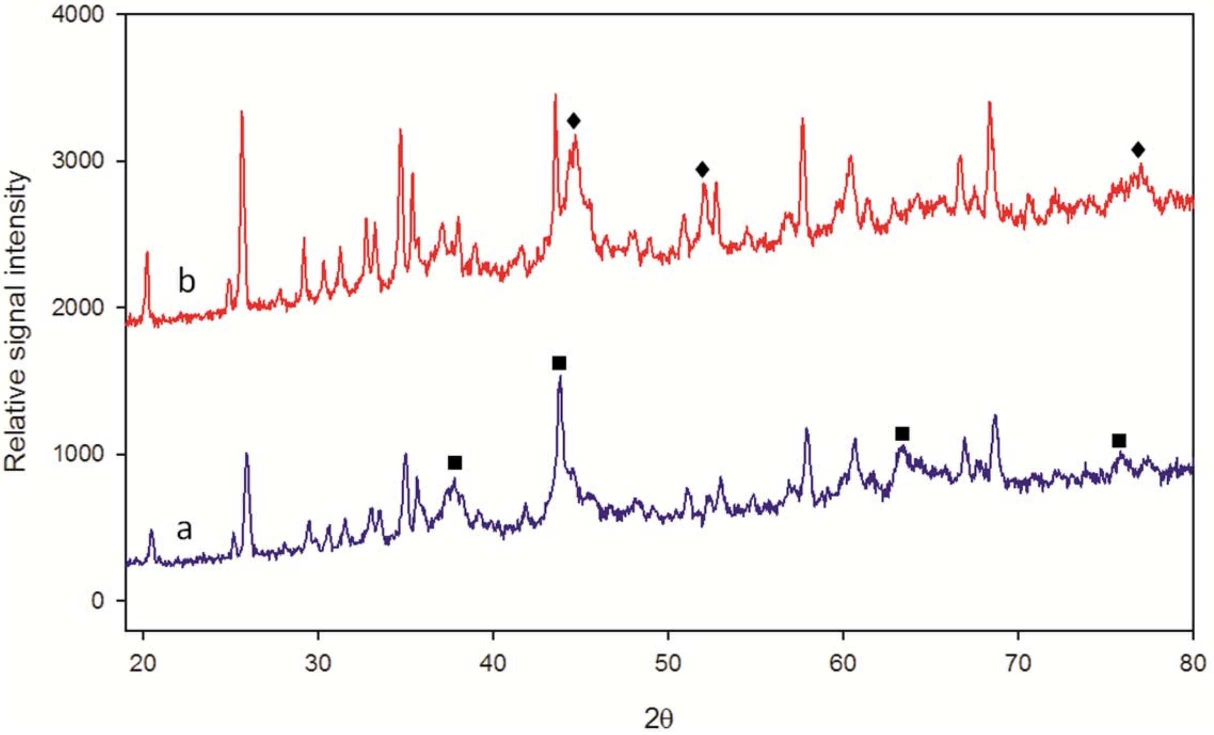

Figure 4.5. **XRD graphs of the fresh (a) and reduced (b) catalyst. Square symbols (■) present phases of NiO and diamond symbols (◆)present phases of Ni^0**

4.5. Experimental results and discussion

Non-catalytic and catalytic steam reforming of acetic acid were performed with different operating parameters such as temperature, residence time, molar steam to carbon ratio (S/C) and mass of the catalyst in the jiggle bed reactor. In order to maintain atmospheric pressure in the reactor, the total volume of the injected liquid (acetic acid + water) was 4 µl. The residence time was taken as the time between the feed injection and the flushing of the product gases by argon into the gas sampling bag. For the non-catalytic experiments, 10 g of silica sand was used as the bed material. For the catalytic experiments, 0.25g, 0.5g or 1.0g of catalyst was mixed with the silica sand to give a total mass of 10g.

Steam reforming of the oxygenated molecules ($C_nH_mO_k$) to produce syngas (H_2+CO) can be described by the following equation:

$$C_nH_mO_k + (n-k)H_2O \rightarrow nCO + \left(n + {}^{m}/_{2} - k\right)H_2 \tag{4.3}$$

So, Equation 4.3 suggests that acetic acid could be converted to syngas with no need for steam:

$$CH_3COOH \rightarrow 2CO + 2H_2 \tag{4.4}$$

However, at the presence of steam, steam reacts with CO through the water-gas shift reaction to produce more hydrogen:

$$2H_2O + 2CO \leftrightarrow 2H_2 + 2CO_2 \tag{4.5}$$

Therefore, combining Equations 4.4 and 4.5, the overall steam reforming of the acetic acid can be shown by Equation 4.6, for a steam to carbon ratio of 1:

$$CH_3COOH + 2H_2O \rightarrow 2CO_2 + 4H_2 \tag{4.6}$$

Although acetic acid could ideally convert completely to syngas through the reactions 4.4 and 4.5, there can be other product gases as well as coke as gasification by-products. For example, according to reactions 4.7 and 4.8, thermal decomposition of acetic acid can produce syngas, steam, light hydrocarbons and coke. Besides, since CO, CO_2 and coke are present inside the reactor, the Boudouard reaction (reaction 4.9) is another important reaction which can affect the CO/CO_2 ratio in the final product gases.

$$CH_3COOH \rightarrow CH_4 + CO_2 \tag{4.7}$$

$$CH_3COOH \rightarrow H_2, CO, CO_2, H_2O, C_2H_4, C_2H_6, C_3H_4, coke, ... \tag{4.8}$$

$$2CO \leftrightarrow CO_2 + C \tag{4.9}$$

In addition, In the presence of steam, the produced hydrocarbons undergo steam reforming reactions towards production of hydrogen and carbon monoxide. For example, reaction 4.10 illustrates how methane can be converted to syngas:

$$CH_4 + H_2O \rightarrow CO + 3H_2 \qquad (4.10)$$

The stoichiometric yield of hydrogen corresponds to the maximum moles of hydrogen which can be produced from complete conversion of acetic acid only through Equation 6; this maximum number of moles could theoretically have been reached with the experiments with a molar S/C of 3 or 6. The yield of hydrogen was defined as the ratio of moles of produced hydrogen in the experiment to the stoichiometric hydrogen yield:

$$\frac{No.of\ moles\ of\ produced\ hydrogen}{Stoichiometric\ yield\ of\ hydrogen} = \frac{[H_2]}{4\times[CH_3COOH]} \qquad (4.11)$$

Molar yields of CO, CO_2, CH_4 were calculated as:

$$\frac{moles\ of\ product}{2\times moles\ of\ acetic\ acid} \qquad (4.12)$$

And molar yields of C_2H_4 and C_2H_6 were calculated as:

$$\frac{moles\ of\ product}{moles\ of\ acetic\ acid} \qquad (4.13)$$

One advantage of the jiggle bed reactor is that it is very convenient to perform a complete test (from feed injection to gas analysis) over a very short period of time i.e. 10 minutes, so it is possible to repeat a test to check out reproducibility of the data and conduct tests under different operating conditions while saving considerable time. However, it must be taken into account that coke as the solid product of the reaction remains in the reactor which must be removed before conducting a new test; otherwise, coke can be gasified during the next test and has a detrimental effect on the calculation of gasification yields. Therefore, after each test, the catalytic bed was regenerated and reduced according to the following in-situ procedure:

1. Coke was burned off with air for 30 seconds
2. Argon was introduced to the reactor for 30 seconds to flush out all air

3. Hydrogen was introduced to the reactor for 5 minutes to remove oxygen adsorbed on the surface and reducing the catalyst
4. Argon was introduced to flush out hydrogen from the reactor for 2 minutes
5. The procedure above was carried out even for non-catalytic tests where there was only silica sand in the reactor.

4.5.1. Non-catalytic results of the acetic acid steam reforming

4.5.1.1. Effect of molar S/C ratio and residence time

Figure 4.6 presents data of non-catalytic steam reforming of acetic acid which was carried out to investigate effect of the steam to carbon ratio (0, 3 and 6) versus residence time (10 s to 90 s) on the yield of the product gases and the total carbon conversion of acetic acid. The temperature used for all tests was 700 °C.

The trend of the yields of product gases versus molar S/C ratio is as expected according to the reactions 4.4 to 4.10 discussed earlier. When only acetic acid is injected to the reactor (molar S/C=0), acetic acid is decomposed to final products, such as hydrogen, carbon monoxide, carbon dioxide, methane and, perhaps, some steam (reaction 4.8). In the absence of sufficient steam, the water gas shift reaction (reaction 4.5) cannot proceed to produce hydrogen and carbon dioxide. In addition, steam reforming reaction of the hydrocarbons (such as reaction 4.10) cannot take place in the absence of sufficient steam. So, it is expected that yields of CO and hydrocarbons should be largest when molar S/C is zero and decrease with increasing molar S/C. Figure 4.6 confirm that yields of methane, C_2 hydrocarbons and carbon monoxide decrease with increasing molar S/C, while yields of hydrogen and carbon dioxide increase.

However, the maximum yield of hydrogen is 0.23, obtained with a 20 s residence time and a molar S/C ratio of 6. Therefore, non-catalytic gasification is not suitable to produce high yields of hydrogen. On the other hand, it might be suitable to produce methane, since the yield of methane is quite high when steam is not present in the reactor; it ranged between 0.14 and 0.25. Methane is a very stable hydrocarbon: although its yield dropped significantly at a molar S/C of 6, it is not possible to convert all methane to syngas in the absence of an appropriate catalyst. According to Figure 4.6, increasing molar S/C is also very effective to increase the carbon conversion of acetic acid. In the absence of steam, conversion is 52% at a 10 s residence time and its maximum value is 82% at a 90 s residence time, while, with a molar S/C ratio of 6, it is 83% at a 10 s residence time and reaches 100% at a 90 s residence time.

The product gas yield increases with increasing residence time and stabilizes for residence times larger than 30 s. At residence times larger than 30s, hydrocarbons are converted to hydrogen, CO and CO_2. Generally, longer residence time does not affect the yields of hydrogen and CO_2. For instance, the yield of hydrogen can not increase beyond 0.23 even at a residence time of 90s.

Figure 4.6 shows a strongly non-monotonic variation of the CO yield with molar S/C. CO is probably produced through the thermal cracking of acetic acid, reforming reactions and the Boudouard reaction and then is consumed through the water gas shift and the Boudouard reactions.

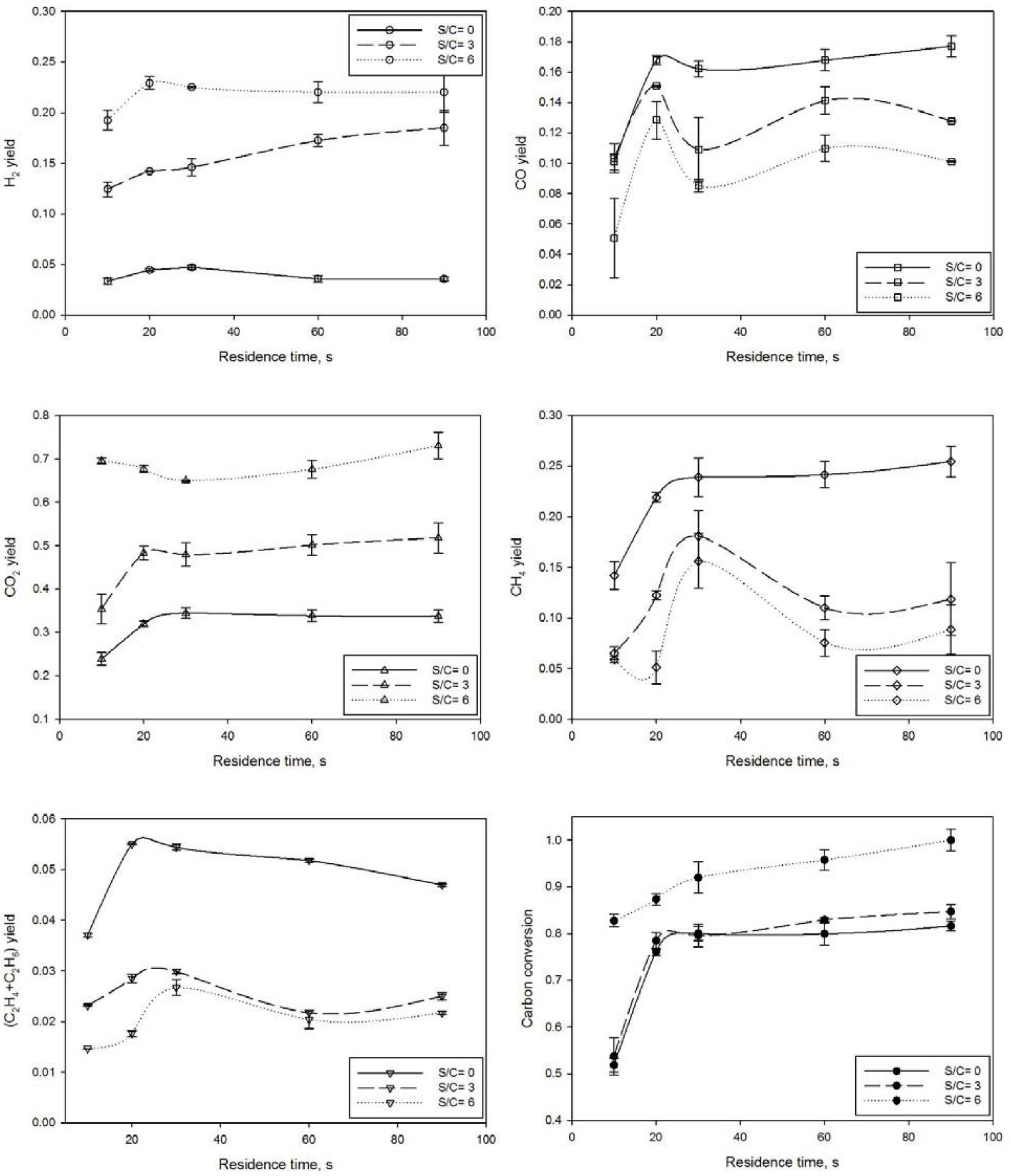

Figure 4.6. **Non-catalytic steam reforming of acetic acid. Effect of S/C ratio versus residence time; T= 700 °C**

4.5.1.2. Effect of temperature

Non-catalytic steam reforming of acetic acid was also carried out at 600°C and 750°C with a 30 s residence time to investigate the effect of temperature on product gas yields and on carbon conversion of acetic acid at different temperatures. Results are presented in Figure 4.7. It is seen that the Steam to Carbon ratio has a similar effect on the yield of the product gases at all tested temperatures i.e. yields of hydrogen and CO_2 increase with increasing molar S/C ratio whereas yields of CO (in relative to CO_2) and hydrocarbons decrease.

Yields of hydrogen and CO increase at higher temperatures. The CO_2 yield decreases with increasing temperature. Production of methane increases with temperature. Yield of C_2 hydrocarbons also increases with temperature for all tested molar S/C ratios. As a result, carbon conversion of acetic acid increases with temperature so that complete conversion is achieved at 750°C when steam is present in the reactor.

In general, by taking yields of CO, CO_2 and hydrocarbons in consideration, results of non-catalytic experiments reveal that the rate of decomposition of the acetic acid (like reactions 4.7 and 4.8) is higher than that of steam reforming and water gas shift reactions because a very low yield of hydrogen is obtained. For example, the maximum yield of hydrogen which was achieved at temperature 750°C and molar S/C ratio of 6 was 0.29. Since high production of hydrogen is a main objective in the steam reforming reactions, it is concluded that the non-catalytic steam reforming process is not a suitable path to hydrogen. An appropriate catalyst must thus be used to drive reforming and water gas shift reactions towards maximum production of hydrogen.

Other than individual yields of hydrogen and CO, the molar H_2/CO ratio is also an important consideration. The molar H_2/CO ratio is less than one when acetic acid is gasified in the reactor in the absence of steam. The maximum value of H_2/CO ratio, which is 5.3, is achieved at 700°C with a molar S/C ratio of 6.

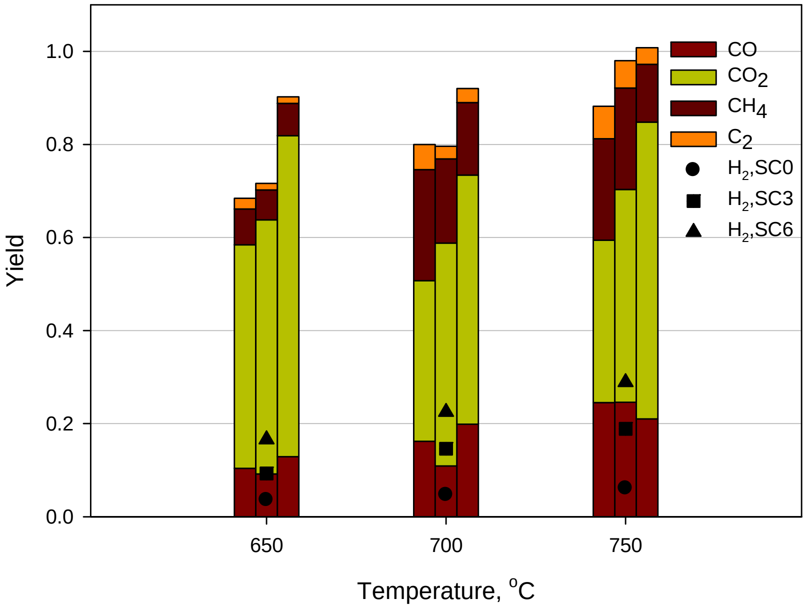

Figure 4.7. **Non-catalytic steam reforming of acetic acid. Effect of temperature. Residence time= 30s. Left, middle and right hand side bars present data of S/C ratios of 0, 3 and 6, respectively**

4.5.2. Catalytic results of the acetic acid steam reforming

Catalytic steam reforming of acetic acid in the jiggle bed reactor was carried out at 700°C with 0.25, 0.5 and 1g of the catalyst X mixed with silica sand so that the total solids mass was 10 g. Molar S/C ratios were 0, 3 and 6. The residence time ranged from 10 to 30 s.

4.5.2.1. Effect of molar S/C ratio and residence time

Figure 4.8 depict the effect of the molar S/C ratio on yields of the product gases and carbon conversion of acetic acid as functions of residence time at 700°C when the mass of catalyst was 0.5 g. Comparing results in Figure 4.8 with the results in Figure 4.6 shows that the catalyst caused steam reforming and water gas shift reactions to become dominant reactions. Compared to non-catalytic experiments, For instance, a significant increase in yield of hydrogen is achieved when catalyst is used (as compared in Figure 4.8).

Taking yields of hydrogen, CO and CO_2 versus molar S/C ratio in consideration, it can be concluded that the catalyst promotes significantly the water gas shift reaction, because the yields of hydrogen and CO_2 increase dramatically with larger molar S/C ratios, while the yield of CO decreases. In addition to an appropriate catalyst, it is realized that a minimum amount of steam is required to maximize the hydrogen yield. In the absence of steam, the maximum hydrogen yield that could theoretically be achieved is 0.5.

The yields of methane and C_2 hydrocarbons are dramatically reduced by the presence of catalyst so that C_2 hydrocarbons were not detected. The effect of steam on catalytic steam reforming of methane can be also seen since the yield of methane which is 0.08 in the absence of steam drops to 0.06 with a molar S/C ratio of 6 at a 10 s residence time. In contrast to the non-catalytic results, a nearly complete carbon conversion of acetic acid is achieved at 700°C. In the absence of steam, onversion is almost 98% for all residence times.

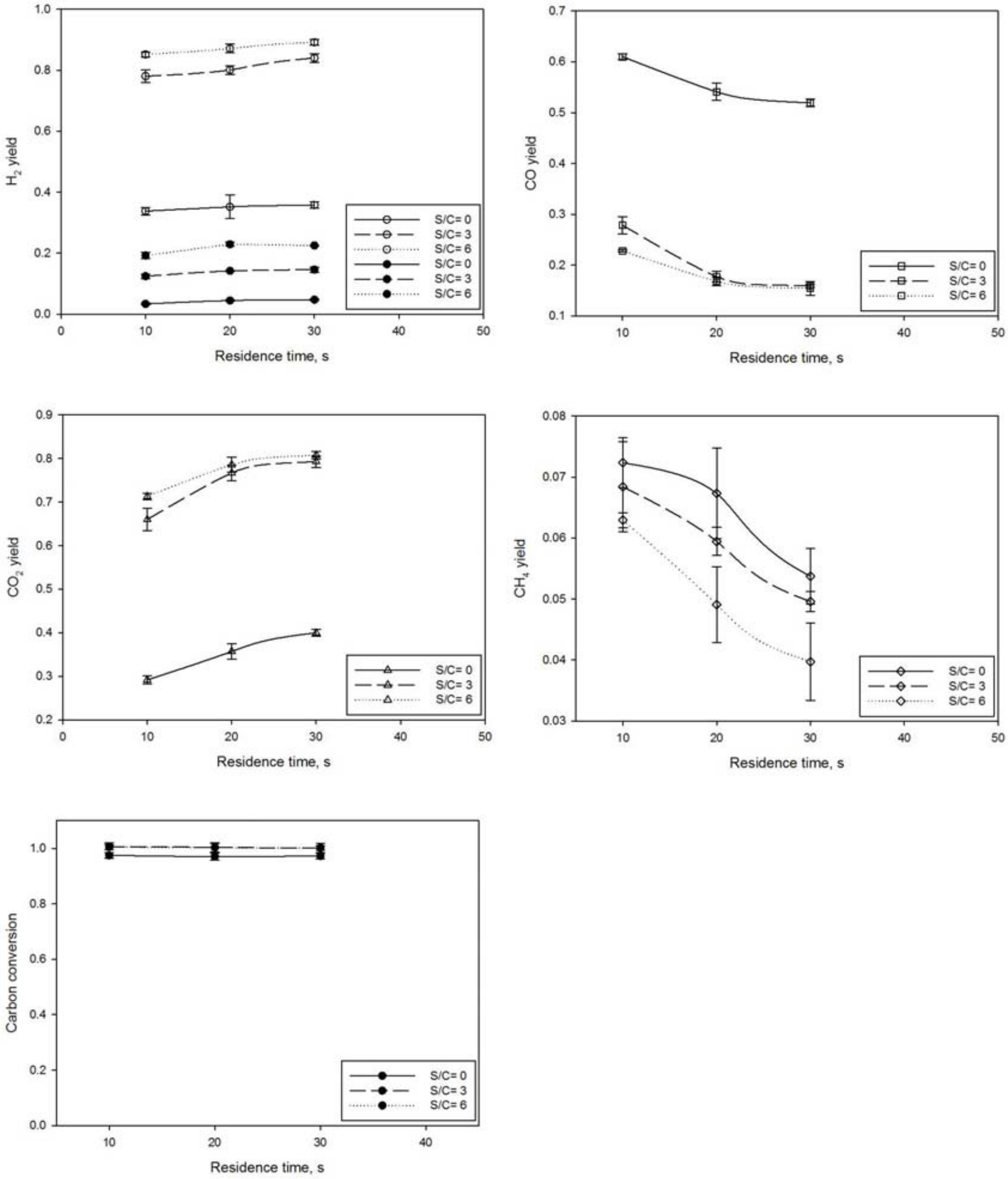

Figure 4.8. **Catalytic steam reforming of acetic acid. Effect of S/C ratio versus residence time; T= 700 °C, catalyst mass= 0.5 g. In case of hydrogen yield: empty symbols present catalytic yields and bold symbols present the non catalytic yields**

4.5.2.2. Effect of catalyst mass

It was seen in the previous section that catalytic steam reforming of acetic acid led to high production of hydrogen through the reforming and water gas shift reactions; however, methane was still present in the reactor. To investigate the effect of catalyst mass on conversion of acetic acid and hydrocarbons as well as on yield of syngas, the mass of catalyst was changed between 0.25 g, 0.5 g and 1 g at 10 s residence time for molar S/C ratios of 0, 3 and 6. The results obtained are presented in Figure 4.9.

It is clear that yield of hydrogen has a direct relationship with the mass of catalyst as it increases when mass of catalyst is increased. However, this relation is not linear; for example, when mass of catalyst is doubled, yield of hydrogen is only slightly increased.

For a molar S/C ratio of zero, the yield of CO increased when catalyst mass was increased from 0.25 g to 0.5 g, but it declined when catalyst mass was 1 g. This is likely because CO, which was produced through the reforming reactions, was initially consumed less in the water gas shift reaction, but rate of water gas shift reaction increased when catalyst mass was increased to 1 g. Decrease in yield of CO_2 can be attributed to the role of the Boudouard reaction in which CO_2 reacts with coke in favor of CO production. It is seen in the Table 4.4 that carbon conversion of acetic acid in the absence of steam was not complete, so the remaining carbon should have been stayed in the reactor as coke. Although production of methane decreased with the extra mass of catalyst, its full conversion was not achieved without steam in the reactor. However, C_2 hydrocarbons which were produced for a catalyst mass of 0.25 g, were completely converted with larger masses of catalyst.

For a molar S/C ratio of 3, the yield of CO showed declining trend as a function of the mass of catalyst, whereas yield of CO_2 had increasing trend. This showed that water gas shift reaction was a dominant reaction at this condition so that CO was consumed towards production of hydrogen and CO_2. It is also noteworthy that methane was converted more by increasing the mass of catalyst, and it was finally converted completely when mass of catalyst was 1 g. In addition, no C_2 hydrocarbon was produced. Despite the case where the catalyst mass was 0.25 g, the carbon conversion was complete for larger masses of catalyst (Table 4.4).

For a molar S/C ratio of 6, an interesting effect of the catalyst mass was seen regarding the yields of CO and CO_2. When the catalyst mass increased from 0.25 g to 0.5 g, the yield of CO increased while the yield of CO_2 dropped, although a different trend was expected. Probably, it can be said that, for a catalyst mass of 0.5 g, the rate of production of CO due to reforming reactions was faster than rate of its consumption through the water gas shift reaction. On the other hand, when the catalyst mass was 1 g, the rate of the water gas shift reaction increased, so that yield of CO_2 increased and the yield of CO decreased. It is interesting that the conversion of acetic acid was complete for a molar S/C ratio of 6 for all tested masses of catalyst (Table 4.4). In addition, no hydrocarbon was among the final products when a catalyst mass of 1g was used.

As illustrated in Table 4.4, the molar H_2/CO ratio was a function of catalyst mass and molar S/C ratio. However, molar S/C ratio had significantly more impact on the molar H_2/CO ratio. When molar S/C ratio was either zero or 3, the molar H_2/CO changed almost following the same order of magnitude as the mass of catalyst. In the case of molar S/C ratio of zero, the molar H_2/CO was between 1.11 and 1.35. This ratio was between 5.61 and 5.88 when molar S/C ratio was 3. On the other hand, the effect of catalyst mass on the molar H_2/CO was very effective when molar S/C ratio was 6. When the catalyst mass was 1 g and molar S/C ratio was 6, the H_2/CO ratio was 15.1, which implies that a significant catalytic activity drives the water gas shift reaction to consume CO and produce hydrogen and CO_2.

Overall, it is realized that the presence of enough steam and the availability of sufficient catalyst must be optimized to reach a high yield of hydrogen and the required H_2/CO ratio. For instance, given that a H_2/CO ratio of 2 is required for the downstream unit when molar S/C ratio is 3 in the stream reforming process, it would be likely possible to produce hydrogen with a lower yield and, instead, to produce CO with a high yield, if the catalyst mass is lower than 0.25 g, which is the lowest mass tested in this research.

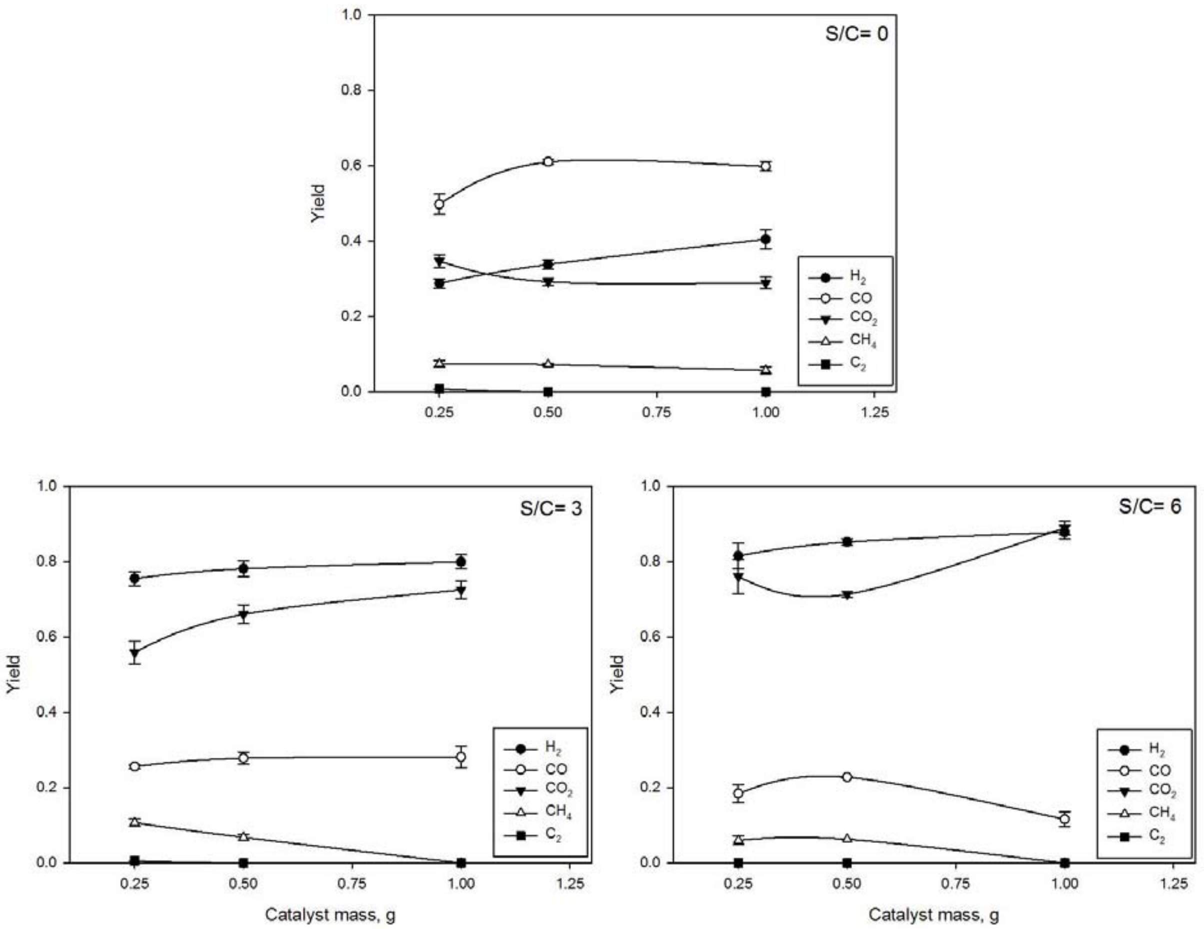

Figure 4.9. **Catalytic steam reforming of acetic acid. Effect of catalyst mass on gas yields. Residence time= 10s, Temperature= 700°C**

Table 4.4. **Carbon conversion, molar H_2/CO and CO/CO_2 ratios as a function of catalyst mass and S/C ratio**

	S/C= 0			S/C= 3			S/C= 6		
	0.25g	*0.5g*	*1g*	*0.25g*	*0.5g*	*1g*	*0.25g*	*0.5g*	*1g*
Conversion	0.925	0.974	0.944	0.931	1.007	1.006	1.004	1.005	1.005
H_2/CO	1.160	1.107	1.354	5.880	5.611	5.690	8.851	9.279	15.091
CO/CO_2	1.432	2.089	2.069	0.457	0.421	0.387	0.242	0.319	0.130

4.5.3. Comparison with literature data

It was not possible to find data in literature that could be compared with our research data because the available literature data were generated with different setups and operating conditions. For example, although nickel based catalysts have been used for steam reforming of acetic acid, they are synthesized with different compositions and physical properties.

The average value of yields obtained in this research from different catalyst masses for a molar S/C ratio of 6 is compared with data reported by Medrano *et al.* [14], who studied the effects of calcium and magnesium on nickel/aluminium catalysts for catalytic steam reforming of acetic acid at 650°C with a molar S/C ratio of 5.58. According to the data in Table 4.5, the yields of product gases and the carbon conversion are very dependent on the catalyst composition. However, a good consistency of trend of the yields is observed between our experimental data and data by Medrano *et al.* . Since the temperature was 700°C in our experiments, complete carbon conversion was achieved.

Vagia and Lemonidou [11] reported their experimental data from three different nickel based catalysts performed at 750°C and molar S/C ratio of 3 which are also compared with average value of yields obtained in this research from different catalyst masses for molar S/C ratio of 3 in Table 4.5. Given that their experiments were carried out at 750°C, a higher hydrogen yield was achieved in their work; regardless, the compositions of the product gases in their work and in this study are consistent.

Therefore, the jiggle bed reactor is an efficient reactor setup which produces reliable data for different operating conditions in addition to the advantage of performing a series of experiments within a short period of time and at a low cost.

***Table 4.5.* Comparison between catalytic experimental data from this study and literature data**

	Medrano *et al.* [14]		This study	Vagia and Lemonidou [11]			This study
Catalyst	*Ni/Al,Ca0.5*	*Ni/Al,Mg0.2*	*X*	*5%Ni*	*10%Ni-1*	*10%Ni-2*	*X*
H_2	0.8445	0.868	0.843	0.88	0.83	0.87	0.776
CO	0.177	0.142	0.176	0.27	0.30	0.31	0.271
CO_2	0.713	0.854	0.787	0.73	0.67	0.69	0.648
CH_4	0.006	0.002	0.040	0.00	0.03	0.00	0.0583
C_2H_4+C_2H_6	0.000	0.000	0.000	0.00	0.00	0.00	0.002
Conversion	0.896	0.999	1.004	1.000	1.000	1.000	1.007

4.6. Conclusions

Non-catalytic and catalytic steam reforming of acetic acid was performed in the jiggle bed reactor. Experiments were repeated 3 times and results were reproducible with less than a 5% error. In addition, changes in operating conditions such as temperature, residence time, molar steam-to-carbon (S/C) ratio and bed material resulted in clear, reproducible and logical changes in the yields of the product gases.

In non-catalytic experiments, the thermal decomposition reactions predominated over the reforming and water gas shift reactions, and the carbon conversion of acetic acid was quite high, while the hydrogen yield was low for all tested molar S/C ratios, temperatures and residence times.

Catalytic steam reforming experiments were conducted at 700°C. Even in the absence of steam, complete carbon conversion of acetic acid was achieved. The hydrogen yield , significantly increased compared to non-catalytic data under similar operating conditions. The reforming and water gas shift reactions were dominant reactions and the hydrogen yield increased with increasing residence time. Increasing molar S/C ratio and the catalyst mass helped increase the acetic acid conversion and the hydrogen yield. On the other hand, CO is also a main product of the steam reforming processes; therefore, an optimum molar S/C ratio and catalyst mass must be selected to maximize the hydrogen yield while achieving the molar H_2/CO ratio that may be required by downstream processes.

Experimental data of the acetic acid catalytic steam reforming were compared with similar data in literature and a satisfactory consistency between the experimental data of this research and those in literature were observed. Therefore, it is realized that the jiggle bed reactor is an efficient novel reactor setup which produces reliable data for different operating conditions in addition to the advantage of performing a series of experiments within a short period of time and at a minimum cost.

References

[1] Latifi, M; Ferrante, L; Briens, C; Berruti, F; “Effects of residence time and temperature on the thermal cracking of bio-oil for syngas production”; ECI Conference, Bioenergy II, Rio de Janeiro, Brazil, March 2009

[2] Latifi M, Ferrante L, Berruti F, Briens C. A Novel Fluidized and Induction Heated Micro Reactor for Catalyst Testing . 2012, Ph.D. Thesis, Chapter 3

[3] Wang D; Czernik S; Montane D; Mann M; Chornet E; “Biomass to Hydrogen via Fast Pyrolysis and Catalytic Steam Reforming of the Pyrolysis Oil or Its Fractions” Ind. Eng. Chem. Res. 1997, 36, 1507-15es

[4] Marquevich M; Czernik S; Chornet E; Montane D; “Hydrogen from Biomass: Steam Reforming of Model Compounds of Fast-Pyrolysis Oil”; Energy & Fuels (1999), 13, 1160-1166

[5] Rioche C; Kulkarni S; Meunier FC; Breen JP; Burch R; “Steam reforming of model compounds and fast pyrolysis bio-oil on supported noble metal catalysts”; Applied Catalysis B: Environmental 61 (2005) 130–139

[6] Galdamez JR, Garcia L, Bilbao R; “Hydrogen production by steam reforming of bio-oil using coprecipitated Ni-Al catalysts. Acetic acid as a model compound”; Energy&Fuels 2005, 19, 1133-1142

[7] Basagiannis AC; Verykios XE; “Reforming reactions of acetic acid on nickel catalysts over a wide temperature range “;Applied Catalysis A: General 308 (2006) 182–193

[8] Takanabe K; Aika K; Inazu K; Baba, T; Seshan K; Lefferts L; “Steam reforming of acetic acid as a biomass derived oxygenate: Bifunctional pathway for hydrogen formation over Pt/ZrO2 catalysts”; Journal of Catalysis 243 (2006) 263–269

[9] Ramos MC, Navascus AI, Garcia L, Bilbao R; “Hydrogen production by catalytic steam reforming of Acetol, a model compound of bio-oil”; Ind. Eng. Chem. Res.; 2007, 46(8), 2399-2406

[10] Medrano JA, Oliva M, Ruiz J, Garcia L, Arauzo J;” Catalytic steam reforming of acetic acid in a fluidized bed reactor with oxygen addition”; Int. J. Hydrogen Energy 33 (2008) 4387-4396

[11] Vagia EC, Lemonidou AA; Hydrogen production via steam reforming of bio-oil components over calcium aluminate supported and noble metal catalysts”; Applied catalysis A: General 351 (2008) 111-121

[12] Davidian T, Guilhaume N, Daniel C, Mirodatos C; “Continuous hydrogen production by sequential catalytic cracking of acetic acid Part I. Investigation of reaction conditions and application to two parallel reactors operated cyclically”; Applied catalysis A: General 335 (2008) 64-73

[13] Davidian T, Guilhaume N, ProvendierH, Mirodatos C; “Continuous hydrogen production by sequential catalytic cracking of acetic acid Part II. Mechanistic features and characterisation of catalysts under redox cycling”; Applied catalysis A: General,337 (2008) 111-120

[14] Medrano J A, Oliva M, Ruiz J, Garcı´a L, Arauzo J; “Catalytic steam reforming of model compounds of biomass pyrolysis liquids in fluidized bed reactor with modified Ni/Al catalysts”; J. Anal. Appl. Pyrolysis 85 (2009) 214–225

[15] Guell B M, Babich I, Nicholas K P, Gardeniers J G E, Lefferts L, Seshan K; “Design of a stable steam reforming catalyst—A promising route to sustainable hydrogen from biomass oxygenates”; Applied Catalysis B: Environmenta, Volume 90, Issues 1–2, 25 July 2009, 38–44

[16] Hu X, Lu G; “Investigation of the steam reforming of a series of model compounds derived from bio-oil for hydrogen production”; Applied Catalysis B: Environmental 88 (2009) 376–385

[17] Hu X, Lu G; “Comparative study of alumina-supported transition metal catalysts for hydrogen generation by steam reforming of acetic acid”; Applied Catalysis B: Environmental 99 (2010) 289–297

[18] Hu X, Lu G; “Acetic acid steam reforming to hydrogen over Co–Ce/Al_2O_3 and Co–La/Al_2O_3 catalysts—The promotion effect of Ce and La addition”; Catalysis Communications 12 (2010) 50–53

[19] Vagia E Ch, Lemonidou A A; “Investigations on the properties of ceria–zirconia-supported Ni and Rh catalysts and their performance in acetic acid steam reforming”; Journal of Catalysis 269 (2010) 388–396

[20] Thaicharoensutcharitthama S, Meeyoo V, Kitiyanan B, Rangsunvigit P, Rirksomboon T; “Hydrogen production by steam reforming of acetic acid over Ni-based catalysts”; Catalysis Today 164 (2011) 257–261

[21] Lu A, Changqing Dong L A, Yang Y, Lei He J Zh; “The influence of Ni loading on coke formation in steam reforming of acetic acid”; Renewable Energy 36 (2011) 930e935

[22] Li Zh, Hu X, Zh L, Lu G; “Renewable hydrogen production by a mild-temperature steam reforming of the model compound acetic acid derived from bio-oil”; Journal of Molecular Catalysis A: Chemical; Volume 355, March 2012, 123–133

CHAPTER 5:

Thermal and Catalytic Gasification of Bio-oils in the Jiggle Bed Reactor for Syngas Production

5.1. Introduction

An increase in energy demand has been seen in the recent decades in different sectors of society. Between 1990 and 2008, total energy consumption in the transportation section increased from 10,051 to 12,510 peta joules in Canada and from 89,312 to 104,875 peta joules in the United States [1]. Fossil fuels have been the main source of energy supply. For example, fossil fuel consumption in Canada and the United States were respectively 75.1% and 84.4% of the total fuel used in 2010 [2]. There is also a big dependence on this energy source. For example, consumption of petroleum was about 19 million barrel per day in 2010 in the United States while 49% of this consumption was supplied from imports [3]. Another challenge with these fuels is that they are sources of large amount of pollutants that create human health problems and global warming. Similar patterns of fossil fuel consumption can be seen in many other countries. Many governments have chosen to promote new technologies to substitute renewable fuels for fossil fuels to reduce greenhouse gas emissions, adhere to environmental regulations, provide some security of supply, and reduce imports.

Natural gas, bio-fuels and hydrogen are well known fuel alternatives. These fuel alternatives can be either used directly or converted to other types of fuels. For example, syngas, a mixture of hydrogen and carbon monoxide that can be produced from steam reforming of natural gas, can be converted to paraffins and olefins through Fischer-Tropsch Synthesis process [4]. Syngas is also a building-block from which a variety of platform chemicals such as methanol or DME can be produced.

Bio-fuels are considered as renewable and clean sources of energy because, when used to substitute fossil fuels, they greatly reduce greenhouse gas emissions and, in some cases, can be ``carbon-negative``. Biomass is a bio-fuel source which has been studied significantly as a fuel alternative for different applications [5-15]. Advancement of biomass technologies can benefit agricultural sectors as well. Biomass is also an appropriate feedstock for syngas production due to its carbon, hydrogen and oxygen contents. Conversion of biomass inside a gasifier in the presence of air or steam directly leads to the production of hydrogen and carbon monoxide [16-19].

There are several advantages in the indirect conversion of biomass to syngas where biomass is firstly pyrolyzed to bio-oil and then bio-oil is gasified to syngas. For example, biomass could be converted to bio-oil in local fields and the bio-oil, which has a much higher energy density than the original biomass, could be transported to a central gasification plant, greatly reducing transportation costs. An additional advantage is that most of the minerals in the original biomass could be locally recycled as pyrolytic biochar, which can be used as a soil amendment or as a source of valuable bio-carbon for a variety of other applications (bio-coal, bio-coke and bio-carbon-based materials – such as catalysts, adsorbents, carbon for composites, bio-cement additives etc.). In addition, valuable biochemicals can be extracted from the raw bio-oil before it is converted to syngas.

Bio-oil is a diverse mixture of oxygenated compounds such as acids, aldehydes, alcohols, ketones, substituted furans derived from cellulose and hemi-cellulose as well as phenolic and cyclic oxygenates derived from lignin. The composition of bio-oil depends on the original biomass and the operating conditions of the fast pyrolysis. As a result, the optimum operating conditions of the gasification process for bio-oil conversion to syngas will likely vary depending upon the type of the original biomass and the pyrolysis conditions. Conversion of bio-oil model compounds to syngas has been studied extensively with different catalysts and operating conditions [20].

Publications on the gasification or steam reforming of actual bio-oils are less numerous than for model compounds. Because of physical properties of bio-oil such as its quick solidification inside the hot injection nozzles, there had been challenges to gasify whole bio-oils, so earlier studies of bio-oil gasification were conducted with the aqueous fraction of bio-oil. By adding water to bio-oil, the aqueous fraction can be separated from the lignin-derived fraction. Since the aqueous fraction contains enough water, high hydrogen yields and carbon conversions can be achieved by gasifying the aqueous fraction. The lignin fraction can also be used to produce different chemical such as adhesives. Garcia *et al.* studied the catalytic steam reforming of the aqueous fraction of bio-oil produced from poplar wood. They used nickel based commercial and synthesized catalysts supported with α-Al_2O_3. The influence of magnesium, lanthanum, cobalt and chromium on the performance of the synthesized catalysts was studied [21]. Czernik *et al.* worked on the catalytic steam reforming of the aqueous phase of bio-oil produced from pine sawdust in a fluidized bed reactor, as well as co-steam reforming of bio-oil and natural gas. They used a commercial steam reforming catalyst [22]. Kechagiopoulos *et al.* worked on the catalytic steam reforming of bio-oil model compounds and also the aqueous fraction of beech wood bio-oil in a fixed bed reactor with a commercial steam reforming catalyst. Lower carbon conversions and hydrogen yields were obtained from the gasification of the aqueous fraction of bio-oil than with the steam reforming of the model compounds. Their investigation revealed that the type of deposited coke from gasification of model compounds was graphitic while the type produced from the aqueous fraction of bio-oil was aromatic [23]. Medrano *et al.* investigated the catalytic steam reforming of the aqueous fraction of pine wood bio-oil model compounds in a fluidized bed reactor. They prepared Ni/Al catalysts with Mg and Ca and obtained larger carbon conversions and hydrogen yields with the catalyst enriched in magnesium [24]. Some developments have been reported to inject whole bio-oil to the gasification reactor in continuous setups. For example, a water cooled spray nozzle was designed and developed through which whole bio-oil can be atomized to a bubbling bed reactor [25].

Fluidized bed reactors have shown better results in term of less coke formation on the catalyst; however, there are some challenges with such reactors such as catalyst attrition. Czernik *et al.* developed a catalyst for fluidized bed reactors to produce hydrogen by catalytic steam reforming of hardwood bio-oil. The developed catalyst was less active than the tested commercial steam reforming catalyst, but displayed an improved attrition resistance [26]. Sakaguchi *et al.* compared non-catalytic and catalytic steam gasification of hardwood bio-oil and bio-oil/bio-char slurry in a fluidized bed reactor with a commercial steam reforming catalyst. They reported that larger carbon conversions were obtained from bio-oil gasification than from bio-oil/bio-char gasification. Although a 3 wt% catalyst loss from the bubbling bed was observed, carbon conversion dropped by 5% after 250 minutes in bio-oil gasification [27]. Seyedyn-Azad *et al.* worked on catalytic steam reforming of a bio-oil in a tubular fixed bed reactor to investigate the effect of catalyst composition and operating conditions. They synthesized Ni/Al_2O_3 catalysts containing nickel between 0 and 18 wt%. Their catalyst with 14.1 wt% nickel content showed the highest carbon conversion and hydrogen yield, but it became significantly deactivated after 1h [28].

Other than testing catalysts, different gasification processes have been also investigated in order to maximize carbon conversion of bio-oil and hydrogen yield and to minimize coke deposition. Davidian *et al.* developed the idea of having a continuous sequential catalytic gasification process having one reactor in which beech wood bio-oil was cracked during the cracking step and then catalyst was regenerated during the regeneration step. They tested a synthesized 10 wt% Ni/Al_2O_3 catalyst and a commercial steam reforming catalyst with composition of 4wt%Ni-2wt%K/La_2O_3-Al_2O_3. The synthesized catalyst showed less activity and was sintered. They have reported that different types of coke were formed on the tested catalysts: whisker deposits on the Ni/Al_2O_3 catalyst and amorphous carbon on the Ni-K/La_2O_3-Al_2O_3 catalyst. The amorphous deposit is more active and can be removed by combustion at lower temperatures [29]. Van Rossum *et al.* worked on non catalytic and catalytic steam gasification of beech wood and pine wood bio-oils in a fluidized bed reactor; their goal was to convert the whole bio-oil to produce a clean syngas, free of hydrocarbons, and with the lowest tar content. They used a Ni-K/La laboratorial catalyst supported on alumina and two commercial steam reforming catalysts. There were problems due to activity loss of the laboratorial catalyst and production of methane as well as secondary and tertiary tars in the fluidized bed reactor. They proposed that it is better to have two reactors in series: a fluidized bed reactor which is loaded with their synthesized catalyst and then a fixed bed reactor loaded with commercial catalysts [30-31]. Wu *et al.* developed the idea of hydrogen production from the sawdust bio-oil via steam reforming in a two-stage catalytic fixed bed reactor to reduce deactivation of the nickel based catalysts and increase carbon conversion and hydrogen yield. The calcined dolomite was used in the first fixed bed reactor for a primary steam reforming of bio-oil and then the commercial Ni/MgO catalyst was used in the second fixed bed reactor in which further catalytic steam reforming reactions between product gases of the previous stage took place [32]. Marda *et al.* investigated non-catalytic partial oxidation (NPOX) of the bio-oil produced from the poplar wood. Their idea was to maximize carbon conversion of the bio-oil to gaseous products through the NPOX process and then to increase the hydrogen yield of in a catalytic reactor where lower temperature and less load of catalyst is required. [33]. Lan *et al.* synthesized a catalyst with formulation of 18wt%Ni/10wt%MgO-10wt%La_2O_3-Al_2O_3 to investigate catalytic steam reforming of bio-oil produced from rice husk in a fixed bed reactor and in a fluidized bed reactor. They gained larger yield of hydrogen and carbon conversion as well as less coke formation on the catalyst in the fluidized bed reactor [34].

Panigrahi *et al.* investigated the effect of residence time on the gasification of hardwood bio-oil in the absence of catalyst to produce syngas and high Btu gases such as methane and olefins. They also studied effect of extra flows of CO_2 (CO_2/N_2), H_2 (H_2/N_2) and steam (H_2O/N_2) on the final yield of the product gases [35-36].

It is realized from the scattering findings in literature that a suitable experimental system would be very helpful to comprehensively study the conversion of different bio-oils to syngas under similar operating conditions. Instead of testing catalysts under different operating conditions in large scale reactor setups, having an appropriate micro reactor to perform similar experiments in a small scale well controlled setup would be beneficial, both in terms of time and money, to investigate the optimum catalyst for bio-oil conversion and production of syngas. The jiggle bed reactor (JBR) is such a novel micro reactor that was designed and developed at the Institute for Chemical and Fuels from Alternative Resources (ICFAR) to test catalysts for bio-oil gasification. This reactor operates as a batch reactor in which catalyst particles are fluidized by vibration and the required heat is supplied by the induction heating method [37]. Promising results were obtained in preliminary experiments of non-catalytic and catalytic steam reforming of acetic acid in the jiggle bed reactor [38].

The objective of this chapter was performing thermal and catalytic gasification of two bio-oils in the jiggle bed reactor to investigate optimum operating conditions such as temperature and residence time as well as catalyst type and mass for maximum production of syngas and bio-oil conversion. In addition, since bio-oils were produced from different biomasses, effect of chemical composition on bio-oil conversion and yield of product gases was investigated.

5.2. Experimental setup and procedure

As the first step of testing bio-oils in the jiggle bed reactor, thermal and catalytic gasification of two fast pyrolysis bio-oils were investigated: a hardwood bio-oil produced by Dynamotive Energy Systems Corporation (Canada) and a birch wood bio-oil produced at ICFAR at 475°C. No additional steam was used in the reactor; nevertheless, different water content of the bio-oils made it possible to study the effect of steam in maximizing carbon conversion of bio-oils and yield of syngas. In order to examine the effects of catalyst (type and mass) on bio-oil gasification as a function of residence time and temperature, two commercial steam reforming nickel based catalystswere tested in the JBR setup: the catalyst X manufactured for steam reforming of light hydrocarbons, and the catalyst Y, manufactured for steam reforming of natural gas. The residence time ranged from 10 to 30 s and the temperature was varied between 700 and 800 °C.

The jiggle bed reactor is a batch fluidized bed micro reactor where the heat required by the gasification reactions is supplied by induction heating. Solid particles are fluidized in a ceramic crucible by vibration which is provided by a linear pneumatic actuator. Frequency of the actuator is 3 Hz and the amplitude of its motion is 0.1 m; these conditions provide smooth fluidization of the bed particles. There is a copper coil around the ceramic crucible. A high voltage current passing on the surface of the coil provides a magnetic field; as a result, hysteresis and eddy currents are induced on the surface of wires inside the crucible. Direction of the magnetic field and direction of the induced currents are alternated with a frequency of about 250 kHz. There is a very small temperature difference between the heating surface and the catalyst bed, which minimizes the parasitic thermal reactions that occur in other reactors [37].

A schematic of the experimental setup is shown in Figure 5.1. Details may be found elsewhere [38].

Since the jiggle bed reactor is a batch setup for injecting micro liters of the liquid feed, Drummond capillary tubes with 4µl volume were used to inject precise amount of the bio-oil to the reactor.

A Varian micro GC CP4900 instrument was used to analyze the product gases H_2, CH_4, CO, CO_2, C_2H_4 and C_2H_6. This micro GC was equipped with three columns 10 m MS5A, 10 m PPU and 8 m 5CB. Helium was used as the carrier gas in the micro GC. Since the product gases were diluted with argon in the gas sampling bag, their concentration was very low. Therefore, the sensitivity of the TCD was set at high level and sampling time was set at 500 ms to be able to observe the peaks of the product gases on the output of the GC analysis. Because the GC did not detect the steam in the product gases, water measurement and, hence, elemental balances could not be performed. GC runs were conducted for 3 minutes.

In order to calculate the yields of the product gases and total carbon conversion, a known volume of an external standard gas was added to the mixture of product gases. Although nitrogen could have been used, it was not ideal because of the risk of contamination from air. Therefore, 500 µl of normal C_4H_{10} was injected into the vacuumed gas sampling bag with a gas tight syringe as the external standard gas. C_4H_{10} was never produced during the gasification tests and was, thus, a suitable external standard gas. Despite the fact that the product gases are mixed with the external standard gas during the gas collection in the gas sampling bag after the test, the gas sampling bag was also squeezed manually for several times to ensure good mixing between the standard gas and the product gases. Experiments were repeated for 3 times to check the reproducibility of the data.

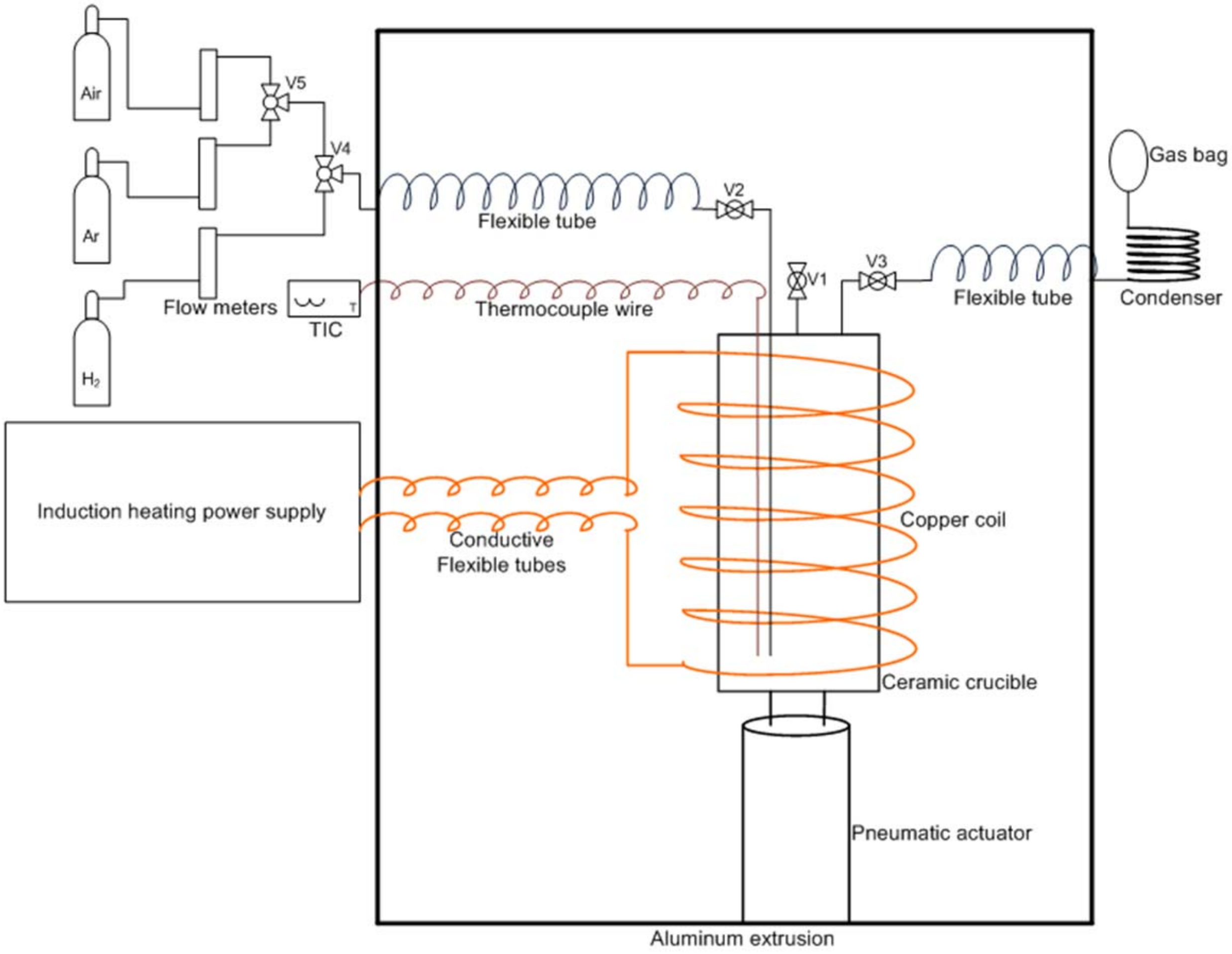
Air
Ar
H₂
Flow meters
V5
V4
Flexible tube
V2
V1
V3
Gas bag
Flexible tube
Condenser
TIC
Thermocouple wire
Induction heating power supply
Conductive
Flexible tubes
Copper coil
Ceramic crucible
Pneumatic actuator
Aluminum extrusion

Figure 5.1. **Schematic of the JBR experimental setup for the catalytic gasification tests**

5.3. Bio-oils

Two different bio-oils were used in this research. The DMB was a bio-oil produced by fast pyrolysis of hardwood at moderate temperatures, in the absence of oxygen, at the Dynamotive Energy Systems Corporation in Canada. This bio-oil had been stored in the lab for three years. As presented in Table 5.1, the elemental composition of the fresh bio-oil is changed and therefore is different from that of the old bio-oil after 3 years so that hydrogen, oxygen and water contents were increased and the carbon content was reduced. Gasification experiments were carried out with the old DBM. The BWB is another bio-oil that was produced at ICFAR through the fast pyrolysis of birch wood in a bubbling fluidized bed reactor at 475°C. The elemental composition of the BWB is also presented in Table 5.1. Despite the fact that DMB and BWB should have different composition of the organic compounds, the water content of the BWB is almost twice as large as the water content of the DMB.

***Table 5.1.* Elemental analysis of Dynamotive (DMB) and ICFAR (BWB) bio-oils**

	Fresh DMB	Old DMB	BWB
H, wt%	7.20	8.04	9.43
C, wt%	41.67	36.30	25.83
N, wt%	0.27	0.30	0.62
O, wt% (balance)	51.13	55.36	64.13
Water content, wt%	24.34	27.52	49.85
General formula	$CH_{2.071}O_{0.920}N_{0.005}$	$CH_{2.624}O_{1.121}N_{0.007}$	$CH_{4.326}O_{1.827}N_{0.019}$
C/H, mol/mol	0.48	0.38	0.23
C/O, mol/mol	1.09	0.87	0.55

5.4. Preparation of the bed material

Pellets of each catalyst were crushed and sieved to achieve a size distribution of 220-350 µm. Since the fresh catalysts were provided in non-reduced form, a 10 g batch of them was initially reduced in-situ in the JBR setup with a flow of 100 ml/min of pure hydrogen for 6 hours at 600 °C for the catalyst X and at 700 °C for the catalyst Y according to the reduction procedures recommended by the manufacturers. Since the reduced catalysts were pyrophoric, the catalytic bed of each catalyst was exposed to steam for an hour before discharge to get passivated; the prepared passivated catalyst was then kept inside desiccators.

The desired mass of a prepared catalyst was mixed with silica sand with a size distribution of 106-220 µm for the gasification tests in the reactor, so that the total mass of the solid particles was 10 g for all experiments. Before starting the experiments, the catalytic bed was reduced in-situ again with a 100 ml/min flow of pure hydrogen at the reaction temperature for 1 hour to make sure that nickels on the surface of catalysts were in the form of free nickel (Ni^0) with no NiO on the surface. The size distribution of the catalyst particles was selected to allow for separation from the silica sand particles after the experiments. Although silica sand and catalyst particles had different size distributions, segregation was not observed in the reactor.

5.5. Catalyst characterization

Surface area analysis of the fresh catalysts was carried out by a surface area analyzer (ASAP 2010) through adsorption of N_2 at 77.35 K. According to Table 2, the catalyst X provides a little larger surface area and pore volume for the catalytic reactions compared to the catalyst Y.

Table 5.2. **Surface and pore analysis of the steam reforming catalysts**

Catalyst	BET surface area, m^2/g	Average pore size$^{\times}$, A°	Total pore volume^{+}, cm^3/g
Fresh catalyst X	15.375	130.049	0.0502
Fresh catalyst Y	12.390	100.731	0.0319

$^{\times}$Adsorption Average Pore Diameter (4V/A° by BET)

$^{+}$Single Point Adsorption Total Pore Volume of pores less than 775.52 A° Diameter at $P/P_0= 0.974$

Data of the X-Ray Fluorescence (XRF) analysis of the fresh catalysts are presented in Table 5.3. The catalysts X and Y include almost similar elements, but they are different in their compositions. Nickel, calcium and lanthanum have noticeable composition differences in the catalysts. For example, estimated total nickel content of the catalysts is X 11.61 wt% while the catalyst Y contains 12 wt% of nickel. The concentration of calcium in the catalyst X is larger than that in the catalyst Y (9 wt% versus 3.4 wt%) whereas the catalyst Y contains 2.12 wt% lanthanum compared to 0.02 wt% lanthanum in the catalyst X.

Nickel is the most important metal in the catalysts designed for the gasification reactions that produce syngas. Although XRF data give an estimation of the total nickel content of the catalysts, it is useful to know how much of the nickel is present on the surface of the catalyst which acts as the active portion of the nickel involved in the catalytic reactions. Therefore, TPR-

TPO analyses on the fresh catalysts were carried out by the AutoChem II 2920 equipment: a sample of the fresh catalyst was oxidized completely by air to convert all nickel elements to nickel oxide. Then, the TPR analysis was started with a flow of hydrogen of 50 cm^3 STP/min with the rate of 10 °C/min until 750 °C when the catalyst was completely reduced. In the next step, the TPO analysis was performed on the reduced catalyst with a flow of oxygen of 50 cm^3 STP/min until 410 °C when the catalyst was completely oxidized. At the end of the TPR analysis, NiO on the surface of catalyst is converted to Ni^0 according to reaction 5.1:

$$NiO + H_2 \rightarrow Ni^0 + H_2O \tag{5.1}$$

Also, at the end of the TPO analysis, Ni^0 on the surface of the catalyst is converted to NiO according to reaction 5.2:

$$Ni^0 + \frac{1}{2}O_2 \rightarrow NiO \tag{5.2}$$

Knowing the consumption of hydrogen and oxygen during the TPR and TPO analyses, respectively, the nickel content on the surface of the catalyst was estimated. Similarly, the TPR-TPO analyses were conducted on the reduced catalysts. Results are presented in Table 5.4. It is realized from the TPR-TPO analyses data that, other than activating the catalyst, reduction of the catalyst has caused a little amount of the nickel element in the bulk of catalyst to move to the surface, so that the available Ni^0 on the surface of catalysts has increased. However, it is important to note that the active portion of nickel is less than half of the total estimated nickel content that takes part in the catalytic reactions. Furthermore, the active portion of the catalyst Y is larger than that in the catalyst X in both fresh and reduced forms.

Table 5.3. **XRF analysis data of the steam reforming catalysts X and Y**

Compound	Mass, wt%		Element	Mass, wt%	
	X	*Y*		*X*	*Y*
Al_2O_3	63.66	68.48	Al	33.69	36.24
NiO	14.78	15.31	Ni	11.61	12.03
CaO	12.66	4.74	Ca	9.05	3.39
SiO_2	1.06	1.59	Si	0.494	0.746
MgO	0.492	0.788	Mg	0.297	0.475
P_2O_5	0.0574	0.0520	Px	0.0250	0.0227
Fe_2O_3	0.0472	0.159	Fe	0.0330	0.111
La_2O_3	0.0251	2.49	La	0.0214	2.12
Sc_2O_3	0.0039		Sc	0.0025	
Lu_2O_3		0.0069	Na		0.164
MnO		0.0024	Lu		0.0061

Table 5.4. **Estimated Ni^0 on the catalyst surface by TPR-TPO analysis (wt%)**

Catalyst	X	Y
Fresh catalyst	4.05-5.31	5.97-6.61
Reduced catalyst	4.35-5.46	6.28-6.60

X-Ray powder Diffraction (XRD) patterns of the fresh and reduced samples of the catalysts X and Y are shown in Figure 5.2. Although similar phases of Ni^0 and NiO have been found, different patterns of the powder diffraction have been identified with both catalysts.

The effect of catalyst reduction is clear on the XRD patterns. Phases of NiO have been disappeared on the reduced catalyst except at 2θ of 43.29°, possibly due to the oxidation of the nickel on the surface when it was exposed to the ambient air. On the other hand, it is noteworthy that phases of active Ni^0 appeared on the surface of the catalyst after its reduction with hydrogen, showing that this catalyst has become active for the catalytic reactions. Other than peaks of NiO and Ni^0 phases, structures of the other phases on both fresh and reduced catalysts are similar. Regarding the catalyst X, the intensity of the peaks is increased after reduction, although it did not change significantly after reduction for the catalyst Y.

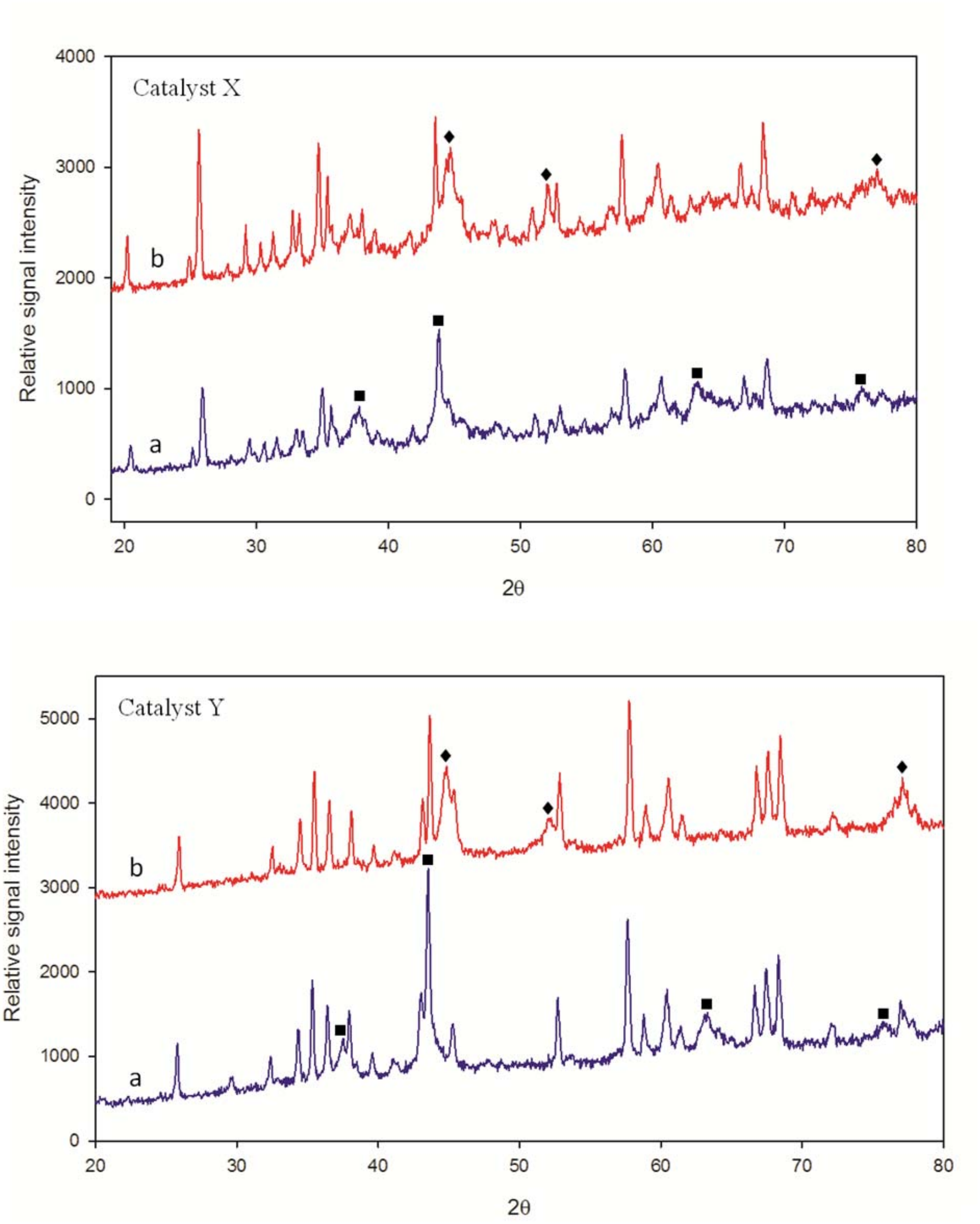

***Figure 5.2.* XRD patterns of the catalysts X and Y: (a) fresh catalyst (b) reduced catalyst; square symbols (■) presents phases of NiO and diamond symbols (♦) presents phases of Ni^0**

5.6. Experimental results and discussion

Non-catalytic and catalytic gasification of the DMB and the BWB bio-oils in the jiggle bed reactor were investigated. The residence time was calculated as the time span from the time the feed was injected until the product gases were flushed by argon into the gas sampling bag. The mass of bed material was 10 g for all experiments. Silica sand was the bed material for non-catalytic tests. In catalytic tests, either 0.5 or 1 g of catalyst was mixed with silica sand.

The Drummond capillary tubes with 4 µl volume were used to introduce the bio-oil into the reactor. This volume was chosen to maintain close-to-atmospheric pressure in the reactor. Since it is important to know the mass of the feed bio-oil for yield and conversion calculations, five capillary tubes were filled with a bio-oil and then the average mass of bio-oil in those tubes was considered as the mass of that bio-oil equivalent to 4 µl volume. To make sure the experimental data were reproducible, experiments were repeated 3 times. Average value of the obtained yield data is reported in this paper. Maximum spread between the replicate data was ±4%.

In the presence of steam, bio-oil with general formula of CH_mO_k (neglecting the nitrogen content) can be converted to syngas (H_2+CO) according to reaction 5.3:

$$CH_mO_k + (1-k)H_2O \rightarrow CO + \left(1 + {}^{m}\!/_{2} - k\right)H_2 \tag{5.3}$$

If there is enough steam in the reactor, the produced CO would react with steam through the water-gas shift reaction to produce more hydrogen:

$$H_2O + CO \leftrightarrow H_2 + CO_2 \tag{5.4}$$

Therefore, summing up reactions 5.3 and 5.4, the overall steam reforming of bio-oil can be expressed by reaction 5.5:

$$CH_mO_k + \left(2 - k\right)H_2O \rightarrow CO_2 + \left(2 + {}^{m}\!/_{2} - k\right)H_2 \tag{5.5}$$

There are a number of other reactions taking place after bio-oil is injected into the reactor. For example, As soon as bio-oil enters the reactor, it decomposes thermally to other forms of the oxygenated molecules (CH_yO_z) as well as some permanent gases (hydrogen, steam, CO, CO_2 and light hydrocarbons) and coke (reaction 5.6). Besides, since CO, CO_2 and coke are available inside the reactor, the Boudouard reaction (reaction 5.7) is another important reaction which can affect the CO/CO_2 ratio in the final product gases.

$$CH_mO_k \rightarrow CH_yO_z + gases\ (H_2, H_2O, CO, CO_2, CH_4, \dots) + coke \tag{5.6}$$

$$2CO \leftrightarrow C + CO_2 \tag{5.7}$$

In addition, in the presence of steam, the produced hydrocarbons undergo steam reforming reactions towards production of hydrogen and carbon monoxide. For example, reaction 10 illustrates how methane can be converted to syngas:

$$CH_4 + H_2O \rightarrow CO + 3H_2 \tag{5.8}$$

In this research we did not add additional water because in industry, the practice is to use a separate water-gas shift reactor, downstream of the gasification reactor, which can be operated at a temperature and with a catalyst optimized for the water-gas shift reaction. In other words, our goal was to maximize the conversion of bio-oil to product gases and conversion of the hydrogen contained in the raw bio-oil, including its own water, to hydrogen gas (H_2). Therefore, the yield of produced hydrogen was defined according to equation 5.9:

$$Y_{H_2}\left(\frac{g}{g}\right) = \frac{mass\ of\ hydrogen\ as\ H_2\ in\ product\ gas}{mass\ of\ H\ in\ the\ raw\ bio\text{-}oil} \tag{5.9}$$

To estimate the number of moles of the bio-oil, bio-oil with a general formula of CH_mO_k was assumed from its elemental composition [28]. Since a maximum of 1 mol of a product gas like CO, CO_2 and CH_4 can be produced per 1 mole of the injected bio-oil, yield of these gases were estimated as:

$$Y_{CO,CO_2,CH_4}\left(\frac{mol}{mol}\right) = \frac{moles\ of\ the\ product\ gas}{moles\ of\ the\ bio\text{-}oil} \tag{5.10}$$

Accordingly, yields of C_2H_4 and C_2H_6 hydrocarbons were estimated by equation 5.11:

$$Y_{C_2H_4,C_2H_6}\left(\frac{mol}{mol}\right) = \frac{moles\ of\ the\ product\ gas}{0.5 \times moles\ of\ the\ bio\text{-}oil} \tag{5.11}$$

The carbon conversion was calculated by summing up the yields of carbon containing product gases.

One advantage of the jiggle bed reactor is that it is very convenient to perform a complete test (from feed injection until end of the gas analysis) for a very short period of time i.e. 10 minutes, so it is possible to repeat a test to check out reproducibility of the data and conduct tests with different operating conditions while a great deal of time is saved. However, it must be taken into account that coke as the solid product of the reaction remains in the reactor which must be removed before conducting a new test; otherwise, coke can be gasified during the next test and have a detrimental effect on the calculation of gasification yields. Therefore, after each test, the catalytic bed was regenerated and reduced according to the following in-situ procedure:

1. Coke was burned off with air for 30 seconds
2. Argon was introduced to the reactor for 30 seconds to flush out air molecules
3. Hydrogen was introduced to the reactor for 5 minutes to remove oxygen molecules on the surface of the catalysts and make them reduced
4. Argon was introduced to flush out hydrogen molecules in the reactor for 2 minutes
5. The procedure above was carried out even for non-catalytic tests where there was only silica sand in the reactor.

5.6.1. Thermal cracking of the bio-oils

Thermal cracking of DMB and BWB bio-oils, i.e. without using any catalyst, was carried out in the jiggle bed reactor at temperatures of 700, 750 and 800 °C for a residence time of 30 s. Such a long residence time was chosen as an extreme condition to investigate whether the absence of catalyst could be compensated with a long residence time. The mass of silica sand was 10 g for all experiments.

The effect of temperature on the yield of the product gases is shown in Figure 5.3. In addition, molar ratios of H_2/CO and CO/CO_2 are compared in Figure 5.4. Complete carbon conversion could not be achieved for either bio-oil. Carbon conversion of the DMB was between 48% at 700°C and 64% at 800°C, and carbon conversion of the BWB was between 52% at 700°C and

72% at 800°C. Not only were carbon conversions low, but also the yield of hydrocarbons was quite high, especially, at lower temperatures.

The hydrogen yield increased with increasing temperature. Hydrogen can be produced through steam reforming of the organic compounds (reaction 5.5), thermal decomposition (reaction 5.6) and steam reforming of the produced hydrocarbons (e.g. reaction 5.8). The hydrogen yield was low between 0.17 and 0.48 from the DMB and between 0.19 and 0.36 from the BWB over the tested temperature range. The larger hydrogen yield of the DMB compared to that of the BWB, which has higher water content (Table 5.1), implies that the rate of hydrogen production through the pathways such as the thermal decomposition of organic compounds was faster than rate of steam reforming reactions in thermal cracking of the DMB.

The methane yield was quite high at 700°C: 0.14 and 0.09 for DMB and BWB, respectively. Figure 5.3 shows that the methane yield decreased with increasing temperature, which indicates an increasing conversion of the produced methane through the steam reforming reaction (reaction 5.8). Complete conversion of methane was not achieved even at 800°C, which can be due to either insufficient steam or the absence of catalyst.

Figure 5.3 shows that the yield of C_2 hydrocarbons was the lowest among the product gases, and increased with increasing temperature. The only unique trend is seen for the BWB thermal cracking, where the yield of C_2 hydrocarbons decreased slightly between 750 and 800 °C.

CO was the main product among the carbon containing gases. As it is illustrated in Figure 5.4, the molar CO/CO_2 ratio was always larger than one, probably because there was not enough steam in the reactor to react with CO through the water gas shift reaction to produce CO_2 and extra hydrogen. For instance, considering the water content of the bio-oils in Table 5.1, it is clear from the data in Figure 5.4 that the molar CO/CO_2 ratio of BWB thermal cracking was lower than that of DMB thermal cracking at similar temperatures. The largest difference between the molar CO/CO_2 ratios of the DMB and the BWB thermal cracking is found at a temperature of 800°C with the yield of CO_2significantly larger in thermal cracking of the BWB, possibly due to a greater influence of the water gas shift reaction for this bio-oil at 800°C.

According to Figure 5.4, the H_2/CO ratio increased with increasing temperature. Although lower yields of hydrogen were achieved from the BWB, larger molar H_2/CO ratios were obtained during its thermal cracking. Given the larger water content of the BWB, it is realized that more CO should have been converted to CO_2 through the water gas shift reaction.

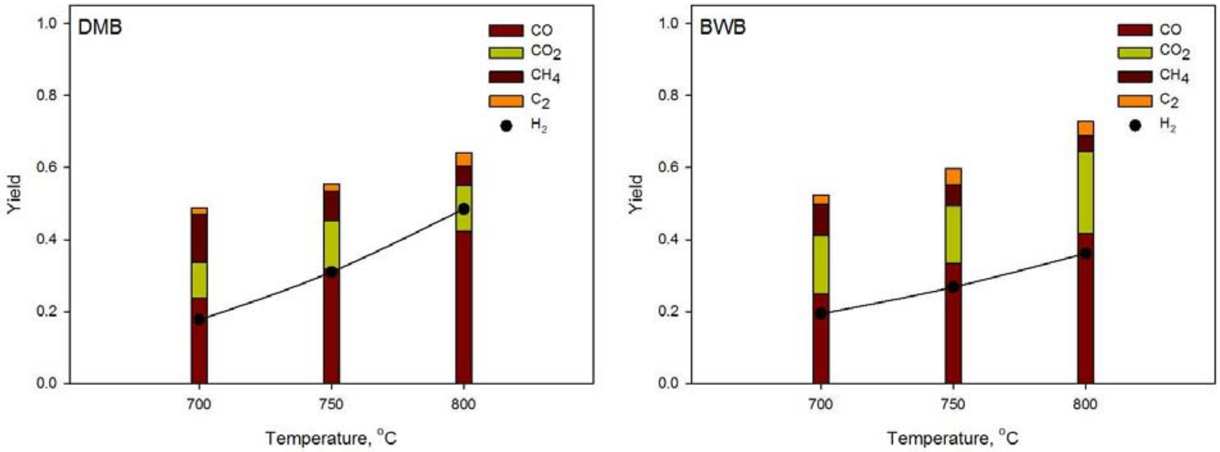

Figure 5.3. **Yield of product gases from thermal cracking of the DMB and the BWB versus temperature. Residence time= 30 s**

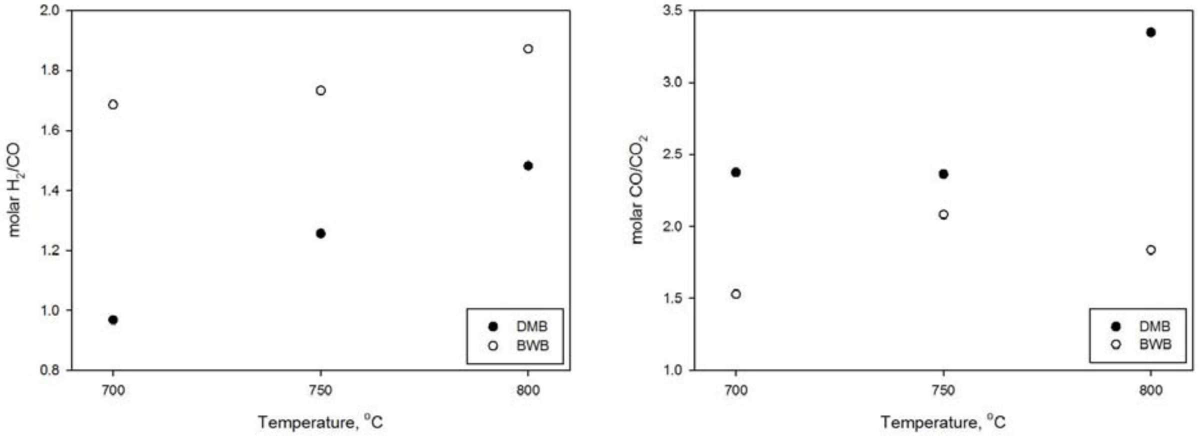

Figure 5.4. **Yield of molar H_2/CO and CO/CO_2 ratios from thermal cracking of the DMB and the BWB; Residence time= 30 s**

5.6.2. Catalytic cracking of the bio-oils

The catalysts X and Y were tested to determine the yield of the product gases as a function of catalyst type and mass, residence time, and temperature, to find out how the hydrogen yield and the carbon conversion can be maximized. Since the DMB and the BWB bio-oils have different elemental compositions and water contents, it is interesting to study how the applied operating conditions can result in different yields of the product gases from the gasification of the tested bio-oils.

5.6.2.1. Effect of catalyst type and mass

The effects of catalyst type and mass on yields of product gases and carbon conversion from the gasification of the DMB and the BWB bio-oils were investigated with the catalysts X and Y. The catalyst mass ranged from 0 (thermal cracking) to 1 g. Figures 5.5 and 5.6 illustrate the yields of the product gases and the carbon conversion for the experiments conducted at a temperature of 800°C and a residence time of 30 s.

The yields of hydrogen, CO and CO_2 increased with increasing catalyst mass (Figure 5.5). The methane yield initially increased because of increased conversion of bio-oils to methane and then decreased with larger catalyst masses that helped convert methane to other gases. The yield of C_2 hydrocarbons was also decreased as the catalyst mass increased. Both catalysts X and Y increased the carbon conversion (Figure 5.6). Thus, the catalysts were effective to convert condensable and large organic compounds in the bio-oils, which could not be cracked in the thermal cracking tests, to permanent gases.

The catalyst X gave higher yields of hydrogen and CO than the catalyst Y. On the other hand, lower yields of hydrocarbons were observed with the catalyst X. This indicates that the catalyst X was more active than the catalyst Y in steam reforming and water gas shift reactions.

Given similar operating conditions and catalyst, the yields of product gases depend on the composition of the organic compounds and the water content of the bio-oils. For example, as with the thermal cracking results of Figure 5.3, although the BWB had larger water content, higher yields of hydrogen were achieved in catalytic gasification of the DMB as shown in Figure 5.5. On the other hand, the influence of steam reforming and water gas shift reactions should have been greater during catalytic gasification of the BWB bio-oil because of presence of more steam in the reactor. For instance, slightly lower yields of CO and larger yields of CO_2 obtained from the BWB than those from the DMB should indicate the effect of its larger water content. Figure 5.5 shows that the yield of CO_2 decreases between 0.5 g and 1 g catalyst mass for the DMB, while it increases for the BWB, which could be due to progress of the water gas shift reaction. Nevertheless, it is noteworthy that, since hydrogen of the water content was considered to calculate the hydrogen yield, such large yields of hydrogen indicate that the bio-oil water was consumed in the catalytic experiments.

Regardless of the type of bio-oil, and under similar conditions, the CO yield was larger than the CO_2 yield: this can be due to low amount of steam in the reactor and, as a result, relatively low rate of the water gas shift reaction. In other words, if sufficient steam could be available in the reactor, the produced CO would partly react with it in favor of higher production of hydrogen and CO_2.

The yield of methane from the BWB cracking drops significantly with 1 g mass of the catalyst X, but there is a very slight decrease with a similar mass of the catalyst Y. It seems that the BWB contains heavy molecules which the catalyst Y is unable to convert directly to hydrogen and CO; therefore, instead, these heavy molecules are probably catalytically cracked to hydrocarbons like methane.

Overall, the catalyst X showed the best performance in terms of larger production of hydrogen and CO as well as carbon conversion of the bio-oils. Although, according to Table 5.4, availability of the nickel on the surface of the catalyst Y was larger, better performance of the catalyst X should be attributed to the larger BET surface area (Table 5.2), and its larger calcium content (Table 5.3).

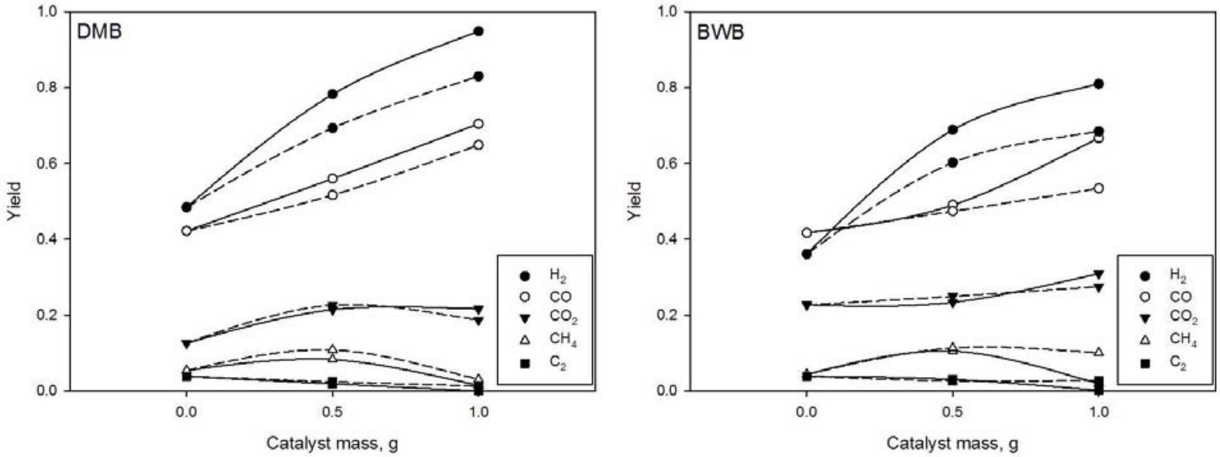

Figure 5.5. **Effect of the catalyst type and mass on yield of product gases from catalytic gasification of the DMB and the BWB, temperature= 800°C, residence time= 30 s. Full and dashed lines represent trend of yields with the catalysts X and Y, respectively.**

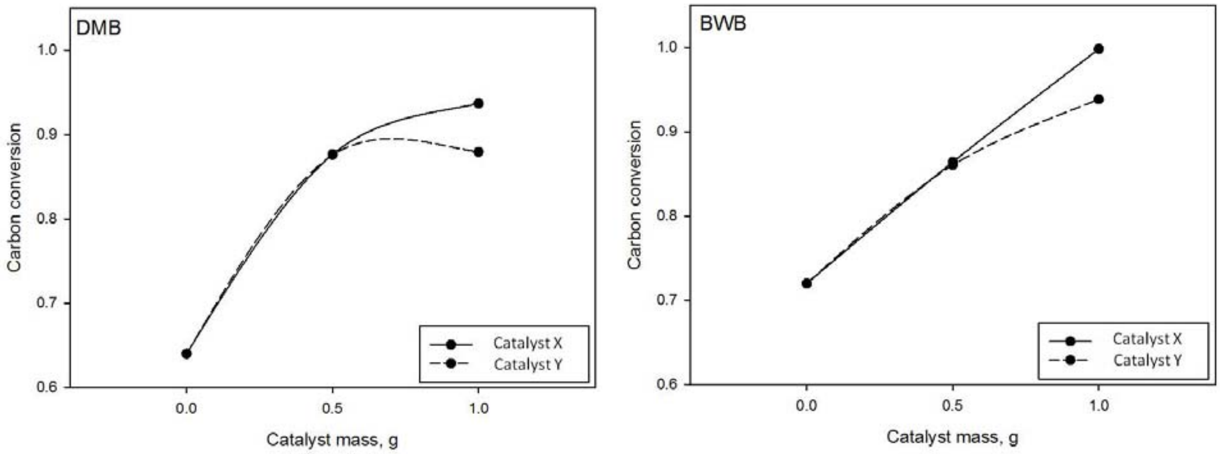

Figure 5.6. **Effect of the catalyst type and mass on carbon conversion from catalytic gasification of the DMB and the BWB, temperature= 800°C, residence time= 30 s. Full and dashed lines represent trend of yields with the catalysts X and Y, respectively.**

5.6.2.2. Effect of residence time

Catalytic gasification of both the DMB and the BWB bio-oils was carried out at 800°C and residence times between 10 s and 30 s. Figure 5.7 shows how the yields of the product gases varied with the residence time when 1 g of the catalyst X was used. The results show that a longer residence time helped increase the yields of hydrogen, CO and CO_2, while hydrocarbons were converted to permanent gases.

A comparison of Figures 5.5 and 5.7 shows that the impact of the catalyst mass on the yield of hydrogen was larger than that of residence time at 800°C.

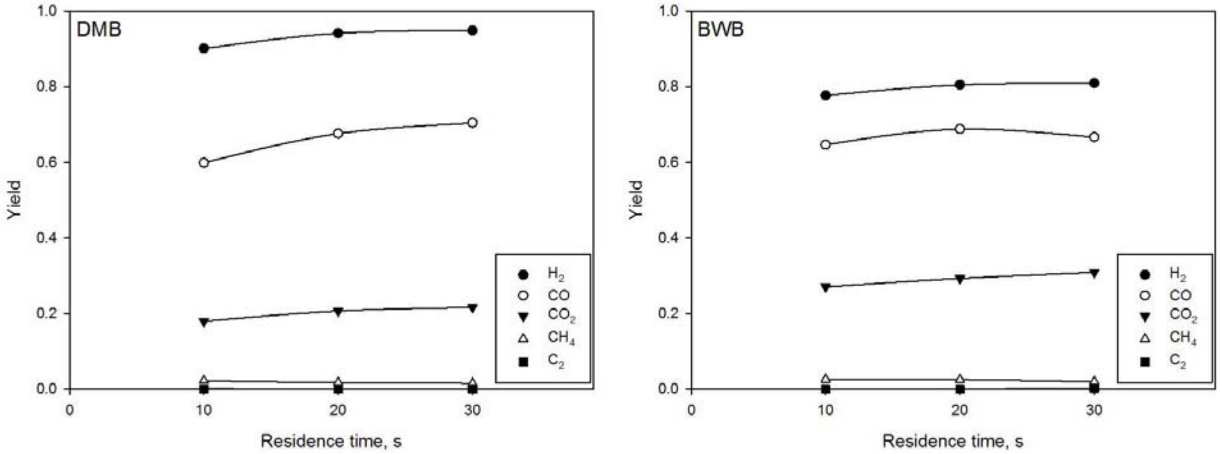

***Figure 5.7.* Effect of residence time on yield of product gases from catalytic gasification of the DMB and the BWB, temperature= 800°C, mass of the catalyst X= 1 g**

5.6.2.3. Effect of temperature

Catalytic gasification of both the DMB and the BWB was conducted with the catalyst X at 700°C, 750°C and 800°C at residence time of 30 s to investigate maximum conversion of the bio-oils and yield of syngas as a function of temperature. The mass of catalyst was 0.5 g and 1 g. The yield of the product gases is illustrated in Figure 5.8. In addition, molar ratios of H_2/CO and CO/CO_2 are compared in Figure 5.9.

In comparison with thermal cracking experiments, Figure 5.3, it is realized from Figure 5.8 that a larger carbon conversion of the bio-oils was achieved in presence of catalyst at all temperatures. In other words, regardless of the composition of the product gases, the catalyst provided good enough conditions for those heavy organic compounds, which did not crack in the absence of catalyst, to be cracked and be converted to permanent product gases. Furthermore, the larger carbon conversions can also be attributed to gasification of deposited coke in the presence of catalyst. Overall, as shown in Figure 5.8, not only total carbon conversion of the bio-oils in the catalytic gasification experiments was larger than that obtained in the thermal cracking experiments, under similar conditions, but it also increased with both temperature and catalyst.

It seen in Figure 5.8 that in opposite to larger water content of the BWB, its carbon conversion, was not noticeably larger than carbon conversion of the DMB; in other words, it was sometimes less, especially at lower temperatures. For example, the carbon conversion of the BWB was 67% and 75% whereas the carbon conversion of the DMB was 69% and 77% at 700°C with 0.5 g and 1 g of catalyst, respectively, which is likely due to some heavier organic compounds in the BWB that could not be converted to the product gases through steam reforming reactions despite having larger water content.

Similarly to the carbon conversion of the bio-oils, at all temperatures, the yield of hydrogen significantly increased in the presence of catalyst compared to the thermal cracking experiments. The yield of hydrogen was also a function of the catalyst mass. On the other hand, the yield of hydrogen did not change significantly as a function of temperature, especially at lower temperatures and lower catalyst mass. It is interesting to note that, at similar temperature and with the same catalyst mass, larger yields of hydrogen were achieved in the DMB catalytic experiments than in the BWB experiments, despite the larger water content of the BWB, indicating alternate pathways of hydrogen production other than stream reforming and water gas shift reactions, such as thermal decomposition reactions.

CO displayed the largest yield among the carbon containing product gases at all temperatures. Its yield increased with temperature and with the mass of catalyst. Therefore, within the tested temperatures, it can be concluded that the steam reforming reactions, such as reactions 5.3 and 5.8, and the Boudoard reaction were the dominant catalytic reactions leading to CO production.

The variation of CO_2 yield as a function of temperature, especially for catalytic gasification of the DMB, is not monotonic. This is probably because the rate of consumption of CO_2 in reactions like the Boudouard reaction is higher than its production rate. It is noteworthy that the maximum yield of CO_2 shown in Figure 5.8 is achieved with the catalytic gasification of the BWB at 800°C where, compared to its yield at the lower temperatures, the rate of its production through the water gas shift reaction should have been larger than its rate of consumption.

According to Figure 5.9, the molar CO/CO_2 ratio increased with temperature. At similar temperatures, larger molar CO/CO_2 ratios were obtained in catalytic gasification of the DMB than that of the BWB. Such results indicate that, in the absence of sufficient steam in the reactor, the rate of water gas shift reaction is low and therefore less hydrogen can be produced; therefore, for instance, larger molar H_2/CO ratios were obtained with the catalytic gasification of the BWB. However, it is noteworthy that along with CO, the production of CO_2 increased accordingly with increasing the catalyst mass because the molar CO/CO_2 ratios did not change significantly as a function of the amount of catalyst. In other words, the larger mass of catalyst was influential to activate the water gas shift reaction.

In comparison with the thermal cracking results, lower yields of methane and C_2 hydrocarbons were obtained in the catalytic gasification of the bio-oils. Taking into consideration that carbon conversion was also higher in the catalytic tests, it can be concluded that the rate of conversion of hydrocarbons greatly increased in the presence of catalyst.

The yield of hydrocarbons was dependant on the catalyst mass. It is clear from the data presented in Figure 5.8 that the production of hydrocarbons increased as a function of temperature when the catalyst mass was 0.5 g; on the other hand, the production of C_2 was zero and the production of methane decreased with temperature at all tested temperatures when the catalyst mass was 1 g.

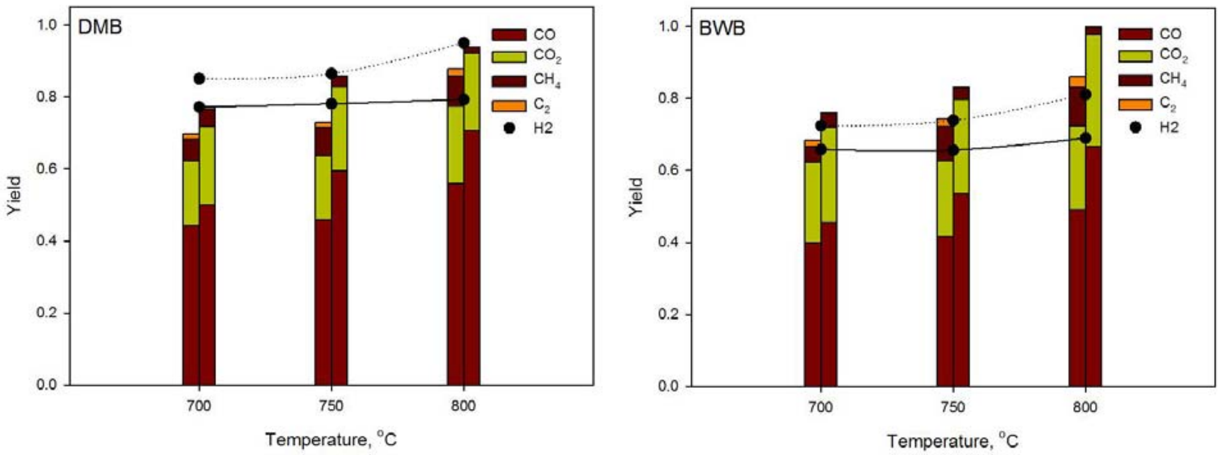

Figure 5.8. **Yield of product gases from catalytic cracking of the DMB and the BWB versus temperature. Residence time= 30s; left hand side bars: mass of the catalyst X= 0.5 g; right hand side bars: mass of the catalyst X= 1 g. Yield of hydrogen is shown with continuous and dashed lines for 0.5 g and 1 g catalyst masses, respectively**

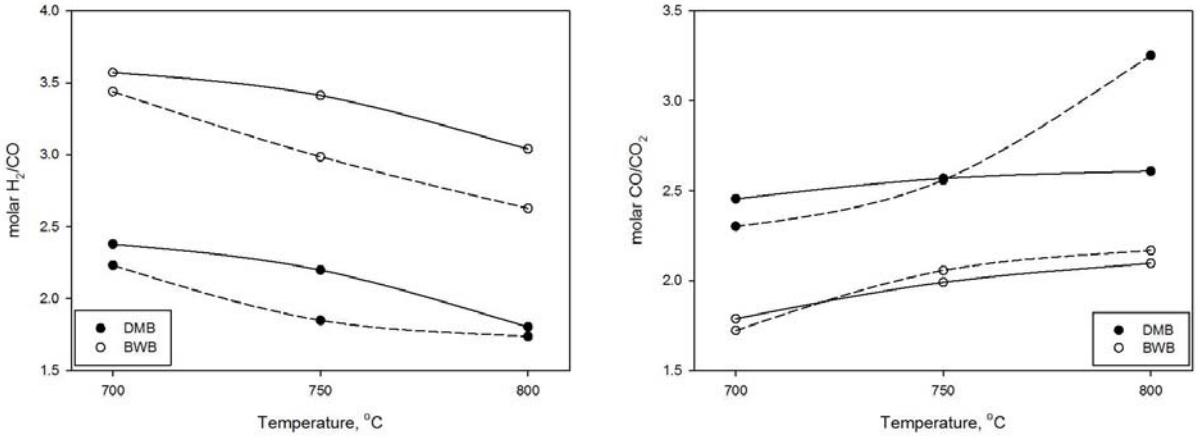

Figure 5.9. **Yield of molar H_2/CO and CO/CO_2 ratios from catalytic cracking of the DMB and the BWB; residence time= 30 s. Mass of the catalyst X= 0.5g (continuous lines) and 1g (dashed lines)**

The molar H_2/CO ratio is a key parameter which needs to be optimized for the downstream processes. As illustrated in Figure 5.9, the molar H_2/CO ratios obtained from the catalytic gasification experiments are larger than those obtained from the thermal cracking tests (Figure 5.4). However, the molar H_2/CO ratios decreased with temperature due to the larger production of CO than the production of hydrogen at higher temperatures. This ratio also decreased with larger catalyst masses.

Given that the carbon conversion of the bio-oils increased with temperature, contrary to trend of the molar H_2/CO ratio, an optimization is required to decide between larger carbon conversion and larger molar H_2/CO ratios. For example, in relation to the catalytic gasification of the DMB in the absence of steam, the molar H_2/CO ratio was lower than 2 at 800°C; hence, if a molar H_2/CO ratio of 2 was required for the downstream process, a water gas shift reactor could be used after the gasification reactor to convert CO to CO_2 in favor of hydrogen production to increase the value of the molar H_2/CO ratio.

By comparing the molar H_2/CO ratios obtained from catalytic gasification of the DMB and the BWB in Figure 5.9, it is evident that larger values of the molar H_2/CO were achieved with the BWB. Given the fact that the BWB had larger water content, it is understood that sufficient presence of steam in the gasification reactor helps to gain high enough value of the molar H_2/CO ratio to avoid having a water gas shift reactor after the gasification reactor.

5.7. Conclusions

Thermal and catalytic gasification of the hardwood bio-oil (DMB) and Birchwood bio-oil (BWB) were carried out in the jiggle bed reactor. Despite the larger water content of the BWB, larger hydrogen yields were achieved from thermal and catalytic cracking of the DMB, which can be attributed to the type of the organic compounds of the DMB and its significant reaction pathways, such as thermal decomposition.

The results of the thermal cracking experiments which were conducted with a residence time of 30 s showed that the total carbon conversion of the bio-oils and yield of hydrogen increased with temperature. The maximum carbon conversion achieved for the DMB and the BWB was 64% and 72%, respectively. The large production of CO and low production of hydrogen in thermal cracking of the bio-oils resulted in the molar H_2/CO ratios less than 2.

The catalyst X had less nickel on its surface, but it showed a better performance than the catalyst Y in terms of maximum production of syngas, minimum production of hydrocarbons and maximum carbon conversion of the bio-oils. This improved performance can be attributed to the larger surface area of the catalyst X and its higher calcium content.

In the presence of both catalysts, the yield of hydrogen and the total carbon conversion of the bio-oils significantly increased. In addition, the yield of hydrocarbons declined noticeably in the catalytic experiments. Overall, the yield of product gases increased with residence time. Yields of hydrogen and CO increased also with catalyst mass at similar residence times.

The yield of hydrogen and the carbon conversion also increased with temperature. On the other hand, the molar H_2/CO ratios obtained in the catalytic tests decreased with temperature. Therefore, an optimization is required to choose a temperature at which maximum carbon conversion and the required molar H_2/CO ratio can be achieved.

Since in the absence of excess steam, low value of the molar H_2/CO ratio can be obtained, either additional steam must be used in the gasification reactor or a secondary water gas shift reactor must be used after the gasification reactor to convert CO to CO_2 and produce extra hydrogen through the water gas shift reaction.

References

[1] North American Transportation Statistics Database.

http://nats.sct.gob.mx/nats/sys/tables.jsp?i=3&id=14

[2] The World Bank. Fossil fuel energy consumption (%) in the countries.

http://data.worldbank.org/indicator/EG.USE.COMM.FO.ZS

[3] Energy department of the United States.

http://energy.gov/science-innovation/energy-sources/fossil

[4] Spath, PL, Dayton DC; “Assessment of Synthesis Gas to Fuels and Chemicals with Emphasis on the Potential for Biomass-Derived Syngas”; National Renewable Energy Laboratory; Colorado; December; 2003

[5] Bedmutha RJ, Ferrante L, Briens C, Berruti F, Inculet I; "Single and two-stage electrostatic demisters for biomass pyrolysis application"; Chemical Engineering and Processing: Process Intensification, 2009, 48, 6, 1112-1120

[6] Xu R, Ferrante L, Briens C, Berruti F; "Flash pyrolysis of grape residues into biofuel in a bubbling fluid bed"; J.Anal.Appl.Pyrolysis, 2009

[7] Berruti F, Muir JR, Hastaoglu MA; "Study of the performance of a large fluidized bed with multiple feed points for flash biomass pyrolysis"; 1989

[8] Sandvig E, Walling G, Daugaard DE, Pletka RJ.; Radlein, Desmond; Johnson, Warren; Brown, R.C.; "The prospects for integrating fast pyrolysis into biomass power systems"; International Journal of Power and Energy Systems, v 24, n 3, p 228-238, 2004, Co-Utilization of Domestic Fuels

[9] Brown RC, Radlein D, Piskorz J; "Pretreatment processes to increase pyrolytic yield of levoglucosan from herbaceous feedstocks"; ACS Symposium Series, v 784, p 123-132, 2001

[10] Scott DS, Paterson L, Piskorz J, Radlein D; "Pretreatment of poplar wood for fast pyrolysis: ate of cation removal"; Journal of Analytical and Applied Pyrolysis, v 57, n 2, p 169-176, February 2001

[11] Scott DS, Piskorz J, Radlein D, Majerski P; "Process for the thermal conversion of biomass to liquids" Biotechnology Advances, v 15, n 3-4, p 799-800, 1997

[12] Scott DS, Majerski P, Piskorz J, Radlein D, Barnickel M; " Production of liquid fuels from waste plastics"; Canadian Journal of Chemical Engineering, v 77, n 5, p 1021-1027, Oct 1999

[13] Scott DS, Majerski P, Piskorz J, Radlein D; " Second look at fast pyrolysis of biomass - the RTI process"; Journal of Analytical and Applied Pyrolysis, v 51, n 1, p 23-37, July 1999

[14] Garg M, Piskorz J, Scott DS, Radlein D; "Hydrogasification of wood"; Industrial and Engineering Chemistry Research, v 27, n 2, p 256-264, Feb 1988

[15] Scott DS, Piskorz J, Radlein D; "Liquid Products from the Continuous Flash Pyrolysis o Biomass"; Industrial & Engineering Chemistry, Process Design and Development, v 24, n 3, p 581-588, Jul 1985

[16] Turner J, Sverdrup G, Mann MK, Maness PC, Kroposki B, Ghirardi M, Evans RJ, Blake D; "Renewable hydrogen production"; International Journal of Energy Research, v 32, n 5, p 379-407, April 2008

[17] Bain RL, Dayton DC, Carpenter DL, Czernik SR, Feik CJ, French RJ, Magrini-Bair KA, Phillips SD; "Evaluation of catalyst deactivation during catalytic steam reforming of biomass-derived syngas"; Industrial and Engineering Chemistry Research, v 44, n 21, p 7945-7956, October 12, 2005

[18] Bain RL; “An overview of biomass gasification”; 2004 AIChE Spring National Meeting, Conference Proceedings, p 547-552, 2004

[19] Sutton D, Kelleher B, Ross JRH; “Review of literature on catalysts for biomass gasification”; Fuel Processing Technology, v 73, n 3, p 155-173, November 13, 2001

[20] Latifi M; Briens C; Berruti F; “Production of Syngas from Bio-oil and its Model Compounds- A Literature Review”; 2012, Ph.D. Thesis, Chapter 1

[21] Garcia L; French R; Czernik S, Chornet E; “Catalytic steam reforming of bio-oils for the production of hydrogen: effects of catalyst composition”; Applied Catalysis A: General 201 (2000) 225–239

[22] Czernik S, French R, Feik C, Chorine E; “Hydrogen by Catalytic Steam Reforming of Liquid Byproducts from Biomass Thermoconversion Processes”; Ind. Eng. Chem. Res. 2002, 41, 4209-4215

[23] Kechagiopoulos PN,Voutetakis SS, Lemonidou AA, Vasalos IA;”Hydrogen production via steam reforming of the aqueous phase of bio-oil in a fixed bed reactor”; Energy & Fuels 2006, 20, 2155-2163

[24] Medrano JA, Oliva M, Ruiz J, Arauzo J; “Hydrogen from aqueous fraction of biomass pyrolysis liquids by catalytic steam reforming in fluidized bed”; energy 36 (2011) 2215-2224

[25] Latifi M, Ferrante L, Briens C, Berruti F; “Effects of residence time and temperature on the thermal cracking of bio-oil for syngas production”; ECI Conference, Bioenergy II, Rio de Janeiro, Brazil, March 2009

[26] Czernik S, Evans R, French R; “Hydrogen from biomass-production by steam reforming of biomass pyrolysis oil”; Catalysis Today 129 (2007) 265–268

[27] Sakaguchi M, Watkinson AP, Ellis N; “Steam gasification of bio-oil and bio-char slurry in a fluidized bed reactor”; Energy&Fuels, 2010, 24, 5181-5189

[28] Seyedeyn-Azad F, Salehi E, Abedi J, Harding T; “Biomass to hydrogen via catalytic steam reforming of bio-oil over Ni-supported alumina catalysts”; Fuel Processing Technology 92 (2011) 563-569

[29] Davidian T; Guilhaume N; Iojoiu E; Provendier H; Mirodatos C; “Hydrogen production from crude pyrolysis oil by a sequential catalytic process”; Applied Catalysis B: Environmental 73 (2007) 116–127

[30] Van Rossum G, Kersten SRA, van Swaaij WPM; “Catalytic and noncatalytic gasification of pyrolysis oil” Ind. Eng. Chem. Res. 2007, 46, 3959-3967

[31] Van Rossum G, Kersten SRA, Van Swaaij WPM; “Staged catalytic gasification/steam reforming of pyrolysis oil”; Ind. Eng. Chem. Res., 2009, 48, 5857-5866

[32] Wu C, Huang M, Sui M, Yan Y, Wang F; “hydrogen production via catalytic steam reforming of fast pyrolysis bio-oil in a two-stage fixed bed reactor system”; Fuel Processing Technology; 89 (2008) 1306-1316

[33] Medrano JA, Oliva M, Ruiz J, Garcia L, Arauzo J; “Catalytic steam reforming of model compounds of biomass pyrolysis liquids in fluidized bed reactor with modified Ni/Al catalysts”; J. Anal. Appl. Pyrolysis 85 (2009) 214-225

[34] Lan P, Xu Q, Zhou M, Lan L, Zhang S, Yan Y; “Catalytic steam reforming of fast pyrolysis bio-oil in fixed bed and fluidized bed reactors”; Chem. Eng. Technology, 2010, 33, No. 12, 2021-2028

[35] Panigrahi S, Chaudhari S T, Bakhshi NN, Dalai AK; “Production of Synthesis Gas/High-Btu Gaseous Fuel from Pyrolysis of Biomass-Derived Oil”; Energy & Fuels 2002, 16, 1392-1397

[36] Panigrahi S, Dalai AK, Chaudhari ST, Bakhshi NN; “Synthesis Gas Production from Steam Gasification of Biomass-Derived Oil”; Energy & Fuels 2003, 17, 637-642

[37] Latifi M, Ferrante L, Berruti F, Briens C. A Novel Fluidized and Induction Heated Micro Reactor for Catalyst Testing . 2012, Ph.D. Thesis, Chapter 3

[38] Latifi M, Briens C, Berruti F. Non-catalytic and Catalytic Steam Reforming of Acetic Acid in the Jiggle Bed Reactor. 2012, Ph.D. Thesis, Chapter 4

CHAPTER 6:

Development of a Thermodynamic Model to Predict the Equilibrium Concentration of Gases from Bio-oil Gasification with Sand or Olivine Catalyst

6.1. Introduction

Fossil fuels including petroleum oil, natural gas and coal are the most common fuels. However, such fuels are not renewable and many countries have to resort to imports to meet their energy needs. Another challenge with these fuels is that they are sources of large amount of pollutants that create human health problems and global warming. Many governments have chosen to promote new technologies to substitute renewable fuels for fossil fuels to reduce greenhouse gas emissions, adhere to environmental regulations, provide some security of supply, and reduce imports [1-3].

Biomass is an attractive renewable source of fuel and energy. Thermochemical processes can convert biomass to a liquid bio-oil or to a syngas [4-18]. Bio-oil can be used directly as a fuel or upgraded to chemicals or fuels. Syngas, which is a mixture of hydrogen and carbon monoxide [19] can be also produced from gasification of bio-oil [20-39]. The advantage of using bio-oil as an intermediate is that, in contrast with both raw biomass and gas, it can easily be produced in small distributed units, stored and transported. Not only can platform chemicals and clean fuels be produced from syngas, but hydrogen is itself an alternative fuel. A high hydrogen production is usually desired: for example, methanol production requires a syngas with a molar H_2/CO ratio of 2. Therefore, maximum hydrogen production has been a major objective in steam reforming/gasification of bio-oil.

Bio-oil is a diverse mixture of oxygenated compounds such as acids, aldehydes, alcohols, ketones, substituted furans derived from cellulose and hemi-cellulose as well as phenolic and cyclic oxygenates derived from lignin. The bio-oil composition depends on the original biomass and the pyrolysis conditions. As a result, the optimum operating conditions of the gasification process will likely vary with the original biomass and the pyrolysis conditions.

An appropriate catalyst is one of the most important operating factors in syngas production. Olivine is a mineral material that has been used by several researchers [40-48] in biomass gasification to crack tars in the product gases. Olivine (with general formula of $(Mg,Fe)_2SiO_4$) has been proven to be attrition resistant in fluidized bed reactors and has catalytic activities in gasification processes because of its iron content [40-42, 44, 45, 47]: It has been stressed in the mentioned references that pre-treatment of olivine is crucial to make it catalytically active. In particular, effect of calcination temperature on the catalytic activity of olivine has been investigated. For example, extensive analytical and experimental studies with olivine and nickel loaded olivine, which were calcined at temperatures between 400°C and 1400°C, reported that the catalytic activity of such materials depends on the calcination temperature because, afterwards, these catalysts can be reduced in the gasification reactor, and at the optimum calcination temperature, maximum amount of iron oxide is extracted from the bulk of olivine. In other words, it has been claimed that iron content of olivine must be in the form of iron oxide when it is introduced in the gasification reactor; gases such as hydrogen and carbon monoxide, which are produced in gasification reactors, reduce the iron oxide to metal iron (Fe^0) that is an active catalyst of gasification reactions.

The objectives of this study are, first to compare bio-oil gasification with inert sand and with olivine with different pretreatments, and, second, to determine whether a model based on thermodynamic equilibrium can predict mole fraction of product gases at different operating conditions.

6.2. Equilibrium model for bio-oil gasification

There are two different approaches to estimate the equilibrium mole fraction of gasification products [49]. One approach minimizes the Gibbs free energy of the gasification products and does not need to consider independent equilibrium reactions between products. The second approach uses the equilibrium constants of the independent reactions to predict the concentrations of the gasification products. Both approaches provide the same results. There are thermodynamic models available in literature to predict the equilibrium yields of gasification products of natural gas and coal using either of the equilibrium approaches [50-57].

The challenge in thermodynamic analysis of products of a gasification process where the feed is a C-H-O mixture like bio-oil is that there are many molecules in the feed with unknown concentrations. Commercial simulation packages such as HYSYS and ASPEN PLUS have been used to simulate equilibrium conditions of model compounds of bio-oil [58-61], but the drawback of the simulators is that the bio-oil composition must be known. This prevents their application to actual bio-oils, since the general consensus is that at least half of the compounds in a bio-oil cannot be identified with current analytical methods [62].

Li *et al.* [63 and 64] developed a thermodynamic model to predict the equilibrium yield of products of coal and biomass gasification based on the minimization of the Gibbs free energy. Ho *et al.* [65] used a HSC Chemistry simulator, which uses a similar approach, to predict the equilibrium yield of the gasification products of some biomasses.

This paper introduces a thermodynamic methodology that uses the equilibrium constants of the independent reactions. This model can be applied for equilibrium analysis of gasification of any feedstock that contains carbon, hydrogen and oxygen. The model solves a set of non-linear equations that includes atomic mass balance equations as well as equilibrium equations.

To apply this model for the gasification of feedstocks such as biomass and bio-oil that have unknown constituents, a general molecular formula is assumed for the feedstock, such as CH_mO_n where m and n represent the elemental composition of the feedstock. The goal is to develop a model that is able to predict the effects of temperature, pressure, feedstock elemental composition and steam to carbon ratio on the equilibrium mole fraction of gasification products including solid carbon. Once the equilibrium mole fractions are known, the energy requirement of the gasification process can also be estimated.

6.2.1. Development of equations

It is assumed that products of gasification at equilibrium conditions are hydrogen, carbon monoxide, carbon dioxide, steam, coke, methane, ethane, ethylene, propane and propylene. Therefore, conversion of a CH_mO_n feed to gasification products can be summarized by equation 6.1:

$$CH_mO_n + b_1H_2O + b_2O_2 \rightarrow a_1H_2 + a_2CO + a_3CO_2 + a_4CH_4 + a_5H_2O_{(g)} + a_6C + a_7C_2H_6 + a_8C_2H_4 + a_9C_3H_{10} + a_{10}C_3H_8 \quad (6.1)$$

Stoichiometric parameters in equation 6.1 represent the number of moles of consumed/produced compounds per one mole of CH_mO_n. Since nitrogen does not participate in gasification reactions, oxygen is included in the equation instead of air. Also, coke is assumed to be produced as pure carbon.

Parameters b_1 and b_2 are inlet and known variables which indicate molar steam to carbon ratio (S/C) and molar oxygen to carbon ratio (O/C) depending on the gasification process. These parameters indicate the amounts of the additional oxygen and steam that are required to obtain certain concentration of the product gases from the gasification reactor. Parameters a_1 through a_{10} are unknown variables which should be calculated by the equilibrium model. With the equilibrium constant modeling approach, independent reactions between product gases should be found first; then equilibrium constant equations should be developed for each independent reaction. Also, three mass balance equations should be developed for carbon, hydrogen and oxygen elements.

Mass balance equations for carbon, hydrogen and oxygen atoms result in equations 6.2 through 6.4:

$$atom\ C: 1 = a_2 + a_3 + a_4 + a_6 + 2a_7 + 2a_8 + 3a_9 + 3a_{10} \tag{6.2}$$

$$atom\ H: m + 2b_1 = 2a_1 + 4a_4 + 2a_5 + 6a_7 + 4a_8 + 10a_9 + 8a_{10} \tag{6.3}$$

$$atom\ O: n + b_1 + 2b_2 = a_2 + 2a_3 + a_5 \tag{6.4}$$

Independent reactions between product gases at equilibrium are according to equations 6.5 through 6.11. These reactions are steam reforming reactions of hydrocarbons and solid carbon as well as water gas shift reaction. Solid carbon is the only species in solid phase while other species are in gas phase at equilibrium.

$$CH_4 + H_2O_{(g)} \leftrightarrow CO + 3H_2 \tag{6.5}$$

$$C_2H_6 + 2H_2O_{(g)} \leftrightarrow 2CO + 5H_2 \tag{6.6}$$

$$C_2H_4 + 2H_2O_{(g)} \leftrightarrow 2CO + 4H_2 \tag{6.7}$$

$$C_3H_8 + 3H_2O_{(g)} \leftrightarrow 3CO + 7H_2 \tag{6.8}$$

$$C_3H_6 + 3H_2O_{(g)} \leftrightarrow 3CO + 6H_2 \tag{6.9}$$

$$CO + H_2O_{(g)} \leftrightarrow CO_2 + H_2 \tag{6.10}$$

$$C + H_2O_{(g)} \leftrightarrow CO + H_2 \tag{6.11}$$

The relation between equilibrium constant and concentration of reactants and products for reaction j can be found with the fugacity of species and the standard Gibbs energy of the reaction j:

$$K_j = \left(\prod \left(\frac{\hat{f_i}}{f_i^{\circ}}\right)^{\nu_i}\right)_j = \left(exp\left(-\frac{\Delta G^{\circ}}{RT}\right)\right)_j \tag{6.12}$$

Where K_j is the equilibrium constant of reaction j, $\hat{f_i}$ is the fugacity of species i among gases at equilibrium, f_i° is the fugacity of pure species i at standard conditions, ν_i is the stoichiometric coefficient of species i in reaction j (negative for reactants and positive for products), ΔG_j° is the standard Gibbs energy of reaction j, T is the temperature in Kelvin and R is the universal constant for gases (8.314 Joule/mole/K).

$\hat{f_i}$ can be estimated from equation 6.13:

$$\hat{f_i} = \hat{\varphi_i} y_i P \tag{6.13}$$

Where $\hat{\varphi_i}$ is the fugacity coefficient of species i at equilibrium mixture, y_i is the mole fraction of species i and P is the equilibrium pressure inside the reactor. $\hat{\varphi_i}$ is assumed unity because the temperature of gasification processes is very high and pressure is almost atmospheric [49], so it can be assumed that there is an ideal mixture of gases inside the gasification reactor.

Furthermore, it is assumed that f_i° is equal to standard pressure of pure species i. Therefore, by some manipulation left term of equation 12 can be written as:

$$K_j = \left(\left(\frac{P}{P^{\circ}}\right)^{\nu} . \prod {y_i}^{\nu_i}\right)_j \tag{6.14}$$

Where:

$$(\nu)_j = (\sum \nu_i)_j \tag{6.15}$$

And, the mole fraction of species i is:

$$y_i = \frac{a_i}{\sum a_i} \tag{6.16}$$

Equation 6.14 illustrates how pressure inside the reactor relates to equilibrium constant of reaction j; however, P/P° is a dimensionless ratio.

Standard Gibbs energy of reaction j in equation 6.12 is calculated by equation 6.17:

$$\left(\frac{\Delta G^{\circ}}{RT} = \frac{\Delta G_r^{\circ} - \Delta H_r^{\circ}}{RT_r} + \frac{\Delta H_r^{\circ}}{RT} + \frac{1}{RT}\int_{T_r}^{T} \Delta C_p^{\circ} dT - \frac{1}{R}\int_{T_r}^{T} \Delta C_p^{\circ} \frac{dT}{T}\right)_j \tag{6.17}$$

Where $(\Delta G_r^{\circ})_j$,and $(\Delta H_r^{\circ})_j$ are the standard Gibbs energy change and the standard enthalpy change, respectively, of reaction j at the reference temperature and are estimated from the Gibbs energy and enthalpy of formation of the species of that reaction :

$$\left(\Delta G_r^{\circ} = \sum \nu_i G_{r,i}^{\circ}\right)_j \tag{6.18}$$

$$\left(\Delta H_r^{\circ} = \sum \nu_i H_{r,i}^{\circ}\right)_j \tag{6.19}$$

Temperature reference, T_r, is 298.15 K. Standard Gibbs energy and enthalpy of formation of the species at equilibrium are presented in Table 6.1.

Table 6.1. **Gibbs energy and enthalpy of formation of products at equilibrium [67]**

Product	H_r°, jol/mol	G_r°, jol/mol
Methane	-7.84×10^4	-5.10×10^4
Ethane	-8.74×10^4	-3.29×10^4
Ethylene	5.23×10^4	6.81×10^4
Propane	-1.04×10^5	-2.35×10^5
Propylene	2.04×10^4	6.27×10^4
H_2	0.00	0.00
CO	-1.11×10^5	-1.37×10^5
CO_2	-3.94×10^5	-3.94×10^5
Water	-2.42×10^5	-2.29×10^5
C	0.00	0.00

There are two integration terms inside equation 6.17 corresponding to the change in heat capacity of the species involved in reaction j. The heat capacities of species in the Chemical Properties Handbook [67] are reported as a function of temperature with the form of:

$$C_p(jol.mol^{-1}.K^{-1}) = A + BT + CT^2 + DT^3 + ET^4 \tag{6.20}$$

Table 6.2 lists the heat capacity coefficients for the gasification products [68].

Table 6.2. **Coefficients for the special heat capacity of gasification products**

	$[68]C_p(jol.mol^{-1}.K^{-1}) = A + BT + CT^2 + DT^3 + ET^4$				
Product	A	B	C	D	E
Methane	34.92	-4.00×10^{-2}	1.92×10^{-4}	-1.53×10^{-7}	3.93×10^{-11}
Ethane	28.17	4.34×10^{-2}	1.89×10^{-4}	-1.91×10^{-7}	5.35×10^{-11}
Ethylene	32.08	-1.48×10^{-2}	2.47×10^{-4}	-2.37×10^{-7}	6.83×10^{-11}
Propane	28.28	1.16×10^{-1}	1.96×10^{-4}	-2.33×10^{-7}	6.87×10^{-11}
Propylene	31.30	7.25×10^{-2}	1.95×10^{-4}	-2.16×10^{-7}	6.30×10^{-11}
H_2	25.40	2.02×10^{-2}	-3.85×10^{-5}	3.19×10^{-8}	-8.76×10^{-12}
CO	29.56	-6.58×10^{-3}	2.01×10^{-5}	-1.22×10^{-8}	2.26×10^{-12}
CO_2	27.44	4.23×10^{-2}	-1.96×10^{-5}	4.00×10^{-9}	-2.99×10^{-13}
Water	33.93	-8.42×10^{-3}	2.99×10^{-5}	-1.78×10^{-8}	3.69×10^{-12}
C	-0.83	3.48×10^{-2}	-1.32×10^{-5}	0.00	0.00

From equation 6.20 and $\tau = T/T_r$:

$$\left(\int_{T_r}^{T} \Delta C_p^{\circ} dT = \Delta A T_r(\tau - 1) + \frac{\Delta B}{2} T_r^2(\tau^2 - 1) + \frac{\Delta C}{3} T_r^3 (\tau^3 - 1) + \frac{\Delta D}{4} T_r^4(\tau^4 - 1) + \frac{\Delta E}{5} T_r^5(\tau^5 - 1)\right)_j \tag{6.21}$$

$$\left(\int_{T_r}^{T} \Delta C_p^{\circ} \frac{dT}{T} = \Delta A ln(\tau) + \Delta B T_r \left(\tau - 1\right) + \frac{\Delta C}{2} T_r^2 (\tau^2 - 1) + \frac{\Delta D}{3} T_r^3(\tau^3 - 1) + \frac{\Delta E}{4} T_r^4(\tau^4 - 1)\right)_j \tag{6.22}$$

Where:

$$(\Delta A = \sum \nu_i A_i)_{\mathrm{j}} \tag{6.23}$$

$$(\Delta \mathrm{B} = \sum \nu_i B_i)_{\mathrm{j}} \tag{6.24}$$

$$(\Delta \mathrm{C} = \sum \nu_i C_i)_{\mathrm{j}} \tag{6.25}$$

$$(\Delta \mathrm{D} = \sum \nu_i D_i)_{\mathrm{j}} \tag{6.26}$$

$$(\Delta E = \sum \nu_i E_i)_{\mathrm{j}} \tag{6.27}$$

Substituting equations 6.14 and 6.17 into equation 6.12 provides a new relationship for each reaction j which associates the molar concentration of gasification products with thermodynamic properties such as temperature, pressure, special heat capacity, Gibbs energy and enthalpy of formation of the species involved in the reaction j.

6.2.2. Development of the solving program

Three mass balance equations and seven equilibrium constant equations developed above form a set of ten non-linear equations to solve ten unknown variables (a_1 through a_{10}). One advantage of the developed equilibrium model is its ability to predict the number of moles of coke at equilibrium. A MATLAB program applying the "fsolve" command from optimization toolbox was developed to solve this set of non-linear equations. A constraint has been defined in the program that none of the values must be negative.

6.2.3. Validation of the equilibrium model

In order to validate the ability of the developed equilibrium model to identify the mole fraction of gasification products, this model was tested for wood and palm oil waste for which equilibrium mole fractions of gasification were predicted using simulators. Results of our model were then compared to the results reported in the references [65] and [66]. Table 6.3 illustrates these comparisons according to equation 6.1. It should be pointed out that equilibrium value of C_2 and C_3 hydrocarbons were estimated to be zero by our developed thermodynamic model considering the operating conditions listed in this table. As shown, there is a very good agreement between reported results in literature and estimated results by our equilibrium model. Therefore, it is verified that the developed equilibrium model is able to predict the equilibrium mole fractions of gasification of any C-H-O feed provided its elemental analysis is known.

Table 6.3. **Comparison of results between equilibrium model and references data**

$$CH_mO_n + b_1H_2O + b_2O_2 \rightarrow a_1H_2 + a_2CO + a_3CO_2 + a_4CH_4 + a_5H_2O + a_6C$$

	b1	b2	a1	a2	a3	a4	a5	a6
Wood [66]: $CH_{1.4}O_{0.59}$								
Temperature: 913 K; Pressure: 1 bar								
Model	0	0	0.430	0.183	0.130	0.062	0.146	0.625
Reference			0.44	0.17	0.13	0.005	0.15	0.64
Temperature: 927 K; Pressure: 1 bar								
Model	0.51	0.21	0.777	0.526	0.361	0.080	0.273	0.034
Reference			0.78	0.5	0.37	0.07	0.29	0.06
Temperature: 1200 K; Pressure: 1 bar								
Model	0	0.3	0.606	0.902	0.097	0.0003	0.093	0.000
Reference			0.61	0.9	0.1	0.0003	0.09	0
Palm oil waste [65]: $CH_{1.69}O_{0.54}$								
Temperature: 833 K-1173 K; Pressure: 1 bar								
Model	0	0	0.682	0.357	0.054	0.044	0.074	0.544
Reference			0.69	0.35	0.05	0.03	0.08	0.56

6.3. Experimental setup and procedures

The jiggle bed reactor is a batch fluidized bed micro-reactor where heat required by the gasification reactions is supplied by induction heating. Solid particles are fluidized in a ceramic crucible by the fast alternating vertical motion provided by a linear pneumatic actuator. The frequency of the actuator is 3 Hz and the amplitude of its motion is 0.1 m; these conditions provide smooth fluidization of the bed particles. There is a copper coil around the ceramic crucible. A high voltage current passing through the coil provides a magnetic field that induces hysteresis and eddy currents within the wires inside the crucible. The directions of the magnetic field and induced currents are alternated with a frequency of about 250 kHz. There is a very small temperature difference between the heating surface and the catalyst bed, which minimizes the parasitic thermal reactions that occur in other reactors [69].

A schematic of the experimental setup is shown in Figure 6.1. Details may be found elsewhere [70].

The Drummond capillary tubes with 4µl volume were used to inject precise amount of the bio-oil into the batch reactor.

A Varian micro GC CP4900 instrument was used to analyze the product gases H_2, CH_4, CO, CO_2, C_2H_4 and C_2H_6. This micro GC was equipped with three columns 10m MS5A, 10m PPU and 8m 5CB. Helium was used as the carrier gas in the micro GC. Since the product gases were diluted with argon in the gas sampling bag, their concentration was very low, requiring a high sensitivity setting of the TCD and a sampling time of 500 ms. Because the GC did not detect the steam in the product gases, water measurement and , hence, elemental balances could not be performed. GC runs were conducted for 3 minutes.

In order to calculate the number of moles of the product gases and the total carbon conversion, a known volume of an external standard gas was added to the mixture of product gases: 500µl of normal C_4H_{10} was injected into the vacuumed gas sampling bag with a gas tight syringe. C_4H_{10} was never produced during the gasification tests and was, thus, a suitable external standard gas. The gas sampling bag was squeezed manually for several times to ensure good mixing between the standard gas and the product gases. Experiments were repeated for 3 times to check the reproducibility of the data.

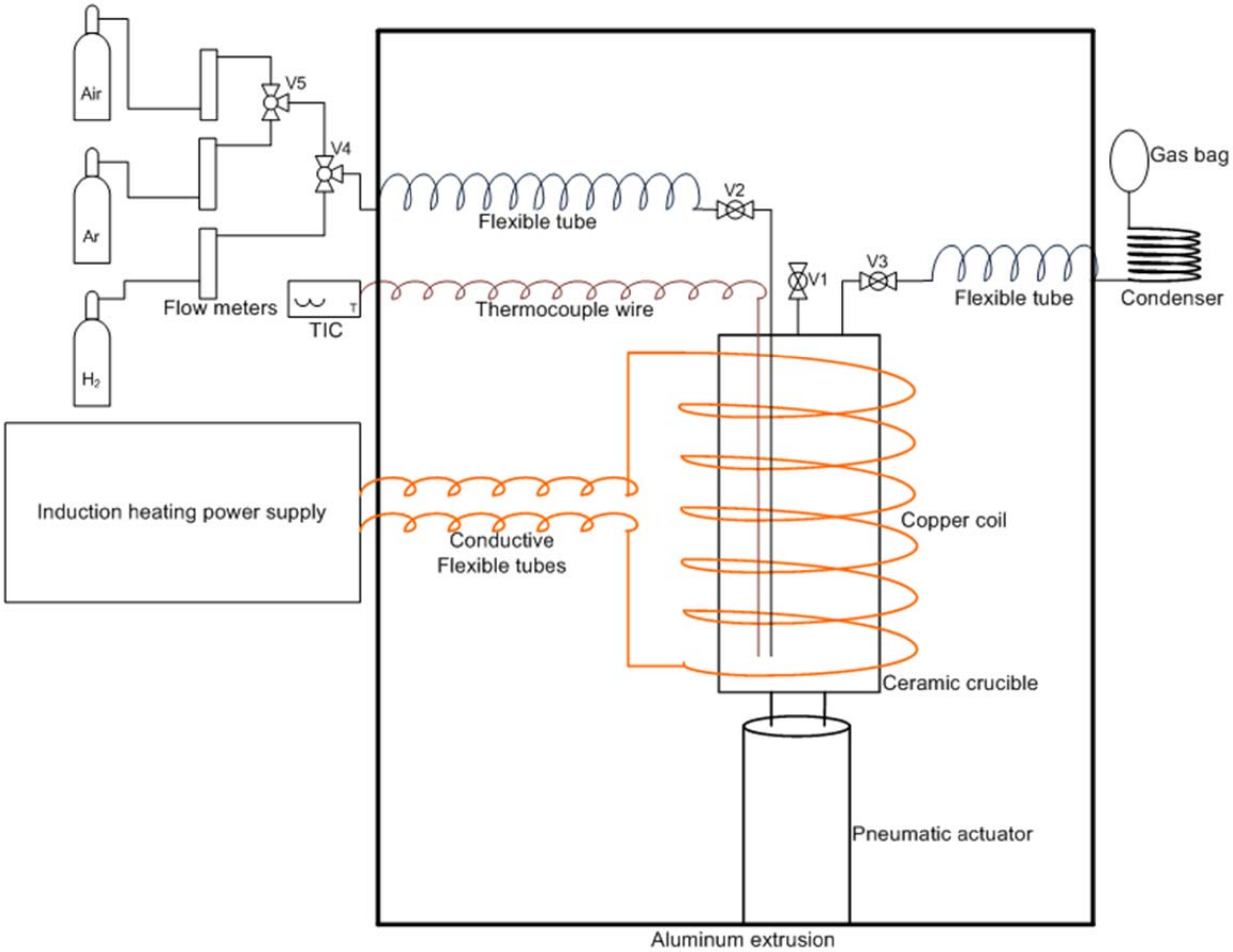
Air
Ar
H2
V5
V4
Flow meters
TIC
Flexible tube
V2
Thermocouple wire
V1
V3
Flexible tube
Gas bag
Condenser
Induction heating power supply
Conductive
Flexible tubes
Copper coil
Ceramic crucible
Pneumatic actuator
Aluminum extrusion

Figure 6.1. **Schematic of the JBR experimental setup for the catalytic gasification tests**

6.4. Experimental materials

6.4.1. Bio-oil characteristics

The bio-oil used in this research was produced by fast pyrolysis of hardwood at moderate temperatures, in the absence of oxygen, at the Dynamotive Energy Systems Corporation in Canada. This bio-oil had been stored in the lab for three years. As presented in table 6.4, elemental composition of the fresh bio-oil is changed and therefore different from that of the old bio-oil after 3 years so that hydrogen and oxygen contents were increased with regard to carbon content. Gasification experimental work was carried out with the old bio-oil.

***Table 6.4.* Elemental analysis of the Dynamotive bio-oils**

	Fresh bio-oil	Old bio-oil
H, wt%	7.20	8.04
C, wt%	41.67	36.30
N, wt%	0.27	0.30
O, wt% (balance)	51.13	55.36
Water content, wt%	24.34	27.52
General formula	$CH_{2.071}O_{0.920}N_{0.0053}$	$CH_{2.624}O_{1.121}N_{0.0065}$
C/H, mol/mol	0.48	0.38
C/O, mol/mol	1.09	0.87

6.4.2. Preparation of the bed material

Silica sand and olivine were used as the bed materials with a size distribution of 106-212 μm. Two samples of olivine calcined at 850°C and 1000°C each for 24 hours and one sample of olivine reduced with hydrogen at 800°C for 24 hours were investigated as the bed materials in the jiggle bed reactor to find out whether metallic iron (Fe^0) or iron oxides are suitable for bio-oil gasification. The calcined samples of olivine had been placed inside a furnace to be calcined whereas the third sample had been placed in the jiggle bed reactor and was reduced in situ by a 100ml/min flow of hydrogen. Since experiments were carried out at 800°C, calcination temperatures were chosen to be higher than the reaction temperature in order to obtain particles with a stable structure in the reactor. The bed mass was 10g in all experiments.

6.4.3. Catalyst characterization

Surface area analyses of the original and the reduced olivine were carried out by the instrument ASAP 2010 through adsorption of N_2 at 77.35 K. According to Table 6.5, reduction of olivine with hydrogen did not significantly change the surface properties of the original olivine. In addition, their BET surface area is very low with very little volume of the pores. In other words, olivine looks like a non-porous material.

Table 6.5. **Surface and pore analysis of olivine**

Catalyst	BET surface area, m^2/g	Average pore size[×], nm	Total pore volume[+], cm^3/g
Original Olivine	2.734	3.751	0.0026
Reduced Olivine	2.144	3.878	0.0021

[×] Adsorption Average Pore Diameter (4V/A° by BET)

[+] Single Point Adsorption Total Pore Volume of pores less than 81.06 nm Diameter at $P/P_0 = 0.976$

To determine the composition of the olivine, Fusion X-Ray Fluorescence (XRF) analysis of the original olivine was carried out. According to Table 6.6, silicate, magnesium and iron are the main components of the olivine although there are traces of other metals.

To estimate the mass of the active metals on the surface of olivine, attempts were made to measure the H_2 consumption of the olivine by TPR and H_2 chemisorption, but it was not possible. Probably because the dominant phase is a silicate, this phase is not reduced easily nor reduced at all at the tested conditions (below 750°C).

Table 6.6. **XRF analysis data of fresh olivine**

Component oxide	Composition, wt%
SiO_2	42.15
TiO_2	< 0.01
Al_2O_3	0.15
Fe_2O_3	7.43
MnO	0.1
MgO	49.74
CaO	0.02
K_2O	0.01
Na_2O	0.1
P_2O_5	< 0.01
Cr_2O_3	0.47
LOI	0.45

X-Ray powder Diffraction (XRD) patterns of the samples of the original olivine, the calcined olivine at 850°C with air, the calcined at 1000°C with air and the reduced olivine with hydrogen are shown in Figure 6.2. Interpretation of the defraction lines has been done according to the information in literature [40, 42].The main lines of the graphs belonging to the original olivine correspond to phases of $(Mg,Fe)_2SiO_4$. Also, phases of estatite $MgSiO_3$ and serpentine $Mg_3Si_2O_5(OH)_4$ are detected on the original Olivine. It is clear that the intensity of these silicate phases has been changed and they are different from the pre-treated samples of olivine due to the thermal conditions of the pre-treatments.

No iron oxide phase was detected on the original olivine and the calcined olivine at 850°C. However, a phase of iron oxide (α-Fe_2O_3) at 2θ of about 33° is available on the sample calcined at 1000°C, which means olivine has gained oxygen in its structure during the calcination. Although not detected on the olivine calcined at 850°C, it is expected that iron oxide should be formed in this sample as well. Regarding the olivine reduced with hydrogen, it is noticeable that there is a phase of metallic iron; in other words, either some iron oxide on the surface of the olivine was reduced or some iron managed to leave bulk of the olivine and stayed on the surface ready for the catalytic reactions.

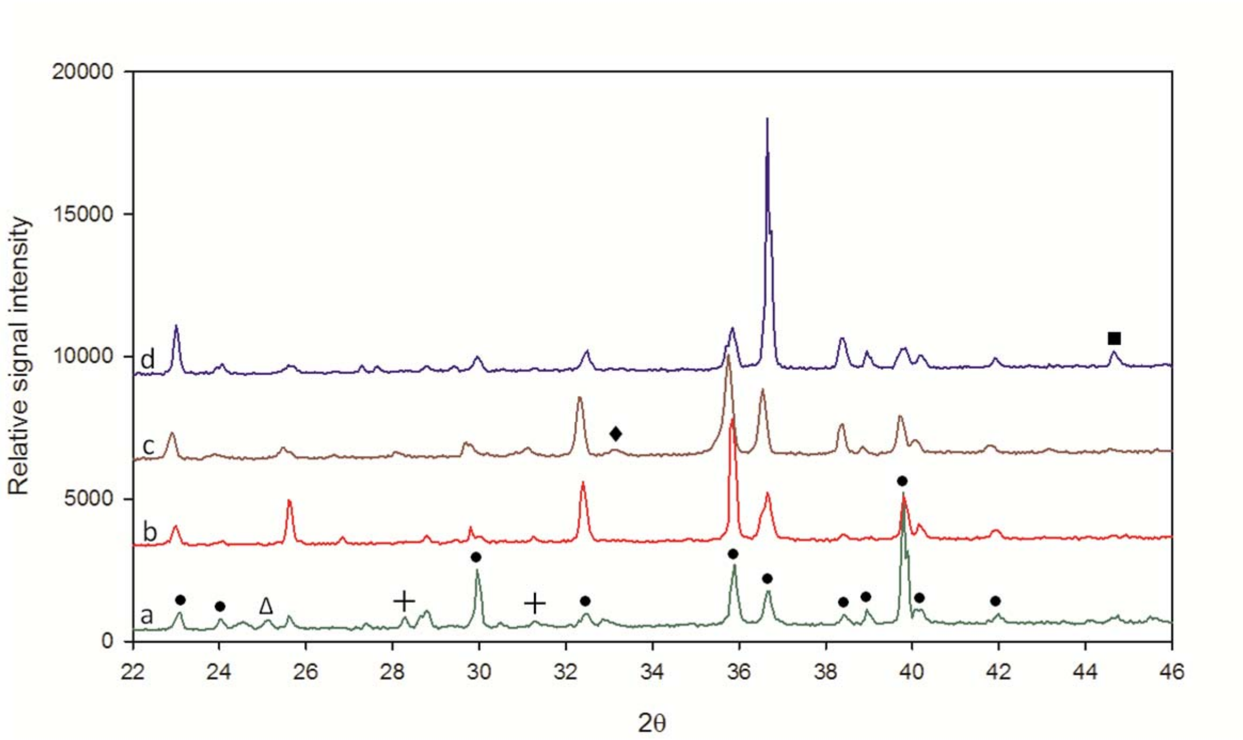

Figure 6.2. **XRD patterns of the (a) original Olivine (b) Olivine calcined at 850°C (c) Olivine calcined at 1000°C and (d) Olivine reduced with hydrogen. ● presents phases of $(Mg,Fe)_2SiO_4$, + presents phase of $MgSiO_3$, Δ presents phase of Mg,Si_2O_5, ♦presents phase of α-Fe_2O_3 and ■ presents phases of metallic iron (Fe^0)**

6.5. Experimental results and discussion

Gasification of bio-oil in the jiggle bed reactor was investigated at 800°C. The effect of the residence time was tested at 10s, 20s, 30s, 60s 120s and 240s, where the residence time was the time between the feed injection and the flushing with argon of the product gases into the gas sampling bag. In order to determine the effect of the bed material on bio-oil conversion and product gases yields, silica sand and pre-treated olivine samples were used in the reactor. The Drummond capillary tubes with 4μl volume were used to introduce the bio-oil into the reactor, which did not change significantly the reactor pressure. Since it is important to know mass of the feed bio-oil for yield and conversion calculations, five capillary tubes were filled with bio-oil and then the average mass of bio-oil content in those tubes was considered as the mass of bio-oil equivalent to a 4 μl volume. To make sure experimental data were reproducible, experiments were repeated 3 times. Average value of the obtained yield data is reported in this paper. Maximum spread between the replicate data was ±4%.

In the presence of steam, bio-oil with general formula of CH_mO_k (neglecting the nitrogen content) can be converted to syngas (H_2+CO) according to reaction 6.28:

$$CH_mO_k + (1-k)H_2O \rightarrow CO + \left(1 + {}^{m}/_{2} - k\right)H_2 \tag{6.28}$$

If there was enough steam in the reactor, the produced CO would react with steam through the water-gas shift reaction to produce more hydrogen:

$$H_2O + CO \leftrightarrow H_2 + CO_2 \tag{6.29}$$

Therefore, summing up reactions 6.28 and 6.29, the overall steam reforming of bio-oil can be expressed by reaction 6.30:

$$CH_mO_k + \left(2 - k\right)H_2O \rightarrow CO_2 + \left(2 + {}^{m}/_{2} - k\right)H_2 \tag{6.30}$$

There are a number of other reactions taking place after bio-oil is injected into the reactor. For example, As soon as bio-oil is entered into the reactor, it decomposes thermally to other forms of the oxygenated molecules (CH_yO_z) as well as some permanent gases (hydrogen, steam, CO, CO_2 and light hydrocarbons) and coke (reaction 6.31). Besides, since CO, CO_2 and coke are available inside the reactor, the Boudouard reaction (reaction 6.32) is another important reaction which can affect the CO/CO_2 ratio in the final product gases.

$$CH_mO_k \rightarrow CH_yO_z + gases\ (H_2, H_2O, CO, CO_2, CH_4, \dots) + coke \tag{6.31}$$

$$2CO \leftrightarrow C + CO_2 \tag{6.32}$$

In addition, in the presence of steam, the produced hydrocarbons undergo steam reforming reactions towards production of hydrogen and carbon monoxide. For example, reaction 6.33 illustrates how methane can be converted to syngas:

$$CH_4 + H_2O \rightarrow CO + 3H_2 \tag{6.33}$$

In this research we did not add additional water because in industry, the practice is to use a separate water-gas shift reactor, downstream of the gasification reactor, which can be operated with a temperature and a catalyst that are optimized for the water-gas shift reaction. In other words, our goal was to maximize the conversion of bio-oil to product gases and conversion of the hydrogen contained in the raw bio-oil, including its own water, to hydrogen gas (H_2). Therefore, the yield of produced hydrogen was defined according to equation 6.34:

$$Y_{H_2}(\frac{g}{g}) = \frac{mass\ of\ hydrogen\ as\ H_2\ in\ product\ gas}{mass\ of\ H\ in\ the\ raw\ bio\text{-}oil} \tag{6.34}$$

To estimate the number of moles of the bio-oil, bio-oil with a general formula of CH_mO_k was assumed from its elemental composition. Since maximum 1 mol of a product gas like CO, CO_2 and CH_4 can be produced per 1 mole of the injected bio-oil, yield of these gases were estimated as:

$$Y_{CO,CO_2,CH_4}(\frac{mol}{mol}) = \frac{moles\ of\ the\ product\ gas}{moles\ of\ the\ bio\text{-}oil} \tag{6.35}$$

Accordingly, yields of C_2H_4 and C_2H_6 hydrocarbons were estimated by equation 6.36:

$$Y_{C_2H_4,C_2H_6}(\frac{mol}{mol}) = \frac{moles\ of\ the\ product\ gas}{0.5 \times moles\ of\ the\ bio\text{-}oil} \tag{6.36}$$

The carbon conversion was calculated by summing up the yields of carbon containing product gases.

Mole fraction of the product gases was assumed as their concentration in the mixture of the detected product gases for the thermodynamic analyses.

One advantage of the jiggle bed reactor is that it is very convenient to perform a complete test (from feed injection until end of the gas analysis) for a very short period of time i.e. 10 minutes, so it is possible to repeat a test to check out reproducibility of the data and conduct tests with different operating conditions while a great deal of time is saved. However, it must be taken into account that coke as the solid product of the reaction remains in the reactor which must be removed before conducting a new test; otherwise, coke can be gasified during the next test and have a detrimental effect on the calculation of gasification yields. Therefore, after each test, the catalytic bed was regenerated and reduced according to the following in-situ procedure:

1. Coke was burned off with air for 30 seconds
2. Argon was introduced to the reactor for 30 seconds to flush out air
3. Hydrogen was introduced into the reactor for 5 minutes to remove oxygen from the surface of the catalysts and reduce the catalyst
4. Argon was introduced for 2 minutes to flush out hydrogen from the reactor

The above procedure was carried out even for non-catalytic tests where there was only silica sand in the reactor.

6.5.1. Equilibrium composition of the product gases versus experimental data

The thermodynamic model developed in this research was used to compare the mole fraction of the product gases obtained with different bed materials at the same operating conditions with the equivalent predicted equilibrium mole fractions.

Figures 6.3 to 6.7 illustrate the evolution with residence time of the experimental mole fraction of the product gases, with different bed materials. Also, equilibrium mole fractions calculated by the model are indicated by a horizontal line. It must be pointed out that the estimated equilibrium mole fractions of the product gases are expressed on a dry basis to be able to compare them with the experimental data. With the exception of the silica sand for which experiments were conducted also at a residence time of 600s, experiments were carried out at residence times of 10s, 20s, 30s, 60s, 120s and 240s for all the tested bed materials.

With the reduced olivine, it is clear that the product gases reach mole fractions near the equilibrium values even at the shortest residence times. This means the reduced olivine acted as an active and effective catalyst that greatly speeded up the reactions.

With sand, the mole fractions of the product gases reached their equilibrium values, but at much longer residence times. A residence time of 600s was, then, required to reach the mole fractions that were achieved in about 20s with the reduced olivine.

With the calcined olivines, the mole fractions of the product gases, especially, hydrogen, CO and CO_2 were far from the equilibrium values. It is seen that the mole fractions of hydrogen, CO and hydrocarbons decrease with increasing residence time and drop below the equilibrium mole fractions whereas the mole fraction of CO_2 increases with increasing residence time and is always above the equilibrium mole fraction. Since the equilibrium mole fractions were calculated according to the elemental composition of the raw bio-oil, this suggests that the calcined olivine acts as an extra source of oxygen in the reactor, which can lead to a large production of CO_2 and steam. This hypothesis is confirmed by the XRD plots of Figure 6.2, which show that α-Fe_2O_3 was formed on the olivine calcined at 1000°C. Such oxide phases should have been also formed on the olivine calcined at 800°C although it was not detected by XRD; therefore, in the presence of reducing gases such as hydrogen in the reactor, iron oxides can be reduced, providing an additional source of elemental oxygen. Elemental analysis of the original olivine, the olivine calcined at 800°C and the olivine calcined at 1000°C by a CHNOS elemental analyzer showed that oxygen content of the calcined olivines had increased relatively compared to the original olivine so that the largest oxygen content was in the olivine calcined at 1000°C. It seems that the calcined olivine works like an oxygen sponge so that the released oxygen reacts with the combustible product gases.

As it can be seen from evolution of the product gas mole fractions versus time with the calcined olivines, it seems that mole fractions tend to reach a new equilibrium at longer residence times. In order to investigate such a new equilibrium condition, the developed model was used to estimate how much oxygen should have been released from the calcined olivines to provide the new equilibrium mole fraction: the stoichiometric factor b_2 in equation 6.1 was changed to reach mole fractions which are close to the experimental data. For instance, as shown in Table 6.7, experimental mole fractions of the product gases from the olivine calcined with air at 800°C obtained after a residence time of 240s are compared with the estimated equilibrium mole fractions where b_2 in equation 6.1 was assumed to be 1.1; in other words, an extra oxygen mass 1.96 times as large as oxygen mass in the injected bio-oil should have been consumed in the reactor to reach the considered experimental mole fractions.

***Table 6.7.* Comparison between estimated equilibrium and experimental mole fractions (dry basis) from olivine calcined at 1000°C. Temperature: 800°C, Residence time: 240s**

	H_2	CO	CO_2	CH_4	$C_2H_4+C_2H_6$
Equilibrium mole fraction	0.091	0.071	0.837	1.13×10^{-7}	0.000
Experimental mole fraction	0.032	0.056	0.823	0.078	6.57×10^{-3}

Regarding the positive effect reported in the literature for calcined olivine in continuous processes, it may be that the calcined olivines were inapropriate catalysts in our batch jiggle bed reactor because of the small bio-oil to catalyst ratio.

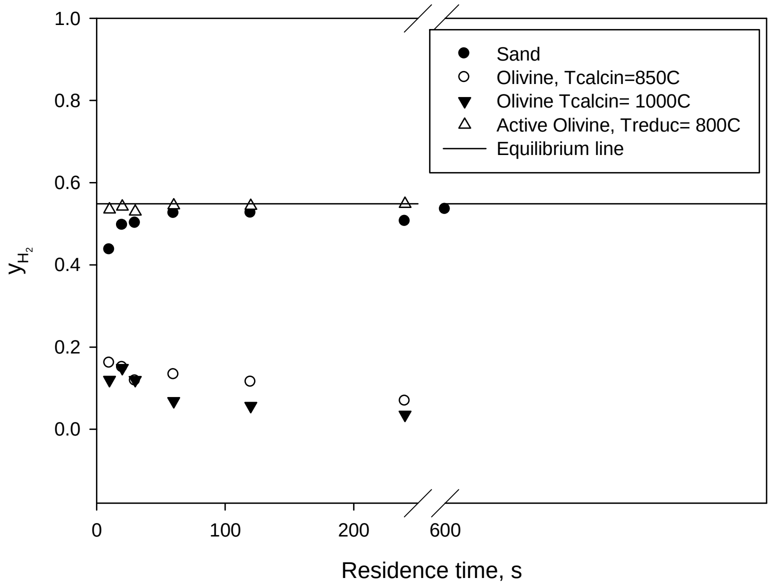

***Figure 6.3.* Measured mole fraction of hydrogen compared to its predicted equilibrium mole fraction, on a dry basis. Bed materials: olivine and sand. Temperature: 800°C**

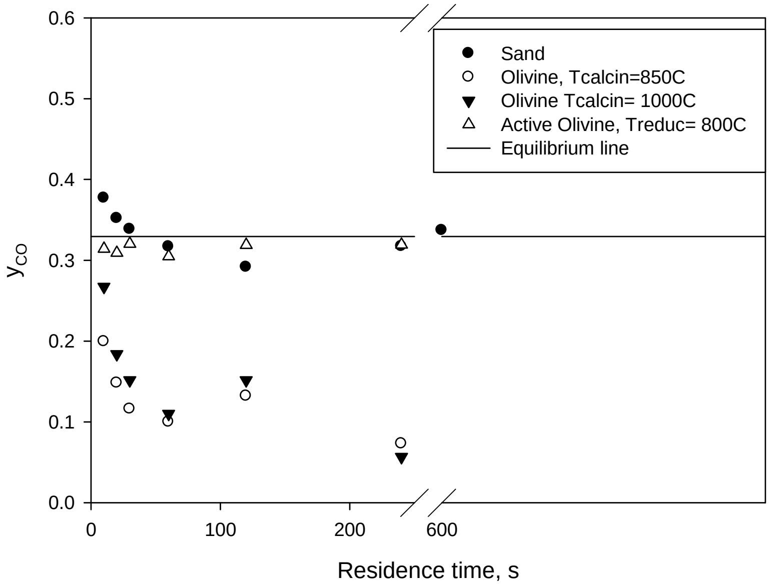

Figure 6.4. **Measured mole fraction of CO compared to its predicted equilibrium mole fraction, on a dry basis.. Bed materials: olivine and sand. Temperature: 800°C**

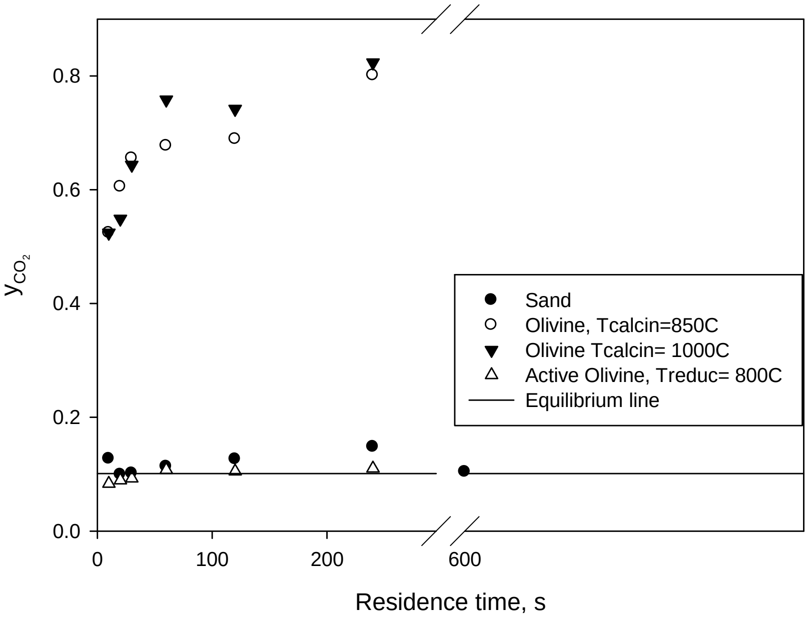

Figure 6.5. **Measured mole fraction of CO_2 compared to its predicted equilibrium mole fraction, on a dry basis. Bed materials: olivine and sand. Temperature: 800°C**

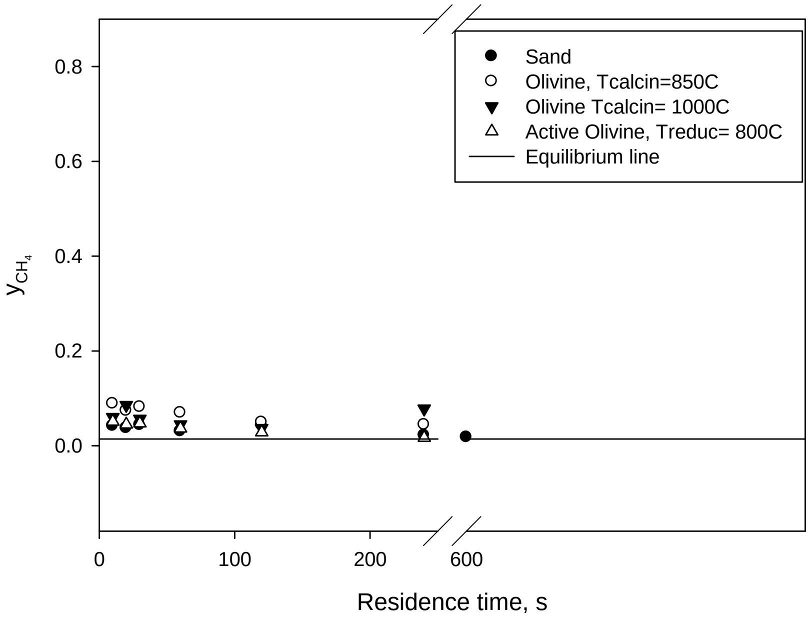

Figure 6.6. **Measured mole fraction of CH_4 compared to its predicted equilibrium mole fraction, on a dry basis. Bed materials: olivine and sand. Temperature: 800°C**

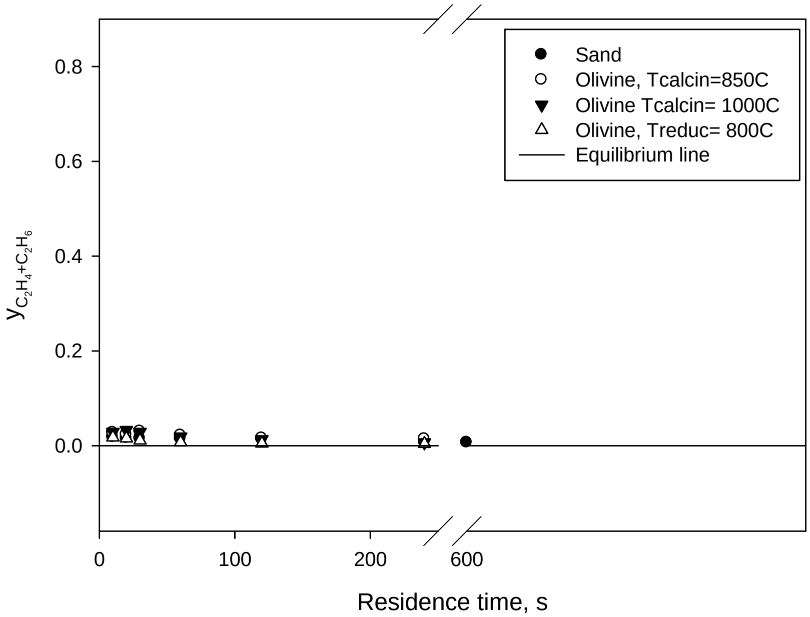

Figure 6.7. **Measured mole fraction of (C_2H_6+C_2H_4) compared to its predicted equilibrium mole fraction, on a dry basis. Bed materials: olivine and sand. Temperature: 800°C**

Since the molar H_2/CO ratio is a key parameter that is essential for downstream processes, the equilibrium model is a useful tool to predict this ratio on the basis of elemental analysis of the feedstock. Figure 6.8 illustrates the predicted molar H_2/CO ratio at equilibrium that is expected from gasification of the Dynamotive bio-oil. It was reached in 30s with the reduced olivine and in 60s with the inert sand. However, a residence time of 60s would not be suitable with sand because full carbon conversion of the bio-oil might not be obtained even at much longer residence times (Figure 6.10).

The predicted molar H_2/CO ratio was 1.65 without the addition of extra steam. The addition of steam would be required if a high value of the molar H_2/CO ratio, such as 2, was required for the downstream process. According to the developed thermodynamic model, it was estimated that a molar H_2/CO ratio of 2 can be obtained at 800°C when additional 0.344g steam per g of bio-oil is injected into the reactor.

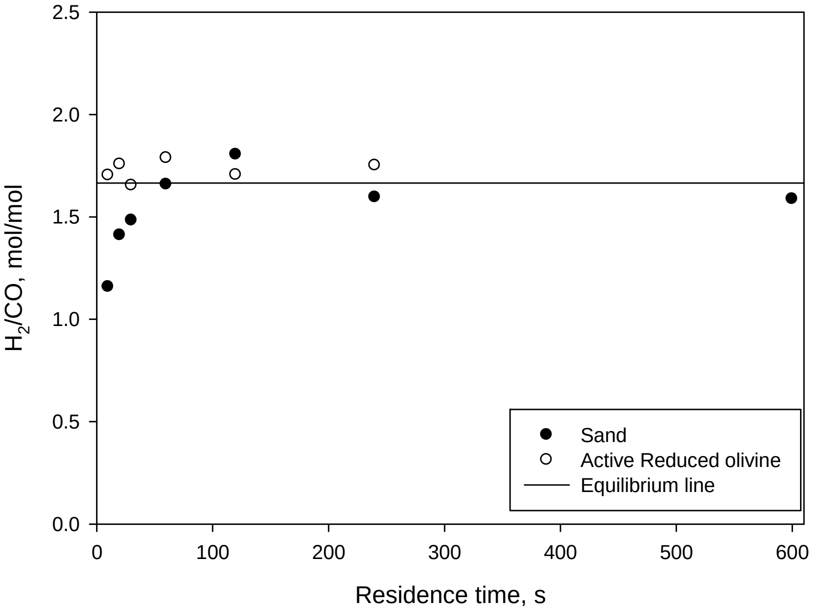

Figure 6.8. **Experimental molar H_2/CO ratio versus predicted molar H_2/CO ratio at equilibrium. Bed materials: olivine and sand. Temperature: 800 °C**

6.5.2. Effect of the bed material on hydrogen yield and bio-oil carbon conversion

Figure 6.9 depicts hydrogen yield versus residence time for the different bed materials used in the jiggle bed reactor. Figure 6.10 also presents carbon conversion of the Dynamotive bio-oil. Silica sand is known to be inert in term of catalytic activity, so this material is a good basis to compare catalytic activity of the pre-treated samples of olivine.

As it can be seen in Figure 6.9, yield of hydrogen was increasing versus residence time for the reduced olivine and silica sand while it had decreasing trend for the calcined olivines. It is also noteworthy that production of hydrogen was quite stable at longer residence times for all the bed materials. In case of the reduced olivine, 83 wt% of hydrogen in bio-oil was converted to hydrogen gas at residence time of 10s and for a 60s residence time, the produced hydrogen gas comprised 93 wt% of the bio-oil hydrogen content. Similar trend of hydrogen yield versus residence time is observed in case of silica sand where the hydrogen yield increased from 0.35 at a residence time of 10s to a maximum hydrogen yield of 0.55 at a residence time of 60s. This indicates that provided enough residence time is available, high hydrogen yields can be achieved through the thermal cracking reactions.

By comparing the reduced olivine and silica sand, it is realized that the reduced olivine was an active catalyst that dramatically reduced the residence time required to reach a desired high hydrogen yield. On the other hand, the hydrogen yield decreased with increasing residence time with calcined olivines, because of the additional oxygen brought by the calcined olivines.

Carbon conversion of bio-oil with the reduced olivine was 96% at the lowest residence time and complete conversion was achieved at longer residence times. Compared to carbon conversion with silica sand where maximum conversion of 66% was gained, it is understood that the reduced olivine was also very effective to crack large molecules inside bio-oil and enhanced reaction between oxygenated molecules and steam according to reaction 6.28.

Although calcination of olivine was found ineffective to increase the yields of hydrogen and CO in this research, the advantage of its oxygen storage can be investigated in cracking complex molecules where an optimum mass of the calcined olivine might be used to partially burn off the heavy molecules to facilitate formation of lighter molecules which can be converted to syngas easier than the original feedstock.

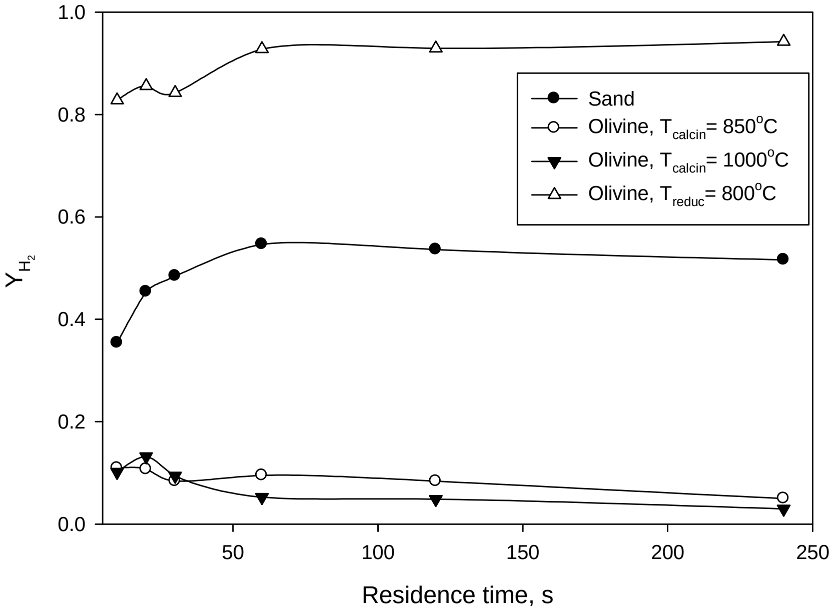

Figure 6.9. **Yield of hydrogen versus residence time. Bed materials: olivine and sand, Temperature 800°C**

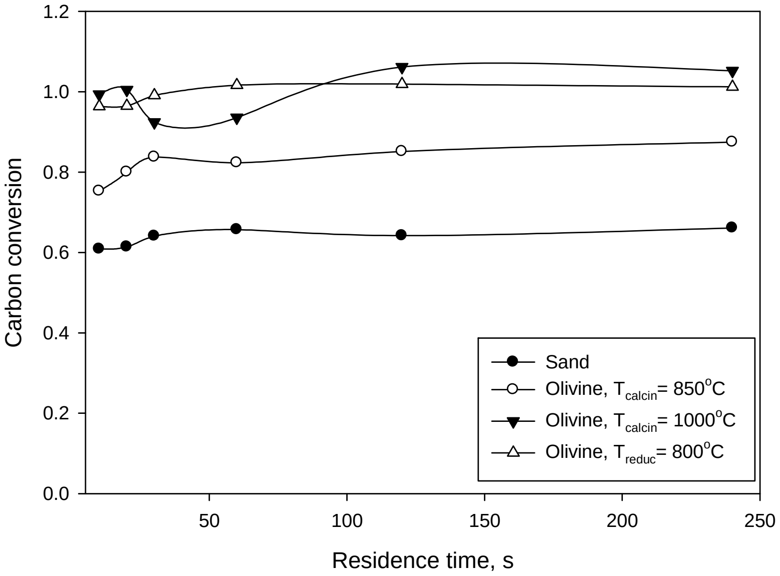

Figure 6.10. **Bio-oil carbon conversion versus residence time. Bed materials: olivine and sand. Temperature 800°C**

6.6. Conclusions

Gasification of the Dynamotive bio-oil was carried out in the jiggled bed reactor, which is a batch-wise fluidized bed micro reactor. Pretreated samples of olivine (calcined with air at 850°C and 1000°C and reduced with hydrogen at 800°C) as well as silica sand were tested as the bed materials.

Despite the literature reports claiming that calcined olivine is a promising biomass gasification catalyst to crack tars and to achieve a high hydrogen yield, experimental data in this research revealed that calcined olivines were inappropriate because oxygen is released from such olivines under gasification conditions. On the other hand, it was discovered that if olivine was reduced in-situ with hydrogen, free iron metals are on the olivine that make it a very active catalyst that results in complete carbon conversion of the bio-oil and a high hydrogen yield at relatively short residence times.

The developed thermodynamic model confirmed that calcined olivines were inappropriate in bio-oil gasification. Product gases produced with the reduced olivine and silica sand, on the other hand, reached the predicted equilibrium concentrations. Since the reduced olivine is a very active catalyst, equilibrium was reached quickly, but took a much longer time with the inert silica sand.

It was also estimated by the thermodynamic model that maximum molar H_2/CO ratio that can be achieved through gasification of the Dynamotive bio-oil in the absence of additional steam is 1.65. According to the model, to reach a molar H_2/CO ratio of 2 would require the addition of 0.344g of additional water per g of bio-oil.

Nomenclatures:

Indices

i	Index of gasification species
j	Index of independent equilibrium reactions
Δ	Change of a parameter or a property

Symbols

A	Coefficient of special heat capacity relation versus temperature
ΔA	Change of coefficient A of all species involved in reaction j at equilibrium

B	Coefficient of special heat capacity relation versus temperature
ΔB	Change of coefficient B of all species involved in reaction j at equilibrium
C	Coefficient of special heat capacity relation versus temperature
ΔC	Change of coefficient C of all species involved in reaction j at equilibrium
D	Coefficient of special heat capacity relation versus temperature
ΔD	Change of coefficient D of all species involved in reaction j at equilibrium
E	Coefficient of special heat capacity relation versus temperature
ΔE	Change of coefficient E of all species involved in reaction j at equilibrium
a_i	Number of moles of species i at equilibrium
b_1	Number of moles of consumed steam per one mole of atom carbon
b_2	Number of moles of consumed oxygen per one mole of atom carbon
$C_{p,i}$	Special heat capacity of species i
$\widehat{f_\iota}$	Fugacity of species i at gaseous mixture at equilibrium
f_i°	Fugacity of pure species i at standard conditions
$\Delta \mathrm{G}_{\mathrm{j}}^{\circ}$	Standard Gibbs energy of reaction j at equilibrium
$(\Delta G_r^{\circ})_j$	Standard Gibbs energy change of reaction j at reference temperature
G_r°	Standard formation Gibbs energy of species i
$(\Delta H_r^{\circ})_j$	Standard enthalpy change of reaction j at reference temperature
H_r°	Standard formation enthalpy of species i
ΔH_C	Combustion energy of a reaction, $\frac{jol}{mol}$
HHV	High heat value of bio-oil, $\frac{jol}{gr}$
K_j	Equilibrium constant of independent reaction j
m	Number of moles of atom hydrogen per one mole of carbon atom on the C-H-O feed
n	Number of moles of atom oxygen per one mole of carbon atom on the C-H-O feed
$M_{w,i}$	Molecular weight of species i, $\frac{gr}{mol}$
O/C	Molar oxygen to carbon ratio
P	Pressure, bar
P°	Standard pressure, bar
Q	External energy required for gasification product to reach equilibrium per 1 mole of CH_mO_n, $\frac{jol}{mol}$
R	Univeral sonstant of gases, 8.314 $\frac{jole}{mol.°K}$
S/C	Molar steam to carbon ratio
T	Temperature, K
T_r	Reference temperature, 298.15 °K
Y_i	Yield of species i
y_i	Mole fraction of species i
$\widehat{\varphi_\iota}$	Fugacity coefficient of species i in equilibrium mixture
ν_i	Stoichiometric coefficient of species i
τ	Ratio between equilibrium temperature and reference temperature

References

[1] North American Transportation Statistics Database. http://nats.sct.gob.mx/nats/sys/tables.jsp?i=3&id=14

[2] The World Bank. Fossil fuel energy consumption (%) in the countries. http://data.worldbank.org/indicator/EG.USE.COMM.FO.ZS

[3] Energy department of the United States. http://energy.gov/science-innovation/energy-sources/fossil

[4] Bedmutha RJ, Ferrante L, Briens C, Berruti F, Inculet I; "Single and two-stage electrostatic demisters for biomass pyrolysis application"; Chemical Engineering and Processing: Process Intensification, 2009, 48, 6, 1112-1120

[5] Xu R, Ferrante L, Briens C, Berruti F; "Flash pyrolysis of grape residues into biofuel in a bubbling fluid bed"; J.Anal.Appl.Pyrolysis, 2009

[6] Berruti F, Muir JR, Hastaoglu MA; "Study of the performance of a large fluidized bed with multiple feed points for flash biomass pyrolysis"; 1989

[7] Sandvig E, Walling G, Daugaard DE, Pletka RJ.; Radlein, Desmond; Johnson, Warren; Brown, R.C.; "The prospects for integrating fast pyrolysis into biomass power systems"; International Journal of Power and Energy Systems, v 24, n 3, p 228-238, 2004, Co-Utilization of Domestic Fuels

[8] Brown RC, Radlein D, Piskorz J; "Pretreatment processes to increase pyrolytic yield of levoglucosan from herbaceous feedstocks"; ACS Symposium Series, v 784, p 123-132, 2001

[9] Scott DS, Paterson L, Piskorz J, Radlein D; "Pretreatment of poplar wood for fast pyrolysis: ate of cation removal"; Journal of Analytical and Applied Pyrolysis, v 57, n 2, p 169-176, February 2001

[10] Scott DS, Piskorz J, Radlein D, Majerski P; "Process for the thermal conversion of biomass to liquids" Biotechnology Advances, v 15, n 3-4, p 799-800, 1997

[11] Scott DS, Majerski P, Piskorz J, Radlein D, Barnickel M; " Production of liquid fuels from waste plastics"; Canadian Journal of Chemical Engineering, v 77, n 5, p 1021-1027, Oct 1999

[12] Scott DS, Majerski P, Piskorz J, Radlein D; " Second look at fast pyrolysis of biomass - the RTI process"; Journal of Analytical and Applied Pyrolysis, v 51, n 1, p 23-37, July 1999

[13] Garg M, Piskorz J, Scott DS, Radlein D; "Hydrogasification of wood"; Industrial and Engineering Chemistry Research, v 27, n 2, p 256-264, Feb 1988

[14] Scott DS, Piskorz J, Radlein D; “Liquid Products from the Continuous Flash Pyrolysis o Biomass”; Industrial & Engineering Chemistry, Process Design and Development, v 24, n 3, p 581-588, Jul 1985

[15] Turner J, Sverdrup G, Mann MK, Maness PC, Kroposki B, Ghirardi M, Evans RJ, Blake D; “Renewable hydrogen production”; International Journal of Energy Research, v 32, n 5, p 379-407, April 2008

[16] Bain RL, Dayton DC, Carpenter DL, Czernik SR, Feik CJ, French RJ, Magrini-Bair KA, Phillips SD; “Evaluation of catalyst deactivation during catalytic steam reforming of biomass-derived syngas”; Industrial and Engineering Chemistry Research, v 44, n 21, p 7945-7956, October 12, 2005

[17] Bain RL; “An overview of biomass gasification”; 2004 AIChE Spring National Meeting, Conference Proceedings, p 547-552, 2004

[18] Sutton D, Kelleher B, Ross JRH; “Review of literature on catalysts for biomass gasification”; Fuel Processing Technology, v 73, n 3, p 155-173, November 13, 2001

[19] Spath PL, Dayton DC; “Assessment of Synthesis Gas to Fuels and Chemicals with Emphasis on the Potential for Biomass-Derived Syngas”; National Renewable Energy Laboratory; Colorado; December; 2003

[20] Rennard D, French R, Czernik S, Josephson T, Schmidt L; “Production of synthesis gas by partial oxidation and steam reforming of biomass pyrolysis oils”; International Journal of Hydrogen Energy, v 35, n 9, p 4048-4059, May 2010

[21] Marda JR, DiBenedetto J, McKibben S, Evans RJ, Czernik S, French RJ, Dean AM; “Non-catalytic partial oxidation of bio-oil to synthesis gas for distributed hydrogen production”; International Journal of Hydrogen Energy, v 34, n 20, p 8519-34, Oct. 2009

[22] Wright MM, Brown RC, Boateng AA.; “Distributed processing of biomass to bio-oil for subsequent production of Fischer-Tropsch liquids”; Biofuels, Bioproducts and Biorefining, v 2, n 3, p 229-238, May/June 2008

[23] Balat M; “Hydrogen-rich gas production from biomass via pyrolysis and gasification processes and effects of catalyst on hydrogen yield”; Energy Sources, v 30, n 5-8, p 552-64, May 2008

[24] Garcia L, French R, Czernik S, Chornet E; “Catalytic steam reforming of bio-oils for the production of hydrogen: effects of catalyst composition”; Applied Catalysis A: General 201 (2000) 225–239

[25] Czernik S, French R, Feik C, Chorine E; “Hydrogen by Catalytic Steam Reforming of Liquid Byproducts from Biomass Thermoconversion Processes”; Ind. Eng. Chem. Res. 2002, 41, 4209-4215

[26] Panigrahi S, Chaudhari ST, Bakhshi NN, Dalai AK; "Production of Synthesis Gas/High-Btu Gaseous Fuel from Pyrolysis of Biomass-Derived Oil"; Energy & Fuels 2002, 16, 1392-1397

[27] Panigrahi S, Dalai AK, Chaudhari ST, Bakhshi NN; "Synthesis Gas Production from Steam Gasification of Biomass-Derived Oil"; Energy & Fuels 2003, 17, 637-642

[28] Kechagiopoulos PN,Voutetakis SS, Lemonidou AA, Vasalos IA;"Hydrogen production via steam reforming of the aqueous phase of bio-oil in a fixed bed reactor"; Energy & Fuels 2006, 20, 2155-2163

[29] Davidian T, Guilhaume N, Iojoiu E, Provendier H, Mirodatos C; "Hydrogen production from crude pyrolysis oil by a sequential catalytic process"; Applied Catalysis B: Environmental 73 (2007) 116–127

[30] Czernik S, Evans R, French R; "Hydrogen from biomass-production by steam reforming of biomass pyrolysis oil"; Catalysis Today 129 (2007) 265–268

[31] Van Rossum G, Kersten SRA, van Swaaij WPM; "Catalytic and noncatalytic gasification of pyrolysis oil" Ind. Eng. Chem. Res. 2007, 46, 3959-3967

[32] Van Rossum G, Kersten SRA, Van Swaaij WPM; "Staged catalytic gasification/steam reforming of pyrolysis oil"; Ind. Eng. Chem. Res., 2009, 48, 5857-5866

[33] Wu C, Huang M, Sui M, Yan Y, Wang F; "hydrogen production via catalytic steam reforming of fast pyrolysis bio-oil in a two-stage fixed bed reactor system"; Fuel Processing Technology; 89 (2008) 1306-1316

[34] Medrano JA, Oliva M, Ruiz J, Garcia L, Arauzo J; "Catalytic steam reforming of model compounds of biomass pyrolysis liquids in fluidized bed reactor with modified Ni/Al catalysts"; J. Anal. Appl. Pyrolysis 85 (2009) 214-225

[35] Sakaguchi M, Watkinson AP, Ellis N; "Steam gasification of bio-oil and bio-char slurry in a fluidized bed reactor"; Energy&Fuels, 2010, 24, 5181-5189

[36] Lan P, Xu Q, Zhou M, Lan L, Zhang S, Yan Y; "Catalytic steam reforming of fast pyrolysis bio-oil in fixed bed and fluidized bed reactors"; Chem. Eng. Technology, 2010, 33, No. 12, 2021-2028

[37] Medrano JA, Oliva M, Ruiz J, Arauzo J; "Hydrogen from aqueous fraction of biomass pyrolysis liquids by catalytic steam reforming in fluidized bed"; energy 36 (2011) 2215-2224

[38] Seyedeyn-Azad F, Salehi E, Abedi J, Harding T; "Biomass to hydrogen via catalytic steam reforming of bio-oil over Ni-supported alumina catalysts"; Fuel Processing Technology 92 (2011) 563-569

[39] Latifi, M; Ferrante, L; Briens, C; Berruti, F; "Effects of residence time and temperature on the thermal cracking of bio-oil for syngas production"; ECI Conference, Bioenergy II, Rio de Janeiro, Brazil, March 2009

[40] Courson C, Makaga E, Petit C, Kiennemann A; "Development of Ni catalysts for gas production from biomass gasification. Reactivity in steam- and dry-reforming"; Catalysis Today 63 (2000) 427-437

[41] Courson C, Udron L, Swierczynski D, Petit C, Kiennemann A; "Hydrogen production from biomass gasification on nickel catalysts Tests for dry reforming of methane"; Catalysis Today 76 (2002) 75-86

[42] Rauch R, Rosch K, Hofbauer H, Swierczynski D, Courson C, Kiennemann A; "Comparison of different olivines for biomass steam gasification"; Sinece in thermal and chemical biomass conversion conference; Victoria BC, Aug 30- Sept 30; 2004

[43] Corella J, Toledo J M, Padilla R; "Olivine or Dolomite as In-Bed Additives in Biomass Gasification with Air in Fluidized Bed; Which Is Better?"; Energy & Fuels 2004, 18, 713-720

[44] Swierczynski D, Courson C, Bedel L, Kiennemann A, Vilminot S; "Oxidation Reduction Behavior of Iron-Bearing Olivines $(Fe_xMg_{1-x})_2SiO_4$ Used as Catalysts for Biomass Gasification"; Chem. Mater. 2006, 18, 897-905

[45] Swierczynski D, Courson C, Bedel L, Kiennemann A, Guille J; "Characterization of Ni-Fe/MgO/Olivine Catalyst for Fluidized Bed Steam Gasification of Biomass"; Chem. Mater. 2006, 18, 4025-4032

[46] Hu G, Xu Sh, Li Sh, Xiao Ch, Liu Sh; "Steam gasification of apricot stones with olivine and dolomite as downstream catalysts"; Fuel Processing Technology 87 (2006) 375-382

[47] Swierczynski D, Libs S, Courson C, Kiennemann A; "Steam reforming of tar from a biomass gasification process over Ni/olivine catalyst using toluene as a model compound"; Applied catalysis B: Environmental 74 (2007) 211-222

[48] Mastellone M L, Arena U; "Olivine as a Tar Removal Catalyst During Fluidized Bed Gasification of Plastic Waste"; AICHE journal, June 2008 Vol. 54, No. 6, 1656-1667

[49] Smith JM, Van Ness HC, Abbott MM; "Introduction to Chemical Engineering Thermodynamics"; sixth edition; 2001

[50] Minutillo M, Perna A, Di Bona D; "Modelling and performance analysis of an integrated plasma gasification combined cycle (IPGCC) power plant"; Energy Conversion and Management 50 (2009) 2837–2842

[51] Semelsberger TA, Brown LF, Borup RL, Inbody MA; "Equilibrium products from autothermal processes for generating hydrogen-rich fuel-cell feeds"; International Journal of Hydrogen Energy 29 (2004) 1047 – 1064

[52] Semelsberger TA, Borup RL; "Thermodynamics of Hydrogen Production from Dimethyl Ether Steam Reforming and Hydrolysis; LosAlamos national laboratory, 2004

[53] Chan SH, Wang HM; "Thermodynamic and kinetic modelling of an autothermal methanol reformer"; Journal of Power Sources 126 (2004) 8–15

[54] Lutza AE, Bradshaw RW, Bromberg L, Rabinovich A; "Thermodynamicanalysis of hydrogen production by partial oxidation reforming"; International Journal of Hydrogen Energy 29 (2004) 809 – 816

[55] Lutz AE, Bradshaw RW, Keller JO; Witmer, DennisE.; "Thermodynamic analysis of hydrogen production by steam reforming"; International Journal of Hydrogen Energy 28 (2003) 159 – 167

[56] Diaz-Somoano M, Martinez-Tarazona MR; "Trace element evaporation during coal gasification based on a thermodynamic equilibrium calculation approach"; Fuel 82 (2003) 137–145

[57] Chan SH, Wang HM; "Thermodynamic analysis of natural-gas fuel processing for fuel cell applications"; International Journal of Hydrogen Energy 25 (2000) 441-449

[58] Seo YS, Shirl, A, Kolaczkowski ST; "Evaluation of thermodynamically favourable conditions for production of hydrogen in three different reforming technologies"; Journal of Power Sources; 108 (2202)) 213-225

[59] Rossia CCRS, Alonsoa CG, Antunesb OAC, Guirardelloc R, Cardozo-Filhoa L; "Thermodynamic analysis of steam reforming of ethanol and glycerine for hydrogen production"; International Journal of Hydrogen Energy 34 (2009) 323-332

[60] Vagia ECh, Lemonidou AA; "Thermodynamic analysis of hydrogen production via autothermal steam reforming of selected components of aqueous bio-oil fraction"; International Journal of Hydrogen Energy 33 (2008) 2489 – 2500

[61] Vagia ECh, Lemonidou AA; "Thermodynamic analysis of hydrogen production via steam reforming of selected components of aqueous bio-oil fraction"; International Journal of Hydrogen Energy 32 (2007) 212 – 223

[62] Hoekstra E, Kersten SRA, Tudos A, Meier D, Hogendoorn KJA; "Possibilities and pitfalls in analyzing (upgraded) pyrolysis oil by size exclusion chromatography (SEC)"; Journal of Analytical and Applied Pyrolysis; Volume 91, Issue 1, May 2011, Pages 76ww8

[63] Li XT, Grace JR, Lima CJ, Watkinson AP, Chen HP; Kim JR; “Biomass gasification in a circulating fluidized bed”; Biomass and Bioenergy 26 (2004) 171 – 193

[64] Li X, Grace JR, Watkinson AP, Lim CJ, ErguÈdenler A; “Equilibrium modeling of gasification: a free energy minimization approach and its application to a circulating fluidized bed coal gasifier”; Fuel 80 (2001) 195-207

[65] Ho LD, Yang H, Yan R, Liang DT; “Prediction of gaseous products from biomass pyrolysis through combined kinetic and thermodynamic simulations”; Fuel 86 (2007) 410–417

[66] Reed TB; “Biomass gasification; Principles and Technology”; Noyes Data Corporation; 1981

[67] Yaws CL; “Chemical Properties Handbook”; 1999

[68] Lide DR; “CRC Handbook of Chemistry and Physics”; 90th edition; Internet version, 2010

[69] Latifi M, Ferrante L, Berruti F, Briens C; “A Novel Fluidized and Induction Heated Micro Reactor for Catalyst Testing”; 2012, Ph.D. Thesis, Chapter 3

[70] Latifi M, Briens C, Berruti F. Non-catalytic and Catalytic Steam Reforming of Acetic Acid in the Jiggle Bed Reactor. 2012, Ph.D. Thesis, Chapter 4

CHAPTER 7:

Conclusions and Recommendations

7.1. Conclusions

Chapter 2 investigates the effects of gas residence time, temperature, bed mass and particle size on the thermal cracking of whole bio-oil in the absence of excess steam in a bubbling fluidized pilot plant. Longer residence times increased vapor phase cracking, producing more syngas with a higher H_2/CO ratio. The results showed that sand had an initial activity which caused higher gasification yields, but, as coke was deposited on the sand, kinetics of the thermal cracking changed and, as a result, gasification yield declined. Higher temperatures always favored gasification, especially at the lower vapor residence times, and bio-oil conversion was very poor at low temperatures. Under all the operating conditions studied in this work, kinetics always controled the thermal cracking reactions and the system was far from thermodynamic equilibrium. Results obtained with Group B and Group A sands were very similar, indicating that mass transfer was not limiting.

Overall, the maximum bio-oil conversion to product gases was less than 45 wt% with thermal cracking, and it was obtained at the maximum temperature of 700 °C and at the maximum vapor residence time of 27 s. Therefore, increasing conversion required either a higher bed temperature or an appropriate catalyst. Effect of excess steam should be investigated to see whether bio-oil conversion would significantly increase.

Since experimental catalyst supply is limited and experimental work with a pilot scale reactor is expensive and time-consuming, a micro test reactor was designed and developed to test the effects of catalyst composition and mass as well as the effect of operating conditions. This unique mechanically agitated small scale setup, defined as “jiggle bed reactor” (JBR), is a batch fluidized micro reactor. As shown in chapter 3, a linear pneumatic actuator was successfully implemented to achieve fluidization conditions in the reaction zone of the JBR, without using any fluidization gas. A new induction heating system was designed and installed to provide a uniform distribution of heat to the bed with a very small temperature difference between the heating surface and the bed. Fluidization and heating of the catalyst bed can, thus, be achieved in a completely non-invasive manner.

A new image processing technique was developed to monitor the fluidization dynamics of the catalyst bed in the JBR. A signal processing technique was used to optimize amplitude and frequency of the pneumatic actuator to achieve the best fluidization conditions. Size distribution and mass of the catalyst particles were optimized with image and signal analyses to enhance fluidization in the JBR.

Heat transfer studies in the JBR showed that induction heating and mechanical fluidization provide a minimum temperature difference between the heating wires and the catalyst bed. Results showed that the maximum fluidization intensity of the bed corresponded to the highest heat transfer coefficient between the heating wires and the catalyst bed.

The JBR was used to conduct precise and reproducible gasification tests over short periods of time. Chapter 4 presented the results of the thermal and catalytic steam reforming of acetic acid, used as model compound, and validated the use of the JBR for the testing of gasification catalysts. Experiments were repeated for 3 times and results were reproducible within 5% data replica. In addition, changes in operating conditions such as temperature, residence time, molar steam-to-carbon ratio and bed material resulted in clear, reproducible and logical changes in the yields of the product gases.

In non-catalytic experiments of acetic acid steam reforming, the thermal decomposition reactions predominated over the reforming and water gas shift reactions, and the carbon conversion of acetic acid was quite high while the hydrogen yield was low for all tested steam-to-carbon ratios, temperatures and residence times.

Complete carbon conversion of acetic acid was achieved in catalytic experiments even in the absence of steam. The hydrogen yield was significantly increased compared to non-catalytic data at similar operating conditions. The reforming and water gas shift reactions were dominant reactions and the hydrogen yield increased with increasing residence time. Increasing the molar steam-to-carbon ratio and the catalyst mass helped increase the acetic acid conversion and the hydrogen yield. On the other hand, CO was also a main product of the steam reforming processes; therefore, an optimum steam-to-carbon ratio and catalyst mass must be selected to maximize the hydrogen yield while achieving the molar H_2/CO ratio that may be required by downstream processes.

Experimental data of the acetic acid catalytic steam reforming were compared with similar data in literature and a satisfactory consistency between the experimental data of this research and those in literature were observed. Therefore, it was realized that the jiggle bed reactor is an efficient newly developed reactor setup which produces reliable data for different operating conditions in addition to the advantage of performing a series of experiments within a short period of time with the minimum cost.

Gasification of actual bio-oils, from hardwood and birchwood, was carried out in the jiggle bed reactor to investigate their conversion into syngas. In Chapter 5, the effects of catalyst type and mass as well as temperature and residence time were studied. Despite the larger water content of the birchwood bio-oil, higher hydrogen yields were achieved from the thermal and catalytic cracking of the hardwood bio-oil, as a result of the type of organic compounds of the DMB.

The results of the thermal cracking experiments, which were conducted at 30 s residence time, showed that both the total carbon conversion and the hydrogen yield increased with temperature. The maximum carbon conversions achieved with the hardwood and the birchwood bio-oils were 64% and 72%, respectively. A large production of CO and a low production of hydrogen resulted in molar H_2/CO ratios less than 2.

The catalysts X and Y were tested for the catalytic gasification of both bio-oils. The catalyst X had less nickel on its surface, but it showed a better performance than the catalyst Y in terms of maximum production of syngas, minimum production of hydrocarbons, and maximum carbon conversion of the bio-oils. This better performance was attributed to the larger surface area of the catalyst X and its higher calcium content.

In the presence of both catalysts, the yield of hydrogen and total carbon conversion of the bio-oils significantly increased. In addition, the yield of hydrocarbons declined noticeably in the catalytic experiments. In overall, the yield of product gases increased with residence time. The yields of hydrogen and CO increased also with catalyst mass at similar residence times.

The yield of hydrogen and the carbon conversion also increased with temperature. On the other hand, the molar H_2/CO ratios obtained in the catalytic tests decreased with temperature. Therefore, an optimization is required to choose a temperature at which maximum carbon conversion and the required molar H_2/CO ratio can be achieved.

Since in the absence of excess steam, low values of the molar H_2/CO ratios can be obtained, either additional steam must be used in the gasification reactor or a secondary water gas shift reactor must be used downstream of the gasification reactor to convert CO to CO_2 and produce extra hydrogen through the water gas shift reaction.

In chapter 6, a comprehensive thermodynamic model was introduced, based on the evaluation of equilibrium constants for the independent reactions between the gasification products. This model can be used to investigate the mole fraction of gasification products at equilibrium for any feedstock with given carbon, hydrogen and oxygen contents. Predictions from this thermodynamic model were compared to experimental results obtained in the jiggle bed reactor, with olivine pretreated under different conditions (calcined with air or reduced with hydrogen).

Despite the literature reports claiming that calcined olivine was a promising biomass gasification catalyst to crack tars and achieve a high hydrogen yield, the experimental data in this research revealed that calcined olivine was actually inappropriate, because oxygen was released from such olivine under gasification conditions. On the other hand, when olivine was reduced in-situ with hydrogen, free iron metal would form on the olivine and make it a very active catalyst resulting in complete carbon conversion of the bio-oil and a high hydrogen yield at relatively short residence times.

The proposed thermodynamic model confirmed that calcined olivine was inappropriate in bio-oil gasification. Product gases produced with the reduced olivine and silica sand, on the other hand, reached the predicted equilibrium concentrations. Equilibrium was reached quickly with the very active reduced olivine catalyst, and much more slowly with the inert silica sand.

The thermodynamic model estimated that the maximum molar H_2/CO ratio that can be achieved through gasification of the hardwood bio-oil in the absence of additional steam was 1.65. According to the model, reaching a molar H_2/CO ratio of 2 would require the addition of 0.34g of additional water per g of bio-oil.

Overall, it is concluded from the experimental work on this thesis that an appropriate catalyst is essential to convert bio-oil to syngas with a high yield at moderate temperatures and residence times. Depending on the required molar H_2/CO ratio for the downstream processes, the model developed in this thesis can be used to predict the optimum amount of excess steam that can be injected either into the gasification reactor or into a secondary water-gas shift reactor.

7.2. Recommendations

Since a good heat transfer and mass transfer can be achieved in a gas-solid fluidized bed, the bubbling bed reactor is a suitable setup for catalytic bio-oil gasification in a continuous flow process, in particular, because less coke can be produced in the bed which deactivates the catalyst in opposite to the fixed bed reactors. It is recommended catalytic experiments should be implemented in the bubbling bed reactor with the optimized catalyst found with jiggle bed reactor to compare the results with the thermal cracking results and to study lifetime of the catalyst during long run experiments.

In this thesis, thermal cracking of whole bio-oil, in the bubbling bed, was conducted in the absence of excess steam. In literature, there are contradicting reports about positive effect of steam to maximize bio-oil conversion and syngas yield through the thermal cracking only. It is recommended some experiments should be performed to prove whether or not thermal steam gasification is a suitable path to increase bio-oil conversion and syngas yield without catalyst.

It is also recommended to study auto thermal bio-oil gasification in the bubbling bed which can be achieved by partly burning the bio-oil with air. Although production of CO_2 would increase, the required heat for the gasification might be supplied through the combustion and, as a result, a considerable amount of electric power could be saved. Having said that, effect of oxygen on the catalyst activity should be investigated.

The jiggle bed reactor is a suitable setup to systematically test gasification catalysts synthesized in the lab at the shortest time and minimum cost. Other than bio-oil gasification tests, the jiggle bed reactor can be easily configured for other applications such as biomass pyrolysis/gasification, coal gasification, pyrolysis of conventional oils and so on. Moreover, the jiggle bed reactor can be used for kinetic studies. In fact, design of the jiggle bed reactor facilitates testing gasification catalysts with different sizes, shapes and masses, as well, with different compositions.

In this thesis, two commercial nickel based steam reforming catalysts were tested. It was also understood through the jiggle bed reactor that iron content of the natural olivine was active for bio-oil gasification. It is recommended some catalysts should be synthesized with olivine as the support and nickel as the deposited active metal with different proportions to investigate integrated effect of iron and nickel on bio-oil conversion and syngas yield. Effect of additional promoters such as lanthanum, magnesium and etc can also be tested on such synthesized catalysts.

In this thesis, activity of olivine was assumed to be mainly due to its iron content according to literature reports. However, Magnesium is also available in olivine. It is suggested three types of catalysts with iron, magnesium and iron/magnesium (with proportions similar to that in olivine) should be synthesized and their catalytic activities be compared with olivine to understand in more detail that which metal is the main active metal and what is the role of each metal in the catalytic gasification tests.

Catalytic experiments in the jiggle bed reactor were conducted for the whole bio-oils, but not with excess steam. It is recommended steam catalytic gasification of bio-oil should be performed to investigate at what steam to carbon ratio, maximum yield of hydrogen with the desired molar H_2/CO can be achieved. Also, it should be investigated whether excess steam is worth adding to the gasification reactor or to a secondary water-gas shift reactor operating at a lower temperature.

The induction heating system was used in a batch-wise reactor in this research. A similar setup can be designed for continuous reactors.

The thermodynamic model developed in this research to predict equilibrium mole fraction of gasification products works with carbon, hydrogen and oxygen elelemntal composition of the feedstock; however, this model can be easily improved for feadstocks containing other elements such as nitrogen and sulphur. It should be investigated whether ash contents can be also predicted with such a thermodynamic model which is based on the equilibrium constants. It is recommended the thermodynamic model on the basis of minimum free Gibb's energy can be used for complex systems with different elements; however, a good solver program including appropriate initial guesses must be developed to get the accurate conversion of the results.

The following improvements of the jiggle bed reactor setup are recommended:

1. An online gas analysis system would facilitate the generation of more experimental data. It is recommended to check out if water can be detected by an online GC or another equipment is required.

2. The operation and the performance of the jiggle bed reactor could be improved by automating the opening of inlet and outlet valves with appropriate timers and by developing a feedstock injection system that could be operated while the reactor is vibrating.

3. The pneumatic actuator has been very effective in achieving the required frequency and amplitudes of the vibrations of the jiggle bed reactor. An electric linear actuator with a stepper motor sized for the maximum required frequency and amplitude as well as the mass of the jiggle bed reactor can be also a good alternative to the pneumatic actuator. Such a linear actuator is

more expensive than a pneumatic actuator, but it is more efficient and user friendly in terms of mechanical life time, accuracy, and strength.

APPENDIX I

A Novel Induction Heating Micro Reactor for Gasification Catalyst Testing

GPE-EPIC
2^{nd} International Congress on Green Process Engineering
2^{nd} European Process Intensification Conference
14-17 june 2009 - Venice (Italy)

A NOVEL INDUCTION HEATING MICROREACTOR FOR GASIFICATION CATALYST-TESTING

S. ROHANI, M. LATIFI, L. FERRANTE, C. BRIENS, F. BERRUTI

♦ Institute for Chemicals and Fuels from Alternative Resources, ICFAR
Department of Chemical and Biochemical Engineering
The University of Western Ontario
London, Ontario N6A 5B9 – Canada
email: srohani2@uwo.ca, **mlatifi@uwo.ca**, **lferran@uwo.ca**, **cbriens@uwo.ca**, **berruti@eng.uwo.ca**

Abstract. The increased interest in alternative energy sources has led to significant developments in the area of biomass gasification and pyrolysis. However, the advances made in this area are limited by the difficulty presented by the testing of the many types of feedstocks, operating conditions and catalysts. With traditional methods of testing, such as the use of pilot plants, the determination of ideal operating parameters requires a great deal of time and money. The use of currently available microreactors also presents several drawbacks. Due to temperature gradients, poor mixing and unrealistic catalyst on stream times, the product distributions obtained from tests carried out in microreactors are not representative of those obtained in large-scale reactors. Temperature gradients, in particular, present a major problem with gasification reactions due to their highly endothermic nature. When the bed is heated through the walls, as is the case with most microreactors, the walls must be kept at a higher temperature than that required at the core to compensate for the heat lost to the reaction. In this study, the construction and validation of a novel microreactor, which minimizes temperature gradients, was carried out. The fluidized bed employed high-frequency induction heating of metal wires placed directly in the bed. The use of inner heating of the bed by wires improved heat transfer, minimized temperature gradients, and also allowed for the temperature of the bed to be kept constant at the Curie point of the wires. A series of tests were carried out in a bed filled with engine oil to determine the number, configuration and diameter of the wires to be used in the bed. Based on the tests, a 25.4 mm diameter bed, consisting of 12 wires with a diameter 2.5 mm placed in a circle, was constructed. The ability of the system to support endothermic gasification reactions was determined by simulating endothermic reactions through the addition of water to a fluidized bed of sand. A bed of fluidized sand particles with diameters ranging between 206 and 250 μm was heated to the Curie point of the carbon steel wires (~680°C) and pulses of water were then injected. A heat transfer coefficient of 473 W/m^2 K between the wires and the bed was measured thereby demonstrating the ability to maintain a constant temperature in the presence of endothermic reactions.

Key-words. biomass gasification, microreactor, induction heating

I.1. INTRODUCTION

The depletion of traditional fuel sources and their increased costs, along with the growing concerns related to greenhouse gases, have led to an increase in research and development in the field of alternative energy sources. The gasification of biomass is one alternative source of energy which has great potential because it not only provides a renewable source of energy, but it also makes use of by-products from agricultural processes, thereby reducing agricultural waste.

One of the challenges associated with catalytic biomass gasification is related to the diversity of feedstocks, catalysts and operating conditions to be used. A need exists for a fast and cost effective means of accurately testing out different catalysts under various operating conditions.

Up to date, the most common tests used are those carried out in pilot plants or those using fixed-bed reactors and fixed fluid-bed reactors (Imhof *et al.*, 2004). Despite the extensive research dedicated to improving the ability of these methods of evaluation to mimic commercial units, the existing methods continue to suffer from numerous drawbacks such as long injection times, long residence times and their inability to simulate mixed-zone kinetics (Corella *et al.*, 1986; Imhof *et al.*, 2004). Alternatively, pilot plants can more accurately mimic full scale operations, but are not as fast, nor as cost effective as the microreactors.

Kraemer at al. (1988) listed several characteristics which a reactor should possess in order to be able to accurately model commercial-scale units. First, the reactor should be able to match the hydrocarbon-catalyst contact time, reactor temperature and catalyst-to-oil ratio of commercial units. Second, axial coke profiles should be minimized to best mimic commercial units. A great deal of research has been carried out to develop reactors meeting these requirements. The Riser Simulator, for example, overcomes the problem of coke profiles present in traditional reactors, such as Berty-style recycle reactors, by generating intense gas-solids mixing through fluidization of the bed (Kraemer *et al.*, 1988).

Another major consideration for a reactor used for the testing of gasification catalysts, which is the focus of this study, is the reactor's ability to minimize unrealistic thermal cracking. Due to the highly endothermic nature of gasification reactions, excessive thermal cracking often occurs at the walls of the reactor. Traditional test reactors suffer from temperature gradients (Rastogi *et al.*, 1988). When reactors heat the gas through the walls of the reactor, the walls must be kept at a significantly higher temperature than that required at the core of the reactor in order to compensate for the heat consumed by the reaction, thereby creating a temperature gradient. Because heat is transferred from a wall to a gas, the heat transfer coefficient is low and the wall temperature must be much higher than the gas temperature. Though some groups have attempted to address this concern by performing runs with inert particles to show the absence of extensive thermal cracking, such results are not adequate to show that thermal cracking does not occur when an endothermic reaction is taking place inside, greatly increasing the need for heat from the walls and, therefore, resulting in a much higher wall temperature.

In pursuing the aim of generating temperature profiles more closely resembling the actual temperature profile, a variety of heating techniques have been employed, including: shock-tube (Ozturk and Merklin, 1995), light irradiation (Boutin *et al.*, 1998), arc, resistive heating (Drummond and Drummond, 1996) and high-frequency induction heating (Tsai *et al.*, 2006).

I.2.EXPERIMENTAL APPROACH

In the present study, a fluidized bed reactor, employing high-frequency induction heating, was developed. Heating of the bed was achieved through induction heating of carbon steel wires placed directly in the bed, instead of the lateral heating through the walls that is commonly used. The choice in the method of heating was made based on the following reasons:

1) Inner heating of the bed is much more efficient than heating through the walls due to direct contact between the heating surface and the fluidized bed. Due to this enhanced heat transfer, the temperature gradient between the core of the reactor and the walls is dramatically reduced.
2) The available area for heat transfer can be increased by using wires.
3) Due to an electromagnetic property of magnetic materials, temperature regulation is facilitated. Magnetic materials can be heated through induction heating up to a temperature known as the Curie point, above which the material loses its ferromagnetic property. As such, in the bed, the wires are heated until they reach their Curie point. At this point, the wires no longer absorb power. As they lose heat to the bed, the temperature of the wires drops below the Curie point, and they again absorb power and generate heat. Through this process, the bed is kept at a constant temperature. Since the Curie point is unique to each type of material, by choosing the appropriate material, the bed can be maintained at the desired target temperature.

Due to the novelty of the idea, a series of experiments were first carried out to determine the position, number and size of the wires which would optimize the heating of the bed. Once the design was completed, the ability of the reactor to maintain the bed at the reaction temperature in the presence of endothermic reactions was tested.

I.3.EXPERIMENTAL EQUIPMENT AND TECHNIQUES

Part I - Design of the Microreactor

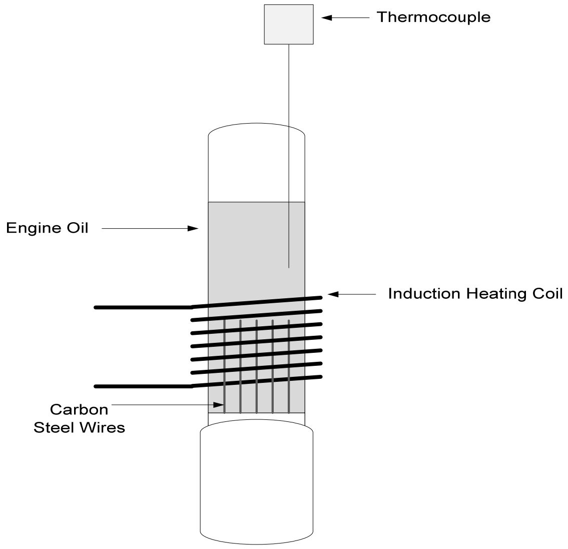

Figure 3 . Experimental set-up employed in Part I

The first set of experiments, used to determine the bed configuration, was carried out in a 30.5 cm long ceramic tube with a diameter of 3.2 cm (see Figure 1). The tube was supported by a stainless steel base. A high frequency power supply (HFPS) was used to provide a high-power, high-frequency alternating output voltage to the induction coil which was cooled by circulating water through the copper tubing. The coil was used to induce current in carbon steel wires placed in the bed. The wires, with diameters ranging from 1.5 to 3.5 mm, were arranged in various configurations and were held in place by a concrete base. The concrete base was placed at the bottom of the ceramic tube, on the stainless steel base, and the column was filled with engine oil so that a thermocouple could be placed inside to measure the temperature of the oil as a function of time. The K-type thermocouple was placed in the engine oil a few centimeters above the induction coil to ensure that the magnetic field created by the induction coil would not affect the thermocouple's ability to measure the temperature. The oil was mixed by bubbling nitrogen. Due to the mixing, the temperature in the column could be assumed to be close to uniform. A data acquisition system was used to record the data from the thermocouple. The system was first set to begin recording the temperature, the cooling water was turned on and then the induction heating system was turned on. Once the oil temperature reached 250 °C, the system was shut off to prevent the oil from boiling and spilling over. The data was plotted to generate a graph depicting the temperature of the oil as a function of time. In order to compare the ability of different wires and wire configurations to heat up the bed, the slopes of the graphs, which corresponded to the change in temperature over time, were compared.

Part II - Validation of the Novel Microreactor for Fluidized Beds with Liquid Injection

The next set of experiments was carried out in the reactor shown in Figure 2. The system consisted of a Mullite thermocouple protector with an I.D. of 2.54 cm and a length of 30.48 cm, supplied by Arklay S. Richards Company (New Highlands, Massachusetts). The ceramic tube was insulated using FiberFrax to minimize heat losses. Silica sand particles with diameters between 206 and 250 μm were fluidized with air flowing through a sparger at a velocity just above the minimum fluidization velocity. The bed was heated by induction heating of rods suspended from a stainless steel disk attached to the sparger tube. The number and configuration of the rods were determined through the first set of experiments. The temperature of the bed was measured by a thermocouple placed inside of the bed, above the induction heating coil.

Water was injected into the bed using a syringe. The injection of water took place once the bed had reached a steady-state temperature (of around 680°C).

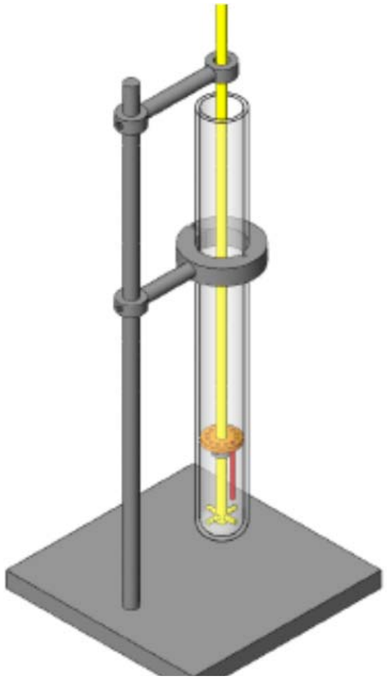

Figure 4 . Experimental set-up employed in

I.4.RESULTS AND DISCUSSION

Part I - Design of the Microeactor

The Effect of the Wire Diameter

For high-frequency induction heating of cylinders, heating can be maximized by setting the ratio between the workpiece diameter and the reference depth of the eddy currents induced in the workpiece at a value of 4.5:1. Increasing the ratio beyond this value, either by increasing the workpiece diameter, or by reducing the reference depth of the eddy currents by changing the frequency, results in little improvement in heating. (Davies, 1990).

In the current study, the frequency of the system, and therefore the depth of the eddy currents, were set at a constant value. Therefore, increasing the diameter of the wires directly increased the ratio between the workpiece diameter and the reference depth of the eddy currents. As Figure 3 shows, the rate of heating was observed to increase with the diameter of the wires over the range of 1– 2.5 mm, but then seemed to level off. These observations are in agreement with past findings which have stated that there is little benefit in increasing the workpiece diameter to a value larger than 4.5 times the reference depth.

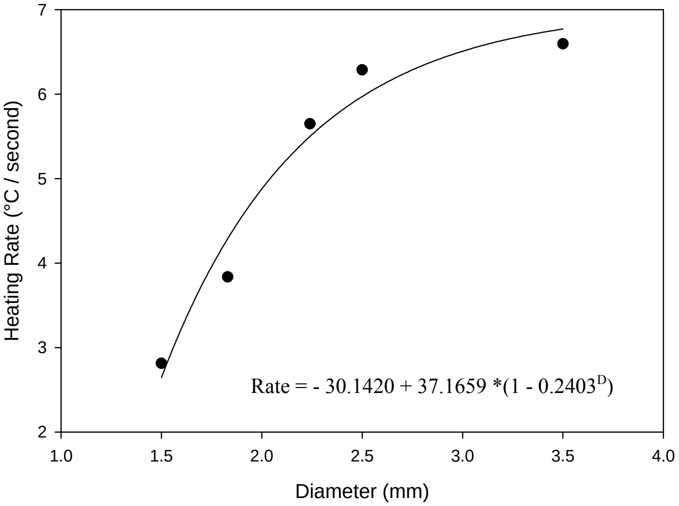

Figure 5 . Effect of the wire diameter on the heating rate

The Effect of the Number of Wires

As the number of wires in the bed is varied, the heating rate changes. In the current experiment, the wires were placed in a circle halfway between the centre and walls of the bed. As Figure 4 shows, the rate of heating was observed to increase linearly with the number of wires in the circle: there was no interference between wires.

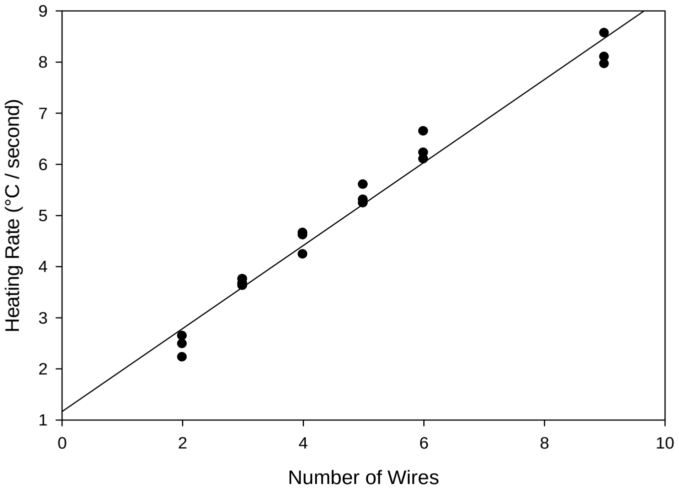

Figure 4 . Effect of the number of wires in the bed on the heating rate

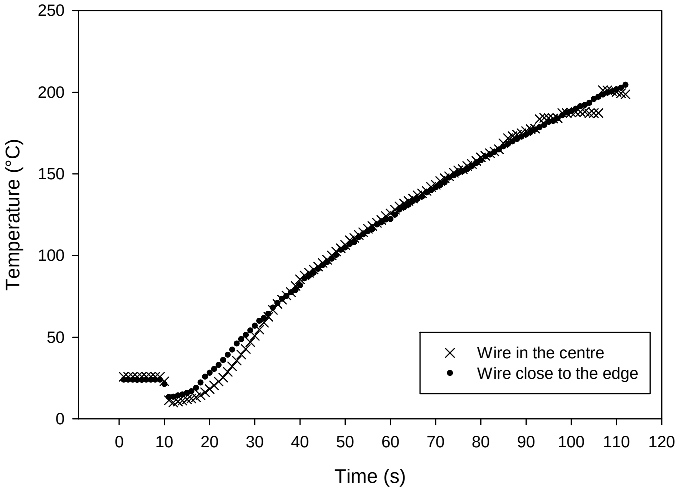

Figure 5 . Effect of the position of a wire on the heating rate

The Effect of the Position of the Wires

In order to determine where the wires should be placed in the reactor, the rate at which the bed was heated when a single wire was placed in the centre of the bed was compared to the heating rate when the wire was placed at the edge of the bed. As Figure 5 shows, the position of the wire seems to have no effect on the rate of heating. Between 100 and 150 ºC, the wire in the centre and the wire heat the oil by 1.84 and 1.85 ºC/s, respectively. The current findings are in agreement with those reported in previous works (Duquenne, 1994).

The Effect of Shielding of Wires

Though the position of a wire was shown to have no effect on the rate of heating for the case with a single wire in the bed, the position of a wire in a bed with numerous wires does affect the rate of heating due to a phenomenon known as shielding. As previously shown, when all wires are placed in a circle, the rate of heating increases linearly with the number of wires. However, with large wires (diameters > 1.83 mm), if a wire is added to the centre of a bed consisting of wires arranged in a circle, the increase in the heating rate due to the added wire is almost negligible. This is because the wire placed in the centre is shielded by those around it. To measure the amount of shielding, six wires were placed in a circle. One wire was then added to the centre of the bed. If there were no shielding, the rate of heating of six wires in a circle and one in the centre of the bed would be equivalent to the rate of heating of seven wires placed in a circle in the bed. However, this was not the case. The seventh wire, placed in the centre of the bed, in experiments with wires with diameters of 2.24 mm and 2.5 mm, generated only around 50 and 20 percent of the heat expected, respectively. Figure 6 shows the % shielding for wires with diameters between 1.5 to 2.5 mm. The shielding % is defined as the fraction of the theoretical amount of heat a wire should add if there were no shielding generated by the addition of a wire to the centre. As Figure 5 shows, the effect of shielding was seen to be most pronounced for wires with larger diameters.

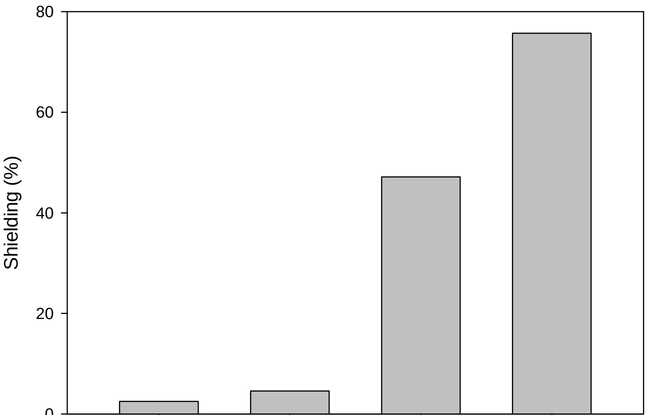

Figure 6 . Shielding effect for 6

The Effect of Configuration of Wires

Three different configurations of wires were also tested out: triangular, circular and square. The results showed no significant difference between the various configurations.

I.5.Overall Design

Based on the results, 2.5 mm diameter wires were chosen. Because heating increases linearly with the number of wires, in order to achieve good heating, the number of wires was chosen to be twelve. More wires could have been used, however, they would have reduced the bed volume and twelve was found to provide sufficient heating. The wires were placed in a circle in order to avoid shielding.

Part II - Validation of the Novel Microreactor for Fluidized Beds with Liquid Injection

After having determined the optimum configuration of the rods in the bed, the ability of the system to heat up a bed of fluidized sand and to support endothermic reactions was tested. Figure 7 shows the temperature profile of the fluidized bed of sand, which was heated until it reached a constant temperature of 680 °C. A pulse of 0.15 mL of water was then injected into the bed, and the system showed a small and short drop in temperature.

A model was developed in order to calculate the heat transfer coefficient between the wires and the bed. The following energy balance equation, which neglects heat losses from the bed, was used:

$$hA(T_w - T_b) = M_s c_p \frac{dT_b}{dt} \qquad [1]$$

Where h is the effective heat transfer coefficient
A is the heat transfer area
T_w, T_b are the wire and bed temperatures
M_s is the mass of sand in the bed
C_p is the specific heat capacity of sand

The following model, developed from equation [1] was obtained:

$$T_b = T_w - (T_w - T_{b0}) * \exp(\frac{hA}{M_s c_p} t)$$

From equation [2], the heat transfer coefficient was estimated to be 473 W/m^2 K based on minimization of the sum of the squares of the error between the measured bed temperature and the calculated bed temperature.

I.6.CONCLUSIONS AND SUMMARY

The design of a novel microreactor employing high-frequency induction heating was carried out. Based on the findings, a bed with twelve wires with diameters of 2.5 mm arranged in a circle was created. Water was injected into the bed and a heat transfer coefficient of 473 W/m^2 K between the wires and the bed was obtained.

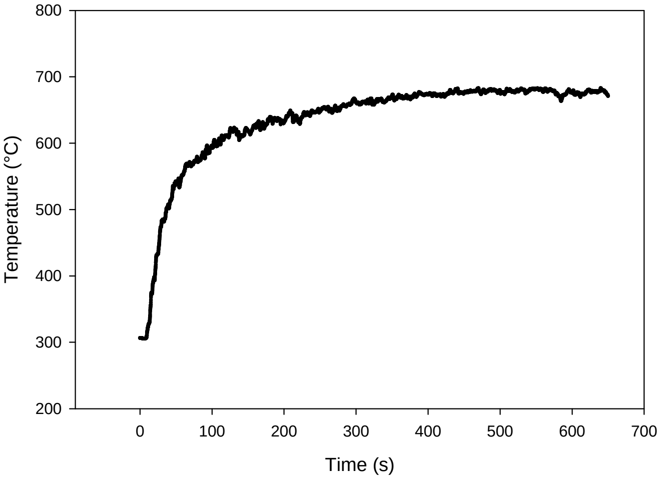

Figure 7. Temperature evolution of the reactor with 0.15 mL of water injected at t = 570 s

REFERENCES

Boutin, O., M. Ferrier, and J. Lede, "Radiant Flash Pyrolysis of Cellulose – Evidence for the Formation of Short Life Time Liquid Species," *Journal of Analytical and Applied Pyrolysis,* **47**, 14 (1998).

Corella, C., A. Fernández, and J. M. Vidal, "Pilot Plant for the Fluid Catalytic Cracking Process: Determination of the Kinetic Parameters of Deactivation of the Catalst," *Ind. Eng. Chem. Prod. Res. Dev.,* **25**, 554 (1986).

Davies, E. J. (1990). *Conduction and Induction Heating*. London, U.K.: P. Peregrinus Ltd.

Drummond, A. F., and I. W. Drummond, "Pyrolysis of Sugar Cane Bagasse in a Wire-Mesh Reactor," *Industrial Engineering and Chemistry Research*, **35**, 1263 (1996).

Duquenne, P., A. Dltour, and G. Lacoste, "Application of Inductive Heating to Granular Media: Modelling of Electrical Phenomena," *The Canadian Journal of Chemical Engineering,* **72,** 975 (1994).

Imhof, P., M. Baas, and J. A. Gonzales, "Fluid Catalytic Cracking Catalyst Evaluation: The Short Contact Time Resid Test," *Catalysis Reviews*, **46**(2), 151 (2004).

Kraemer, D. W., de Lasa, H. I., "Catalytic Cracking of Hydrocarbons in a Riser Simulator," *Ind. Eng. Chem. Res.*, **27**, 2002 (1988).

Ozturk, Z., and J. F. Merklin, "Rapid Pyrolysis of Cellulose with Reactive Hydrogen Gas in a Single-Pulse Shock Tube," *Fuel*, **74**(11), 91 (1995).

Rastogi, A., W. Y. Svrcek, and L. A. Behie, "Novel Microreactor with Quench System for Kinetic Study of Propane Pyrolysis," *AIChE Journal,* **34**(9), 1417 (1988).

Tsai, W. T., M.K. Lee, and Y. M. Chang, "Fast Pyrolysis of rice straw, sugarcane bagasse and coconut shell in an induction-heating reactor," *J. Anal. Appl. Pyrolysis,* **76**, 230 (2006).

APPENDIX II

Characterization of Moisture Distribution in a Fluidized bed

II.1. Introduction

The performance of several important industrial processes, such as fluid coking or fluid catalytic cracking, is dependent on the good distribution of liquid feed sprayed into a fluidized bed of hot inert or catalytic solid particles, respectively. In the fluid coking process, which operates at about 550^{o}C, bitumen is spray-atomized with steam and injected into a fluidized bed of hot coke particles providing the heat required to crack heavy hydrocarbons into lighter products. The quality of the liquid injection has a significant impact on agglomerate formation and on the yield of valuable liquid (Knapper *et al.*, 2003). Imperfect liquid distribution results in the formation of agglomerates that hinder heat transfer to the reacting liquid, slowing the cracking reactions, increasing coke formation, and causing fouling of coker internals.

The objective of this study was the development of simple and reliable methods for the determination of the moisture distribution in a fluidized bed. In particular, the study aimed at the investigation and optimization of the liquid distribution in a cold fluidized bed, using water and sand, for example, to simulate the spraying of hot bitumen on hot coke particles in industrial fluid cokers. McDougall *et al.* (2004) have shown that the water-sand system is a good room temperature simulator the hot bitumen-coke system, as there is nearly perfect wettability of the solids by the liquids in both cases.

Fluidization quality is strongly affected by the presence of liquid. As a fluidized bed gets wetter, its cohesivity increases and this reduces bed fluidity. McDougall *et al.* (2004) examined different methods to evaluate the fluidization quality, such as a falling ball to measure the bed viscosity, a funnel to measure the gravity flow time of a bed sample, a movable column top to determine the Transport Disengaging Height (TDH), and pressure transducers to monitor the kinetics of bed de-aeration.

Several researchers have monitored bed fluidity with pressure fluctuations. When a liquid is sprayed into a fluidized bed, the fluidization quality can degrade to the extent of affecting the bed pressure drop, which Tardos *et al.* (1985), Stusch *et al.* (2001) and McLaughlin *et al.* (2001) used to assess de-stabilization and de-fluidization in wet fluidized beds. Briens *et al.* (2003) were able to detect the more subtle degradation in bed fluidity, which occurs at lower liquid concentrations, by analyzing the signals from dynamic pressure transducers.

McDougall *et al.* (2004) showed that, as a fluidized bed becomes wet and agglomerates form, the flux of entrained particles above the TDH decreases and their size distribution changes. Benoni *et al.* (1994) had observed similar results when particles agglomerated due to electrostatic effects.

The falling ball method was applied by McDougall *et al.* (2004) and Kai *et al.* (1991) to measure the apparent viscosity of a wet fluidized bed. McDougall *et al.* (2004) showed that the velocity of a ball falling through a fluidized bed was affected by the presence of liquid in the bed.

Renganathan *et al.* (2005) monitored the fluctuations of the local voidage in a fluidized bed by applying a conductance method. They showed that the maximum of the Root Mean Square (RMS) of voidage fluctuations can be related to the average bed voidage.

The injection of liquids into fluidize solids may create agglomerates of particles bound together by the liquid. The additional objective of this study is to develop and evaluate several experimental tools to measure the various types of moisture in fluidized beds: i) free moisture, or water coating individual particles; (ii) micro-agglomerates, which are fluidized; and (iii) macro-agglomerates, which are too large to remain fluidized and, consequently, settle to the bottom of the bed. These tools can be applied to evaluate the performance of liquid spray nozzles in fluidized beds.

II.2. Equipment

The experiments were performed in a Plexiglas fluidized bed column with a rectangular cross section 0.5 m in length and 0.1 m wide. The bed material used in this study was Barco 71 silica sand from Opta minerals with a Sauter diameter of 200 μm and a density of 2650 kg/m3. In each experiment, the bed was filled with 45 kg of dry sand.

In order to fluidize the bed uniformly, a porous plate distributor was used. The fluidization velocity was set at 0.12 m/s during liquid injection and then reduced to 0.07 m/s. The fluidization air flowrate was controlled and measured with a calibrated 1.4 mm sonic orifice

This unit was equipped with a liquid line, to inject the water into the fluidized bed, and an air line, to atomize the liquid into small droplets and, consequently, increase the interaction area between liquid and solid. The atomization air was supplied from a high pressure cylinder at a constant pressure controlled by a pressure regulator. A calibrated sonic orifice, with a diameter of 1.4 mm, was used to measure the air flowrate. A simple type of pre-mixer, called Bilateral Flow Conditioner (BFC) (McCracken *et al.*, 2005) was used to efficiently mix liquid and atomizing air upstream of the spray nozzle.

Two types of spray nozzles were used in this study. The first nozzle, called TEB, is shown in Figure II.1. It is a scaled down version of industrial spray nozzles patented by Base *et al.* (1999). In industrial processes, the flowrate of atomization gas must be minimized; for example, in the Fluid Coking process, the flowrate of atomization steam must be minimized to reduce energy costs, increase the coker capacity and reduce wastewater flows. The ratio of the atomization gas mass flowrate to the liquid mass flowrate, or "Air to Liquid Ratio" (ALR), typically ranges from 0.5 to 2 %. With such ALR values, the liquid distribution is far from perfect, and agglomerates are typically formed in the fluidized bed. The second type of nozzle used in this work was a "high ALR nozzle" (Figure II.2), consisting of a 3.6 mm diameter hollow cylinder and operating with an ALR of 50 %.

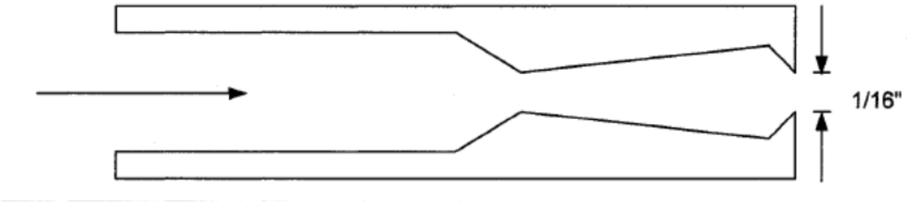

Figure II.1: TEB Spray Nozzle geometry

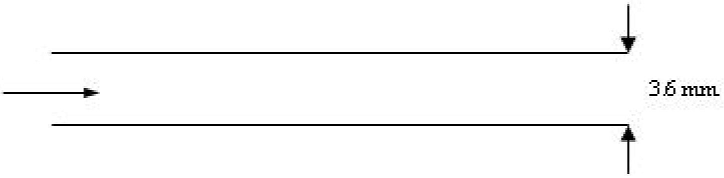

Figure 0II.2: “High ALR” hollow cylinder shaped nozzle

Preliminary experiments used a method first developed by House *et al.* (2008) to show that no agglomerates were formed when liquid was injected into the fluidized bed with the high ALR nozzle. This method was originally used to characterize the initial liquid-solid contact in a fluidized bed by injection of a sugar solution. After an injection of such solution, the bed was defluidized and allowed to slowly dry. The sugar would act as binder and maintain the integrity of granules formed during the initial contact of the injected liquid with the sand particles. Similarly to House *et al.* (2008), a solution of 22 wt% sucrose and 8 wt% glucose was used to match the viscosity of bitumen at the injection temperature used in industry. Figure II.3 shows that no agglomerates were formed when the “high ALR nozzle” was used.

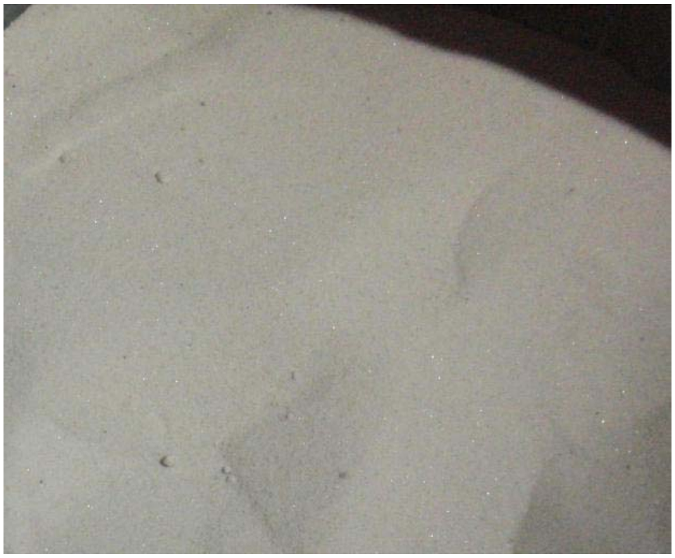

Figure 0II.3: a sample of bed collected sand after spray with “high ALR” nozzle

II.3. Types of Moisture Distribution in a Fluidized Bed

Preliminary studies showed that, when liquid is spray-atomized into a fluidized bed, the moisture is distributed throughout the bed in three different forms, (a) free moisture, (b) micro-agglomerates, and (c) macro-agglomerates, as illustrated in Figure II.4. Figure II.4a shows the ideal case, when all the liquid injected spreads on the surface of individual particles, without forming any agglomerate. Such liquid is called “free moisture”. This does not occur with practical spray nozzles, since a fraction of the injected liquid always forms agglomerates.

Micro-agglomerates refer to the small and light agglomerates that remain suspended within a fluidized bed under normal operating conditions (Figure II.4b). Such agglomerates can be found in samples taken through the wall of the fluidized bed. Figure II.5 shows an example of micro-agglomerates sampled from a fluidized bed; these agglomerates were solidified by using the sugar injection and drying method, based on the method developed by House *et al.* (2008). The proportion of the injected liquid which is trapped within micro-agglomerates is called “micro-agglomerate moisture”.

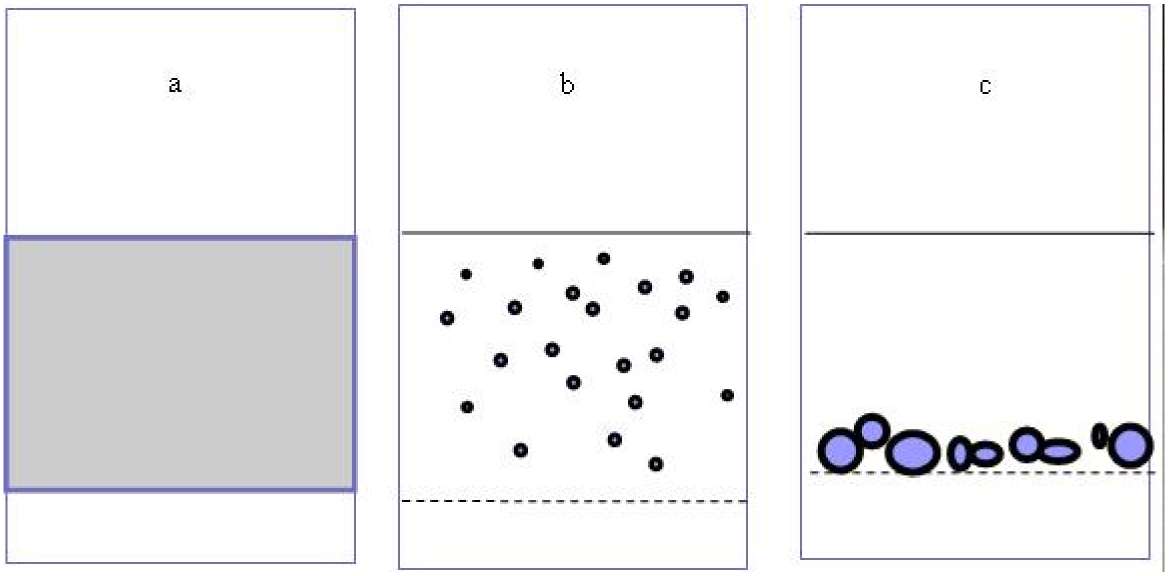

Figure 0II.4: a) Free moisture b) Micro-agglomerates c) Macro-agglomerates

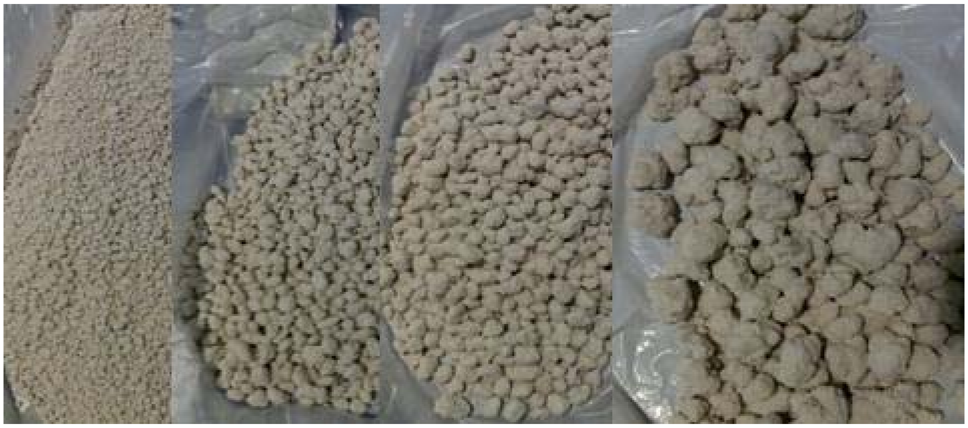

Figure II.5: Micro-agglomerates from experiments with injection of sugar solutions

The third type of moisture is trapped within macro-agglomerates (Figure II.4c). The density and size of the macro-agglomerates is such that they cannot be fluidized and, therefore, sink to the bottom of the bed above the gas distributor. Such agglomerates will not be present in samples taken through the wall of the fluidized bed. Figure II.6 shows an example of macro-agglomerates recovered from the bottom of a fluidized bed, which were collected with the sugar injection and drying method. The proportion of the injected liquid which is trapped within macro-agglomerates is called “macro-agglomerate moisture”.

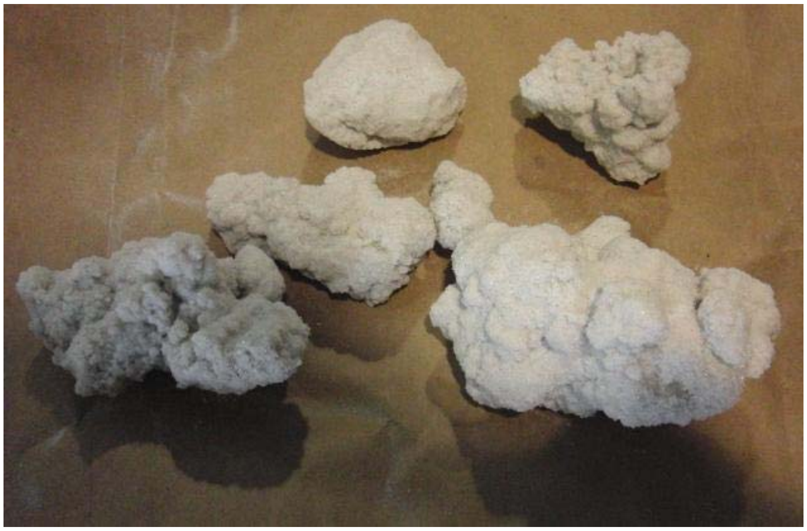

Figure 0II.6: Macro-agglomerates from sugar experiments

II.4. Quantitative methods for the Evaluation of the Moisture Distribution in a Fluidized Bed

Three different types of measurement were conducted in this study:

1) The overall moisture of the fluidized bed (X1), i.e. the total amount of water present in the fluidized bed, was obtained by mass balance.
2) Fluidized solids were sampled through the wall of the fluidized bed and the total moisture of the sample was measured (X2).
3) The free moisture (X3) was measured either from measurements performed directly in the fluidized bed or from sampled bed material.

The micro-agglomerate moisture can be obtained from (X2 – X3) while the macro-agglomerate moisture can be estimated from (X1 – X2).

II.4.1 Total Bed Moisture

The overall moisture of the fluidized bed, i.e. the total amount of water present in the fluidized bed, was obtained by mass balance, knowing the mass of injected water at the start of the experiment and the mass of water evaporated since then, which was calculated from the bed temperature and relative humidity of the fluidization gas leaving the bed. Preliminary experiments indicated that the gas leaving the bed was saturated in water vapor.

II.4.2. Total Sample Moisture

Two methods, Karl Fischer titrations and evaporative weight loss measurements, were used to obtain the total free moisture of a sample of bed solids.

II.4.2.1 Karl Fischer Titration

Karl Fischer titration was invented in 1935 by the German chemist Karl Fischer. It uses a volumetric titration to determine the amount of water in a sample.

In this study, known amounts of wet solids and dry methanol were mixed. The mixture was then centrifuged to obtain a particle-free sample of the wet methanol solution, which was titrated to determine its water content.

Unfortunately, our tests indicated that the Karl Fischer titration is not sensitive enough for the accurate determinate of the moisture content of in solids samples with a liquid to solid ratio below 0.12wt%.

II.4.2.2 Evaporative Weight Loss

Another way to measure the moisture content of a sample of wet solids is to use a moisture analyzer. This type of analyzer is a balance that is equipped with a heating system that is able to vaporize the water from a sample: this increases the accuracy of the standard weight loss method by reducing the number of manipulations. In this work, a moisture balance (HG63 Halogen Moisture Analyzer from Mettler Toledo) has been used.

II.4.3. Free Moisture

Several methods were investigated for the determination of the free moisture of a solid sample. Several samples were prepared with a known amount of water, using a mechanical blender to eliminate any agglomerate, so that all the sample moisture was in the form of free moisture. The free moisture of each sample was characterized as the liquid to solid mass ratio (L/S) and experimentally measured using the following methods:

II.4.3.1 Funnel flow

This method is based on the assumption that free moisture makes particles cohesive and that this cohesivity slows gravity flow through a funnel. For these experiments, two different funnels with included angles of 60 degrees and spout diameters of 4 mm and 12 mm were chosen. Figures II.7 and II.8 show that the free moisture greatly affected the time required for 70 g of solids to flow through the funnel. However, this method can only determine the effects of free moisture on flowing time over a narrow range of values: below L/S values of 0.8 %, there was no effect of free moisture on the flow time while, above 0.12%, particles would not flow through the funnel.

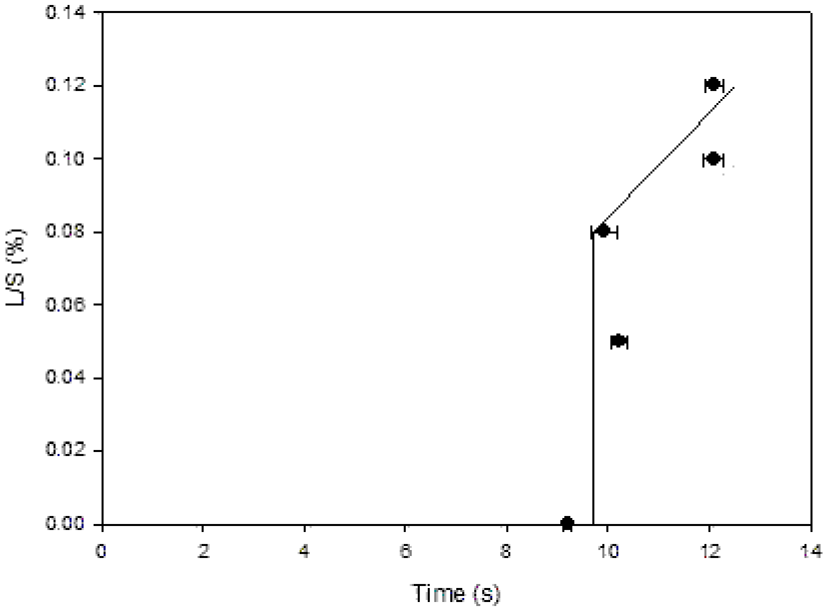

Figure 0II.7: L/S versus funnel flowing time –funnel with 12 mm spout, 70 g sample

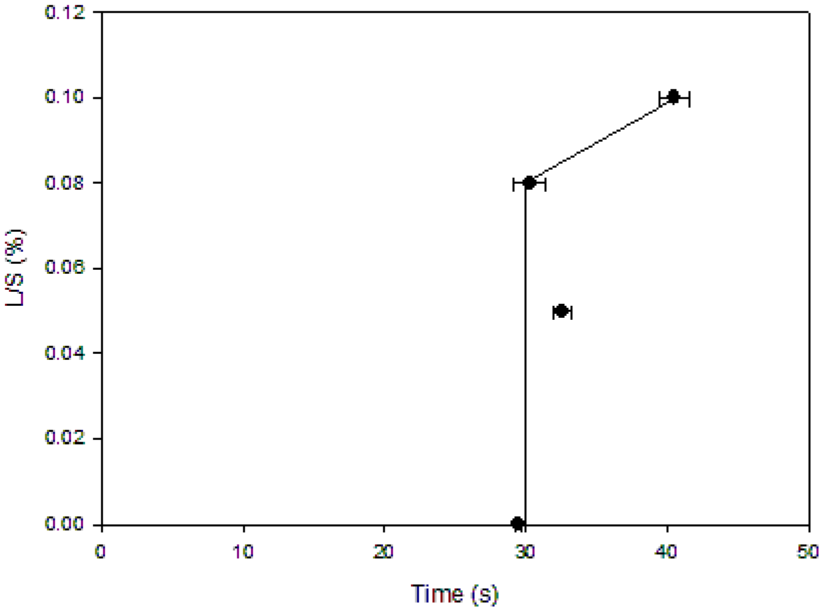

Figure II.8: L/S versus funnel flowing time –funnel with 4 mm spout, 70 g sample

II.4.3.2 Avalanche test

A revolution powder analyzer determines the cohesivity of a powder from its avalanching behavior. The equipment contains a rotating drum, a video camera that captures the resulting avalanches and software that characterizes the avalanches. In this work, a Revolution powder analyzer from Mercury Scientific (Rev 2007) was used. Figure II.9 shows that the avalanching behavior of a wet sample is completely different from that of a dry sample. This study considered three different avalanche characteristics: the avalanche time, the avalanche power standard deviation and the surface fractal.

The avalanche time is the average time interval between avalanches: it normally increases as a powder becomes more cohesive. Figure II.10 shows that the avalanche time increases with increasing free moisture. However, the avalanche time is not sensitive enough for free moistures greater than 0.07 % (Figure II.10).

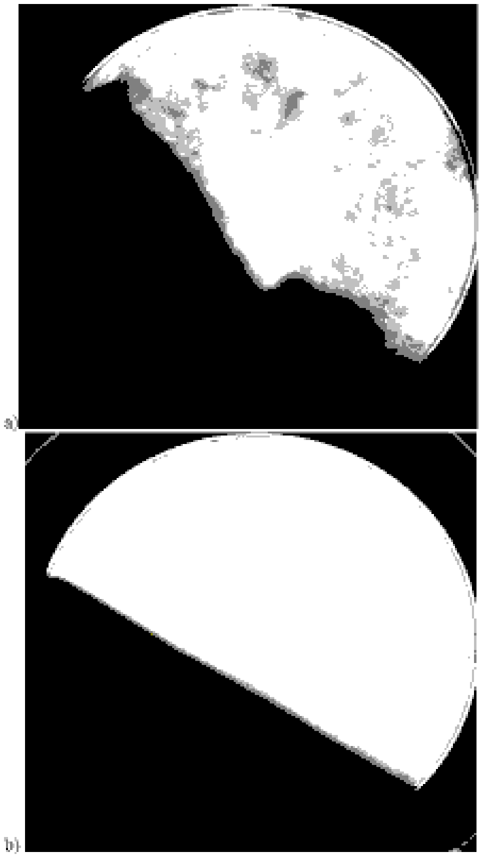

Figure 0II.9: Images from the Revolution powder analyzer: (a) Wet sand with L/S = 0.1%, (b) Dry sand

The power of each avalanche is the difference between the beginning height of the avalanche to the ending height of the avalanche; as a powder becomes more cohesive, avalanches become less regular and the standard deviation of the avalanche power increases. Figure II.11 shows results similar to those obtained with the avalanche time: a higher sensitivity at low moistures and a poor sensitivity for free moistures greater than 0.07%.

The surface fractal is the fractal dimension of the surface of the powder and characterizes the irregularity of the powder surface; as a powder becomes more cohesive, its surface becomes less regular and its surface fractal increases. Figure II.12 shows that, in contrast with the previous two avalanche characteristics, the fractal dimension can provide sufficient sensitivity for an accurate determination of free moistures greater than 0.07 %.

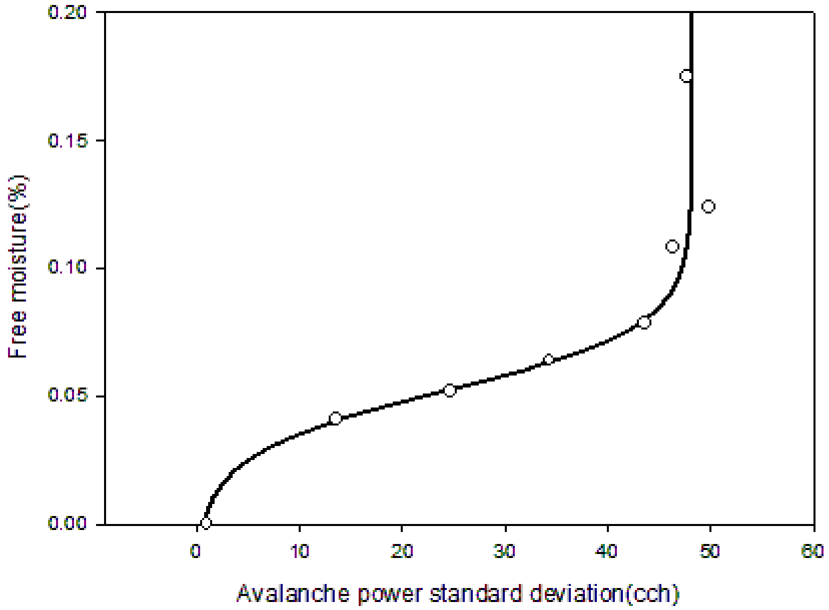

Figure 0.10: Avalanche time vs. free moisture

Based on these results, the recommendations is to first use the avalanche power standard deviation to estimate the free moisture of the sample. If the estimated moisture is greater than 0.07 %, then the surface fractal can be used to get more accurate moisture.

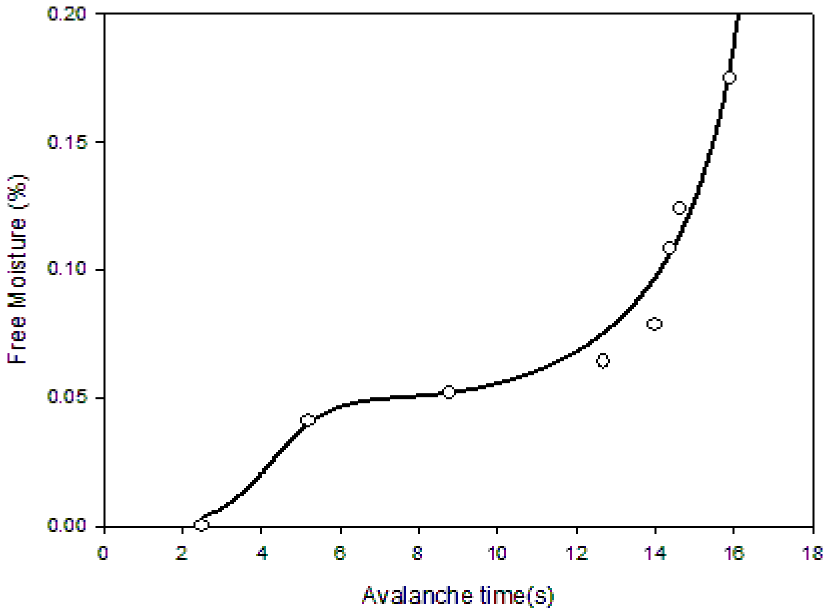

Figure 0II.11: Avalanche power standard deviation vs. free moisture

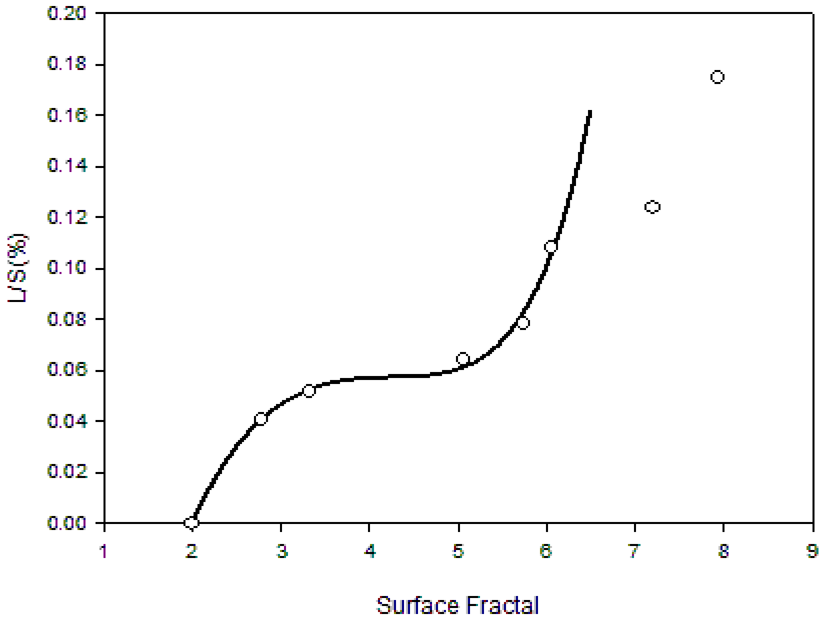

Figure 0II.12: Surface fractal vs. free moisture

II.4.3.3 Angle of Repose

The angle of repose is the angle that a powder forms at rest with a horizontal plane. The angle of repose increases as a powder becomes more cohesive.

Figure II.13 shows that the angle of repose cannot be used to determine free moistures smaller than 0.08 %. On the other hand, it is sensitive at higher moistures.

The bulk density of a powder can be determined from angle of repose experiments, using the radius r and the height h of the angle formed when a mass m of powder is poured:

$$\rho b = \frac{m}{\left[\pi r^2 h / 6\right]} \qquad [II.1]$$

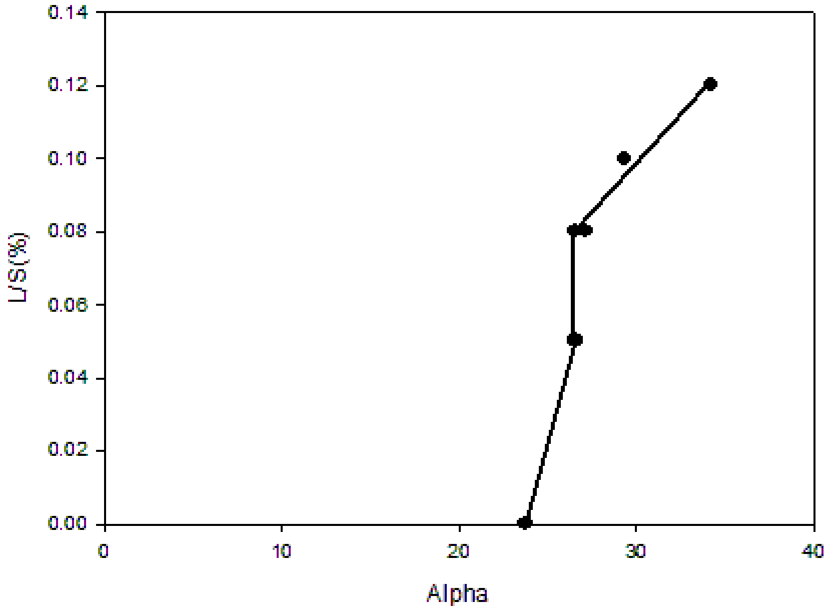

Figure 0II.13: Angle of repose

Figure II.14 shows that the bulk density varies with the free moisture, but this method is not a very sensitive.

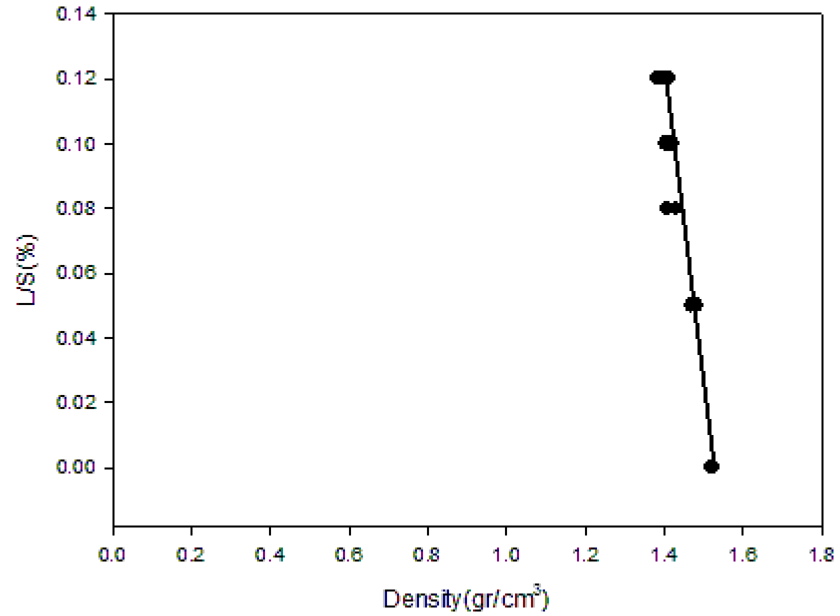

Figure II.14: Powder density as determined from the angle of repose measurements

II.4.3.4. Hausner ratio

One important characteristic to evaluate powder cohesivity is the Hausner ratio, defined as the ratio of tapped bulk density to bulk loose density. The Hausner ratio increases as a powder becomes more cohesive. Figure II.15 shows that it cannot be used to determine the free moisture, probably because its measurement is not accurate enough to detect the very small changes caused by the free moisture.

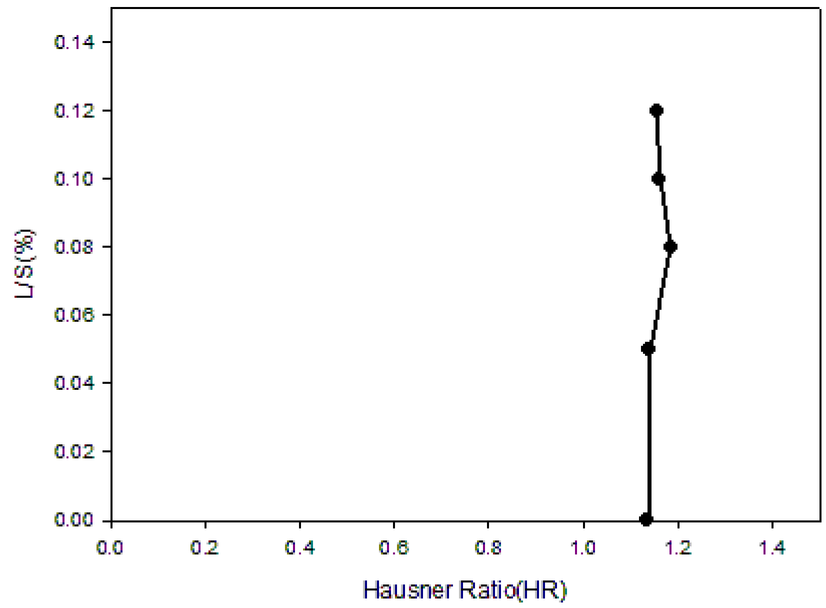

Figure II.15: HR vs. L/S (%)

II.4.3.5. Electrical conductance method

The electrical conductance method was developed by Portoghese *et al.* (2008) to evaluate the distribution of sprayed liquid in a gas-solid fluidized bed. Leach *et al.* (2009) adapted the electrical conductance method to study the impact of spray nozzle geometry on liquid distribution in fluid beds. It was found that the presence of water increased the electrical conductance of a defluidized, packed bed and that, as the liquid spreads through the bed; it provides additional pathways for the electrical current, increasing the bed conductance (Leach *et al.*, 2008). Portoghese *et al.* (2008) and Leach *et al.* (2009) found that more stable and accurate measurements of the liquid distribution in a fluidized bed could be achieved by defluidizing the bed just before measuring its conductance.

In this study, the electrical conductance method is first applied to wet solids samples prepared with a mechanical blender. It is then used in a fluidized bed, following the method developed by Portoghese *et al.* (2008) and Leach *et al.* (2009).

II.4.3.5.1. Preliminary tests in a small cell

A wet solids sample was prepared with a mechanical blender, as for the other tests. This sample was poured in a small, custom-built 11 cm x 11 cm cell, where it was packed. Electrodes on the walls were connected to a signal generator that provided a sinusoidal, 100 Hz current with a constant voltage of 7.74 V (Vapp). A small, 100 KΩ resistor (R_1) was inserted in series along the electrical circuit: the voltage drop across this resistor (V_m) provided the intensity of the current flowing through the circuit.

The following equation shows how the conductance can be calculated by applying the Kirchhoff's current law.

$$I = \frac{V_{app}}{R_1 + R_{bed}} = \frac{V_m}{R_1} \qquad \text{[II.2]}$$

Then this can be rearranged in following equation.

$$R_{bed} = R_1 \left[\frac{V_{app}}{V_m} - 1 \right] \qquad \text{[II.3]}$$

The inverse of this expression is defined as the bed conductance.

$$G_{bed} = \frac{1}{R_{bed}} \qquad \text{[II.4]}$$

The instantaneous bed conductance could then be measured from the two voltages V_{app} and V_m, which were acquired with a data acquisition system and a Labview program.

Preliminary tests were conducted by adding wet micro-agglomerates and macro-agglomerates to the solids in the cell. They showed that the agglomerates did not have a detectable effect on the electrical conductance (although after a long time, there was some detectable impact as water slowly diffused out of the agglomerates and into the bed material contained in the cell). This method can, therefore, be used to measure the free moisture.

Figure II.16 shows that free moistures larger than 0.05 % can be accurately measured with the electrical conductance. The moderate scatter that was observed with replicate experiments may result from the difficulty of achieving an identical packing of the powder in the cell: performing measurements directly in the fluidized bed would eliminate this error, as well as any sampling error.

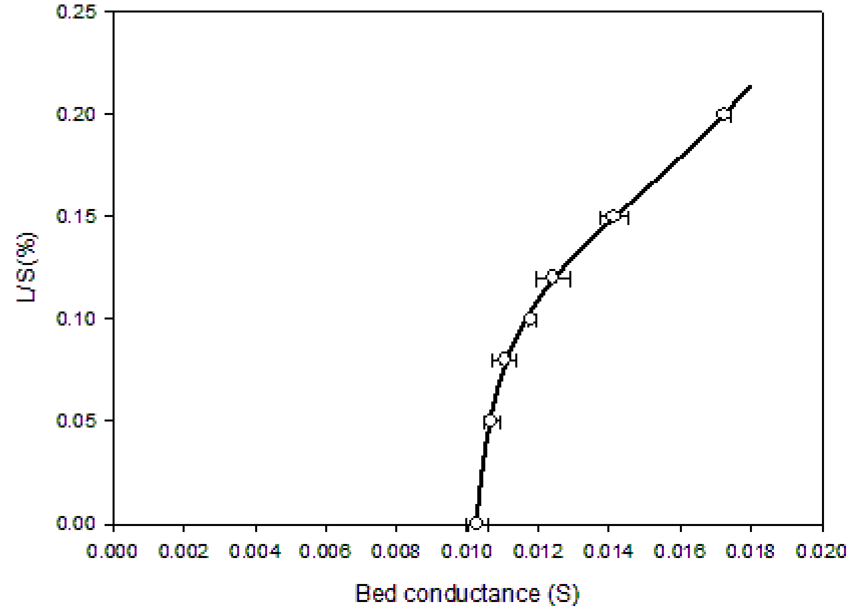

Figure II.16: Small cell conductance result

II.4.3.5.2. Fluidized bed measurements

The conductance measurements in the fluidized bed used an experimental procedure similar to the procedures developed by Portoghese *et al.* (2008) and Leach *et al.* (2009). First, the fluidization velocity was set at 12 cm/s and then 162 ml of water were injected over about 40 s with the "high ALR" spray nozzle. With this nozzle and this low flowrate, no agglomerates were formed. After 90 s, the fluidization is shut off. Some experiments were conducted with a longer fluidization time to verify that no agglomerates had been formed, as agglomerates would be broken over a longer fluidization time.

Five electrodes were placed at different heights on one side wall of bed. These electrodes were 5 cm x 20 cm metal strips and their location is shown in Figure II.17. A large, common electrode covered the opposite wall. The electrical circuit is shown in Figure II.18 and the local bed conductance was evaluated with the same equations used for the small cell.

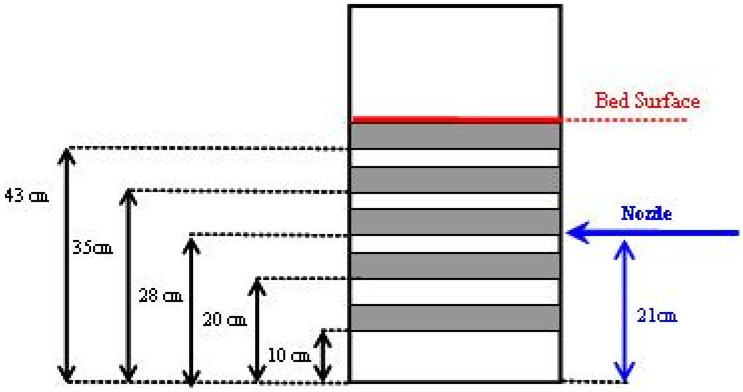

Figure 0II.17: Electrodes locations

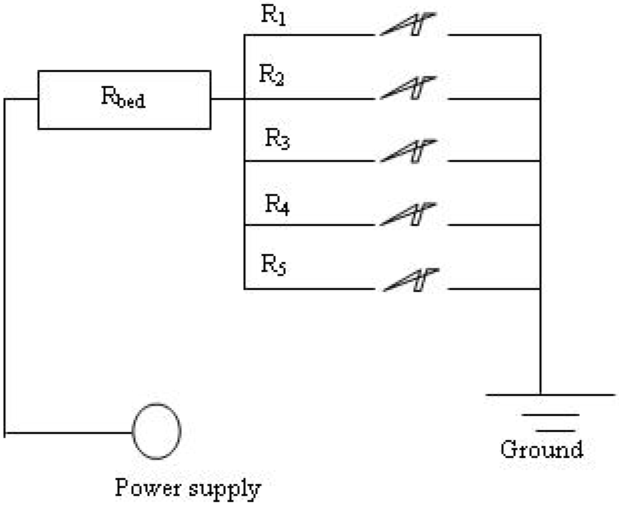

Figure 0II.18: Circuit diagram

Figure II.19 shows how the bed conductance varied during a typical experiment with a regular spray nozzle, which produced agglomerates. During the water injection in the fluidized bed, there was a rapid increase in conductance due to the increased concentration of electrical conductive water. The bed was then defluidized: the bed conductance first increased quickly as the bed slumped and then increased slowly as water slowly diffused from wet agglomerates. During the subsequent refluidization period, the conductance first dropped quickly as the bed expanded, it then increased slightly, peaked and decreased: at first, the free moisture increased as the free moisture generated by agglomerates breakup predominated while at the end, the free moisture decreased as drying by the fluidization gas became predominant. Figure II.19 shows the results obtained with the high ALR nozzle: the main difference is that, during the refluidization period, there was no peak in free moisture since, in the absence of agglomerates, there was no free moisture generated from agglomerates breakup.

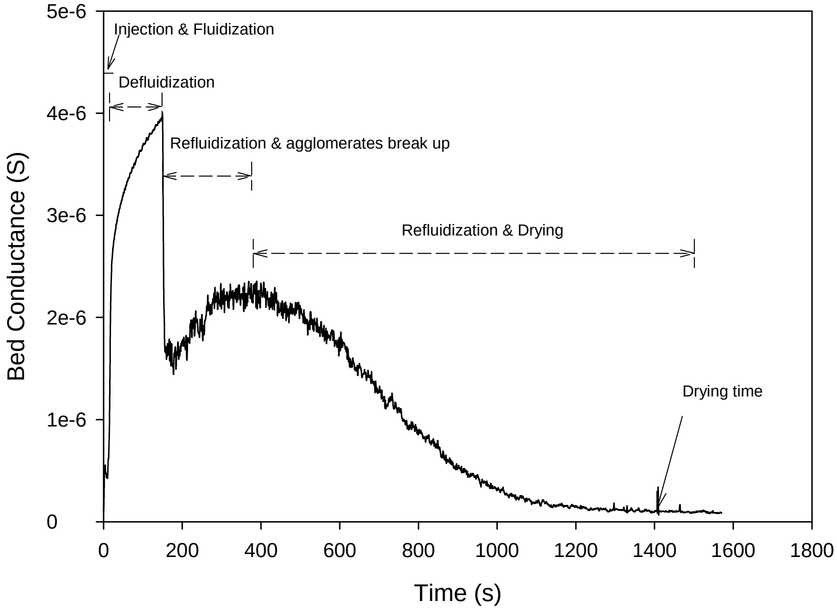

Figure II.19: Bed conductance variation with time, for a regular spray nozzle

Leach *et al.* (1988) proposed to use the variation of the bed conductance with time to characterize the distribution of liquid sprayed into a fluidized bed. They defined two "Nozzle Performance Indices". The first index, "NPI1", is the average of the conductance of the defluidized bed, between the times of 0 s and 150 s, after the end of the liquid injection. If the liquid is well distributed and the free moisture is high, the average bed conductance will be high, as shown by the experiments in the small cell. The second index, "NPI3", is the slope of the bed conductance vs. the logarithm of the time, taken few seconds after the end of the liquid injection. It is a measurement of the rate at which liquid spreads by diffusion from the micro-agglomerates when the bed is defluidized. The small cell experiments show that if the liquid is perfectly distributed as free moisture, NPI3 will be 0: it is therefore unsuitable for the determination of the free moisture.

A calibration curve was obtained by using the high ALR spray nozzle conductance results, as illustrated in Figure II.20. The x axis shows the bed conductance measured a few seconds after the start of the defluidization period, thus resulting from the initial liquid solid contact and not affected by diffusion.

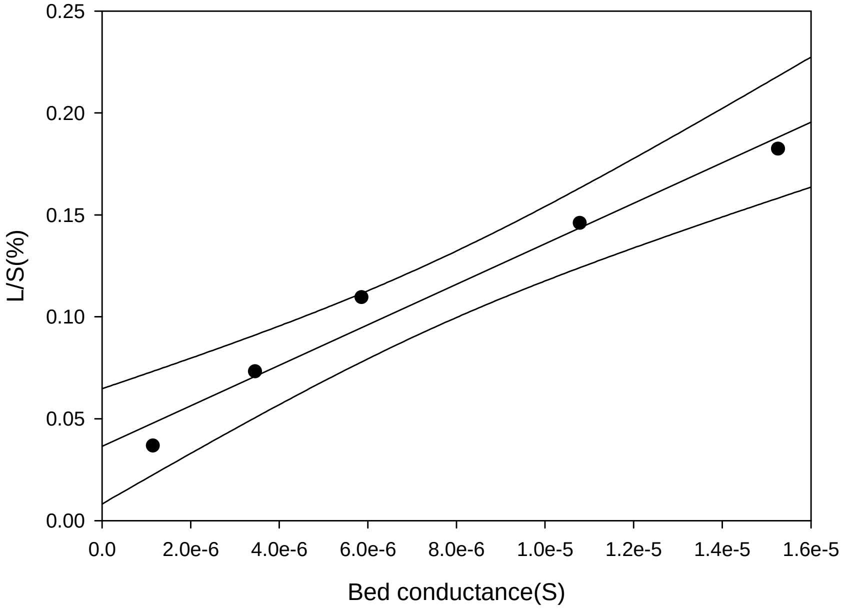

Figure II.20: 95% confidence calibration curve, bed conductance vs. free moisture

Agglomerates were not formed when the high ALR nozzle was used to spray water into the fluidized bed. Figure II.21 shows that when the high ALR spray nozzle was used, the conductance of the defluidized bed (between 100 and 150 s) did not change significantly with time. This is in contrast with the results obtained with a regular spray nozzle, for which the conductance increased with time as water slowly diffused out of the agglomerates (Figure II.19). The absence of agglomerates with the high ALR nozzle was verified by performing the sugar test under the same operating conditions. As the sugar dried under defluidized conditions, it would have preserved any agglomerate. After drying, the bed was emptied and no agglomerate was found, as shown in Figure II.3.

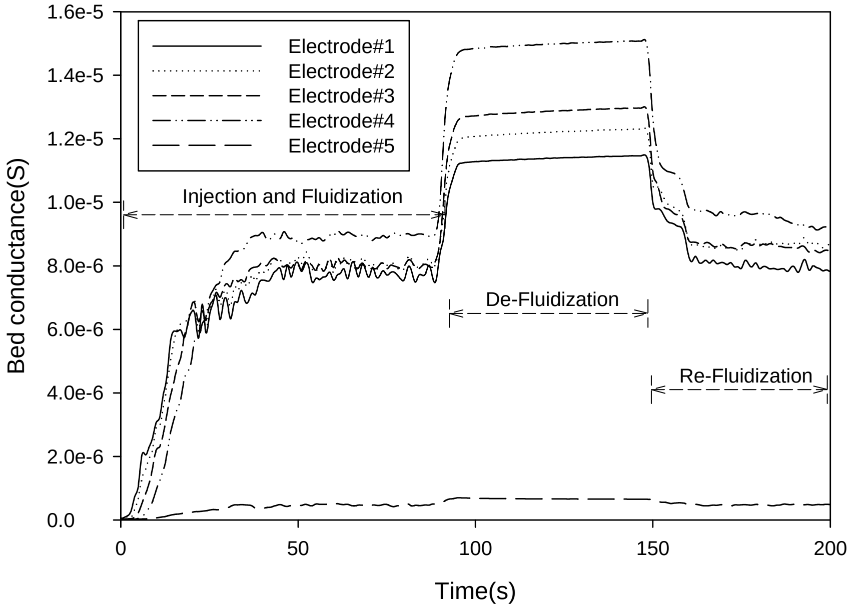

Figure II.21: Variation with time of the bed conductance when using the high ALR nozzle

II.4.3.6. Variations in Bed Height

Free moisture makes the particles cohesive and affects the fluidization quality, while micro-agglomerates and macro-agglomerates have a negligible effect on fluidization quality. Quantifying the fluidization quality can, thus, be used to determine the free moisture. The variation of the bed height as liquid was injected in the fluidized bed, as the bed was defluidized and, finally, as the bed was refluidized, provides a way to quantify the fluidization quality, the cohesivity of the bed particles and, therefore, the free moisture.

A video recording of the fluidized bed was taken through its transparent Plexiglas wall, using a camera operating at a speed of 29 frames/s. An image analysis procedure was then used to determine the instantaneous bed height from this recording.

The movie was first converted to individual pictures. For example, for a 120 second movie, 3479 pictures were created. A dedicated Matlab program analyzed these pictures and calculated the coefficient of variation (standard deviation / mean) of each pixel in the pictures. When a bed is fluidized, the bed surface fluctuates and the bed height can thus be obtained at every lateral location from the pixel where the coefficient of variation is highest, as shown in Figure II.22.

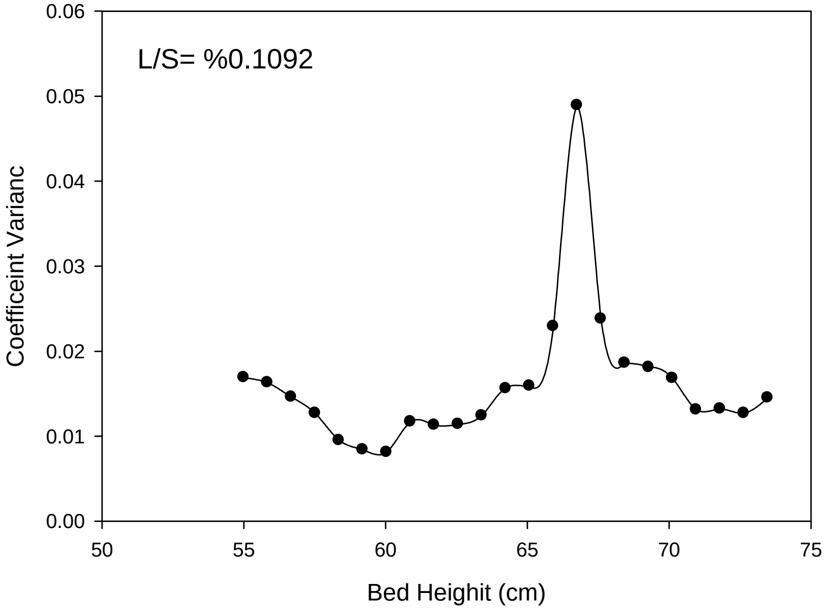

Figure 0II.22: Coefficient of variation vs. height

Figure II.23 shows that the variation of the bed height with time was completely different for a dry bed and a bed wetted with liquid injected with the high ALR nozzle. The same procedure was used as for the conductance measurements: first, the fluidization velocity was set at 12 cm/s and then 162 ml of water were injected over about 40 s with the high ALR spray nozzle; after 90 s, the fluidization was interrupted. In both cases, the initial fluidized bed height was about 65 cm. When the dry bed was defluidized, its height dropped to about 59 cm. When the high ALR nozzle was used to inject water into the bed, the bed height gradually increased to a maximum of about 73 cm and then slowly decreased to a defluidized height of 68 cm.

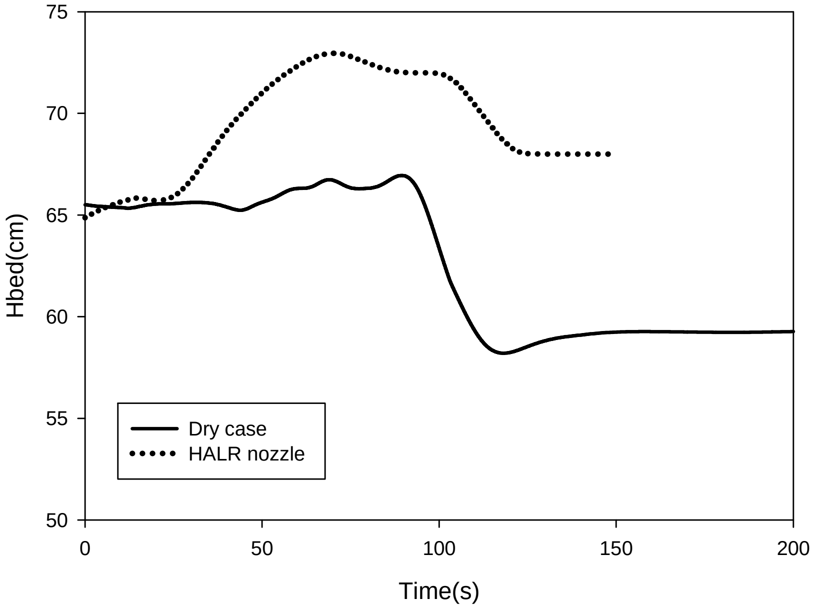

Figure II.23: Bed height changes as the bed is defluidized, for 2 cases: a dry bed and a bed wetted with the high ALR nozzle

Figure II.24 shows how the free moisture could be obtained from the maximum fluidized bed height. Accurate values can be obtained for free moistures ranging from 0.07 to 0.18 %. Below 0.07%, the change in cohesivity cannot be detected. Above 0.2%, the bed becomes completely bogged.

Similar results were obtained from the defluidized bed height, as shown in Figure II.25. The defluidized bed height seems a more sensitive method at the low moistures, but the reproducibility seems worse.

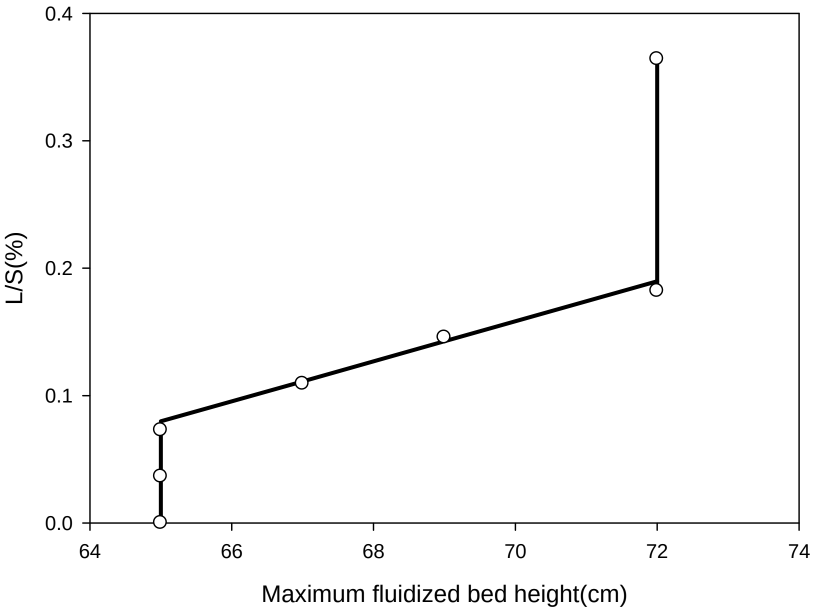

Figure II.24: Maximum fluidized bed height changes with free moisture

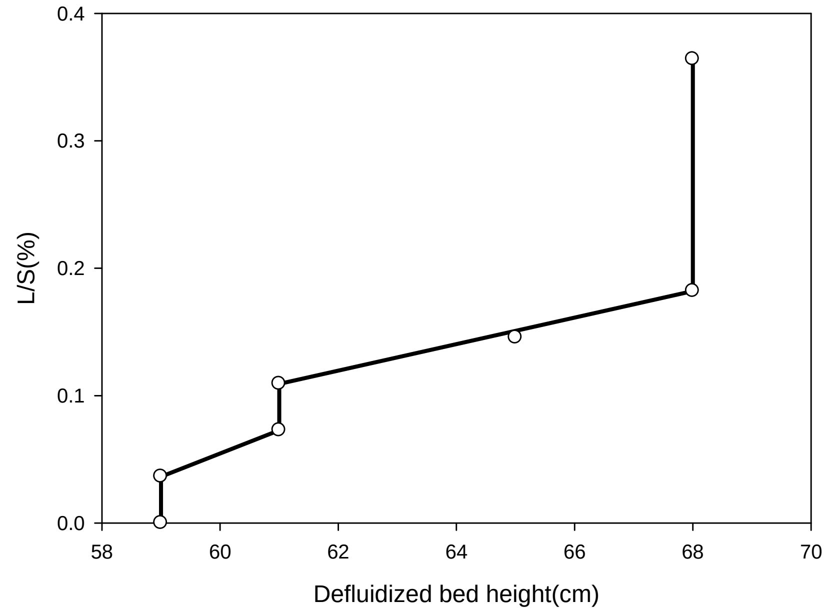

Figure II.25: Maximum de-fluidized bed height changes with free moisture

II.5. Effect of the Atomization Gas Flowrate on the Moisture Distribution in a Fluidized Bed

A small regular nozzle (TEB) (see Figure II.1) was tested with air-to-liquid ratio (ALR) values ranging from 0 to 2%. This range of ALR values is typical for industrial nozzles of the same type as the TEB nozzle. The objective of these tests was to demonstrate how the experimental methods developed in this paper can be used to quantify the effect of the ALR on the distribution of the bed moisture among free moisture, micro-agglomerates and macro agglomerates.

The conductance method described in section 1.4.3.5.2 was found to be the most convenient and accurate method to determine the free moisture and, therefore, it was used in this work.

The moisture in macro-agglomerates was obtained by considering that the macro-agglomerates segregate and, as such, they are only present in the bottom region of the bed. Figure II.19 indicates how the drying time was obtained from the bed conductance measurements. Figure II.26 shows the difference between the drying time (t1) of the solids in the top region of the bed, measured with electrode #1, and the drying time (t5) of the solids in the bottom region of the bed, measured by electrode #5. The time t5 is much longer than the time t1 because macro-agglomerates dry and break up much more slowly than the micro-agglomerates present in the upper part of the bed. Drying takes place in two stages: in the first stage, there is significant free moisture in the bed, which results from the original free moisture and from micro-agglomerates, while in the second stage, most of the bed is dry and the macro-agglomerates are slowly drying out.

Separate measurements indicated that the air leaving the fluidized bed, during drying, was saturated with water vapor. Its temperature was approximately constant during the drying period. Therefore, the time t5 is proportional to the total moisture while the time t1 is proportional to the sum of the free moisture and the moisture contained in micro-agglomerates. The fraction of the injected water that is contained in macro-agglomerates can thus be obtained from the following equation:

$$Fraction\ of\ total\ moisture\ in\, macro - agglomerte\, s = \frac{(t5 - t1)}{t5} \qquad [II.5]$$

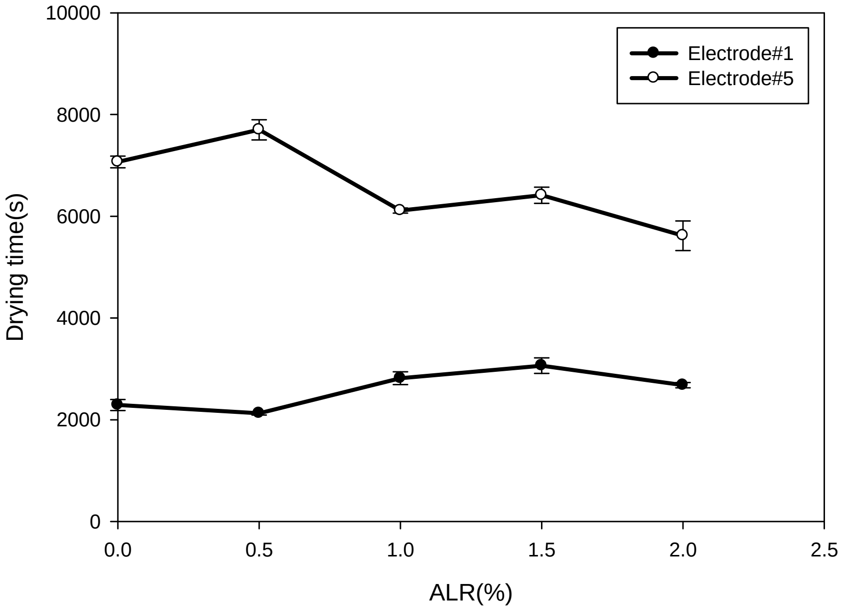

Figure 0II.26: The difference between drying time of Elec#1 and Elce#5

This method for the determination of the moisture contained in macro-agglomerates was validated by conducting experiments where the water was injected into the fluidized bed as in the regular experiments. Once the bed had been defluidized, however, most of the solids were carefully vacuumed out, leaving only a layer of about 10 cm at the bottom of the bed. The solids in this bottom layer were weighed, dried in an oven and weighed again to obtain their total moisture. This provided a direct measurement of the moisture contained in the macro-agglomerates, assuming the free and micro-agglomerate moistures are the same in the bottom layer as in the rest of the bed. Table 1 shows that there was a reasonably good agreement between the two measurement methods.

Table 0II.1: Macro-agglomerates moisture measurements with two different methods

ALR	Macro-agglomerates moisture from drying time	Macro-agglomerates from the bottom layer drying experiments
0	67%	70%
1	52%	50%
2	53%	51%

Figure II.27 shows that the ALR of the TEB spray nozzle has a strong impact of the distribution of the injected water in the fluidized bed. The macro-agglomerate moisture dropped with increasing ALR while the free moisture increased. Figure II.27 also indicates that, even at a 2% ALR, the TEB nozzle provides a distribution that is far from perfect, since over 50% of the injected liquid is contained in macro-agglomerates.

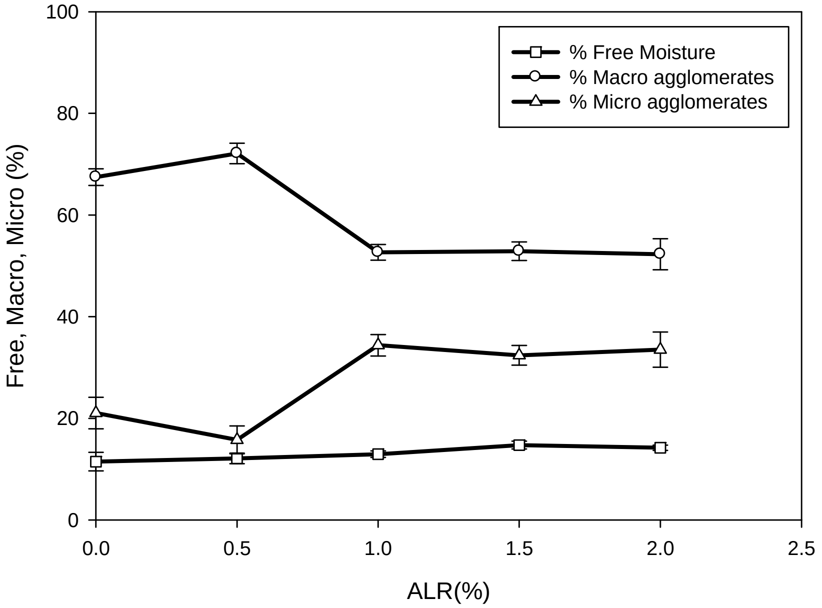

Figure 0II.27: Effect of the ALR on the moisture distribution, using the TEB nozzle

Conclusions

Of all the methods that were investigated, to measure how a liquid injected into a fluidized bed is distributed on the fluidized particles, the methods based on the in-situ measurements of the bed conductance have been demonstrated to be the most convenient and accurate. Bed conductance measurements in the top region of the bed provide the free moisture, i.e. the liquid distributed on individual particles, while conductance measurements in the bottom region provide the moisture trapped in macro-agglomerates.

These methods were applied to the study of the effect of the atomization gas flowrate on the performance of a scaled-down nozzle, of a type used in industrial applications. Increasing the atomization gas flowrate increased the free moisture and reduced the moisture trapped in macro-agglomerates.

References

Base, T.E., Chan, E.W., Kennett, R.D., Emberley, D.A., (1999) Nozzle for atomizing liquid in two phase flow. *United States patent, 6003789.*

Benoni, D., Briens, C.L, Baron, T., Duchesne, E., Knowlton, T.M. (1994). A procedure to determine particle agglomeration in a fluidized bed and its effect on entrainmen., *Powder technology, Vol. 78*, 33-42.

Briens, C., McDougall, S., Chan, E. (2003). online-detection of bed fluidity in a fluidized bed coker. *Powder Technology*

House, P., Briens, C., Berruti, F., Chan, E., August (2008). Effect of spray nozzle design on liquid–solid contact in fluidized beds. *Powder Technology, Volume 186*, Issue 1, Pages 89-98.

Kai, T., Murakami, M., Yamasaki, K.I., Takahashi, T., Relationship between apparent bed viscosity and fludization quality in a fluidized bed with fine particles. *J. Chem. Eng. Japan, Vol. 24*, No. 4. 494-500

Knapper, B., Gray, M., Chan, E., Mikula, R. (2003). Measurement of Efficiency of Distribution of Liquid Feed in a Gas-Solid Fluidized Bed Reactor. *International Journal of Chemical Reactor Engineering, Vol. 1.*

Leach A, Portoghese F, Briens C, Berruti F. (2008). New, rapid method for the evaluation of the liquid-solid contact resulting from liquid injection into a fluidized bed. *Powder Technology. 184,* 44–51.

Leach, A., Chaplin, G., Briens, C., Berruti, F., (2009). Comparison of the performance of liquid–gas injection nozzles in a gas–solid fluidized bed. *Chemical Engineering and Processing 48,* 780–788.

McCracken, T.W., (2005) Mixing arrangements for atomizing flow in multi phase flow. *United States patent, US 2005/0001062 A1*

McDougall, S. L.,Ssaberian, M., Briens, C., Berruti, F. Chan, E. (2004). Characterization of fluidization quality in fludized beds of wet particles. *International Journal of Chemical reactor Engineering, Vol. 2.*

McLaughlin, L.J., Rhodes, M.J. (2001) Prediction of fluidized bed behavior in the presence of liquid bridges. *Powder Technology. Vol. 114.*

Portoghese, F., House, P., Berruti, F., Briens, C., Adamiak, K., Chan, E. (2008), Electric conductance method to study the contact of injected liquid with fluidized particles. *American Institute of Chemical Engineers AIChE.*

Renganathan, T., Krishnaiah, K. (2005). Voidage characteristics and prediction of bed expansion in liquid-solid inverse fluidized bed. *Chemical Engineering Science.*

Strusch, J., Riehle, C., Mleczko, L. (2001). Development of a method for preparing particles for the investigations of defluidization phenomena in cold flow models. Bayer, *Nuremberg, PARTEC.*

Tardos, G., Mazzone, D., Pfeffer, R. (1985). Destabilization of fluidized beds due to agglomeration - part II:Experimental verification, *Can. J. Chem. Eng., Vol. 63*, 384-389.

CURRICULUM VITAE

EDUCATION

Ecole Polytechnique de Montreal (February 2012-present)
Post Doctoral Fellow

Western Universty, London, Ontario, Canada (September 2006- April 2012)
Ph.D. candidate in Chemical Engineering
Research Group: Institute for Chemicals and Fuels from Alternative Resources (ICFAR)
Thesis: “Thermal and catalytic gasification of bio-oil in fluidized bed reactors to produce syngas”

The University of Tehran, Tehran, Iran (2001-2003)
M.Sc. in Chemical Engineering
Thesis: “Retrofit for debottlenecking of heat exchanger networks designed by pinch technology method”

The University of Mazandaran, Babolsar, Iran (1996-2000)
B.Sc. in Chemical Engineering
Thesis: “Simulation of an atmospheric distillation tower of the crude oil by PROII- Tehran refinery”

EDUCATIONAL AWARDS

1. Western Engineering Scholarship (September 2006- January 2012)

2. Graduate research thesis award (2006-2007 and 2009-2010)

3. Second prize for the best presentation in the “fluidized bed reactors” session, Research Bridges Symposium, Sarnia Research Park, Sarnia, Ontario, Canada (May 2010)

4. Certified as the top graduate among master’s students of Chemical Engineering, Faculty of Engineering, The University of Tehran, Tehran, Iran (September 2003)

ACADEMIC WORK EXPERIENCE

1. Research assistant (September 2006- February 2012)

   Institute for Chemicals and Fuels from Alternative Resources (ICFAR),
   Department of Chemical and Biochemical Engineering, Faculty of Engineering,
   Western University

   - Development and upgrading of renewable energy resources
   - Fluidization engineering
   - Gasification and pyrolysis processes
   - Operation of the bench scale fluidized bed reactors
   - Synthesis and screening of heterogeneous catalysts
   - Design and construction of micro test reactors
   - Thermodynamic modeling of chemical reactions
   - Induction heating
   - Design of the linear pneumatic actuators
   - Image analysis with MATLAB
   - Gas analysis
   - Elemental analysis of chemical compounds

2. Teaching assistant (September 2006- April 2010)

   Department of Chemical and Biochemical Engineering, Faculty of Engineering,
   Western University

3. Representative of graduate students and member of the graduate committee (May 2008- August 2010)

   Department of Chemical and Biochemical Engineering, Faculty of Engineering,
   Western University

4. Founder and chair of the Chemical Engineering Graduate Society (CGS) (September 2009- August 2010)

   Department of Chemical and Biochemical Engineering, Faculty of Engineering,
   Western University

5. Founder and member of the editorial board of "Grad Gab" (September 2009- August 2010)

   The news letter of graduate students of Chemical Engineering, Department of Chemical and Biochemical Engineering, Faculty of Engineering, Western University

6. Co-chair of the Research Bridges Symposium (May 2010)

The first annual Chemical and Biochemical Engineering students' research presentation to academia and industries, Department of Chemical and Biochemical Engineering, Faculty of Engineering, Western University, Sarnia Research Park, Sarnia, Ontario

7. Research assistant (September 2001- August 2003)
   Department of Chemical Engineering, Faculty of Engineering, the University of Tehran, Iran
   - Grass root and retrofit analysis of heat exchanger networks by pinch technology method
   - Exergy analysis of chemical processes
   - Simulation of chemical processes by HYSYS

8. Member of Board of Directors (September 2001- August 2002)
   Society of Alumni Graduates, Faculty of Engineering, the University of Mazandaran, Iran

9. Teaching assistant (February 1999; February2000)
   Department of Chemical Engineering, Faculty of Engineering, the University of Mazandaran, Iran
   - Chemical Engineering Thermodynamics; 2 terms

10. Chair of the Society of Undergraduate Chemical Engineering Students (September 1999- June 2000)
    Department of Chemical Engineering, Faculty of Engineering, the University of Mazandaran, Iran

11. Chair of the "Farayand-e-Khazar" (September 1999- June 2000)
    The Newsletter of undergraduate Chemical Engineering students, Department of Chemical Engineering, Faculty of Engineering, the University of Mazandaran, Iran

12. Representative of the Student Committee of the Society of Iranian Chemical Engineers (September 1999-June 2000)
    Department of Chemical Engineering, Faculty of Engineering, the University of Mazandaran, Iran

PROFESSIONAL WORK EXPERIENCE

1. Iranian Offshore Engineering and Construction Company (IOEC), Tehran, Iran (February 2006- September 2006)
   Procurement and process engineer, Process group, Commercial department

2. Research Institute of Petroleum Industry (RIPI), Tehran, Iran (August 2005- February 2006)
   Researcher, FCC project, Division of process engineering development

3. Petrochemical Research and Technology Company, Tehran, Iran (April 2004- August 2005)
   Researcher, Department of non polymeric researches

4. Department of Chemical Engineering, Faculty of Engineering, University of Tehran, Tehran, Iran (September 2003- March 2004)
   Research assistant, feasible study of retrofit for energy saving on heat exchangers network of Behran Oil company using pinch technology method

VOLUNTEER WORK EXPERIENCE

1. Iranian Society of London Ontario (ISLO), London, Ontario, Canada (October 2009- May 2010)
   Member of the Board of Directors

2. CHRW radio station, 94.9 FM, Western University, London, Ontario, Canada (October 2006- November 2009)
   Host of the multicultural radio shows
   - President of Radio Navaye Iran

3. International Student Centre, Western University, London, Ontario, Canada (April 2008-December 2008)
   Volunteer peer guide to assist new international students to get comfortably settled in a new living and educational environment

VOLUNTEER WORK AWARDS

1. Award for the best multicultural show during 2008-2009 by CHRW radio station (February 2009)

2. Award for the best outstanding volunteer during 2008-2009 by CHRW radio station (February 2009)

PATENT

- Lead Inventor for the Jiggle Bed Reactor. A report of invention has been issued to the Western University Ontario

PUBLICATIONS- JOURNAL PAPERS

1. **Latifi, M**; Ferrante, L; Berruti, F; Briens, C; "A Novel Fluidized and Induction Heated Micro Reactor for Catalyst Testing"; to be submitted to the AICHE journal

2. **Latifi, M**; Briens, C; Berruti, F; "Production of Syngas from Bio-oil and its Model Compounds- A Literature Review"; to be submitted to the International Journal of Chemical Reactor Engineering

3. **Latifi, M**; Ferrante, L; Briens, C; Berruti, F; "Effects of Residence Time and Temperature on the Thermal Cracking of Bio-oil for Syngas Production"; to be submitted to Canadian Journal of Chemical Engineering
4. **Latifi, M**; Briens, C; Berruti, F; "Non-catalytic and Catalytic Steam Reforming of Acetic Acid in the Jiggle Bed Reactor"; to be submitted to the Journal of Fuel Processing Technology
5. **Latifi, M**; Briens, C; Berruti, F; "Thermal and Catalytic Gasification of Bio-oils in the Jiggle Bed Reactor for Syngas Production"; to be submitted to the International Journal of Hydrogen Energy
6. **Latifi, M**; Briens, C; Berruti, F; "Development of a Thermodynamic Model to Predict the Equilibrium Concentration of Gases from Bio-oil Gasification with Sand or Olivine Catalyst"; to be submitted to the International Journal of Hydrogen Energy
7. Farkhondeh, M; Soleimani, **M; Latifi**, M; Briens, C; Berruti, F; "Characterization of Moisture Distribution in a Fluidized bed"; to be submitted to Journal of Power Technology
8. **Latifi, M**; Panjeshahi, M; Tahuni, N; "Debottlenecking of the Heat Exchanger Networks Designed by the Pinch Technology Method"; Iranian Journal of Energy; 2005

PUBLICATIONS- CONFERENCE PAPERS AND PRESENTATIONS

1. **Latifi, M**; Ferrante, L; Briens, C; Berruti, F; “Development of a Novel Vibrating Reactor for Testing Bio-oil Gasification Catalysts”; Bioenergy III: Present and New Perspectives on Biorefineries; Lanzarote; Canary Islands; Spain; May 22-27
2. **Fotovat, F**; Chaouki, J; Bergthorson, J; Latifi, M; “ The influence of Biomass Properties on the Fluidization Hydrodynamics of Solid Mixtures Containing Biomass”; Bioenergy III: Present and New Perspectives on Biorefineries; Lanzarote; Canary Islands; Spain; May 22-27
3. **Latifi, M**; Briens, C; Berruti, F; “Introducing a Novel Mini Fluidized Reactor for Gasification Processes”; Research Bridges symposium; Sarnia research park; Sarnia; Ontario; Canada; May 5, 2010
4. **Latifi, M**; Ferrante, L; Briens, C; Berruti, F; “ Bio-oil Gasification to Produce Syngas”; Agricultural and Biorefinery Innovation Network (ABIN) conference; the University of Western Ontario; London; Ontario; Canada; March 14-16, 2010
5. **Latifi, M**; Ferrante, L; Briens, C; Berruti, F; “ Bio-oil Gasification to Produce Syngas”; Institute of Chemicals and Fuels for Alternative Resources (ICFAR) seminar; Niagara Falls; Ontario; Canada; February 28- March 2, 2010
6. **Latifi, M**; Briens, C; Berruti, F; “Thermal Cracking of Bio-oil for Syngas Production”; 8th World Congress of Chemical Engineering (WCCE8); Montreal; Quebec; Canada, August 23-27, 2009
7. **Rohani, S**; Latifi, M; Briens, C; Berruti, F; “Development and Testing of a Novel Induction Micro Reactor to Test Catalysts for Bio-oil Gasification”; 8th World Congress of Chemical Engineering (WCCE8); Montreal; Quebec; Canada, August 23-27, 2009
8. **Rohani, S**; Latifi, M; Briens, C; Berruti, F; “A Novel Induction Heating Micro Reactor for Gasification Catalyst-Testing”; GPE-EPIC congress; Venice; Italy; June 14-17, 2009
9. **Latifi, M**; Ferrante, L; Briens, C; Berruti, F; “Effect of Residence Time and Temperature on Thermal Cracking of Bio-oil for Syngas Production”; Bioenergy-II: Fuels and Chemical from Renewable Resources; Rio de Janeiro; Brazil; March 8-13, 2009
10. **Latifi, M**; Panjeshahi, M; Tahuni, N; “Debottlenecking of Heat Exchanger Networks, already Designed by Pinch Design Method”; 17th International

Congress of Chemical and Process Engineering (CHISA congress); Prague; Czech Republic; August 27-31, 2006

11. **Latifi, M**; Panjeshahi, M; “Technology Transfer in Transportation Sector Regarding Climate Change Mitigation and Reduction”; 10th National Congress of Iranian Chemical Engineers (in Persian), Zahedan, Iran, 2005
12. **Latifi, M**; Jafari Nasr, M.R.; Masoumi, M; “Study of Mass Transfer and its Effect on the Rate of Gas-Liquid Reactions with Homogeneous Catalysts”; 10th National Congress of Iranian Chemical Engineers (in Persian), Zahedan, Iran, 2005
13. **Latifi, M**; Panjeshahi, M; Tahuni, N; “Investigation of Heat Exchanger Networks with Increased Flow Rates"; National Congress of Energy (in Persian), Tehran, Iran, 2005
14. **Latifi, M**; Sotudeh, R; Mostoufi, N; “Simulation of Melamine Plant in Low Pressure Processes”; 8th National Congress of Iranian Chemical Engineers (in Persian), Mashhad, Iran, 2003